REPORT DOCUMENTATION PAGE

FORM APPROVED
OMB No. 0704-0188

Public reporting burden for this collection of information is estimated to average 1 hour per response, including the time for reviewing instructions, searching existing data sources, gathering and maintaining the data needed and completing and reviewing the collection of information. Send comments regarding this burden estimate or any other aspect of the collection of information, including suggestions for reducing the burden to Washington Headquarters Services, Directorate for Information Operations and Reports, 1215 Jefferson Davis Highway, Suite 1204, Arlington, VA 22202-4302 and to the Office of Management and Budget, Paperwork Reduction Project (0704-0188), Washington, DC 20503.

1. AGENCY USE ONLY (Leave blank)	2. REPORT DATE 5/1/96	3. REPORT TYPE AND DATES COVERED FINAL 12/93 TO 12/96

4. TITLE AND SUBTITLE OF REPORT
THEORETICAL AND EXPERIMENTAL STUDIES IN NONLINEAR
MECHANICAL SYSTEMS

5. FUNDING NUMBERS

6. AUTHOR(S)
SRI NAMACHCHIVAYA AND MONICA M. DOYLE

F49620-93-1-0063

7. PERFORMING ORGANIZATION NAME(S) AND ADDRESS(ES)
UNIVERSITY OF ILLINOIS
AERO & ASTRO ENGINEERING
306 TALBOT LAB
104 S. WRIGHT
URBANA, IL 61801

8. PERFORMING ORGANIZATION REPORT NUMBER:

UILU ENG 96-504

9. SPONSORING/MONITORING AGENCY NAME(S) AND ADDRESS(ES)
AFOSR/NA
Bolling AFB DC 20332-6448

NA

AFOSR-TR-96

0274

11. SUPPLEMENTARY NOTES:

12a. DISTRIBUTION AVAILABILITY STATEMENT
Approved for public release;
distribution unlimited

19960617 152

13. ABSTRACT (Maximum 200 words)

The stability and bifurcation behavior of mechanical systems parametrically excited by small periodic or stochastic perturbations is studied. The almost-sure stability is defined by the sign of the maximal Lyapunov exponent, the exponential growth rate of solutions to a linear stochastic system. A perturbative approach is employed to construct an asymptotic expansion for the maximal Lyapunov exponent of a four-dimensional gyroscopic dynamical system driven by a small intensity real noise. The perturbative technique developed is then applied to study the lateral vibration instability in rotating shafts subject to stochastic axial loads and stationary shafts in cross flow with randomly varying flow velocity. The local and global bifurcation behavior of nonlinear deterministic gyroscopic and consevative systems subject to periodic parametric excitation is also examined. Throughout this work, it is assumed that the dissipation, imperfections and amplitudes of parametric excitations are small. In this way, it is possible to treat these problems as weakly Hamiltonian systems. Most of the analysis presented here is based on the recent work of perturbed Hamiltonian systems. (P.T.O.)

14. SUBJECT TERMS	15. NUMBER OF PAGES: 137
	16. PRICE CODE

17. SECURITY CLASSIFICATION OF REPORT: U	18. SECURITY CLASSIFICATION OF THIS PAGE U	19. SECURITY CLASSIFICATION OF ABSTRACT U	20. LIMITATION OF ABSTRACT U

ONRCHI COMPUTER V 1.0   11/94   DTIC QUALITY INSPECTED 1   STANDARD FORM 298 (REV 2-89)

FINAL TECHNICAL REPORT

THEORETICAL AND EXPERIMENTAL STUDIES IN NONLINEAR MECHANICAL SYSTEMS UNDER HARMONIC AND STOCHASTIC EXCITATION

N. Sri Namachchivaya and Monica M. Doyle

Principal Investigator: N. Sri Namachchivaya
Nonlinear Systems Group
University of Illinois at Urbana-Champaign
Urbana, IL 61801
Department of Aeronautical and Astronautical Engineering

May 1, 1996

Contents

List of Figures

iv

List of Tables

Chapter 1

INTRODUCTION

1.1 Introduction

The primary concern in the analysis of dynamical systems is the determination and prediction of steady-state motions and their corresponding stability. A steady-state (or *fixed point* in state space) is defined to be stable if the solution returns to this state after being perturbed from it. This point is locally stable if it is stable with respect to small perturbations and globally stable if robust to large perturbations. Consider the motion of a general dynamical system described by the following ordinary differential equation:

$$\dot{x} = f(x, \mu), \quad x \in \mathbf{R}^d \tag{1.1}$$

where x is the state vector and μ represents a collection of parameters on which the motion depends. These parameters may or may not depend on time. The vector function $f(x, \mu)$ may contain both linear and nonlinear terms. Lyapunov showed that the local stability of a fixed point of Eq. (1.1), denoted by $\bar{x}$, can be completely categorized by the equations of motion linearized about this point provided none of the eigenvalues have zero real part.

The stability analysis of the system in Eq. (1.1) becomes more difficult when the parameter μ depends on a random process. Since most practical dynamical systems are subject to some form of noise, this situation cannot be ignored. The determination of conditions under which the resulting *stochastic* system is stable (in some sense) is of great interest to both researchers and practitioners in the area of machine and component vibration as well as system reliability.

There are several ways of defining the stability of a fixed point $\bar{x}$ in a stochastic system. The two most prevalent definitions are almost-sure stability and moment stability. If the fixed point is almost-surely stable, or stable with probability 1 (w.p.1), then as time tends to infinity, the state of the system approaches this equilibrium from all starting values except for those contained in a set of measure zero. This can be expressed in terms of probabilities as

$$P\left\{ \lim_{t \to \infty} \| x(t; x_0) - \bar{x} \| < \epsilon \right\} = 1 \tag{1.2}$$

where $\epsilon \ll 1$. If Eq. (1.2) is linear, it is always possible to translate this fixed point to the origin, i.e. $\bar{x} = 0$. Thus, for an almost-surely stable fixed point, as time progresses, the system response decays to zero. However, from the applications viewpoint, one may not be satisfied with such guarantees since such a process may still exceed some threshold values or may possess a slow rate of decay. Although sample solutions may be stable w.p.1, the mean square response of the system

2

for the same parameter values may grow exponentially. For this reason, it is wise to also consider the behavior of the moments (of certain order) of the response over time. A fixed point is said to be stable in the pth moment if

$$\lim_{t \to \infty} E\left[\| \, x(t; x_0) - \bar{x} \, \|^p\right] = 0$$

The first portion of this research deals with the determination of the effect of adding parametric noise to linear mechanical systems for which the corresponding deterministic system is stable. Specifically, the almost-sure and moment stability for the resulting linear stochastic systems will be examined. Both two- and four-dimensional systems, parametrically excited by noise, are considered. The analysis in two dimensions considers general single-degree-of-freedom systems perturbed by noise. The results of this analysis can be applied to study the stability of any two-dimensional linear system in which the corresponding deterministic system is exponentially stable. In the four-dimensional case addressed here, the corresponding deterministic system is gyroscopic. The results obtained have a wide range of applications including rotating shafts (drive shafts, helicopter rotor shafts, etc.), pipes conveying fluid, moving belts (such as band saws) and cylinders in a cross flow. In the most realistic cases, these gyroscopic systems are subject to some type of noise. The methods developed through this research provide a means of determining the almost-sure and moment stability of these four-dimensional system as a function of the system parameters. In all cases, the amplitude of the noise is assumed to be small.

While current research efforts are continuously providing a greater understanding of the behavior of autonomous nonlinear dynamical systems, much work remains to be done in the area of deterministic nonautonomous nonlinear dynamics. In particular, the study of global bifurcations and the analytical prediction of chaotic dynamics in such systems is an area which is still evolving. Most realistic models of physical systems contain nonlinear terms in the ordinary (or partial) differential equations governing the evolution of the states. In the study of the response and stability of nonlinear dynamical systems, the location and characterization of bifurcation points is of primary importance. A *bifurcation* refers to a qualitative change in the response of a dynamical system as a parameter passes some critical value. The parameter value at which this qualitative change takes place is the *bifurcation point*.

The focus of the deterministic portion of this research is the study of the bifurcation behavior of nonlinear gyroscopic systems. In the absence of dissipation and nonconservative forces, a gyroscopic system is Hamiltonian. Throughout this work, it is assumed that the dissipation, imperfections and amplitudes of parametric excitations are small. Thus, one can treat these problems as weakly Hamiltonian systems. Most of the analysis is based on the recent work of perturbed Hamiltonian systems. Since in the Hamiltonian treatment, the momenta p and coordinates q constitute $2n$ independent variables, Hamilton's equations allow a much wider range of transformations than the point transformations. This enlargement of the class of possible transformations, which includes all $2d$ independent variables p and q, is one of the important advantages of the Hamiltonian treatment.

The study of the bifurcation behavior in a small region of state space surrounding the fixed point (or limit cycle) or in a small neighborhood of the bifurcation point is referred to as local analysis. In a local bifurcation, the stability of one fixed point or limit cycle is lost and a branching, or bifurcating, solution emerges. These local bifurcation scenarios arise in the dynamics governed by the variational equations.

There are many phenomena which cannot be explained by local analysis alone. These solutions are, for the most part, global in the sense that they do not lie in the small neighborhood of state space or in a small neighborhood of the parameter at which the fixed point or the limit cycle

3

goes through a local bifurcation. Recent results on persistence of quasiperiodic motions facilitate the development of global techniques to detect such complicated dynamics. It is imperative to understand the response, stability and both local and global bifurcation behavior of such nonlinear dynamical systems prior to their use as integral and reliable elements of mechanical systems.

The analytical techniques developed in this research are used to predict the local and global bifurcation behavior of the dynamical system and estimate the nontrivial response in the post-critical regions. While these techniques seem to provide researchers with the ability to predict the behavior of many practical dynamical systems without the expense and delay of complicated experiments, the accuracy of the approximations (as well as that of the mechanical models) is not fully known. Before relying on the results of such modeling and reduction techniques in the analysis of complex systems, it is imperative to verify the local and global behavior of simple (lower dimensional) dynamical systems through direct experimentation. Thus, the final phase of this research involves the design and construction of an experimental rig. This rig will serve as a test bed for direct experimental verification of results obtained from the various approximation techniques employed in the analysis of nonlinear differential equations. The theoretical results will serve as a guideline for locating stability boundaries and predicting post-critical behavior. The extent to which the theoretical and experimental results match will provide an insight into the accuracy of the mathematical models and theoretical approximations. The experiments will, in turn, guide the development and refinement of the theories developed to incorporate any new phenomena observed.

1.2 Objectives

The current research addresses both the stability and dynamics of mechanical systems in the presence of deterministic as well as stochastic parametric excitations. The overall goal of this research is two-fold:

- In the case of deterministic excitations, the primary objective is the development of techniques to detect the nonlinear behavior of a class of gyroscopic systems including experimental verification of theoretical results.

- The second part of this investigation involves the formulation and development of methods to analyze the complex interactions between noise, stability, and nonlinearities inherent in mechanical systems.

1.3 Impact of This Research

The work performed under this grant will have direct impact on the design of advanced mechanical/structural components and system reliability. The following points highlight the primary contributions of the completed work:

- analytical prediction of stability limits (or limits of "safe" operation),

- analytical prediction of regions of parameter space in which chaotic motions may exist,

- experimental verification of the accuracy of these predictions and

- understanding of instability mechanisms necessary for development of techniques to control unwanted dynamics.

The techniques developed throughout this research should provide a deeper insight into the dynamics of more complicated systems and will, ultimately, lead to the design of more efficient and reliable components.

1.4 Researchers Working on the Grant

Faculty (PI): Navaratnam, N. Sri, Associate Professor, Aeronautical and Astronautical Engineering

Post Docs: Doyle, Monica M., PhD (AAE, UIUC 1995), US citizen

Graduate Students: Doyle, Monica M., Doctoral candidate (degree completed May, 1995) Aeronautical and Astronautical Engineering, US citizen (1/4 assistance)

Pluta, Gregory, Masters candidate (degree completed December, 1994) Aeronautical and Astronautical Engineering, US citizen (1/4 assistance)

McDonald, Robert, Doctoral candidate, Aeronautical and Astronautical Engineering, US citizen (1/4 assistance)

1.5 Articles in Peer-reviewed Publications, Journals, Book Chapters and Editorships of Books

1. N. Sri Namachchivaya and S. Talwar, "Maximal Lyapunov and Rotation Numbers for Co-Dimension Two Stochastic Bifurcation", *Journal of Sound and Vibration*, Vol. 169(3), 1993, pp. 349-372.

2. N. Sri Namachchivaya, Monica M. Doyle, W. F. Langford and Nolan W. Evans, "Normal Form for Generalized Hopf Bifurcation with Non-Semisimple 1:1 Resonance", *Journal of Applied Mathematics and Physics (ZAMP)*, Vol. 45, 1994, pp. 312-335.

3. M. M. Doyle and N. Sri Namachchivaya, "Almost-Sure Asymptotic Stability of a General Four-Dimensional System Driven by Real Noise", *Journal of Statistical Physics*, Vol. 75(3/4), 1994, pp. 525-555.

4. Win-Min Tien, N. Sri Namachchivaya and Anil K. Bajaj, "Nonlinear Dynamics of a Shallow Arch with External and 1:2 Internal Resonances", *International Journal of Nonlinear Mechanics*, Vol. 29(3), 1994, pp. 349-366.

5. Win-Min Tien, N. Sri Namachchivaya and N. Malhotra, "Nonlinear Dynamics of a Shallow Arch with External and 1:1 Internal Resonances", *International Journal of Nonlinear Mechanics*, Vol. 29(3), 1994, pp. 367-386.

6. M. M. Doyle and N. Sri Namachchivaya, "Almost-Sure Asymptotic Stability of a General Four-Dimensional System Driven by Real Noise", *Journal of Statistical Physics*, Vol. 75(3/4), 1994, pp. 525-555.

7. O.M. O'Reilly, N. Malhotra and N. Sri Namachchivaya, "Reversible Dynamical Systems: Dissipation-Induced Destabilization and Follower Forces", *Applied Mathematics and Computation*, Vol. 70, 1995, pp.273-282.

8. N. Malhotra and N. Sri Namachchivaya, "Externally Excited Two Degree of Freedom Coupled Nonlinear Oscillators", *Nonlinear Dynamics* Vol. 8, 1995, pp.85-109.

9. N. Sri Namachchivaya, M. M. Doyle and N.K. Malhotra, "Some Aspects of Chaotic and Stochastic Dynamics for Structural Systems", *Sadhana-Journal of the Indian Academy of Sciences* Vol. 20, 1995, pp. 583-613.

1.6   Conference Publications

1. S. Talwar and N. Sri Namachchivaya, "Almost-Sure Stability of Structural Systems Under Combined Stochastic and Harmonic Excitation", *3nd International Symposium on Stochastic Structural Dynamics*, San Juan, Puerto Rico, January 1995.

2. M. Doyle, N. Sri Namachchivaya and H. J. Van Roessel, "Asymptotic Stability of Structural Systems Based on Lyapunov Exponents and Moment Lyapunov Exponents", *3nd International Symposium on Stochastic Structural Dynamics*, San Juan, Puerto Rico, January 1995.

3. N. Malhotra and N. Sri Namachchivaya, "Global Bifurcations in Periodically Excited Shallow Arch Structures", *Proceedings of the 10th Engineering Mechanics Conference*, Vol. 2, ed. Steve Sture, Boulder, CO, pp. 742-745, May 1995.

4. M. Doyle, N. Sri Namachchivaya and L. Arnold, "Small Noise Expansion of Moment Lyapunov Exponents for Two Dimensional Systems", *IUTAM Symposium on Advances in Nonlinear Stochastic Mechanics*, Trondheim, Norway, July 1995.

5. N. Malhotra and N. Sri Namachchivaya, "Nonlinear Dynamics of a Spinning Disc", 15th *ASME Biennial Conference on Mechanical Vibrations and Noise*, Boston, MA, September 1995.

1.7   Honors/Awards Received During Grant Lifetime

Honor/Award: Presidential Young Investigator
    Honor/Award Recipient: N. Sri Namachchivaya
    Awarding Organization: National Science Foundation
    Month/Year Received: May 1990

Honor/Award: Senior Xerox Award for Outstanding Faculty Research
    Honor/Award Recipient: N. Sri Namachchivaya

Awarding Organization: Xerox Corporation & University of Illinois
Month/Year Received: May 1993

Honor/Award: Visiting Scientist Fellowship
    Honor/Award Recipient: N. Sri Namachchivaya
    Awarding Organization: The Fields Institute for Research in
        Mathematical Sciences
    Month/Year Received: January - June 1993

Honor/Award: Keynote Lecture on Stochastic Dynamics
        University College London
    Honor/Award Recipient: N. Sri Namachchivaya
    Awarding Organization: IUTAM
    Month/Year Received: July 1993

1.8   Outline of the Report

In Chapter 2, conditions on the almost-sure stability of a general four-dimensional gyroscopic system subjected to parametric real noise excitation is examined. In the absence of noise, the system under consideration in Chapter 2 is critical and possesses two pairs of purely imaginary eigenvalues with non-commensurable frequencies. In this chapter, a perturbative technique is developed which involves solving a series of *forward* Kolmogorov equations to obtain higher and higher orders in the formal expansion for the invariant density. In this case, no restrictions on the structure of the stochastic terms are imposed and all possible singularities of the invariant density are examined. The results of the perturbative method developed in this chapter are applied to the prediction of lateral vibration instability in rotating shafts subject to stochastic axial loads and stationary shafts in cross flow with randomly varying flow velocity.

Throughout this research, the dynamics and stability of a rotating shaft, one of the most fundamental components of mechanical and power generating systems, will be the motivating problem. In Chapter 3, the partial differential equations of motion of the rotating shaft are derived. The dynamics and stability of this structure may be affected by a time-dependent force imparted by the action of nearby components. These inputs are included as time-dependent parameters in the equations of motion of the component under investigation and may lead to large amplitude vibrations or chaotic motion. The partial differential equations are reduced to ordinary differential equations via a Galerkin approximation assuming only the first mode to be excited. These equations are then checked using the Rayleigh-Ritz technique.

An investigation of the stability and local bifurcation behavior of the rotating shaft is carried out in Chapter 4. The method of averaging is applied to the Hamiltonian. This yields a set of autonomous differential equations governing the transverse motion of the shaft. The stability of the trivial (non-vibratory) solution is examined and the stability boundaries under various parametric resonance conditions are presented. These boundaries are given in terms of the amplitude and frequency of the parametric excitation. The post-critical nontrivial solution branches and their corresponding stability are also calculated.

In one of the parametric resonance cases of Chapter 4, the system at criticality (and in the absence of dissipation) possesses two coincident pairs of purely imaginary eigenvalues. The linear system is in non-semisimple 1:1 internal resonance and the trivial solution loses stability through a Hamiltonian Hopf bifurcation.

Chapter 5 describes The global dynamics of a shallow arch structure subjected to a spatially and temporally varying force is investigated under the conditions of principal *subharmonic resonance* and various conditions of *internal resonance* near single mode periodic motions. We describe two different mechanisms leading to chaotic behavior in the class of systems under consideration. The method of averaging is used to obtain the first order approximation of the system response for one-to-two internal resonance and a second order averaging procedure is used to study the system response under one-to-one resonance conditions. In the first part, a higher dimensional Melnikov type perturbation method is used to analytically show that the arch structure, in the absence of any dissipation mechanism, may exhibit chaotic dynamics in the sense of Smale horseshoe for one-to-two internal resonance case. These chaotic motions result from the existence of orbits *heteroclinic to a normally hyperbolic invariant torus* which corresponds to the hyperbolic periodic orbit in the averaged system. In this case, the presence of small dissipation causes the the phase flow to get attracted to the trivial solution. In the second part, the effect of dissipation is also included to study the global dynamics associated with one-to-one internal resonance case, where using a new perturbation technique (due to [48]) we show the existence of *Silnikov type homoclinic orbit* to a fixed point in the perturbed system, and consequently the chaotic behavior. The numerical simulations are also performed to confirm the theoretical predictions and hence the existence of complicated dynamics in the shallow arch system.

Chapter 6 describes the set-up of the rotating shaft experiment. Finally, in Chapter 7, the results and contributions of this work are summarized. Suggestions for future research in deterministic as well as stochastic dynamics are also included.

Chapter 2

ALMOST-SURE ASYMPTOTIC STABILITY OF SYSTEMS DRIVEN BY REAL NOISE

2.1 Introduction

One of the primary concerns in the analysis of dynamical systems is the determination of the stability of the steady state solutions. This analysis becomes more difficult when these systems are excited by a stochastic process. The stability of a linear stochastic system can be defined in several ways. The weakest, or least conservative, definition is that of stability in distribution. A more conservative estimate of the stability boundary is described by stability in probability. Thus, if a system is stable in probability, it is also stable in distribution. The last two definitions of stability in the stochastic sense are stability in the rth mean and almost-sure stability, or stability with probability one. If a dynamical system excited by noise is stable according to either of these definitions, it is stable in distribution and in probability, as well. However, r^{th} mean and almost-sure stability do not imply each other, i.e. a system can be almost surely stable while its 2nd moments grow exponentially. Kozin and Sugimoto [50], with extensions by Arnold [5], established a characterization between moment stability and almost-sure stability for linear Itô stochastic differential equations when the process is ergodic on the entire surface of the n-sphere. It was shown that the region of sample stability is the limit of the regions of rth moment stability for r approaching zero.

Stability in the almost-sure sense is determined by the sign of the maximal Lyapunov exponent. It was shown by Arnold and Kliemann [6] that, for a linear system with stochastic parametric excitation, the Lyapunov exponents are analogous to the real part of the eigenvalue of the corresponding deterministic system. Thus, the maximal Lyapunov exponent yields the almost-sure asymptotic stability of the linear system. One can also define the stochastic analog of the imaginary part of the eigenvalue; the rotation number determines the asymptotic rate of rotation for the stochastically perturbed system.

In this chapter, the maximal Lyapunov exponent and rotation number for a general four-dimensional linear system excited by noise are approximated. For the case when the noise is white, Khas'minskii [46] presented necessary and sufficient conditions under which the system is stable with probability one without explicit mention of the Lyapunov exponent. The studies by

9

Kozin and Prodromou [49] and Mitchell and Kozin [59] yielded results for second order systems and a complete examination by Nishioka [67] considered the effects of all possible singularities that may be present in a one-dimensional diffusion process.

In the case of ergodic but non-white noise excitation, few results are available. The existing results are due to Arnold et al. [7] and Pardoux and Wihstutz [70]. A survey paper of 1991 by Pinsky and Wihstutz [71] summarizes the previous work on this topic. A more recent investigation was performed by Sri Namachchivaya [79] in which the almost-sure stability of dynamical systems under the combined influence of stochastic and harmonic excitation was examined.

As in most of the studies involving multidegree-of-freedom systems reported to date, the analytical results in [79] were derived under the condition that only one mode is critical while the remaining modes are strongly stable. This, however, is not necessarily true in all physical systems. For this reason, it is imperative to determine the almost-sure asymptotic stability of multidegree-of-freedom dynamical systems with more than one critical mode. The maximal Lyapunov exponent and rotation number for stochastically perturbed codimension two bifurcations have been calculated via the method of averaging by Sri Namachchivaya and Talwar [82]. In [82], averaging was applied to obtain a set of approximate Itô equations for amplitudes and phases. However, in order to completely decouple the amplitude and phase equations, certain restrictive conditions on the manner in which the noise entered the equations were imposed.

The focus of this chapter is to approximate the maximal Lyapunov exponents for a four-dimensional system with two critical modes perturbed by a small intensity multiplicative real noise process. The approach adopted here is the perturbation method developed by Sri Namachchivaya and Van Roessel [83]. Using this approach, no restrictions on the structure of the stochastic terms in the equations of motion are necessary to decouple the amplitude and phase equations. Thus, the results presented here are for a general four-dimensional system parametrically perturbed by a real noise process. The frequencies are assumed to be non-commensurable in order to obtain a unique invariant measure. Furthermore, to make the problem tractable, the infinitesimal generator associated with the noise process is assumed to have an isolated simple zero eigenvalue.

Section 2.2 describes the formulation of the mathematical problem. General results for the probability density for all possible singular cases are presented in section 2.3 and the maximal Lyapunov exponent is evaluated in section 2.4 and the rotation number for each case in section 2.5. Section 2.7 summarizes the contributions of this research.

2.2 Statement of the Problem

The problem under investigation is a general two-degree-of-freedom mechanical system with two critical modes in the absence of damping. Physically, this represents a deterministic system at the point of a Hopf bifurcation. The addition of small dissipation shifts the eigenvalues of the deterministic system slightly into the left half plane. In the most realistic cases, all mechanical systems are acted on by noise. Depending on the mechanical parameters, the effects of this noise on a system near a deterministic bifurcation point may be catastrophic. The goal of this chapter is to determine the effects of small amplitude multiplicative noise on the almost-sure stability of a dynamical system near criticality. To this end, consider a linear stochastic system governed by the following equations of motion:

$$\dot{x} = Ax + \varepsilon f(\xi(t))Bx \,, \quad x \in \mathbf{R}^4 \tag{2.1}$$

10

Appropriate scaling of the matrix A yields

$$A = A_0 - \varepsilon^2 A_1$$

where

$$A_0 = \begin{bmatrix} 0 & \omega_1 & 0 & 0 \\ -\omega_1 & 0 & 0 & 0 \\ 0 & 0 & 0 & \omega_2 \\ 0 & 0 & -\omega_2 & 0 \end{bmatrix} \quad \text{and} \quad A_1 = \begin{bmatrix} \delta_1 & 0 & 0 & 0 \\ 0 & \delta_1 & 0 & 0 \\ 0 & 0 & \delta_2 & 0 \\ 0 & 0 & 0 & \delta_2 \end{bmatrix}$$

The matrix B is described by $B = [b_{ij}]$ and the quantities δ_1 and δ_2 are damping parameters. The matrix A_1 describes the versal deformation of the deterministic linear system. In this analysis, it is assumed that the frequencies ω_1 and ω_2 are non-commensurable. The term $\xi(t)$ is a small intensity real noise process defined on a smooth connected one-dimensional Riemannian manifold M (with or without boundary). The smooth function $f : M \to \mathbf{R}$ is assumed to have zero mean.

Before proceeding, a brief description of some of the results of Oseledec's Multiplicative Ergodic Theorem [68], as related to four-dimensional systems, is necessary. Consider the linear stochastic system in Eq. (2.1) under the assumption that $\xi(t)$ is ergodic. According to the Multiplicative Ergodic Theorem, the Lyapunov exponent of the solution of Eq. (2.1), $x(t; x_0)$, for the the initial condition x_0 $(x_0 \neq 0)$ is

$$\lambda(x_0) = \lim_{t \to \infty} \frac{1}{t} \log \| x(t; x_0) \| \tag{2.2}$$

where $\lambda(x_0)$ takes on one of r fixed or non-random values $\lambda_1 < \cdots < \lambda_r$. Which λ_i is realized depends on the initial condition x_0. The multiplicities of the Lyapunov exponents sum to the dimension of the system, n (in this case, $n = 4$). Associated with each λ_i there exists a random linear invariant subspace E_i, known as an Oseledec space, such that $E_1 \oplus E_2 \oplus \cdots \oplus E_r = \mathbf{R}^n$, with

$$\lim_{t \to \pm\infty} \frac{1}{t} \log \| x(t; x_0) \| = \lambda_i \text{ iff } x(t; x_0) \in E_i \setminus \{0\}$$

The dimension of each Oseledec space E_i is given by the multiplicity of the associated Lyapunov exponent, λ_i.

The effects of deterministic detuning and noise on the Lyapunov exponents of the system under consideration are depicted in Figure 2.1. In the absence of noise and detuning, all eigenvalues lie on the imaginary axis. The addition of negative detuning stabilizes the system. In this case, as shown, all Lyapunov exponents are negative. In the presence of both deterministic detuning and noise, generically one expects four distinct Lyapunov exponents. The maximum of these, λ_1, determines the almost-sure stability of the stochastic system.

The stability of the system described by Eq. (2.1) was studied by Sri Namachchivaya and Talwar [82] using the method of stochastic averaging to derive a set of approximate Itô equations for the amplitudes and phases. Using that method, it is necessary to impose certain restrictive conditions on the matrix B in order to completely decouple the amplitude and phase equations which was essential for the calculations. Employing the following notation

$$H_{ij}^{\pm} = b_{2i-1,2j} \pm b_{2i,2j-1} \quad \text{and} \quad J_{ij}^{\pm} = b_{2i,2j} \pm b_{2i-1,2j-1}$$

these restrictions are given as

$$H_{12}^- J_{21}^+ + H_{21}^- J_{12}^+ = 0 \quad \text{and} \quad H_{21}^+ J_{12}^- - H_{12}^+ J_{21}^- = 0 \tag{2.3}$$

11
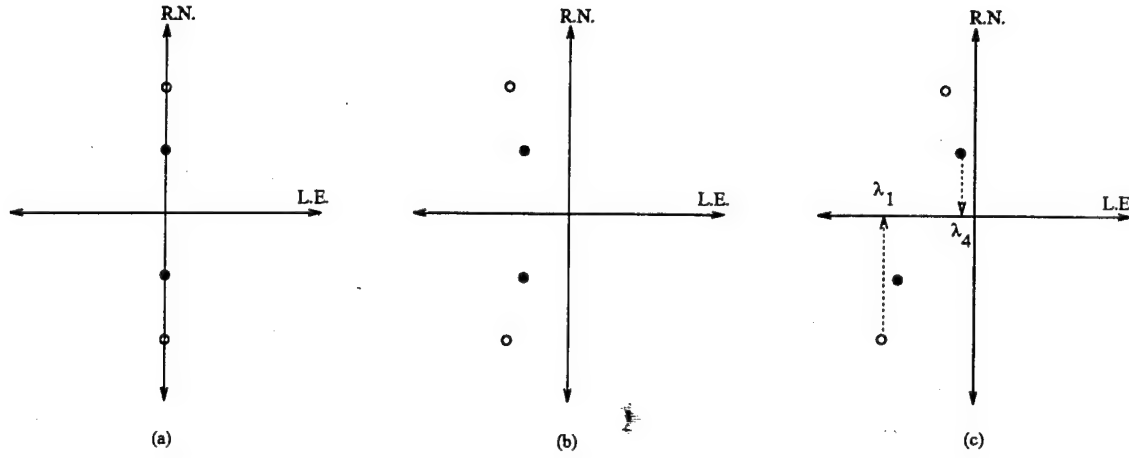
Figure 2.1: Effect of detuning and noise on system stability: (a) zero noise and detuning, (b) detuning only, (c) noise and detuning. (R.N.= Rotation number, L.E.= Lyapunov exponent)

and either

$$H_{11}^- = H_{22}^- = 0 \quad \text{or} \quad J_{11}^+ = J_{22}^+ = 0 \tag{2.4}$$

Examples of systems in which these conditions are satisfied include the double oscillator described by Sri Namachchivaya and Ariaratnam [80] and Ariaratnam and Xie [4] and problems with a symmetric B matrix. These conditions are also satisfied by the system considered by Sri Namachchivaya and Van Roessel [83]. In the present analysis, no restrictions on the structure of the B matrix are required to decouple the amplitude and phase equations. Thus, the results obtained here are for the most general case of Eq. (2.1). The analysis presented in this chapter is based heavily on the work completed by Sri Namachchivaya and Van Roessel in [83].

Let G denote the infinitesimal generator of $\xi(t)$ in Stratonovich form, i.e.

$$G(\xi) = \mu(\xi)\frac{\partial}{\partial \xi} + \frac{1}{2}\sigma^2(\xi)\frac{\partial^2}{\partial \xi^2}$$

The generator may be rewritten as

$$G(\xi) = X_0(\xi) + \frac{1}{2}\sum_{i=1}^{r} X_i^2(\xi)$$

This is known as the Hörmander form for the differential generator. As in [83], assume that G has an isolated simple zero eigenvalue. This implies that $u \equiv constant$ is the only solution of $Gu = 0$. Consequently, the adjoint operator G^* must also have an isolated simple zero eigenvalue. The results obtained from this analysis are applicable when the manifold M is of arbitrary dimension. For the case in which M is one-dimensional, the normalized invariant measure $v(\xi)\,d\xi$ satisfying the Fokker-Planck equation $G^*v(\xi) = 0$ can be written in terms of scale measure and speed density as

$$v(\xi) = m(\xi)\left[c_1 S(\xi) + c_2\right]$$

12

where

$$S(\xi) = \int^{\xi} s(\eta)d\eta \ , \quad m(\xi) = [\sigma^2(\xi)s(\xi)]^{-1}$$

$$s(\xi) = \exp\left\{-\int^{\xi} \frac{2\mu(\eta)}{\sigma^2(\eta)}d\eta\right\}$$

The constants c_1 and c_2 are determined using boundary and normality conditions, respectively.
The usual transformation, i.e.

$$x_{2i-1} = r_i \cos\phi_i \ , \quad x_{2i} = r_i \sin\phi_i \ \text{ and } \ \rho_i = \log(r_i) \ , \quad i = 1, 2$$

yields amplitude and phase equations of the form

$$\dot{\rho}_i = \varepsilon^2 \left[\tilde{p}_i(\phi)\right] + \varepsilon \left[p_i\left(e^{(\rho_j - \rho_i)}, \phi\right)\right] f\left(\xi(t)\right) \tag{2.5}$$

$$\dot{\phi}_i = \left[\omega_i + \varepsilon^2 \tilde{h}_i(\phi)\right] + \varepsilon \left[h_i\left(e^{(\rho_j - \rho_i)}, \phi\right)\right] f\left(\xi(t)\right) \tag{2.6}$$

In this form, the amplitude and phase equations are coupled by the presence of terms of the form $e^{(\rho_j - \rho_i)}$ for $i \neq j$. Since $e^{(\rho_j - \rho_i)}$ is always positive, one can introduce a one-to-one mapping $e^{(\rho_j - \rho_i)} = \tan\theta, \theta \in (0, \pi/2)$. Thus, applying the following transformations to the original system

$$x_1 = e^{\rho} \cos\phi_1 \cos\theta \ , \quad x_2 = -e^{\rho} \sin\phi_1 \cos\theta$$

$$x_3 = e^{\rho} \cos\phi_2 \sin\theta \ , \quad x_4 = -e^{\rho} \sin\phi_2 \sin\theta$$

yields the following set of equations for the amplitude ρ, phase variables (ϕ_1, ϕ_2, θ) and noise process ξ:

$$\dot{\rho} = \varepsilon f(\xi)q_1(\phi_1, \phi_2, \theta) + \varepsilon^2 \tilde{q}_1(\theta) \tag{2.7}$$

$$\dot{\phi}_i = \omega_i + \varepsilon f(\xi)h_i(\phi_1, \phi_2, \theta) + \varepsilon^2 \tilde{h}_i(\phi_1, \phi_2, \theta) \tag{2.8}$$

$$\dot{\theta} = \varepsilon f(\xi)q_2(\phi_1, \phi_2, \theta) + \varepsilon^2 \tilde{q}_2(\theta) \tag{2.9}$$

$$d\xi = \mu(\xi)dt + \sigma(\xi) \circ dW_t \tag{2.10}$$

The explicit expressions for q_i, $\tilde{q}_i$ and h_i, $(i = 1, 2)$ used in Eqs. (2.7)-(2.10) are

$$
\begin{aligned}
q_1(\phi_1, \phi_2, \theta) = & \ \frac{1}{2}(J_{11}^+ - J_{11}^- \cos 2\phi_1 - H_{11}^+ \sin 2\phi_1) \cos^2\theta \\
& + \frac{1}{2}(J_{22}^+ - J_{22}^- \cos 2\phi_2 - H_{22}^+ \sin 2\phi_2) \sin^2\theta \\
& + \frac{1}{2}\left[(J_{12}^+ + J_{21}^+) \cos(\phi_1 - \phi_2) - (J_{12}^- + J_{21}^-) \cos(\phi_1 + \phi_2) \right. \\
& \left. + (H_{12}^- - H_{21}^-) \sin(\phi_1 - \phi_2) - (H_{12}^+ + H_{21}^+) \sin(\phi_1 + \phi_2)\right] \cos\theta \sin\theta \\
\tilde{q}_1(\theta) = & \ -\delta_1 \cos^2\theta - \delta_2 \sin^2\theta \\
h_1(\phi_1, \phi_2, \theta) = & \ \frac{1}{2}(H_{11}^- - H_{11}^+ \cos 2\phi_1 + J_{11}^- \sin 2\phi_1) \\
& + \frac{1}{2}\left[H_{12}^- \cos(\phi_1 - \phi_2) - H_{12}^+ \cos(\phi_1 + \phi_2) \right. \\
& \left. - J_{12}^+ \sin(\phi_1 - \phi_2) + J_{12}^- \sin(\phi_1 + \phi_2)\right] \tan\theta
\end{aligned}
$$

13

$$h_2(\phi_1, \phi_2, \theta) = \frac{1}{2}(H_{22}^- - H_{22}^+ \cos 2\phi_2 + J_{22}^- \sin 2\phi_2)$$

$$+ \frac{1}{2}\left[H_{21}^- \cos(\phi_1 - \phi_2) - H_{21}^+ \cos(\phi_1 + \phi_2) \right.$$

$$\left. + J_{21}^+ \sin(\phi_1 - \phi_2) + J_{21}^- \sin(\phi_1 + \phi_2) \right] \cot \theta$$

$$q_2(\phi_1, \phi_2, \theta) = \frac{1}{2}\left[J_{22}^+ - J_{11}^+ + J_{11}^- \cos 2\phi_1 + H_{11}^+ \sin 2\phi_1 \right.$$

$$\left. - J_{22}^- \cos 2\phi_2 - H_{22}^+ \sin 2\phi_2 \right] \cos \theta \sin \theta$$

$$+ \frac{1}{2}\left[-J_{12}^+ \cos(\phi_1 - \phi_2) + J_{12}^- \cos(\phi_1 + \phi_2) \right.$$

$$\left. - H_{12}^- \sin(\phi_1 - \phi_2) + H_{12}^+ \sin(\phi_1 + \phi_2) \right] \cos^2 \theta$$

$$+ \frac{1}{2}\left[J_{21}^+ \cos(\phi_1 - \phi_2) - J_{21}^- \cos(\phi_1 + \phi_2) \right.$$

$$\left. - H_{21}^- \sin(\phi_1 - \phi_2) - H_{21}^+ \sin(\phi_1 + \phi_2) \right] \sin^2 \theta$$

$$\tilde{q}_2(\theta) = (\delta_1 - \delta_2) \sin \theta \cos \theta$$

Given the structure of the A_1 matrix, it can be shown that $\tilde{h}_i \equiv 0$ for $i = 1, 2$.

The processes $(\phi_1, \phi_2, \theta, \xi)$ are independent of the amplitude ρ and form a diffusive Markov process with associated generator

$$L^\varepsilon = L^0 + \varepsilon L^1 + \varepsilon^2 L^2$$

where, in general

$$L^0 = \sum_{i=1}^{2} \omega_i \frac{\partial}{\partial \phi_i} + G(\xi),$$

$$L^1 = f(\xi) \left[q_2 \frac{\partial}{\partial \theta} + \sum_{i=1}^{2} h_i \frac{\partial}{\partial \phi_i} \right],$$

$$L^2 = \tilde{q}_2 \frac{\partial}{\partial \theta} + \sum_{i=1}^{2} \tilde{h}_i \frac{\partial}{\partial \phi_i}$$

For this particular A_1 matrix, $L^2 = \tilde{q}_2 \frac{\partial}{\partial \theta}$. Next, define the function $Q^\varepsilon(\phi_1, \phi_2, \theta, \xi)$ to be the right hand side of Eq. (2.7) such that

$$Q^\varepsilon = Q^0 + \varepsilon Q^1 + \varepsilon^2 Q^2$$

In the present analysis, Q^ε can be written in terms of $f(\xi), q_1$ and $\tilde{q}_1$ as follows:

$$Q^\varepsilon(\phi_1, \phi_2, \theta, \xi) = \varepsilon f(\xi) q_1(\phi_1, \phi_2, \theta) + \varepsilon^2 \tilde{q}_1(\theta)$$

Then, according to Oseledec's multiplicative ergodic theorem [68], assuming the operator L^ε to be ergodic, the maximal Lyapunov exponent is given by

$$\lambda^\varepsilon = \langle Q^\varepsilon, p^\varepsilon \rangle = \int_0^{\pi/2} \int_M \int_0^{2\pi} \int_0^{2\pi} Q^\varepsilon p^\varepsilon \, d\phi_1 \, d\phi_2 \, d\xi \, d\theta$$

where p^ε is the unique ergodic invariant measure associated with the generator L^ε, i.e. p^ε solves the Fokker-Planck equation given by

$$L^{\varepsilon^*} p^\varepsilon = 0$$

provided the process ξ is strongly elliptic. The strong ellipticity condition guarantees that there exists a smooth and everywhere positive invariant measure p^ε on M. The condition for strong ellipticity is given by

$$dim LA(X_1, \cdots, X_r)(\xi) = dim M \quad \forall \xi \in M$$

where LA denotes the Lie algebra associated with the vector fields.

Construct a formal expansion of the invariant measure, i.e.

$$p^\varepsilon = p^0 + \varepsilon p^1 + \cdots + \varepsilon^N p^N + \cdots$$

Substituting this expansion and the expansion for L^ε into the Fokker-Planck equation yields the following sequence of Poisson equations to be solved for $p^0, p^1, p^2, \ldots$:

$$
\begin{aligned}
L^{0^*} p^0 &= 0 \\
L^{0^*} p^1 &= -L^{1^*} p^0 \\
L^{0^*} p^2 &= -L^{1^*} p^1 - L^{2^*} p^0
\end{aligned}
\tag{2.11}
$$

This yields the following expression for the maximal Lyapunov exponent:

$$
\begin{aligned}
\lambda^\varepsilon &= \langle Q^0, p^0 \rangle + \varepsilon \left[\langle Q^1, p^0 \rangle + \langle Q^0, p^1 \rangle \right] + \\
&\quad \varepsilon^2 \left[\langle Q^2, p^0 \rangle + \langle Q^1, p^1 \rangle + \langle Q^0, p^2 \rangle \right] + \cdots
\end{aligned}
$$

A proof that this expansion is, in fact, asymptotic begins with the construction of the adjoint problem $L^\varepsilon F^\varepsilon = Q^\varepsilon$ with $F^\varepsilon = F^0 + \varepsilon F^1 + \cdots + \varepsilon^N F^N$ as in [7]. In this expression, $F^0, F^1, \cdots, F^N$ are such that

$$\left(L^0 + \varepsilon L^1 + \varepsilon^2 L^2 \right) \left(F^0 + \varepsilon F^1 + \cdots + \varepsilon^N F^N \right)$$
$$= Q^\varepsilon - \left(q^0 + \varepsilon q^1 + \cdots + \varepsilon^N q^N \right) + \varepsilon^{N+1} \left\{ L^1 F^N + L^2 F^{N-1} \right\} + \varepsilon^{N+2} \left\{ L^2 F^N \right\}$$

The functions $q^0, q^1, \cdots, q^N$ are independent of θ, ϕ_1 and ϕ_2 and satisfy the equations

$$
\begin{aligned}
L^0 F^0 &= Q^0 - q^0 \\
L^0 F^1 &= Q^1 - q^1 - L^1 F^0 \\
L^0 F^2 &= Q^2 - q^2 - L^1 F^1 - L^2 F^0 \\
&\;\;\vdots \\
L^0 F^N &= -q^N - L^1 F^{N-1} - L^2 F^{N-2}
\end{aligned}
$$

Next, define the truncated density $\tilde{p}^\varepsilon = p^0 + \varepsilon p^1 + \cdots + \varepsilon^N p^N$ and assume $v(\xi)$ is the marginal of both p^ε and $\tilde{p}^\varepsilon$ on M. Employing Eqs. (2.11), the error introduced by truncating λ^ε at an arbitrary order $N \geq 0$ is given by

$$
\begin{aligned}
\langle Q^\varepsilon, p^\varepsilon \rangle - \langle Q^\varepsilon, \tilde{p}^\varepsilon \rangle &= \\
- \;\; & \varepsilon^{N+1} \Big[\langle L^1 F^N + L^2 F^{N-1}, p^\varepsilon - \tilde{p}^\varepsilon \rangle + \langle L^{1^*} p^N + L^{2^*} p^{N-1}, F^\varepsilon \rangle \\
& \quad - \langle Q^1, p^N \rangle - \langle Q^2, p^{N-1} \rangle \Big] \\
- \;\; & \varepsilon^{N+2} \Big[\langle L^2 F^N, p^\varepsilon - \tilde{p}^\varepsilon \rangle + \langle L^{2^*} p^N, F^\varepsilon \rangle - \langle Q^2, p^N \rangle \Big]
\end{aligned}
$$

Suppose that the functions $p^0, p^1, \cdots, p^N$ and $F^0, F^1, \cdots, F^N$ are such that all inner products above are well defined. Since p^ε is unknown, one can assume that $p^0, p^1, \cdots, p^N$ are constructed such that

$$\sup_{\phi,\theta,\xi} \left| L^1 F^N + L^2 F^{N-1} \right| \le K_1 < \infty \quad \text{and} \quad \sup_{\phi,\theta,\xi} \left| L^2 F^N \right| \le K_2 < \infty$$

Applying the above estimate, it is clear that the expansion for a fixed $N \ge 0$ is a valid asymptotic expansion. These results are summarized in the following theorem.

Theorem 1 *Assume the operator L^ε to be hypoelliptic and p^ε to be the unique ergodic invariant measure associated with the generator L^ε, i.e. p^ε solves the Fokker-Planck equation given by*

$$L^{\varepsilon^*} p^\varepsilon = 0$$

Then, by constructing a formal expansion for p^ε and the function F^ε such that the adjoint problem becomes $L^\varepsilon F^\varepsilon = Q^\varepsilon$, the expansion for the maximal Lyapunov exponent can be written as

$$\lambda^\varepsilon = \langle Q^\varepsilon, p^\varepsilon \rangle \;=\; \langle Q^0, p^0 \rangle + \varepsilon \left[\langle Q^1, p^0 \rangle + \langle Q^0, p^1 \rangle \right] +$$
$$\varepsilon^2 \left[\langle Q^2, p^0 \rangle + \langle Q^1, p^1 \rangle + \langle Q^0, p^2 \rangle \right] + \cdots$$

Moreover, this expansion is asymptotic provided

$$\sup_{\phi,\theta,\xi} \left| L^1 F^N + L^2 F^{N-1} \right| \le K_1 < \infty \quad \text{and} \quad \sup_{\phi,\theta,\xi} \left| L^2 F^N \right| \le K_2 < \infty$$

Since $Q^0 = 0$, the expression for the maximal Lyapunov exponent reduces to

$$\lambda^\varepsilon = \varepsilon \langle Q^1, p^0 \rangle + \varepsilon^2 \left[\langle Q^2, p^0 \rangle + \langle Q^1, p^1 \rangle \right] + \cdots$$

where p^0 and p^1 satisfy the Poisson equations above with the periodic boundary conditions

$$p^0(\phi_1, \phi_2, \theta, \xi) = p^0(\phi_1 + 2\pi, \phi_2, \theta, \xi) = p^0(\phi_1, \phi_2 + 2\pi, \theta, \xi)$$

$$p^1(\phi_1, \phi_2, \theta, \xi) = p^1(\phi_1 + 2\pi, \phi_2, \theta, \xi) = p^1(\phi_1, \phi_2 + 2\pi, \theta, \xi)$$

Solving the $O(1)$ Poisson equation with appropriate boundary conditions and considering the non-commensurability condition on the natural frequencies yields

$$p^0(\xi, \theta) = \frac{v(\xi) F(\theta)}{4\pi^2}$$

where $v(\xi)$ is the invariant measure satisfying $G^* v = 0$. Note that for arbitrary $F(\theta)$, the inner product $\langle Q^1, p^0 \rangle = 0$ due to the periodic boundary conditions on ϕ_1 and ϕ_2 *and* the zero mean assumption on $f(\xi)$. The maximal Lyapunov exponent, up to $O(\varepsilon^2)$, reduces to

$$\lambda^\varepsilon = \varepsilon^2 \left[\langle Q^2, p^0 \rangle + \langle Q^1, p^1 \rangle \right] \tag{2.12}$$

The $O(\varepsilon)$ Poisson equation and its adjoint are

$$L^{0^*} p^1 = -L^{1^*} p^0 \quad \text{and} \quad L^0 u = 0$$

16

and the associated solvability condition is

$$\langle L^{1^*}p^0, u \rangle = 0 \quad \forall u \in ker(L^0) \tag{2.13}$$

Due to the assumption on G and the boundary conditions on ϕ_1 and ϕ_2,

$$ker(L^0) = \{C(\theta) : C \text{ is an arbitrary function of } \theta\}$$

The solvability condition of Eq. (2.13) reduces to

$$\int_0^{\pi/2} \tilde{F}(\theta)C(\theta)\,d\theta = 0$$

where

$$\tilde{F}(\theta) = \int_M f(\xi)v(\xi) \int_0^{2\pi} \int_0^{2\pi} \left[\frac{\partial}{\partial \theta}(q_2 F) + F \sum_{i=1}^2 \frac{\partial h_i}{\partial \phi_i} \right] d\phi_1 d\phi_2 d\xi$$

which must hold for arbitrary $C(\theta)$. This implies

$$\tilde{F}(\theta) = 0$$

This condition is automatically satisfied due to the periodicity of ϕ_1 and ϕ_2. Thus, it is not possible to determine $F(\theta)$ using the $O(\varepsilon)$ solvability condition. One can, however, find an expression for p^1 in terms of $F(\theta)$. To do so, rewrite the $O(\varepsilon)$ Poisson equation as

$$\left(G^* - \omega_i \sum_{i=1}^2 \frac{\partial}{\partial \phi_i} \right) p^1 = -\frac{f(\xi)v(\xi)}{4\pi^2} R(\phi_1, \phi_2, \theta) \tag{2.14}$$

where

$$
\begin{aligned}
R(\phi_1, \phi_2, \theta) = \\
&- \frac{1}{2}\left(J_{22}^+ - J_{11}^+ \right) \left[(c_\theta^2 - s_\theta^2)F + \frac{1}{2}s_{2\theta}\frac{\partial F}{\partial \theta} \right] \\
&- \left[\left(1 + \frac{1}{2}c_{2\theta} \right) F + \frac{1}{4}s_{2\theta}\frac{\partial F}{\partial \theta} \right] \left(J_{11}^- c_{2\phi_1} + H_{11}^+ s_{2\phi_1} \right) \\
&- \left[\left(1 - \frac{1}{2}c_{2\theta} \right) F - \frac{1}{4}s_{2\theta}\frac{\partial F}{\partial \theta} \right] \left(J_{22}^- c_{2\phi_2} + H_{22}^+ s_{2\phi_2} \right) \\
&+ \frac{1}{2}\left[(2c_\theta s_\theta + t_\theta) F + s_\theta^2\frac{\partial F}{\partial \theta} \right] \left(J_{12}^+ C^- - J_{12}^- C^+ + H_{12}^- S^- - H_{12}^+ S^+ \right) \\
&+ \frac{1}{2}\left[\left(2c_\theta s_\theta + \frac{1}{t_\theta} \right) F - c_\theta^2\frac{\partial F}{\partial \theta} \right] \left(J_{21}^+ C^- - J_{21}^- C^+ - H_{21}^- S^- - H_{21}^+ S^+ \right)
\end{aligned}
$$

In the above expression, $c_{(\cdot)} = \cos(\cdot)$, $s_{(\cdot)} = \sin(\cdot)$, $t_{(\cdot)} = \tan(\cdot)$, $C^\pm = \cos(\omega_1 \pm \omega_2)$ and $S^\pm = \sin(\omega_1 \pm \omega_2)$.

Introduce an auxiliary time t such that Eq. (2.14) becomes

$$\left(\frac{\partial}{\partial t} - G^* + \omega_i \sum_{i=1}^2 \frac{\partial}{\partial \phi_i} \right) p_t^1 = \frac{f(\xi)v(\xi)}{4\pi^2} R(\phi_1, \phi_2, \theta) \tag{2.15}$$

17

The density p^1 is the stationary solution of Eq. (2.15) and solves Eq. (2.14), i.e.

$$p^1(\phi_1, \phi_2, \theta, \xi) = \lim_{t \to \infty} \left[p_t^1(\phi_1, \phi_2, \theta, \xi, t) \right]$$

Employing the transformation

$$\tau = \frac{1}{2} \left[t + \frac{1}{2} \left(\frac{\phi_1}{\omega_1} + \frac{\phi_2}{\omega_2} \right) \right] , \quad s = \frac{1}{2} \left[t - \frac{1}{2} \left(\frac{\phi_1}{\omega_1} + \frac{\phi_2}{\omega_2} \right) \right]$$

and $\Upsilon = \omega_1 \phi_2 - \omega_2 \phi_1$ in Eq. (2.15) yields

$$\left(\frac{\partial}{\partial \tau} - G^* \right) p_t^1 = \frac{H(\xi)}{4\pi^2} R\left(\phi_1(\tau, s, \Upsilon), \phi_2(\tau, s, \Upsilon), \theta \right) \tag{2.16}$$

where $H(\xi) = f(\xi)v(\xi)$. Equation (2.16) is an inhomogeneous boundary value problem. This problem can be transformed into a homogeneous initial value problem using Duhamel's principle with zero initial conditions (see, for example, [92]). The solution to Eq. (2.16) can then be written as

$$p_t^1(\tau, s, \Upsilon, \xi) = \frac{1}{4\pi^2} \int_0^\tau R\left(\phi_1(\tau - T, s, \Upsilon), \phi_2(\tau - T, s, \Upsilon), \theta \right) K(\xi, T) \, dT$$

where $g(\xi, T; \eta, 0)$ is the transient density which solves

$$\frac{\partial g}{\partial t} = G^* g , \quad g(\xi, 0; \eta, 0) = \delta(\xi - \eta)$$

and

$$K(\xi, T) = \int_M H(\eta) g(\xi, T; \eta, 0) \, d\eta$$

The final form of $p^1(\phi_1, \phi_2, \theta, \xi)$ is found by taking the limit as $\tau \to \infty$:

$$p^1(\phi_1, \phi_2, \theta, \xi) = \frac{1}{4\pi^2} \int_0^\infty R(\omega_1 T - \phi_1, \omega_2 T - \phi_2, \theta, T) \, K(\xi, T) \, dT \tag{2.17}$$

In Eq. (2.17), $R(\omega_1 T - \phi_1, \omega_2 T - \phi_2, \theta, T)$ contains $F(\theta)$ and its derivatives which have yet to be determined. This can be accomplished with the aid of the $O(\varepsilon^2)$ solvability condition. Recall the $O(\varepsilon^2)$ Poisson equation

$$\left(G^* - \omega_i \sum_{i=1}^2 \frac{\partial}{\partial \phi_i} \right) p^2 = \chi_0(\phi_1, \phi_2, \theta, \xi) + \chi_1(\phi_1, \phi_2, \theta, \xi) \tag{2.18}$$

where

$$\chi_0 = \frac{\partial}{\partial \theta} \left(\tilde{q}_2 p^0 \right) \quad \text{and} \quad \chi_1 = f(\xi) \left[\frac{\partial}{\partial \theta} \left(q_2 p^1 \right) + \sum_{i=1}^2 \frac{\partial}{\partial \phi_i} \left(h_i p^1 \right) \right]$$

This yields

$$L^{0^*} p^2 = \chi_0 + \chi_1$$

and the corresponding solvability condition

$$\langle \chi_0 + \chi_1, v(\xi) C(\theta) \rangle = 0 \quad \forall \, C(\theta) \in ker(L^0)$$

18

Evaluating the solvability condition for arbitrary $C(\theta)$ yields the following ordinary differential equation for $F(\theta)$:

$$-\frac{d}{d\theta}\left[\Phi(\theta)F(\theta)\right] + \frac{1}{2}\frac{d^2}{d\theta^2}\left[\Psi^2(\theta)F(\theta)\right] = 0 \qquad (2.19)$$

where

$$\Psi^2(\theta) = A\,\cos^2 2\theta + B\cos 2\theta + C$$

$$\Phi(\theta) = -\frac{1}{2}(\tilde{\lambda}_1 - \tilde{\lambda}_2)\sin 2\theta + \Psi^2(\theta)\cot 2\theta$$

This is indeed the diffusion equation in θ. This describes the stochastic coupling between ρ_1 and ρ_2 in Eq. (2.5).

Throughout the remainder of this chapter, the following notation will be used:

$$\alpha_{ij} = \frac{1}{8}\left[(H_{ij}^{-2} + J_{ij}^{+2})S(\Omega^-) + (H_{ij}^{+2} + J_{ij}^{-2})S(\Omega^+)\right]$$

$$\beta_i = \frac{1}{8}(H_{ii}^{+2} + J_{ii}^{-2})S(2\omega_i)$$

$$\mu = \frac{1}{8}\left[(H_{12}^+H_{21}^+ + J_{12}^-J_{21}^-)S(\Omega^+) - (H_{12}^-H_{21}^- - J_{12}^+J_{21}^+)S(\Omega^-)\right]$$

$$\gamma_1 = \frac{1}{4}(H_{21}^-J_{12}^+ + H_{12}^-J_{21}^+)\Gamma(\Omega^-)$$

$$\gamma_2 = \frac{1}{4}(H_{21}^+J_{12}^- - H_{12}^+J_{21}^-)\Gamma(\Omega^+)$$

$$\gamma = \frac{1}{16}(J_{11}^+ - J_{22}^+)^2 S(0) + \frac{1}{4}(\beta_1 + \beta_2) - \frac{1}{4}(\alpha_{12} + \alpha_{21}) - \frac{1}{2}\mu$$

The sine and cosine spectrums are defined, respectively, as

$$\Gamma(\omega) = 2\int_0^\infty R(T)\sin\omega T\,dT \quad \text{and} \quad S(\omega) = 2\int_0^\infty R(T)\cos\omega T\,dT$$

where $R(T)$ is the autocorrelation of $f(\xi)$, i.e.

$$R(T) = \int_M f(\xi)K(\xi, T)\,d\xi$$

and $\Omega^\pm = \omega_1 \pm \omega_2$. Employing this notation, one can write

$$A = -\gamma$$

$$B = -\frac{1}{2}(\alpha_{12} - \alpha_{21}) = -\frac{1}{2}\alpha^-$$

$$C = \gamma + \frac{1}{2}(\alpha_{12} + \alpha_{21}) = \gamma + \frac{1}{2}\alpha^+$$

$$\lambda_i = -\delta_i + \beta_i \quad \text{and} \quad \tilde{\lambda}_i = \lambda_i + \gamma_i$$

where λ_1 and λ_2 are the Lyapunov exponents for the case when the modes in Eq. (2.1) are decoupled.

Equation (2.19) can be rewritten as

$$\frac{d}{d\theta}\left\{-\Phi(\theta)F(\theta) + \frac{1}{2}\frac{d}{d\theta}\left[\Psi^2(\theta)F(\theta)\right]\right\} = 0 \qquad (2.20)$$

19

Let $A_{st}(\theta)$ be the term in the brackets. Then, $A_{st}(\theta)$ must be constant with respect to θ, i.e. $A_{st}(\theta) = A_{st}$. By examining Eq. (2.20), one can see that there may be singularities in the open interval $(0, \pi/2)$. All possible singular cases must be considered when attempting to solve this expression for $F(\theta)$. The location of the singular points and the behavior of the diffusion process in the presence of these singularities will be examined in the next section.

2.3 Evaluation of Solutions

The solution to the Fokker-Planck equation can be written as

$$F(\theta) = m(\theta)[2\,A_{st}\,S(\theta) + c] \tag{2.21}$$

where the scale and speed measures are defined in terms of Φ and Ψ as

$$m(\theta) = [\Psi^2(\theta)\,s(\theta)]^{-1}$$

$$s(\theta) = \exp\left\{ -\int^\theta \frac{2\,\Phi(\eta)}{\Psi^2(\eta)}d\eta \right\} \quad \text{and} \quad S(\theta) = \int^\theta s(\eta)\,d\eta$$

and $F(\theta)$ satisfies boundary and normality conditions. The boundary conditions for $F(\theta)$, as well as the evolution of the process when singularities exist, will be discussed in this section. One can rewrite $s(\theta)$ as

$$s(\theta) = e^{b(\theta)}$$

where

$$b(\theta) = \int^\theta \frac{2\,\Phi(\eta)}{\Psi^2(\eta)}d\eta = \ln|\sin 2\theta| + (\tilde{\lambda}_2 - \tilde{\lambda}_1)\beta(\theta)$$

In terms of the parameters A, B and C,

$$\beta(\theta) = -\frac{1}{2}\int^{\cos 2\theta} \frac{dt}{At^2 + Bt + C}$$

The last integral can be broken down into the following 6 cases:

1. $A, B, C \neq 0$
2. $B = 0$ and (i) $A, C \neq 0$, (ii) $A = 0, C \neq 0$, (iii) $A \neq 0, C = 0$
3. $C = 0$ and $A, B \neq 0$
4. $A = 0$ and $B, C \neq 0$
5. $A = C = 0$ and $B \neq 0$
6. $A = B = C = 0$

Singularities in the $F(\theta)$ process are θ values satisfying either

$$\Psi^2(\theta) = 0 \quad \text{or} \quad \Phi(\theta) = \infty$$

These singularities can be classified according to Feller's scheme as entrance, exit, natural or regular boundaries of a region of state space [25]. The following definitions, summarized by Karlin and

Taylor in [45], are needed in order to classify the behavior of a stochastic process at a singular point θ_s and to determine the type of boundary present:

$$S(\theta_s, \theta] = \int_{\theta_s}^{\theta} s(\eta) \, d\eta \,, \quad M(\theta_s, \theta] = \int_{\theta_s}^{\theta} m(\eta) \, d\eta$$

$$\Sigma(\theta_s) = \int_{\theta_s}^{\theta} S(\theta_s, \xi] dM(\xi) = \int_{\theta_s}^{\theta} \left\{ \int_{\eta}^{\theta} m(y) \, dy \right\} s(\eta) \, d\eta$$

$$N(\theta_s) = \int_{\theta_s}^{\theta} M(\theta_s, \xi] dS(\xi) = \int_{\theta_s}^{\theta} \left\{ \int_{\eta}^{\theta} s(y) \, dy \right\} m(\eta) \, d\eta$$

In the above definitions, $S(\theta_s, \theta]$ and $M(\theta_s, \theta]$ are the scale and speed measures, respectively. The explicit dependence on θ_s is dropped. In this case, the notation $S(\theta)$ and $M(\theta)$ is used. The last two quantities defined above measure the time it takes to reach the boundary of the state space starting from the interior ($\Sigma(\theta_s)$) and the time required to reach the interior beginning at the boundary ($N(\theta_s)$). In the above definitions, θ_s is a left boundary. Analogous definitions are employed when θ_s is a right boundary.

An *entrance boundary* cannot be reached from the interior of the state space but it is possible for the process to begin at such a point. The singular point is an entrance boundary if and only if

$$S(\theta_s, \theta] = \infty \quad \text{and} \quad N(\theta_s) < \infty$$

Once the process reaches an *exit boundary*, it is impossible to re-enter the interior. The necessary and sufficient conditions for a singular point to be an exit are

$$M(\theta_s, \theta] < \infty \quad \text{and} \quad \Sigma(\theta_s) < \infty$$

An exit boundary within the state space implies that the process eventually exits a portion of the space and enters another region. The direction in which this boundary is traversed depends upon the sign of the drift term $\Phi(\theta)$ as follows:

$$\Phi(\theta) = \begin{cases} < 0 & \text{left (backward) shunt} \\ > 0 & \text{right (forward) shunt} \\ = 0 & \text{trap} \end{cases}$$

A diffusion process can neither reach in finite mean time nor be started from a *natural (Feller) boundary*. A singular point is a natural boundary if and only if

$$N(\theta_s) = \infty \quad \text{and} \quad \Sigma(\theta_s) = \infty$$

Finally, a *regular boundary* allows the diffusion process to both enter and leave. The criteria for a regular boundary are

$$S(\theta_s, \theta] < \infty \quad \text{and} \quad M(\theta_s, \theta] < \infty$$

21
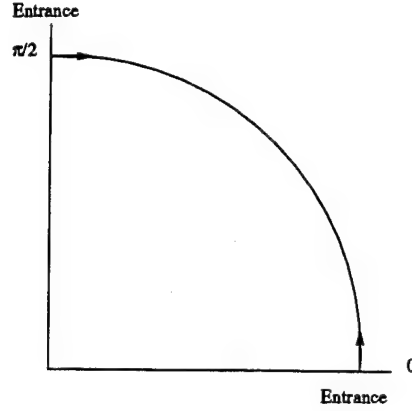
Figure 2.2: Boundary behavior for singular cases 1, 2i $(AC > 0)$, 2ii and 4.

In this investigation, all possible singular cases will be examined. The function $F(\theta)$ will be computed and the behavior of the process at the singular points will be determined.

Employing the above criteria, it can be shown that for all 6 cases, the boundary points $\theta = 0, \pi/2$ are entrance boundaries. Since $S(0) = -\infty$ and $S(\pi/2) = \infty$, in order for $F(\theta)$ to remain positive throughout the interval, it must be that $A_{st} = 0$ in Eq. (2.21), i.e. the zero-flux property. This leaves

$$F(\theta) = c\, m(\theta) \tag{2.22}$$

where c is the normalizing parameter. The expressions for $m(\theta)$ and the normalizing constant c for each case are given below.

Case 1: $A,\ B,\ C \neq 0$

$$\Psi^2(\theta) = -\gamma \cos^2 2\theta - \frac{1}{2}(\alpha_{12} - \alpha_{21})\cos 2\theta + \gamma + \frac{1}{2}(\alpha_{12} + \alpha_{21})$$

The only singularities for this case are the entrance boundaries $\theta = 0$ and $\theta = \pi/2$ as shown in Figure 2.2. Define the discriminant $\Delta = 4AC - B^2$ and consider the cases: $\Delta > 0$, $\Delta = 0$ and $\Delta < 0$.

For $\Delta > 0$:

$$m(\theta) = \frac{\sin 2\theta}{\Psi^2(\theta)} \exp\left\{ \frac{-(\tilde{\lambda}_2 - \tilde{\lambda}_1)}{\sqrt{\Delta}} \tan^{-1}\left(\frac{2A\cos 2\theta + B}{\sqrt{\Delta}} \right) \right\}$$

and

$$M(\theta) = \frac{1}{\tilde{\lambda}_2 - \tilde{\lambda}_1} \exp\left\{ \frac{-(\tilde{\lambda}_2 - \tilde{\lambda}_1)}{\sqrt{\Delta}} \tan^{-1}\left(\frac{2A\cos 2\theta + B}{\sqrt{\Delta}} \right) \right\}$$

For $\Delta = 0$:

$$m(\theta) = \frac{\sin 2\theta}{\Psi^2(\theta)} \exp\left\{ \frac{(\tilde{\lambda}_2 - \tilde{\lambda}_1)}{2A\cos 2\theta + B} \right\}$$

22

and

$$M(\theta) = \frac{1}{\tilde{\lambda}_2 - \tilde{\lambda}_1} \exp\left\{\frac{(\tilde{\lambda}_2 - \tilde{\lambda}_1)}{2A\cos 2\theta + B}\right\}$$

For $\Delta < 0$:

$$m(\theta) = \frac{\sin 2\theta}{\Psi^2(\theta)} \exp\left\{\frac{(\tilde{\lambda}_2 - \tilde{\lambda}_1)}{\sqrt{-\Delta}} \tanh^{-1}\left(\frac{2A\cos 2\theta + B}{\sqrt{-\Delta}}\right)\right\}$$

and

$$M(\theta) = \frac{1}{\tilde{\lambda}_2 - \tilde{\lambda}_1} \exp\left\{\frac{(\tilde{\lambda}_2 - \tilde{\lambda}_1)}{\sqrt{-\Delta}} \tanh^{-1}\left(\frac{2A\cos 2\theta + B}{\sqrt{-\Delta}}\right)\right\}$$

In all of the above cases for Δ, the normalizing constant c is

$$c = [M(\pi/2) - M(0)]^{-1}$$

where the appropriate $M(\theta)$ must be used.

Case 2i: $B = 0$ and $A, C \neq 0$

$$\Psi^2(\theta) = -\gamma \cos^2 2\theta + \gamma + \alpha$$

$B = 0$ implies $\alpha_{12} = \alpha_{21} = \alpha$. As in Case 1, the singularities at $\theta = 0, \pi/2$ are entrance boundaries. There is, however, an additional singularity in this case at

$$\theta = \theta_s = \frac{1}{2}\cos^{-1}\sqrt{\frac{-C}{A}}$$

which is valid only when $AC < 0$. The function $m(\theta)$ is given by

$$m(\theta) = \begin{cases} \frac{\sin 2\theta}{\Psi^2(\theta)} \exp\left\{\frac{-(\tilde{\lambda}_2 - \tilde{\lambda}_1)}{2\sqrt{AC}} \tan^{-1}\left(\frac{\sqrt{AC}}{C}\cos 2\theta\right)\right\} & AC > 0 \\[2em] \frac{\sin 2\theta}{\Psi^2(\theta)} \exp\left\{\frac{(\tilde{\lambda}_2 - \tilde{\lambda}_1)}{2\sqrt{-AC}} \tanh^{-1}\left(\frac{\sqrt{-AC}}{C}\cos 2\theta\right)\right\} & AC < 0 \end{cases}$$

In order to determine the normalizing constant c, it is necessary to consider the two cases $AC > 0$ and $AC < 0$ separately. For $AC > 0$, since no singularity exists in the open interval $(0, \pi/2)$, c is simply

$$c = \frac{1}{2}(\tilde{\lambda}_2 - \tilde{\lambda}_1)\text{csch}\left\{\frac{(\tilde{\lambda}_2 - \tilde{\lambda}_1)}{2\sqrt{AC}} \tan^{-1}\left(\frac{\sqrt{AC}}{C}\right)\right\}$$

When $AC < 0$, it can be shown that the point $\theta = \theta_s$ is a left or right shunt, depending on the sign of $\Phi(\theta_s)$ where

$$\Phi(\theta_s) = \frac{1}{2}(\tilde{\lambda}_2 - \tilde{\lambda}_1)\sqrt{1 + \frac{C}{A}}$$
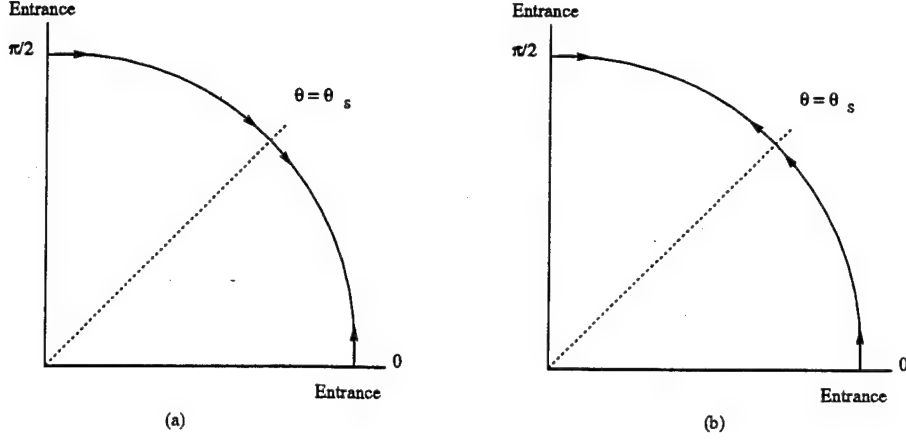
Figure 2.3: Boundary behavior for singular case 2i $(AC < 0)$ and case 2iii: (a) $\tilde{\lambda}_1 > \tilde{\lambda}_2$, (b) $\tilde{\lambda}_1 < \tilde{\lambda}_2$.

For $\tilde{\lambda}_1 > \tilde{\lambda}_2$:

$$F(\theta) = \begin{cases} c\, m(\theta) & \theta \in (0, \theta_s) \\ \\ 0 & \theta \in (\theta_s, \pi/2) \end{cases}$$

In this case, the point $\theta = \theta_s$ is a left shunt. A process starting from a point in the region $\theta \in (\theta_s, \pi/2)$ will eventually leave this region and be shunted over to the portion of state space bounded by $\theta \in (0, \theta_s)$. This leads to a build up of probability in the region $\theta \in (0, \theta_s)$.

For $\tilde{\lambda}_1 < \tilde{\lambda}_2$:

$$F(\theta) = \begin{cases} 0 & \theta \in (0, \theta_s) \\ \\ c\, m(\theta) & \theta \in (\theta_s, \pi/2) \end{cases}$$

Here, $\theta = \theta_s$ is a right shunt. A process starting from a point in the region $\theta \in (0, \theta_s)$ will eventually be shunted over to the region bounded by $\theta \in (\theta_s, \pi/2)$ and the probability accumulates in this region. In both cases,

$$c = \left|\tilde{\lambda}_2 - \tilde{\lambda}_1\right| \exp\left[\frac{\left|\tilde{\lambda}_2 - \tilde{\lambda}_1\right|}{2A}\right]$$

The singular behavior for this case is summarized in Figure 2.3.

Case 2ii: $B = 0$ and $A = 0$, $C \neq 0$

$$\Psi^2(\theta) = \alpha$$

As in Case 1, the only singularities are at $\theta = 0, \pi/2$ (see Figure 2.2) and $m(\theta)$ and c are given by:

$$m(\theta) = \frac{\sin 2\theta}{\alpha} \exp\left\{\frac{-(\tilde{\lambda}_2 - \tilde{\lambda}_1)}{2\alpha} \cos 2\theta\right\}$$

24

and

$$c = \frac{\tilde{\lambda}_2 - \tilde{\lambda}_1}{2} \operatorname{csch} \left[\frac{\tilde{\lambda}_2 - \tilde{\lambda}_1}{2\alpha} \right]$$

Case 2iii: $B = 0$ and $A \neq 0$, $C = 0$

$$\Psi^2(\theta) = \alpha \cos^2 2\theta$$

In addition to the singularities at the boundaries $\theta = 0, \pi/2$, there is also a singular point at $\theta = \pi/4$. As in Case 2i, the sign of $\Phi(\theta_s)$ determines the behavior of the process at this point. In this case

$$\Phi(\theta_s) = \frac{1}{2}(\tilde{\lambda}_2 - \tilde{\lambda}_1)$$

For $\tilde{\lambda}_1 > \tilde{\lambda}_2$:

$$F(\theta) = \begin{cases} c\, m(\theta) & \theta \in (0, \pi/4) \\\\ 0 & \theta \in (\pi/4, \pi/2) \end{cases}$$

Thus, the point $\theta = \pi/4$ is a left shunt. This leads to a build up of probability in the region $\theta \in (0, \pi/4)$.

For $\tilde{\lambda}_1 < \tilde{\lambda}_2$:

$$F(\theta) = \begin{cases} 0 & \theta \in (0, \pi/4) \\\\ c\, m(\theta) & \theta \in (\pi/4, \pi/2) \end{cases}$$

Here, $\theta = \pi/4$ is a right shunt and the probability accumulates in the region $\theta \in (\pi/4, \pi/2)$. In both of the above cases,

$$m(\theta) = \frac{\sin 2\theta}{\Psi^2(\theta)} \exp \left\{ \frac{(\tilde{\lambda}_2 - \tilde{\lambda}_1)}{2\alpha} \sec 2\theta \right\}$$

and

$$c = \left| \tilde{\lambda}_2 - \tilde{\lambda}_1 \right| \exp \left[\frac{\left| \tilde{\lambda}_2 - \tilde{\lambda}_1 \right|}{2\alpha} \right]$$

Figure 2.3 summarizes the behavior of the diffusion process for this case.

Case 3: $C = 0$ and $A, B \neq 0$

$$\Psi^2(\theta) = A \cos^2 2\theta + B \cos 2\theta$$

In this case, the singular points are located at

$$\theta = \frac{\pi}{4} \quad \text{and} \quad \theta = \theta_s = \frac{1}{2} \cos^{-1} \left(\frac{-B}{A} \right) = \frac{1}{2} \cos^{-1} \left(\frac{\alpha^-}{\alpha^+} \right)$$

as well as at the boundaries $\theta = 0, \pi/2$.

25

For $\tilde{\lambda}_1 > \tilde{\lambda}_2$ and $B < 0$:

$$F(\theta) = c_1 \begin{cases} m(\theta) & \theta \in (0, \theta_s) \\ \\ \delta(\theta - \pi/4) & \theta \in (\theta_s, \pi/2) \end{cases}$$

By Feller's scheme, the point $\theta = \theta_s$ is an entrance and $\theta = \pi/4$ is an exit boundary.

For $\tilde{\lambda}_1 > \tilde{\lambda}_2$ and $B > 0$:

$$F(\theta) = c_1 \begin{cases} m(\theta) & \theta \in (0, \pi/4) \\ \\ \delta(\theta - \theta_s) & \theta \in (\pi/4, \pi/2) \end{cases}$$

The singularity at $\theta = \theta_s$ is an exit and $\theta = \pi/4$ is an entrance boundary.

For $\tilde{\lambda}_1 < \tilde{\lambda}_2$ and $B < 0$:

$$F(\theta) = c_2 \begin{cases} \delta(\theta - \theta_s) & \theta \in (0, \pi/4) \\ \\ m(\theta) & \theta \in (\pi/4, \pi/2) \end{cases}$$

The point $\theta = \theta_s$ is an exit and $\theta = \pi/4$ is an entrance.

For $\tilde{\lambda}_1 < \tilde{\lambda}_2$ and $B > 0$:

$$F(\theta) = c_2 \begin{cases} \delta(\theta - \pi/4) & \theta \in (0, \theta_s) \\ \\ m(\theta) & \theta \in (\theta_s, \pi/2) \end{cases}$$

The singular point $\theta = \theta_s$ is an entrance boundary and $\theta = \pi/4$ is an exit. The boundary behavior for this case is depicted in Figure 2.4. In all cases,

$$m(\theta) = \frac{\sin 2\theta}{\Psi^2(\theta)} \left| -\alpha^+ + \alpha^- \sec 2\theta \right|^{\frac{\tilde{\lambda}_1 - \tilde{\lambda}_2}{\alpha^-}}$$

and

$$c_1 = \frac{\tilde{\lambda}_2 - \tilde{\lambda}_1}{\tilde{\lambda}_2 - \tilde{\lambda}_1 - (2\alpha_{21})^{\frac{\tilde{\lambda}_1 - \tilde{\lambda}_2}{\alpha^-}}} \quad , \quad c_2 = \frac{\tilde{\lambda}_2 - \tilde{\lambda}_1}{\tilde{\lambda}_2 - \tilde{\lambda}_1 + (2\alpha_{12})^{\frac{\tilde{\lambda}_1 - \tilde{\lambda}_2}{\alpha^-}}}$$

Case 4: $A = 0$ and $B, C \neq 0$

$$\Psi^2(\theta) = \frac{1}{2}\alpha^+ - \frac{1}{2}\alpha^- \cos 2\theta$$

The only singular points for this case are at the boundaries $\theta = 0, \pi/2$ (see Figure 2.2) since the singular point defined by

$$\theta_s = \frac{1}{2}\cos^{-1}\left(\frac{\alpha^+}{\alpha^-}\right)$$

can be shown to coincide with either $\theta = 0$ or $\theta = \pi/2$ due to the condition

$$0 \leq \left|\frac{\alpha^+}{\alpha^-}\right| \leq 1$$

26
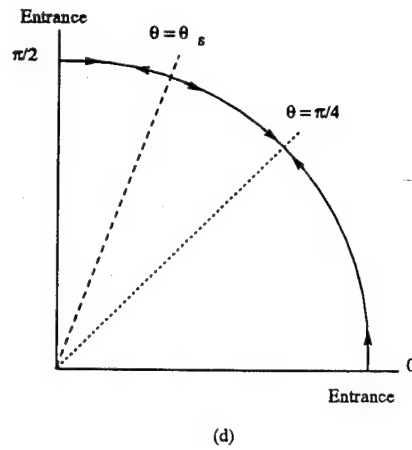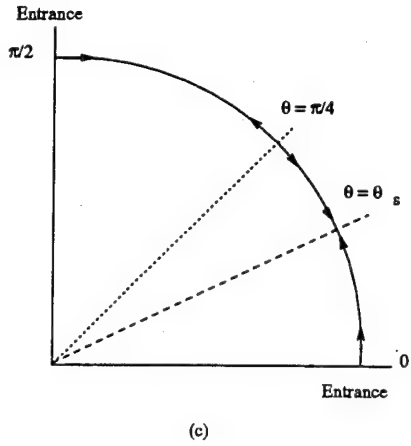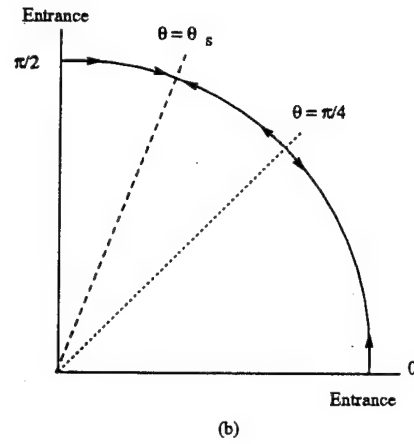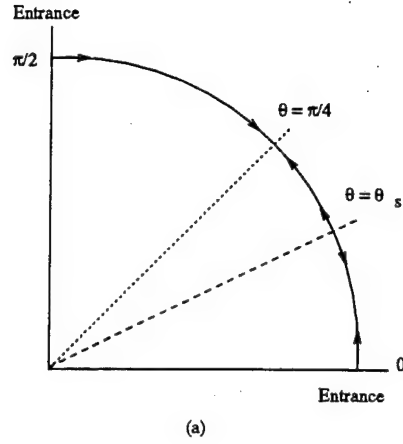
Figure 2.4: Boundary behavior for singular case 3: (a) $\tilde{\lambda}_1 > \tilde{\lambda}_2$, $B < 0$, (b) $\tilde{\lambda}_1 > \tilde{\lambda}_2$, $B > 0$, (c) $\tilde{\lambda}_1 < \tilde{\lambda}_2$, $B < 0$, (d) $\tilde{\lambda}_1 < \tilde{\lambda}_2$, $B > 0$

In this case,

$$m(\theta) = \frac{\sin 2\theta}{\Psi^2(\theta)} \left| -\alpha^+ + \alpha^- \cos 2\theta \right|^{\frac{\tilde{\lambda}_2 - \tilde{\lambda}_1}{\alpha^-}}$$

and

$$c = \frac{\tilde{\lambda}_2 - \tilde{\lambda}_1}{(2\alpha_{12})^{\frac{\tilde{\lambda}_2 - \tilde{\lambda}_1}{\alpha^-}} - (2\alpha_{21})^{\frac{\tilde{\lambda}_2 - \tilde{\lambda}_1}{\alpha^-}}}$$

Case 5: $A = C = 0$ and $B \neq 0$

Satisfying $A = C = 0$ requires the following conditions:

$$\gamma = 0 \quad \text{and} \quad \alpha^+ = 0$$

Since $\alpha^+ = \alpha_{12} + \alpha_{21}$, where α_{12} and α_{21} are non-negative quantities, the second requirement implies $\alpha_{12} = \alpha_{21} = 0$. For $B \neq 0$, the following condition must hold

$$\alpha^- \neq 0$$

These cannot be satisfied simultaneously. Thus, the case 5 singularity is not possible.

Case 6: $A = B = C = 0$

$$\Psi^2(\theta) = 0 \quad \forall \; \theta \in (0, \pi/2)$$

This corresponds to the case of two uncoupled oscillators. In this case, the diffusion process is singular for all values of θ and a function $F(\theta)$ satisfying the normality condition over the interval $(0, \pi/2)$ cannot be found. However, as stated previously, the Lyapunov exponents for this situation are λ_1 and λ_2. The maximal Lyapunov exponent is simply the greater of the two.

2.4 Maximal Lyapunov Exponents

The maximal Lyapunov exponent given by Eq. (2.12) can now be calculated. Letting

$$J(\theta) = \Psi^2(\theta) + \frac{1}{2}(\tilde{\lambda}_1 - \tilde{\lambda}_2) \cos 2\theta$$

and

$$\tilde{c} = \frac{1}{2}(\tilde{\lambda}_1 + \tilde{\lambda}_2) - \frac{1}{2}(\gamma_1 + \gamma_2) + \mu$$

and considering terms up to $O(\varepsilon^2)$ only yields the following for the expansion in λ^ε:

$$\lambda^\varepsilon = \varepsilon^2 \left\{ \int_0^{\frac{\pi}{2}} J(\theta) F(\theta) \, d\theta + \tilde{c} \int_0^{\frac{\pi}{2}} F(\theta) \, d\theta \right\} \tag{2.23}$$

Integration by parts and substitution of the appropriate $F(\theta)$ yields the maximal Lyapunov exponent for each of the singular cases.

28

Case 1: A, B, $C \neq 0$ For all cases ($\Delta > 0$, $\Delta = 0$, $\Delta < 0$), using the appropriate $M(\theta)$:

$$\lambda^\varepsilon = \varepsilon^2 \left\{ \frac{1}{2}(\tilde{\lambda}_2 - \tilde{\lambda}_1) \frac{[M(\pi/2) + M(0)]}{[M(\pi/2) - M(0)]} + \tilde{c} \right\}$$

Case 2i: $B = 0$ and A, $C \neq 0$

For $AC > 0$:

$$\lambda^\varepsilon = \varepsilon^2 \left\{ \frac{1}{2}(\tilde{\lambda}_2 - \tilde{\lambda}_1) \coth \left[\frac{(\tilde{\lambda}_2 - \tilde{\lambda}_1)}{\sqrt{AC}} \tan^{-1} \left(\frac{\sqrt{AC}}{C} \right) \right] + \tilde{c} \right\}$$

For $AC < 0$, recall, there is an additional singularity at $\theta = \theta_s$. The maximal Lyapunov exponent is given by

$$
\lambda^\varepsilon = \varepsilon^2 \left\{ \frac{|\tilde{\lambda}_2 - \tilde{\lambda}_1|}{2} \exp \left[\frac{|\tilde{\lambda}_2 - \tilde{\lambda}_1|}{2} \left(1 - \frac{1}{\sqrt{-AC}} \tanh^{-1} \left[\frac{\sqrt{-AC}}{C} \right] \right) \right] \right.
$$
$$
\left. + \frac{|\tilde{\lambda}_2 - \tilde{\lambda}_1|}{2} (\tilde{\lambda}_1 - \tilde{\lambda}_2) \frac{\sqrt{-AC}}{A} \exp \left[\frac{|\tilde{\lambda}_2 - \tilde{\lambda}_1|}{2A} \right] + \tilde{c} \right\}
$$

Case 2ii: $B = 0$ and $A = 0$, $C \neq 0$

$$\lambda^\varepsilon = \varepsilon^2 \left\{ \frac{1}{2}(\tilde{\lambda}_2 - \tilde{\lambda}_1) \coth \left[\frac{\tilde{\lambda}_2 - \tilde{\lambda}_1}{2\alpha} \right] + \tilde{c} \right\}$$

Case 2iii: $B = 0$ and $A \neq 0$, $C = 0$

$$\lambda^\varepsilon = \varepsilon^2 \left\{ \frac{1}{2} \left| \tilde{\lambda}_2 - \tilde{\lambda}_1 \right| + \tilde{c} \right\}$$

Case 3: $C = 0$ and A, $B \neq 0$

For $\tilde{\lambda}_1 > \tilde{\lambda}_2$ and $B < 0$:

$$\lambda^\varepsilon = \varepsilon^2 \left\{ \frac{1}{2} \left(\tilde{\lambda}_2 - \tilde{\lambda}_1 \right) \left[\frac{(2\alpha_{21})^{\frac{\tilde{\lambda}_1 - \tilde{\lambda}_2}{\alpha^-}}}{\tilde{\lambda}_2 - \tilde{\lambda}_1 - (2\alpha_{21})^{\frac{\tilde{\lambda}_1 - \tilde{\lambda}_2}{\alpha^-}}} \right] + \tilde{c} \right\}$$

For $\tilde{\lambda}_1 > \tilde{\lambda}_2$ and $B > 0$:

$$\lambda^\varepsilon = \varepsilon^2 \left\{ \frac{1}{2} \left(\tilde{\lambda}_2 - \tilde{\lambda}_1 \right) \left[\frac{(2\alpha_{21})^{\frac{\tilde{\lambda}_1 - \tilde{\lambda}_2}{\alpha^-}} - \frac{\alpha^-}{\alpha^+} \left(\tilde{\lambda}_2 - \tilde{\lambda}_1 \right)}{\tilde{\lambda}_2 - \tilde{\lambda}_1 - (2\alpha_{21})^{\frac{\tilde{\lambda}_1 - \tilde{\lambda}_2}{\alpha^-}}} \right] + \tilde{c} \right\}$$

29

For $\tilde{\lambda}_1 < \tilde{\lambda}_2$ and $B < 0$:

$$\lambda^\varepsilon = \varepsilon^2 \left\{ \frac{1}{2} \left(\tilde{\lambda}_2 - \tilde{\lambda}_1 \right) \left[\frac{(2\alpha_{12})^{\frac{\tilde{\lambda}_1 - \tilde{\lambda}_2}{\alpha^-}} - \frac{\alpha^-}{\alpha^+} \left(\tilde{\lambda}_2 - \tilde{\lambda}_1 \right)}{\tilde{\lambda}_2 - \tilde{\lambda}_1 + (2\alpha_{12})^{\frac{\tilde{\lambda}_1 - \tilde{\lambda}_2}{\alpha^-}}} \right] + \tilde{c} \right\}$$

For $\tilde{\lambda}_1 < \tilde{\lambda}_2$ and $B > 0$:

$$\lambda^\varepsilon = \varepsilon^2 \left\{ \frac{1}{2} \left(\tilde{\lambda}_2 - \tilde{\lambda}_1 \right) \left[\frac{(2\alpha_{12})^{\frac{\tilde{\lambda}_1 - \tilde{\lambda}_2}{\alpha^-}}}{\tilde{\lambda}_2 - \tilde{\lambda}_1 + (2\alpha_{12})^{\frac{\tilde{\lambda}_1 - \tilde{\lambda}_2}{\alpha^-}}} \right] + \tilde{c} \right\}$$

Case 4: $A = 0$ and $B, C \neq 0$

$$\lambda^\varepsilon = \varepsilon^2 \left\{ \frac{1}{2} \left(\tilde{\lambda}_2 - \tilde{\lambda}_1 \right) \left[\frac{(2\alpha_{12})^{\frac{\tilde{\lambda}_2 - \tilde{\lambda}_1}{\alpha^-}} + (2\alpha_{21})^{\frac{\tilde{\lambda}_2 - \tilde{\lambda}_1}{\alpha^-}}}{(2\alpha_{12})^{\frac{\tilde{\lambda}_2 - \tilde{\lambda}_1}{\alpha^-}} - (2\alpha_{21})^{\frac{\tilde{\lambda}_2 - \tilde{\lambda}_1}{\alpha^-}}} \right] + \tilde{c} \right\}$$

Case 6: $A = B = C = 0$

$$\lambda^\varepsilon = \varepsilon^2 \max \left(\lambda_1, \lambda_2 \right)$$

It is important to note that when the conditions of Eq. (2.3) are imposed, $\gamma_1 = \gamma_2 = 0$, the maximal Lyapunov exponent given by Eq. (2.23) is identical to that obtained via the method of averaging (refer to [82]).

2.5   Rotation Numbers

The Multiplicative Ergodic Theorem for rotation numbers is given in a recent paper by Arnold and San Martin [8] in which a general method for calculating the rotation numbers, ρ_{ij}, of the canonical planes $p_{ij} = \text{span}(E_i, E_j)$ is given. The spaces E_i and E_j are the Oseledec spaces described earlier. The rotation number of any other plane will pick the value ρ_{ij} whenever this plane has p_{ij} as the strongest component. In the current calculations, three angles have been introduced. Thus, by definition, there would be a rotation number associated with each angle giving the exponential rotation rate. Since these angles are not defined with respect to canonical bases, the rotation numbers cannot be readily related to those given in [8]. However, it is clear that if the plane of x_1-x_2 corresponds to any of the p_{ij}'s, then one can relate α_1 to ρ_{ij}, where α_1 is the rotation number corresponding to the first degree-of-freedom. A similar relation exists for α_2. The relationship between the results of Arnold and San Martin and those presented here must be further investigated.

In terms of the invariant measure p^ε, the rotation numbers are given as

$$\alpha_i^\varepsilon = \langle H_i^\varepsilon, p^\varepsilon \rangle \qquad (2.24)$$

30

where
$$H_i^\varepsilon(\phi_1, \phi_2, \theta, \xi) = \omega_i + \varepsilon f(\xi) h_i(\phi_1, \phi_2, \theta) + \varepsilon^2 \tilde{h}_i(\phi_1, \phi_2, \theta)$$

Again, for A_1 as given, $\tilde{h}_i = 0$. The rotation number given by Eq. (2.24) can be rewritten as

$$\alpha_i^\varepsilon = \langle \omega_i, p^0 \rangle + \varepsilon \left[\langle \omega_i, p^1 \rangle + \langle f(\xi) h_i, p^0 \rangle \right] + \varepsilon^2 \left[\langle \omega_i, p^2 \rangle + \langle f(\xi) h_i, p^1 \rangle + \langle \tilde{h}_i, p^0 \rangle \right] \qquad (2.25)$$

where ω_i is a constant and p^ε is scaled such that p^1 and p^2 have mean zero. The last term is zero due to the structure of the A_1 matrix. Due to the periodic boundary conditions on ϕ_1 and ϕ_2, as well as the zero mean assumption on $f(\xi)$, one has

$$\langle f(\xi) h_i, p^0 \rangle = 0$$

Hence, Eq. (2.25) reduces to

$$\alpha_i^\varepsilon = \omega_i + \varepsilon^2 \langle f(\xi) h_i, p^1 \rangle \qquad (2.26)$$

Making use of the following definitions:

$$\begin{aligned}
\hat{\alpha}_{12} &= \frac{1}{8} \left[(H_{12}^{-2} + J_{12}^{+2}) \Gamma(\Omega^-) + (H_{12}^{+2} + J_{12}^{-2}) \Gamma(\Omega^+) \right] \\
\hat{\alpha}_{21} &= \frac{1}{8} \left[(H_{21}^{-2} + J_{21}^{+2}) \Gamma(\Omega^-) - (H_{21}^{+2} + J_{21}^{-2}) \Gamma(\Omega^+) \right] \\
\hat{\beta}_i &= \frac{1}{8} (H_{ii}^{+2} + J_{ii}^{-2}) \Gamma(2\omega_i) \\
\hat{\mu}_1 &= \frac{1}{8} \left[(-H_{12}^- H_{21}^- + J_{12}^+ J_{21}^+) \Gamma(\Omega^-) \right] \\
\hat{\mu}_2 &= \frac{1}{8} \left[(H_{12}^+ H_{21}^+ + J_{12}^- J_{21}^-) \Gamma(\Omega^+) \right] \\
\hat{\gamma}_1 &= \frac{1}{4} (H_{21}^- J_{12}^+ + H_{12}^- J_{21}^+) S(\Omega^-) \\
\hat{\gamma}_2 &= \frac{1}{4} (H_{21}^+ J_{12}^- - H_{12}^+ J_{21}^-) S(\Omega^+)
\end{aligned}$$

the rotation numbers may be written as

$$\alpha_1 = \omega_1 - \varepsilon^2 \left\{ \hat{\beta}_1 + \frac{1}{2} (\hat{\gamma}_2 - \hat{\gamma}_1) + (\hat{\mu}_1 + \hat{\mu}_2) + \frac{1}{2} \hat{\alpha}_{12} \lim_{\theta \to \frac{\pi}{2}} [\sec(\theta) F(\theta)] \right\} \qquad (2.27)$$

$$\alpha_2 = \omega_2 - \varepsilon^2 \left\{ \hat{\beta}_2 - \frac{1}{2} (\hat{\gamma}_2 + \hat{\gamma}_1) - (\hat{\mu}_1 - \hat{\mu}_2) + \frac{1}{2} \hat{\alpha}_{21} \lim_{\theta \to 0} [\csc(\theta) F(\theta)] \right\} \qquad (2.28)$$

By substituting the appropriate $F(\theta)$ into the above expressions, the rotation numbers can be explicitly determined for each of the possible singular cases.

2.6 Applications

The focus of this section is to apply the results of the perturbation method described in the preceding sections to investigate the almost-sure stability of general four-dimensional mechanical systems. The applications presented here include a gyroscopic system and a nonconservative system involving fluid-structure interaction. Specifically, the examples considered are: a rotating shaft subjected to a small amplitude stochastic axial load and a stationary cylinder under the influence of a stochastically fluctuating lift force. It will be shown in the first of these that A_1 need not be strictly diagonal.
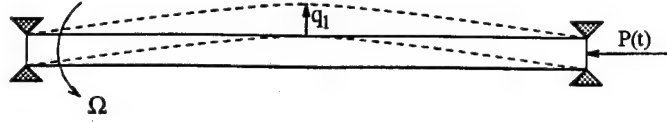
Figure 2.5: Pinned-pinned rotating shaft subjected to time-dependent axial load.

2.6.1 Rotating Shaft Subject to Random Axial Load

Rotating systems are an integral part of modern machinery. Much work has been done to examine the stability and response of such systems subjected to periodic excitations. The dynamics and response of rotating systems have been studied extensively. Sri Namachchivaya and Ariaratnam [2, 3] examined the general conservative linear and nonlinear gyroscopic systems. Yazici [91] analyzed the general problem of such stability in the presence of damping. In most practical situations, the system is subjected to excitations which are not purely deterministic. The combined effects of harmonic and stochastic excitations on the mean square stability of rotating systems was examined by Sri Namachchivaya [78]. The almost-sure stability of rotating systems under the influence of white or real noise excitation has been studied by Sri Namachchivaya and Talwar [82] using the method of averaging. In this system, the amplitude and phase equations decouple. Thus, no restrictions on the stochastic terms are necessary.

In this first application, consider a shaft pinned at each end and rotating at constant rate Ω and study the almost-sure stability of the trivial solution of Eq. (2.1). The system is shown in Figure 2.5. The shaft is subjected to a compressive axial load $P(t)$ which is composed of a mean load P_0 plus a small amplitude, zero mean real noise excitation $f(t)$. The linear equations of motion are [2]

$$M\ddot{q} + \left(2G + \varepsilon^2 D\right)\dot{q} + Kq = \varepsilon f(t)q \tag{2.29}$$

where $q = (q_1, q_2)^T$, the vector of generalized coordinates representing the displacement of the shaft center-line in the two principal directions. M, G, K and D are 2×2 constant matrices: M contains mass-like terms, G represents the gyroscopic terms $(G = -G^T)$, K contains stiffness terms and D arises from internal damping. These matrices have the following forms:

$$M = \begin{bmatrix} I & 0 \\ 0 & I \end{bmatrix}, \quad G = \begin{bmatrix} 0 & -\Omega \\ \Omega & 0 \end{bmatrix}$$

$$K = \begin{bmatrix} \bar{\omega}_1^2 - \Omega^2 & 0 \\ 0 & \bar{\omega}_2^2 - \Omega^2 \end{bmatrix} = \begin{bmatrix} k_1 & 0 \\ 0 & k_2 \end{bmatrix} \quad \text{and} \quad D = \begin{bmatrix} d_1 & 0 \\ 0 & d_2 \end{bmatrix}$$

where

$$\bar{\omega}_i^2 = \frac{\pi^2}{mL^2}\left(EI_i\left(\frac{\pi}{L}\right)^2 - P_0\right), \quad i = 1, 2$$

Letting $y_{2i-1} = q_i$ and $y_{2i} = \dot{q}_i$ yields the state space representation

$$\dot{y} = \left(\tilde{A}_0 - \varepsilon^2 \tilde{A}_1\right)y + \varepsilon f(t)\tilde{B}y$$

32

where

$$\tilde{A}_0 = \begin{bmatrix} 0 & 1 & 0 & 0 \\ -k_1 & 0 & 0 & 2\Omega \\ 0 & 0 & 0 & 1 \\ 0 & -2\Omega & -k_2 & 0 \end{bmatrix}$$

$$\tilde{A}_1 = \begin{bmatrix} 0 & 0 & 0 & 0 \\ 0 & d_1 & 0 & 0 \\ 0 & 0 & 0 & 0 \\ 0 & 0 & 0 & d_2 \end{bmatrix} \quad \text{and} \quad \tilde{B} = \begin{bmatrix} 0 & 0 & 0 & 0 \\ 1 & 0 & 0 & 0 \\ 0 & 0 & 0 & 0 \\ 0 & 0 & 1 & 0 \end{bmatrix}$$

Transforming to real Jordan form yields the following equations:

$$\dot{x} = \left(A_0 - \varepsilon^2 A_1 \right) x + \varepsilon f(t) B x$$

with

$$A_0 = \begin{bmatrix} 0 & \omega_1 & 0 & 0 \\ -\omega_1 & 0 & 0 & 0 \\ 0 & 0 & 0 & \omega_2 \\ 0 & 0 & -\omega_2 & 0 \end{bmatrix},$$

$$A_1 = \frac{1}{\omega_1^2 - \omega_2^2} \begin{bmatrix} d_1(\omega_1^2 - k_2) & 0 & d_1\frac{\omega_2}{\omega_1}(\omega_1^2 - k_2) & 0 \\ 0 & d_2(\omega_1^2 - k_1) & 0 & d_2(\omega_2^2 - k_1) \\ -d_1\frac{\omega_1}{\omega_2}(\omega_2^2 - k_2) & 0 & -d_1(\omega_2^2 - k_2) & 0 \\ 0 & -d_2(\omega_1^2 - k_1) & 0 & -d_2(\omega_2^2 - k_1) \end{bmatrix}$$

and

$$B = \frac{1}{\omega_1^2 - \omega_2^2} \begin{bmatrix} 0 & -\frac{1}{\omega_1}(\omega_1^2 - k_2) & 0 & -\frac{1}{\omega_1}(\omega_1^2 - k_2) \\ \frac{1}{\omega_1}(\omega_1^2 - k_1) & 0 & -\frac{1}{\omega_2}(\omega_2^2 - k_2) & 0 \\ 0 & \frac{1}{\omega_2}(\omega_2^2 - k_2) & 0 & \frac{1}{\omega_2}(\omega_2^2 - k_2) \\ -\frac{1}{\omega_1}(\omega_1^2 - k_1) & 0 & -\frac{1}{\omega_2}(\omega_2^2 - k_1) & 0 \end{bmatrix}$$

The eigenvalues of A_0, $\pm i\omega_r (r = 1, 2)$, are given by

$$\omega_r = \sqrt{\frac{1}{2}\left(\bar{\omega}_1^2 + \bar{\omega}_2^2 + 2\Omega^2 \pm \sqrt{(\bar{\omega}_1^2 - \bar{\omega}_2^2)^2 + 8\Omega^2(\bar{\omega}_1^2 + \bar{\omega}_2^2)} \right)}$$

where "+" corresponds to ω_1 and "−" to ω_2. Note that if the matrix $A_1 = [a_{ij}]$ is full, δ_i is then

$$\delta_i = \frac{1}{2}\left(a_{2i-1,2i-1} + a_{2i,2i} \right), \quad i = 1, 2$$

The off-diagonal terms in A_1 introduce additional damping terms in the equations of motion for ρ, ϕ_1, ϕ_2 and θ. However, in the calculation of the maximal Lyapunov exponent, the coefficients of these new terms are periodic in ϕ_1 and ϕ_2 and drop out in the course of the analysis. Thus, the presence of these off-diagonal terms does not alter the expressions for the top Lyapunov exponent obtained in [23]. In this example,

$$\delta_i = \frac{(-1)^{i+1}}{2(\omega_1^2 - \omega_2^2)}\left\{ (d_1 + d_2)(\omega_i^2 + \Omega^2) - d_1\bar{\omega}_2^2 - d_2\bar{\omega}_1^2 \right\}, \quad i = 1, 2$$

33

For the general case,

$$H^{\pm} = \frac{1}{\omega_1^2 - \omega_2^2} \begin{bmatrix} -\frac{1}{\omega_1}(\omega_1^2 - k_2) \pm \frac{1}{\omega_1}(\omega_1^2 - k_1) & -\frac{1}{\omega_1}(\omega_1^2 - k_2) \pm \frac{1}{\omega_2}(\omega_2^2 - k_1) \\ \frac{1}{\omega_2}(\omega_2^2 - k_2) \mp \frac{1}{\omega_1}(\omega_1^2 - k_1) & \frac{1}{\omega_2}(\omega_2^2 - k_2) \mp \frac{1}{\omega_2}(\omega_2^2 - k_1) \end{bmatrix}$$

and

$$J^{\pm} = \begin{bmatrix} 0 & 0 \\ 0 & 0 \end{bmatrix}$$

Consider the case of band limited, or band-pass, noise. In this situation, $S(\omega)$ has significant values only for ω in the range $0 \leq \omega_0 - b/2 \leq \omega \leq \omega_0 + b/2$ where b is the bandwidth and ω_0 is .the central frequency. The correlation time of a band limited stochastic process is $O(1/b)$. The relaxation time of the amplitude process is $O(1/\varepsilon^2)$. If $b \gg \varepsilon$, the Markov approximation remains valid.

For $\omega_0 = 2\omega_i$:

$$A = -\frac{(\bar{\omega}_1^2 - \bar{\omega}_2^2)^2}{32\omega_i^2 (\omega_1^2 - \omega_2^2)^2} S(2\omega_i)$$

$$B = 0$$

$$C = \frac{(\bar{\omega}_1^2 - \bar{\omega}_2^2)^2}{32\omega_i^2 (\omega_1^2 - \omega_2^2)^2} S(2\omega_i)$$

$$\lambda_i = \tilde{\lambda}_i = -\delta_i + \frac{(\bar{\omega}_1^2 - \bar{\omega}_2^2)^2}{8\omega_i^2 (\omega_1^2 - \omega_2^2)^2} S(2\omega_i)$$

with $i = 1, 2$. For $\omega_0 = \omega_1 \pm \omega_2$:

$$A = \frac{S(\Omega^{\pm})}{32(\omega_1^2 - \omega_2^2)^2} \left\{ 6(\omega_2 \mp \omega_1)^2 + \frac{1}{\omega_1^2 \omega_2^2}(\omega_1^2 + \omega_2^2)(k_1^2 + k_2^2) \right.$$
$$\left. \mp \frac{1}{\omega_1 \omega_2} \left[2(k_1^2 + k_2^2) - 3(\omega_1 \mp \omega_2)^2 (k_1 + k_2) \right] \right\}$$

$$B = \frac{S(\Omega^{\pm})}{16\omega_1 \omega_2 (\omega_1^2 - \omega_2^2)} \left\{ \frac{(k_2^2 - k_1^2)}{\omega_1 \omega_2} \mp (k_1 - k_2) \right\}$$

$$C = \frac{-S(\Omega^{\pm})}{32(\omega_1^2 - \omega_2^2)^2} \left\{ 2(\omega_2 \pm \omega_1)^2 - \frac{1}{\omega_1^2 \omega_2^2}(\omega_1^2 + \omega_2^2)(k_1^2 + k_2^2) \right.$$
$$\left. \mp \frac{1}{\omega_1 \omega_2} \left[2(k_1^2 + k_2^2) - (\omega_1 \mp \omega_2)^2 (k_1 + k_2) \right] \right\}$$

and $\lambda_i = \tilde{\lambda}_i = -\delta_i$. The stability boundaries for the above cases are plotted in Figure 2.6 for the following parameter values: $\bar{\omega}_1 = 1.0$, $\bar{\omega}_2 = \sqrt{2}$, $\varepsilon = 0.1$ and $S(\omega_0) = 0.02$. The damping parameters d_1 and d_2 can be defined in terms of a single parameter ζ as $\zeta = d_i/(2\bar{\omega}_i)$.

Next, consider the case of broadband excitation, i.e. $S(2\omega_1) = S(2\omega_2) = S(\Omega^{\pm}) = S$. This yields

$$A = \frac{S}{32(\omega_1^2 - \omega_2^2)^2} \left\{ \frac{(\omega_1^2 + \omega_2^2)}{\omega_1^2 \omega_2^2}(k_1 + k_2)^2 + 12(\omega_1^2 + \omega_2^2) - 12(k_1 + k_2) \right\}$$

34
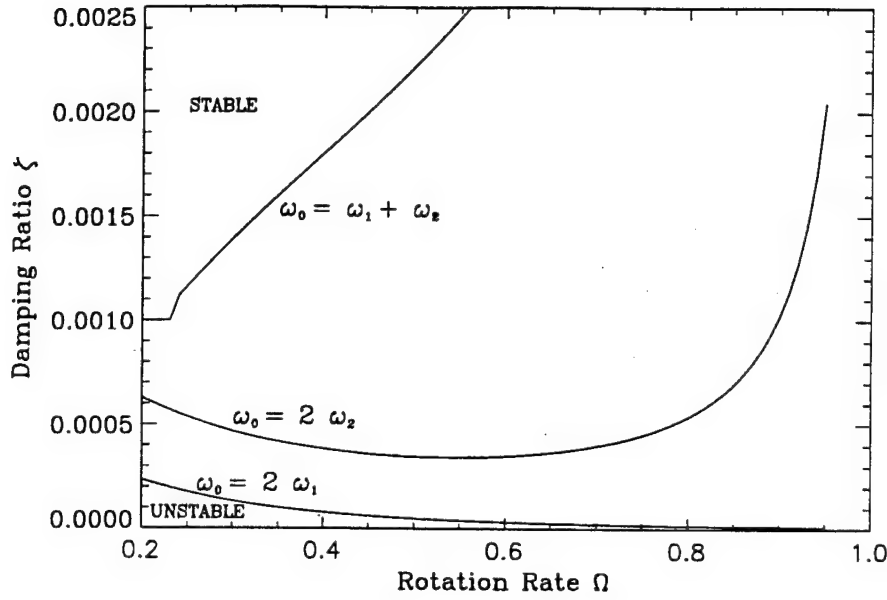
Figure 2.6: Stability boundaries for the rotating shaft for $\omega_0 = \omega_1$, ω_2 and $\omega_1 + \omega_2$.

$$B = \frac{-S(k_1^2 - k_2^2)}{8\omega_1^2\omega_2^2(\omega_1^2 - \omega_2^2)}$$

$$C = \frac{S}{32(\omega_1^2 - \omega_2^2)^2}\left\{\frac{3(\omega_1^2 + \omega_2^2)}{\omega_1^2\omega_2^2}(k_1^2 + k_2^2) - 6(\omega_1^2 + \omega_2^2) + 4(k_1 + k_2)\right\}$$

$$\lambda_i = \tilde{\lambda}_i = -\delta_i + \frac{(\bar{\omega}_1^2 - \bar{\omega}_2^2)^2 S}{8\omega_i^2(\omega_1^2 - \omega_2^2)^2}, \quad i = 1, 2$$

When the shaft is symmetric, $\bar{\omega}_1 = \bar{\omega}_2 = \bar{\omega}$, $d_1 = d_2 = d$ and the eigenvalues reduce to

$$\omega_1 = \bar{\omega} + \Omega \quad \text{and} \quad \omega_2 = \bar{\omega} - \Omega$$

The matrices A_1 and B become

$$A_1 = \begin{bmatrix} \delta_1 & 0 & \delta_2 & 0 \\ 0 & \delta_1 & 0 & -\delta_2 \\ \delta_1 & 0 & \delta_2 & 0 \\ 0 & -\delta_1 & 0 & \delta_2 \end{bmatrix} \quad \text{and} \quad B = \frac{1}{2\bar{\omega}}\begin{bmatrix} 0 & -1 & 0 & -1 \\ 1 & 0 & -1 & 0 \\ 0 & -1 & 0 & -1 \\ -1 & 0 & 1 & 0 \end{bmatrix}$$

where $\delta_i = d\omega_i/(2\bar{\omega})$. This yields

$$A = \frac{S(\Omega^+)}{8\bar{\omega}^2}, \quad B = C = 0$$

$$\lambda_i = \tilde{\lambda}_i = -\delta_i, \quad i = 1, 2$$

35
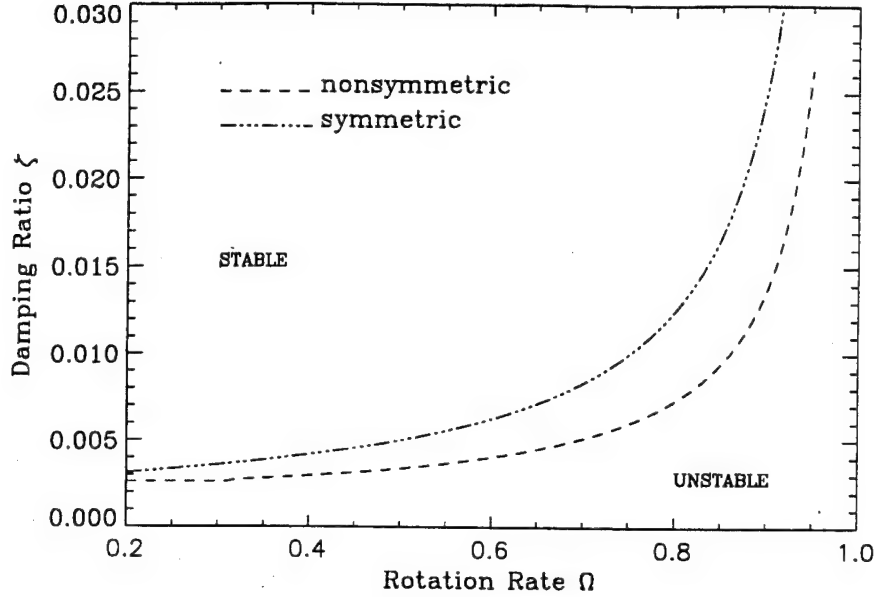
Figure 2.7: Stability boundary for the rotating shaft under broadband excitation

Since $\omega_1 > \omega_2$, one can easily show $\tilde{\lambda}_2 > \tilde{\lambda}_1$ and the top Lyapunov exponent reduces to

$$\lambda^\varepsilon = \varepsilon^2 \left\{ \frac{-d(\bar{\omega} - \Omega)}{2\bar{\omega}} + \frac{1}{8\bar{\omega}^2} S(\Omega^+) \right\}$$

The resulting stability boundaries for the symmetric (with $\bar{\omega} = 1.0$) and unsymmetric cases are depicted in Figure 2.7 in the Ω-ζ space. This system was examined by Sri Namachchivaya and Talwar [82] using the method of stochastic averaging. The results obtained by the two methods are identical.

By setting the noise spectrum to zero in the maximal Lyapunov exponent, the eigenvalues of the deterministic system can be recovered. In each of the above cases, the coefficients of the spectra are positive. Thus, the maximal Lyapunov exponents are greater than the deterministic eigenvalues. Therefore, the effect of noise is always destabilizing in this system.

2.6.2 Flow-induced Oscillations

As a final example, consider the wake-oscillator model of Hartlen and Currie [35] which describes the influence of a stochastically fluctuating lift force on a stationary circular cylinder normal to the flow. Unlike the first example, this system does not satisfy the decoupling conditions necessary for the implementation of averaging. The method of averaging, therefore, cannot be applied to determine the almost-sure stability of this system. The linear system is described by the following second order differential equations

$$\ddot{x} + \beta \dot{x} + x = a(W_0 + \varepsilon^2 \eta + \varepsilon f(\xi))^2 C_L$$

36
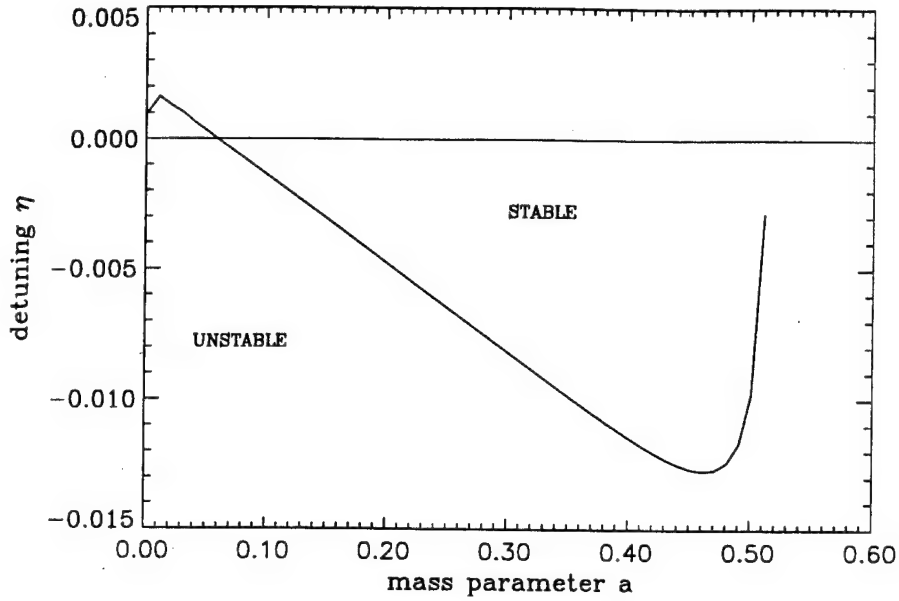
Figure 2.8: Stability boundary for the case of broadband excitation in the flow-induced oscillation problem

$$\ddot{C}_L - \alpha(W_0 + \varepsilon^2\eta + \varepsilon f(\xi))\dot{C}_L$$
$$+ (W_0 + \varepsilon^2\eta + \varepsilon f(\xi))^2 C_L = b\dot{x}$$

where W_0 is the dimensionless mean flow velocity, β represents a mechanical damping parameter, a is a mass factor, b an interaction parameter and α is a Van der Pol parameter. The quantity η is the deterministic detuning term describing the variation of the mean flow velocity from some critical value and $f(\xi)$ represents a stochastic variation in the flow velocity. The variable x describes the dimensionless displacement of the cylinder transverse to both the flow direction and cylinder axis and C_L represents the instantaneous lift coefficient. Letting $y_1 = C_L$, $y_2 = \dot{C}_L$, $y_3 = x$ and $y_4 = \dot{x}$, the first order equations of motion become

$$\dot{y} = \tilde{A}y$$

where

$$\tilde{A} = \begin{bmatrix} 0 & 1 & 0 & 0 \\ -\tilde{W}^2 & \alpha\tilde{W} & 0 & b \\ 0 & 0 & 0 & 1 \\ a\tilde{W}^2 & 0 & -1 & -\beta \end{bmatrix}$$

37

and $\tilde{W} = W_0 + \varepsilon^2 \eta + \varepsilon f(\xi)$. Putting this in the form of Eq. (2.1) yields

$$
A_0 = \begin{bmatrix} 0 & 1 & 0 & 0 \\ -W_0^2 & \alpha W_0 & 0 & b \\ 0 & 0 & 0 & 1 \\ aW_0^2 & 0 & -1 & -\beta \end{bmatrix}, \quad
A_1 = \begin{bmatrix} 0 & 0 & 0 & 0 \\ 2W_0\eta & -\alpha\eta & 0 & 0 \\ 0 & 0 & 0 & 0 \\ -2aW_0\eta & 0 & 0 & 0 \end{bmatrix}
$$

and

$$
B = \begin{bmatrix} 0 & 0 & 0 & 0 \\ -2W_0 & \alpha & 0 & 0 \\ 0 & 0 & 0 & 0 \\ 2aW_0 & 0 & 0 & 0 \end{bmatrix}
$$

The characteristic equation for the matrix A_0 is given by

$$
\lambda^4 - c_1\lambda^3 + c_2\lambda^2 - c_3\lambda + \lambda = 0
$$

where $c_1 = \alpha W_0 - \beta$, $c_2 = 1 + W_0^2 - \alpha\beta W_0$, $c_3 = W_0(abW_0 + \alpha - \beta W_0)$ and $c_4 = W_0^2$. In order to insure that A_0 possesses two pairs of purely imaginary eigenvalues, the following restrictions are placed on the parameter ranges of interest:

$$
c_1 = c_3 = 0 , \quad c_2 > 0 \quad \text{and} \quad c_2^2 - 4c_4 > 0
$$

The conditions $c_1 = 0$ and $C_3 = 0$ implies the following parameter relations:

$$
\alpha = \frac{abW_0}{W_0^2 - 1} \quad \text{and} \quad \beta = \alpha W_0
$$

The eigenvalues are then given by

$$
\pm i\omega_1 = \pm i\sqrt{\frac{c_2}{2} + \sqrt{\left(\frac{c_2}{2}\right)^2 - c_4}}
$$

and

$$
\pm i\omega_2 = \pm i\sqrt{\frac{c_2}{2} - \sqrt{\left(\frac{c_2}{2}\right)^2 - c_4}}
$$

Letting $b = 0.4$ (as in [35]) and $W_0 = \sqrt{2}$, the above restrictions yield the following range for the mass parameter $0.001 < a < .5177$.

In the deterministic system, when the above conditions are satisfied, the trivial solution $\| x \| = 0$ is unstable for all flow velocities near W_0 (except at $\tilde{W} \equiv W_0$) and for all values of the mass parameter a within the specified range. The point $\tilde{W} = W_0$ represents a bifurcation. For $\tilde{W} < W_0$, no stable solution exists. However, for $\tilde{W} > W_0$, one stable and one unstable periodic orbit exist. Hence, the only point at which the trivial solution is stable is $\tilde{W} \equiv W_0$, i.e. $\eta \equiv 0$.

In the current analysis, the almost-sure asymptotic stability of the trivial solution alone is considered. Using the parameter values given above, it can be shown that, under broadband excitation, the system falls into the case 1 singularity category with $\Delta < 0$. The almost-sure stability boundary for the trivial solution in $\eta - a$ parameter space is depicted in Figure 2.8. The

38

solid line at $\eta = 0$ represents the locus of parameter values for which the trivial solution of the deterministic system is stable.

For the stochastic case, the parameter regions for which the non-oscillatory state is stable or unstable are labeled in Figure 2.8. Note that for small values of the mass parameter a, the addition of broadband noise destabilizes the point $\eta = 0$. As a increases, $\eta = 0$ becomes stable. Furthermore, the addition of noise creates entire regions of parameter space for which the cylinder exhibits no transverse oscillations in the steady state. For higher values of the mass parameter, e.g. $0.2 < a < 0.5$, the stability of the trivial steady state is more robust to variations in the mean flow velocity.

2.7   Conclusions

In this chapter, an asymptotic expansion for the maximal Lyapunov exponent, the exponential growth rate of solutions to a linear stochastic system, and the rotation numbers for a general four-dimensional dynamical system driven by a small intensity real noise process were constructed. Stability boundaries, defined as the point at which the maximal Lyapunov exponent becomes zero can be obtained provided the natural frequencies are non-commensurable and the infinitesimal generator associated with the noise process has an isolated simple zero eigenvalue. This last assumption was made to make the solution tractable.

The asymptotic expansion for the maximal Lyapunov exponent was calculated for two practical dynamical systems. The advantage of this method over the method of stochastic averaging is the applicability of the perturbation approach to problems in the form of Eq. (2.1) without imposing any conditions on the form of the B matrix. For systems in which these conditions hold, the expressions for the maximal Lyapunov exponent and the rotation numbers calculated here reduce to those presented by Sri Namachchivaya and Talwar in [82]. When these conditions are violated, as in the example involving flow-induced vibrations of a cylinder, the method of averaging cannot be employed. In such cases, the perturbation method described in [23] provides the top Lyapunov exponents and, thus, the almost-sure stability boundaries.

It is worth pointing out that there are some other quantities that may be obtained asymptotically employing the current technique. One can use Liouville's theorem to calculate the sum of the Lyapunov exponents as the expected value of the trace of the complete linear coefficient matrix, i.e. $E\left(\text{Trace}[A_0 + A_1 + Bf(\xi)]\right) = \sum_{i=1}^{4} \lambda_i$. Considering the definition of the matrices A_0 and A_1 and the zero mean assumption on the noise process, the sum of the Lyapunov exponents is simply $2(\delta_1 + \delta_2)$. In two-dimensional systems, the trace and the top Lyapunov exponent completely describe the spectrum. However, the author is not aware of methods of describing the complete spectrum for systems with dimension greater than two. It should also be noted that the smallest Lyapunov exponent can be obtained by following the same procedure given here with time reversed. In this case, attention must be paid to the various generators describing the noise process.

The ability to predict the almost-sure stability boundaries of a stationary solution of a random dynamical system is of great importance in practical engineering problems. For a system operating within the almost-sure stability limits, all sample solutions except for a set of measure zero tend to the stationary solution as time goes to infinity. However, one may not be satisfied with such guarantees since a sample stable process may still exceed some threshold values or may possess a slow rate of decay.

39

Chapter 3

EQUATIONS OF MOTION OF A ROTATING SHAFT

3.1 Introduction

Any motion of a rigid body which has a dominant component of its angular velocity about an axis of symmetry is called a gyroscopic motion. Gyroscopic systems are integral components in many power generating systems. The dynamics and stability of a component modeled as a gyroscopic system may be affected by a time-dependent force imparted by the action of nearby components. These inputs appear as time-dependent parameters in the equations of motion of the component under investigation and may lead to large amplitude vibrations or complicated dynamics.

One of the most fundamental components of mechanical systems such as turbines, pumps, generators, etc., is a rotor. It is, therefore, not surprising that through the years considerable effort has been directed toward obtaining a better understanding of rotordynamics. Although for some purposes, it is sufficient to model the rotor as a rigid body, it is more appropriate in most situations to incorporate deformable rotor models. This investigation deals primarily with shaft-like rotors in which the longitudinal axis of the shaft coincides with the axis of rotation. There are two distinct motions a rotating shaft may exhibit: *rotation* and *whirling*. When a non-whirling shaft rotates, the axis of the rotor is stationary but each section of the rotor at right angles to the axis rotates about the axis. When a non-rotating shaft whirls, every point in the section executes the identical orbital motion without any change in the orientation of the section. Rotation is a necessary function of a shaft, while whirling is always an undesirable motion which introduces vibration, noise and additional loading on the rotor and its bearings. Whirling, in extreme cases, can cause failure. A recent paper by Crandall [17] gives an excellent physical insight into these problems. When the axis of the rotating shaft bends, gyroscopic torques are generally created which couple the transverse bending vibrations in the orthogonal planes, and thereby promote whirling forms of motion. In addition, bending can give rise to mid-plane stretching. Thus, it may be essential to consider nonlinear strain-displacement relations in obtaining the equations of motion.

In the study of the response and stability of dynamical systems, the location and characterization of bifurcations points is of primary importance. Consider the system

$$\dot{x} = f(x, \mu) , \quad x \in \mathbf{R}^d \tag{3.1}$$

with solution $x(t; x_0)$ where $f(x, \mu)$ is a d-dimensional (possibly nonlinear) vector function which

depends on a parameter μ. A *bifurcation* refers to a qualitative change in the response $x(t; x_0)$ as the parameter μ passes some value μ_0. μ is called the *bifurcation parameter* and the value of μ at which this qualitative change takes place is the *bifurcation point*.

The study of the bifurcation behavior in a small region of state space surrounding the fixed point (or limit cycle) or in a small neighborhood of the bifurcation point is referred to as local analysis. In a local bifurcation, the stability of one fixed point or limit cycle is lost and a branching, or bifurcating, solution emerges. These local bifurcation scenarios are described by the dynamics in the variational equations. The results must be interpreted according to the physics of the problem. For example, constant amplitude standing or traveling waves correspond to the case of fixed points, amplitude modulated standing or traveling waves to the case of limit cycles. In addition to these, there are many phenomena which cannot be explained by local analysis alone. These solutions are, for the most part, global in the sense that they do not lie in the small neighborhood of state space or in a small neighborhood of the parameter at which the fixed point or the limit cycle goes through a local bifurcation.

It is imperative to understand the response, stability and both local and global bifurcation behavior of such nonlinear dynamical systems prior to their use as integral and reliable elements of mechanical systems. Recently, considerable effort has been directed toward obtaining a better understanding of the nonlinear behavior and instability mechanisms of rotating shafts. When viewed in a rotating reference frame, the rotating shaft may be classified as a gyroscopic system. The dynamics and response of rotating and gyroscopic systems have been studied extensively in the literature [2, 3, 43, 76, 77, 91].

In this chapter, the dynamics and stability of a rotating shaft subjected to a dynamic axial load will be investigated. The Lagrangian equations of motion for simply supported and fixed-end shafts are derived in Section 3.2. In Section 3.3, the Hamiltonian equations of motion are obtained from the Lagrangian equations via a Legendre transformation. In addition to the rotating shaft, there are many examples of engineering systems which are modeled by gyroscopic systems. Problems of practical interest include the lateral vibrations of a pipe conveying fluid, the transverse vibrations of moving belts (such as band saws), etc. The dynamics of these systems are governed by equations very similar to those derived in this chapter. While the motivation for this chapter is the study of the dynamics of the rotating shaft, the analysis presented in the two subsequent chapters may be applied to any of these problems.

3.2 Derivation of the Lagrangian Equations of Motion

In this section, the equations governing the transverse vibrations of a rotating shaft subjected to a time-dependent axial load are derived. The geometry of the shaft of length L and constant cross-sectional area A is depicted in Figure 3.1. In the subsequent analysis, the time-dependent component of the axial load is assumed to be periodic and the shaft is assumed to be free from torque. This models a perturbation to the compressive axial load imparted by adjacent components. If these components are rotating or reciprocating at a constant rate, the additional excitation they impart consists of a small amplitude oscillating force with fixed period. The resulting axial load may be written as $P(t) = P_0 + \mu \cos(\nu t) H(t)$ where $H(t)$ is the Heaviside function. Thus the periodic perturbation is turned on at time $t = 0$. This corresponds to a step discontinuity in the axial load at $t = 0$. Since the goal of this investigation is to study the steady state behavior of the shaft, the transient effects of this discontinuity may be ignored. This model also assumes that

41
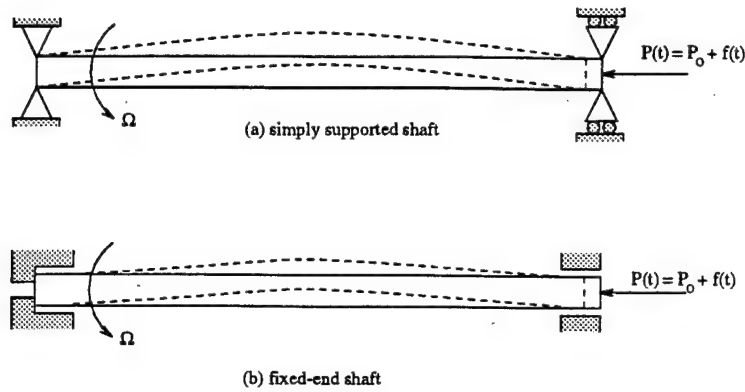
Figure 3.1: Geometry of simply supported and fixed-end shafts showing undeformed (solid line) and deformed (dashed line) configurations.

the shaft is rotating in torque-free bearings (e.g. ideal superconducting or magnetic bearings). The latter restriction may be relaxed by considering additional terms describing the torque and resulting twist in the shaft. For clarity in presenting the method of analysis, the effect of torque has been omitted. Two types of end conditions are examined: simply supported ends (pinned-pinned) and fixed ends (clamped-clamped).

The nonlinearities in the final equations of motion stem from the geometry of the mechanical problem. The longitudinal displacement of each section of the shaft is a result of axial compression, which generates linear terms, as well as the overall shortening effect of lateral displacements, which generates cubic terms in the final equations of motion describing the lateral displacement of the shaft center line. This shortening effect is due to the fact that the end of the shaft at $x = L$ is free to move axially.

The equations of motion are derived here using the energy method. The potential energy, including the combined effects of bending and compression, and the kinetic energy are calculated and combined to form the Lagrangian. Hamilton's Principle of Least Action yields the partial differential equations describing the transverse motion of the shaft. Applying a modal approximation reduces these to ordinary differential equations governing the amplitude of vibration in each of the two principal directions.

The total strain energy contains contributions from the effects of axial compression and bending strain. The strain due to axial compression is simply $\epsilon_{comp} = u_x(x, t)$. The bending strain can be calculated from the geometry of the deformed center-line with the aid of Figure 3.2. Consider the arc length ds of a differential element of the shaft center line. This length is determined by

$$ds = \sqrt{dx^2 + dv^2 + dw^2} = dx\sqrt{1 + \left(\frac{\partial v}{\partial x}\right)^2 + \left(\frac{\partial w}{\partial x}\right)^2}$$

where dx is the projection of ds onto the x-axis. Let v be the displacement of the shaft centerline along the y axis and w the displacement along the z axis. Then dv and dw represent differential changes in the coordinates v and w, respectively. Writing the partial derivatives as v_x and w_x, where the subscript indicates differentiation with respect to the longitudinal variable x, and expanding
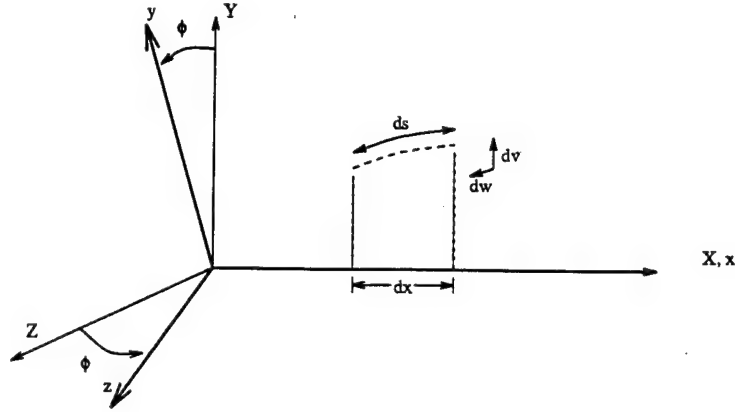
Figure 3.2: Differential element of the deformed centerline showing longitudinal displacements due to bending alone.

the square root in a binomial series yields

$$ds = \left[1 + v_x^2 + w_x^2\right]^{\frac{1}{2}} dx = \left[1 + \frac{1}{2}\left(v_x^2 + w_x^2\right)\right] dx + h.o.t.$$

The effect of bending on this differential element is to shift the points on the center line by an amount $ds - dx$ in the direction of $x = 0$. The overall axial displacement of a point on the shaft center line is the sum of the effects of all displacements up to that point. Thus, one can superimpose the effects of bending and compression on the axial displacement of a point. For an incompressible material, the axial displacement of a point on the shaft originally at x is given (to second order) by the integral

$$\int_0^x \left(\frac{ds}{d\xi} - 1\right) d\xi = \frac{1}{2}\int_0^x \left(v_\xi^2 + w_\xi^2\right) d\xi$$

Including the effects of axial compression $u(x,t)$, the total displacement $h(x,t)$ of a point originally at x is

$$h(x,t) = u(x,t) + \frac{1}{2}\int_0^x \left(v_\xi^2 + w_\xi^2\right) d\xi$$

Note that this displacement is defined to be positive in the negative x-direction.

The curvature vector of the deformed center-line is

$$\vec{\kappa} \cong \frac{v_{xx}\hat{e}_v + w_{xx}\hat{e}_w}{\left[1 + v_x^2 + w_x^2\right]^{\frac{3}{2}}}$$

where $\hat{e}_v$ and $\hat{e}_w$ are unit vectors in the v and w directions, respectively. Expanding the denominator in a binomial series yields the following second order approximation for the curvature vector:

$$\vec{\kappa} = \left(v_{xx}\hat{e}_v + w_{xx}\hat{e}_w\right)\left[1 - \frac{3}{2}\left(v_x^2 + w_x^2\right)\right]$$

The radius of curvature of the center-line is defined to be

$$\rho = \frac{1}{|\vec{\kappa}|}$$

43
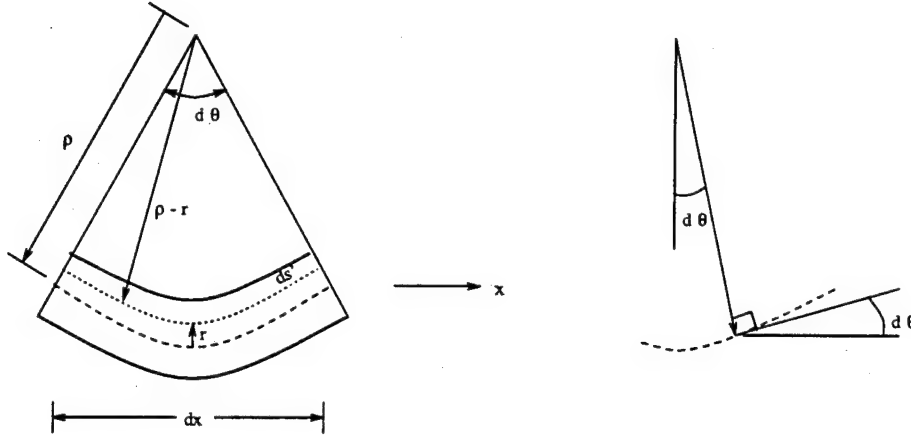
Figure 3.3: Geometry of the deformed center-line.

where $|\vec{\kappa}|$ is the magnitude of the vector $\vec{\kappa}$. With the aid of Figure 3.3, the bending strain can be written as

$$\epsilon = \frac{ds' - dx}{dx} = \frac{(\rho - r)d\theta - dx}{dx} = (\rho - r)\frac{d\theta}{dx} - 1$$

But the term $\frac{d\theta}{dx}$ is simply $1/\rho$. The strain due to axial bending is given by

$$\epsilon_{bend} = -\left(r_v v_{xx} + r_w w_{xx}\right)\left[1 - \frac{3}{2}\left(v_x^2 + w_x^2\right)\right] = -(r_v \kappa_v + r_w \kappa_w)$$

Assuming constant cross-sectional area A along the length of the shaft, and combining the effects of axial and bending strain, the total strain energy is then

$$U = \frac{EA}{2}\int_0^L u_x^2 dx + \frac{E}{2}\int_{volume}\left[\left(r_v^2\kappa_v^2 + r_w^2\kappa_w^2 r_v r_w \kappa_v \kappa_w\right) - 2u_x\left(r_v\kappa_v + r_w\kappa_w\right)\right]dVol$$

The area moments of inertia are defined as

$$I_v = \int_{area} r_v^2 dA \ , \quad I_w = \int_{area} r_w^2 dA \ \text{ and } \ I_{vw} = \int_{area} r_v r_w dA$$

Assuming $\hat{e}_v$ and $\hat{e}_w$ define principal axes, $I_{vw} \equiv 0$. Furthermore, since the center-line of the shaft is the centroid of the cross-sections,

$$\int_{area} r_v dA = \int_{area} r_w dA \equiv 0$$

Finally, the total strain energy in the shaft is given by

$$U = \frac{EA}{2}\int_0^L u_x^2 dx + \frac{EI_v}{2}\int_0^L v_{xx}\left[1 - 3\left(v_x^2 + w_x^2\right)\right]dx + \frac{EI_w}{2}\int_0^L w_{xx}\left[1 - 3\left(v_x^2 + w_x^2\right)\right]$$

An additional contribution to the total potential energy comes from the work done on the system by the external force $P(t)$ applied at $x = L$. This work is defined as follows:

$$W(t) = \vec{P}(t) \cdot \vec{h}(L,t) = P(t)h(L,t)$$

44
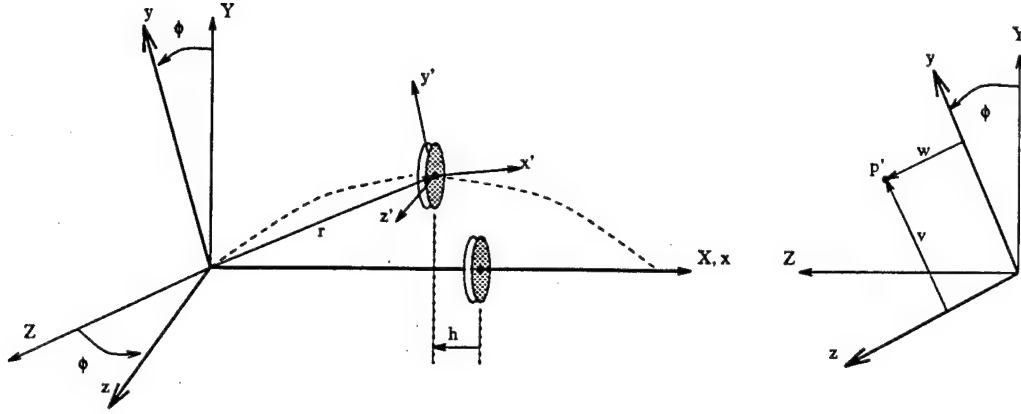
Figure 3.4: Stationary, rotating and body-fixed reference frames.

As defined, the work done by $P(t)$ is positive since $P(t)$ acts in the direction of positive displacement $h(x,t)$. The potential energy generated by this force is

$$\mathcal{V} = -W(t)$$

and the total potential energy is

$$\Pi = U + \mathcal{V}$$

The total kinetic energy of the system is the sum of the translational kinetic energy of the center of mass $T_{c.m.}$ and the kinetic energy due to the rotation of the body about its center of mass T_{rot}. Consider Figure 3.4 depicting the stationary (X, Y, Z), rotating (x, y, z) and body-fixed (x', y', z') coordinate systems. The vector $\vec{r}$ locates the center-line p' at a particular cross-section. In the rotating reference frame, the vector $\vec{r}$ is

$$\vec{r} = (x - h)\hat{e}_x + v\hat{e}_y + w\hat{e}_z$$

where, again, $\hat{e}$ represents a unit vector in the specified direction. By definition,

$$\left(\frac{d\vec{r}}{dt}\right)_{XYZ} = \left(\frac{d\vec{r}}{dt}\right)_{xyz} + \vec{\omega} \times \vec{r}$$

where $\vec{\omega} = \dot{\phi}\hat{e}_x = \Omega\hat{e}_x$ is the angular velocity vector. Taking the appropriate derivative and cross product yields

$$\left(\frac{d\vec{r}}{dt}\right)_{XYZ} = h_t\hat{e}_x + (v_t - \Omega w)\hat{e}_y + (w_t + \Omega v)\hat{e}_z$$

The kinetic energy of the center of mass is

$$T_{c.m.} = \frac{1}{2} \int_{volume} \rho \left|\left(\frac{d\vec{r}}{dt}\right)_{XYZ}\right|^2 dVol = \frac{1}{2} \int_0^L \left[\int_{area} \rho dA\right] \left|\left(\frac{d\vec{r}}{dt}\right)_{XYZ}\right|^2 dx$$

45

In the above expression, ρ is the density of the shaft material and is assumed constant along the length of the shaft. Define m to be the mass per unit length. This yields

$$T_{c.m.} = \frac{m}{2} \int_0^L \left| \left(\frac{d\vec{r}}{dt} \right)_{XYZ} \right|^2 dx$$

or

$$T_{c.m.} = \frac{m}{2} \int_0^L \left[h_t^2 + (v_t - \Omega w)^2 + (w_t + \Omega v)^2 \right] dx \tag{3.2}$$

Consider a volume element $dVol = dA\, dx$ with mass density ρ. The distance from the shaft center-line to the element is given by the vector

$$\vec{r} = y'\hat{e}_{y'} + z'\hat{e}_{z'}$$

Note that the unit vectors $\hat{e}_{y'}$ and $\hat{e}_{z'}$ in the body-fixed frame are identical to $\hat{e}_v$ and $\hat{e}_w$, respectively, used in the derivation of the potential energy. For consistency with Figure 3.4, $\hat{e}_{y'}$ and $\hat{e}_{z'}$ will be used in this section to describe the (x', y', z') coordinate system. The rotational kinetic energy is described by the expression

$$T_{rot} = \frac{1}{2} \int_{volume} \rho \dot{r}^2 dVol$$

where $\dot{r} = \vec{\omega'} \times \vec{r}$ and $\vec{\omega'}$ describes the angular velocity of the element about the displaced center-line. In determining this angular velocity, Choi et al. [16] include the effects of tilting cross-sections. The resulting angular velocity vector has nonzero components in all three coordinate directions of the body-fixed frame. In this analysis, only small deflections in the first mode (in both v and w directions) will be considered. In this situation, the contribution to the kinetic energy from these additional tilting terms is extremely small. Furthermore, the inclusion of these terms adds considerable complexity to the equations of motion. Therefore, in this analysis, the effects of tilting will not be considered. Thus, the angular speed of the element about the deformed center-line is identical to the angular speed of the deformed center-line about its undeformed position. The angular velocity of the element, however, is along $\hat{e}_{x'}$ and is given by $\vec{\omega'} = \dot{\phi}\hat{e}_{x'} = \Omega\hat{e}_{x'}$. Substituting these expressions into T_{rot} yields

$$T_{rot} = \frac{1}{2}\vec{\omega'} \int_{volume} \rho \left[r_2\vec{\omega'} - (\vec{r} \cdot \vec{\omega'})\vec{r} \right] dVol$$

Define the polar mass moment of inertia as

$$J_p = J_{y'} + J_{z'} \quad \text{where} \quad J_{y'} = \int_{area} \rho z'^2 dA, \quad J_{z'} = \int_{area} \rho y'^2 dA$$

and note that since $\hat{e}_{y'}$ and $\hat{e}_{z'}$ are principal axes

$$\int_{area} \rho z'y' dA \equiv 0$$

Finally, the kinetic energy of rotation is given by

$$T_{rot} = \frac{L}{2}J_p\Omega^2 \tag{3.3}$$

46

Combining Eqs. (3.2) and (3.3), the total kinetic energy can be written as

$$T = \frac{m}{2} \int_0^L \left[h_t^2 + (v_t - \Omega w)^2 + (w_t + \Omega v)^2 \right] dx + \frac{L}{2} J_p \Omega^2 \tag{3.4}$$

Hamilton's Principle of Least Action states that the motion of a system from time t_0 to t_1 is such that the integral of the Lagrangian L over this interval has a stationary value for the correct path of the motion [30]. That is, the most desirable (lowest energy) path is the one which makes the variation of this integral zero.

The Lagrangian is

$$L = T - \Pi$$

Let

$$\delta J = \delta \int_{t_0}^{t_1} L \, dt = \delta \int_{t_0}^{t_1} (T - \Pi) \, dt = 0$$

Making the appropriate substitutions and integrating by parts yields an integral containing δu, δv and δw. Since these variations are independent, the corresponding coefficients must all be identically 0 in order to insure the stationarity of J. The partial differential equations of motion are

$$- mh_{tt} + EAu_{xx} = 0 \tag{3.5}$$

$$- m\left(v_{tt} - 2\Omega w_t - \Omega^2 v\right) - (Nv_x)_x$$
$$- EI_v \left(v_{xxxx} - \frac{3}{2} \left[(v_x^2)_{xx} v_x \right]_x - 3 \left[v_{xx} w_x^2 \right]_{xx} \right) - 3EI_w \left[w_{xx}^2 v_x \right]_x = 0 \tag{3.6}$$

$$- m\left(w_{tt} + 2\Omega v_t - \Omega^2 w\right) - (Nw_x)_x$$
$$- EI_w \left(w_{xxxx} - \frac{3}{2} \left[(w_x^2)_{xx} w_x \right]_x - 3 \left[w_{xx} v_x^2 \right]_{xx} \right) - 3EI_v \left[v_{xx}^2 w_x \right]_x = 0 \tag{3.7}$$

with boundary conditions

$$u(0,t) = 0 , \qquad -EAu_x(L,t) + P(t) = 0$$
$$v(0,t) = v(L,t) = 0 \qquad \text{and} \quad w(0,t) = w(L,t) = 0$$

At this point, no assumption is made on the moment or slope at the boundaries. These will be determined by the bearing conditions. In Eqs. (3.6) and (3.7), $N(x,t)$ represents the total axial force, i.e.

$$N(x,t) = P(t) - m \int_x^L h_{tt}(\xi,t) d\xi$$

where $N(x,t)$ is defined to be positive in the negative x-direction. With the aid of Eq. (3.5), $N(x,t)$ may be expressed as a function of $u(x,t)$ instead of $h(x,t)$ as follows:

$$N(x,t) = P(t) - EA \int_x^L u_{\xi\xi}(\xi,t) d\xi$$

47

The equations describing the transverse motion of the shaft depend on the axial displacement $u(x,t)$. Equation (3.5) can be written explicitly in terms of $u(x,t)$ as

$$u_{tt} - \alpha^2 u_{xx} = -f(x,t) \tag{3.8}$$

where

$$\alpha^2 = \frac{EA}{m} \quad \text{and} \quad f(x,t) = \frac{1}{2}\frac{\partial^2}{\partial t^2}\int_0^x \left(v_\xi^2(\xi,t) + w_x^2(\xi,t)\right) d\xi$$

The boundary and initial conditions are

$$u(0,t) = 0 \quad, \quad u_x(L,t) = \frac{P(t)}{EA} = \frac{P_0 + H(t)\mu\cos\nu t}{EA} = f_0(t)$$

$$u(x,0) = \frac{P_0 x}{EA} \quad \text{and} \quad u_t(x,0) = 0 \tag{3.9}$$

The solution of Eq. (3.8) presents severe difficulties due to the presence of $f(x,t)$. This term arises from the motion of the end point where the axial load is applied. As stated above, the longitudinal motion of a point on the shaft is the combined effect of compression as well as longitudinal motion induced by lateral displacements. The effect of bending is to shift points on the center line toward $x = 0$. The term $f(x,t)$ describes the effect of this lateral motion on the acceleration (in the x direction) of a point on the center-line. It is easy to see that this contribution to the longitudinal acceleration is on the order of the acceleration in the lateral direction. Since only small center-line deflections are being considered here, the velocities and accelerations in the lateral directions are extremely small when compared to the velocity u_t or acceleration u_{tt} of a compression wave traveling along the axis of the shaft. Thus, the major contribution to the dynamics in the axial direction results from axial compression and not lateral motion. For this reason, the effects of lateral displacements in Eq. (3.8) governing the dynamics in the longitudinal direction may be neglected. The solution of Eq. (3.8) with $f(x,t) = 0$, given by Bolotin [14], is

$$u(x,t) = \frac{P_0 x}{EA}\left(\frac{\alpha\mu}{\nu\cos\frac{\nu L}{\alpha}}\right) H(t)\cos\nu t\,\sin\frac{\nu x}{\alpha} \tag{3.10}$$

In order to simplify the analysis, it is desirable to reduce Eqs. (3.6) and (3.7) from partial differential equations to a set of ordinary differential equations using some a priori knowledge of the response. This reduction can be accomplished via several techniques. Two of these techniques, the Galerkin method and the Rayleigh-Ritz method, will be employed and the resulting ordinary differential equations of motion will be compared. For details of each of these methods, see, for example, Forray [29], Stakgold [84] and Zauderer [92].

First consider the Galerkin approach in which the following system of (possibly nonlinear) partial differential equations of motion are given:

$$\mathcal{F}_i\left(v(x,t), w(x,t)\right) = 0\,, \quad i = 1,2 \tag{3.11}$$

with some specified boundary conditions. Suppose $v(x,t)$ and $w(x,t)$ can be approximated by

$$v_n(x,t) = q_1(t)\phi(x) \quad \text{and} \quad w_n(x,t) = q_2(t)\phi(x) \tag{3.12}$$

48

where $\phi(x)$ is chosen such that $v_n(x,t)$ and $w_n(x,t)$ satisfy the given boundary conditions. While these approximations satisfy the boundary conditions, they do not necessarily satisfy Eq. (3.11). Thus

$$\mathcal{F}_i\left(v_n(x,t), w_n(x,t)\right) = R_{n_i}(x) \,, \quad i = 1, 2$$

where $R_{n_i}(x)$ represents the residual, or error. In the vibratory response of a mechanical system, all modes of vibration are present. Thus, if instead the functions $v(x,t)$ and $w(x,t)$ are represented by infinite series, i.e.

$$v(x,t) = \sum_{k=1}^{\infty} q_1(t)\phi_k(x) \quad \text{and} \quad w(x,t) = \sum_{k=1}^{\infty} q_2(t)\phi_k(x)$$

where $\phi_k(x)$ describes the shape of the kth mode, then the residual term vanishes. However, consideration of an infinite number of modes is not feasible. Hence, attention here is focused on the loss of stability of the trivial solution of Eq. (3.11) and the subsequent emergence of first mode $(k = 1)$ oscillations which dominate the response near subharmonic and combination resonances. For this analysis, the approximations given in Eq. (3.12) are sufficient with q_1 and q_2 representing the time-dependent amplitudes of vibration of the center-line in the v and w directions, respectively.

The Galerkin method requires that the residual $R_{n_i}(x)$ be orthogonal to the coordinate function $\phi(x)$ over the entire coordinate domain. This implies

$$\int_0^L R_{n_i}(x)\phi(x)dx = 0 \,, \quad i = 1, 2$$

or equivalently

$$\int_0^L \mathcal{F}_i\left(v_n(x,t), w_n(x,t)\right)\phi(x)dx = 0 \,, \quad i = 1, 2$$

Application of this method to Eqs. (3.6) and (3.7) yields

$$m\left[\ddot{q}_1 - 2\Omega\dot{q}_2 - \Omega^2 q_1\right]\int_0^L \phi^2 dx$$

$$+EI_v\left[q_1\int_0^L \phi_{xxxx}\phi dx - \frac{3}{2}q_1^3\int_0^L \left[(\phi_x^2)_{xx}\phi_x\right]_x \phi dx - 3q_1 q_2^2\int_0^L \left[\phi_{xx}\phi_x^2\right]_{xx}\phi dx\right]$$

$$+3EI_w q_1 q_2^2\int_0^L \left[\phi_{xx}^2\phi_x\right]_x \phi dx + q_1\int_0^L [N\phi_x]\phi dx = 0$$

$$m\left[\ddot{q}_2 + 2\Omega\dot{q}_1 - \Omega^2 q_2\right]\int_0^L \phi^2 dx$$

$$+EI_w\left[q_2\int_0^L \phi_{xxxx}\phi dx - \frac{3}{2}q_2^3\int_0^L \left[(\phi_x^2)_{xx}\phi_x\right]_x \phi dx - 3q_1^2 q_2\int_0^L \left[\phi_{xx}\phi_x^2\right]_{xx}\phi dx\right]$$

$$+3EI_v q_1^2 q_2\int_0^L \left[\phi_{xx}^2\phi_x\right]_x \phi dx + q_2\int_0^L [N\phi_x]\phi dx = 0$$

Using the following identities

$$\int_0^L \left[\phi_{xx}\phi_x^2\right]_{xx}\phi dx = -\int_0^L \left[\phi_{xx}^2\phi_x\right]_x \phi dx = \int_0^L \phi_x^2\phi_{xx}^2 dx$$

$$\int_0^L \left[(\phi_x^2)_{xx}\phi_x \right]_x \phi \, dx = 4 \int_0^L \phi_x^2 \phi_{xx}^2 \, dx$$

$$\int_0^L \phi_{xxxx}\phi \, dx = \int_0^L \phi_{xx}^2 \, dx$$

and

$$\int_0^L \left[N\phi_x \right] \phi \, dx = -P(t) \int_0^L \phi_x^2 \, dx + EA \int_0^L \left\{ \int_x^L u_{\xi\xi} d\xi \right\} \phi_x^2 \, dx$$

the above equations of motion may be rewritten as

$$m \left[\ddot{q}_1 - 2\Omega\dot{q}_2 - \Omega^2 q_1 \right] \int_0^L \phi^2 \, dx$$

$$+ EI_v \left[q_1 \int_0^L \phi_{xx}^2 \, dx - 3q_1 \left(2q_1^2 + q_2^2 \right) \int_0^L \phi_x^2 \phi_{xx}^2 \, dx \right] - 3EI_w q_1 q_2^2 \int_0^L \phi_x^2 \phi_{xx}^2 \, dx$$

$$- Pq_1 \int_0^L \phi_x^2 \, dx + q_1 EA \int_0^L \left\{ \int_x^L u_{\xi\xi} d\xi \right\} \phi_x^2 \, dx = 0 \qquad (3.13)$$

$$m \left[\ddot{q}_2 + 2\Omega\dot{q}_1 - \Omega^2 q_2 \right] \int_0^L \phi^2 \, dx$$

$$- 3EI_v q_1^2 q_2 \int_0^L \phi_x^2 \phi_{xx}^2 \, dx + EI_w \left[q_2 \int_0^L \phi_{xx}^2 \, dx - 3q_2 \left(q_1^2 + 2q_2^2 \right) \int_0^L \phi_x^2 \phi_{xx}^2 \, dx \right]$$

$$- Pq_2 \int_0^L \phi_x^2 \, dx + q_2 EA \int_0^L \left\{ \int_x^L u_{\xi\xi} d\xi \right\} \phi_x^2 \, dx = 0 \qquad (3.14)$$

Next consider the Rayleigh-Ritz approach. Again, assume that only the first mode (in each of the principal directions) is excited by the parametric forcing $P(t)$. The above system of partial differential Eqs. (3.6) and (3.7) may be reduced to a set of ordinary differential equations by employing the approximations

$$v_n(x,t) = q_1(t)\phi(x) \quad \text{and} \quad w_n(x,t) = q_2(t)\phi(x)$$

where $\phi(x)$ describes the mode shape of the first mode and q_1 and q_2 represent the time-dependent amplitudes of vibration of the center-line in the v and w directions, respectively. The function $\phi(x)$ is identical to that used in the Galerkin approach. Unlike the Galerkin approach, however, application of the Rayleigh-Ritz method requires the existence of a functional in the form of a definite integral which is to be made stationary. This is the basis of Hamilton's Principle which was employed above in deriving Eqs. (3.6) and (3.7). Therefore, the functional for this problem is J, the time integral of the Lagrangian.

The approximations $v_n(x,t)$ and $w_n(x,t)$ are then substituted into the Lagrangian for $v(x,t)$ and $w(x,t)$. Note that in solving Eq. (3.8) for the axial displacement, the term

$$f(x,t) = \frac{1}{2}\frac{\partial^2}{\partial t^2} \int_0^x \left(v_\xi^2(\xi,t) + w_x^2(\xi,t) \right) d\xi$$

was neglected since the longitudinal inertia associated with lateral vibrations is small. This term appears in the translational kinetic energy and in the Lagrangian through the square of the axial

velocity, i.e.

$$h_t^2 = u_t^2 + 2u_t \left(q_1\dot{q}_1 + q_2\dot{q}_2\right) \int_0^x \phi_\xi^2 d\xi + \left(q_1\dot{q}_1 + q_2\dot{q}_2\right)^2 \left(\int_0^x \phi_\xi^2 d\xi\right)^2$$

In this expression, u_t represents the velocity of the axial compression wave which is, in general, very large. The second term is the product of a large quantity (the velocity of the compression wave) and a very small quantity resulting from longitudinal motion induced by lateral vibrations. For consistency in the derivation, this term will be retained. The last term is small and will be neglected in the Lagrangian. The resulting Lagrangian is

$$\begin{aligned}
L = \int_0^L \Bigg\{ &\frac{m}{2}\left[u_t^2 + (\dot{q}_1 - \Omega q_2)^2\,\phi^2(x) + (\dot{q}_2 + \Omega q_1)^2\,\phi^2(x) + \frac{1}{2}\Omega^2 J_p\right] \\
&+ \frac{m}{2}\left[2u_t\left(q_1\dot{q}_1 + q_2\dot{q}_2\right)\int_0^x \phi_\xi^2 d\xi + (q_1\dot{q}_1 + q_2\dot{q}_2)^2\left(\int_0^x \phi_\xi^2 d\xi\right)^2\right] \\
&- \frac{EA}{2}u_x^2 - \frac{E}{2}\left(I_v q_1^2 + I_w q_2^2\right)\phi_{xx}^2(x)\left[1 - 3\left(q_1^2 + q_2^2\right)\phi_x^2(x)\right] \\
&+ \frac{P(t)}{2}\left(q_1^2 + q_2^2\right)\phi_x^2(x)\Bigg\} dx + P(t)u(L,t) \qquad (3.15)
\end{aligned}$$

In the above expression, the ($\dot{}$) represents the total derivative with respect to time, $()_x$ represents the total derivative with respect to the longitudinal coordinate and, as before, $()_t$ denotes the partial derivative with respect to time.

The Lagrangian equations of motion are obtained using

$$\frac{d}{dt}\left(\frac{\partial L}{\partial \dot{q}_i}\right) - \frac{\partial L}{\partial q_i} = Q_i, \quad i = 1, 2 \qquad (3.16)$$

where q_i are the generalized coordinates and Q_i represent the generalized forces which are not derivable from a potential function. This term includes the effects of internal and external damping. At this point, only forces derivable from a potential have been considered. In the absence of dissipation, the equations of motion become

$$\begin{aligned}
m\;&\left[\ddot{q}_1 - 2\Omega\dot{q}_2 - \Omega^2 q_1\right]\int_0^L \phi^2 dx \\
&+ EI_v\left[q_1\int_0^L \phi_{xx}^2 dx - 3q_1\left(2q_1^2 + q_2^2\right)\int_0^L \phi_x^2\phi_{xx}^2 dx\right] - 3EI_w q_1 q_2^2\int_0^L \phi_x^2\phi_{xx}^2 dx \\
&- Pq_1\int_0^L \phi_x^2 dx + EAq_1\int_0^L \left(\int_0^x u_{\xi\xi}d\xi\right)\phi_x^2 dx = Q_1 \qquad (3.17) \\
m\;&\left[\ddot{q}_2 + 2\Omega\dot{q}_1 - \Omega^2 q_2\right]\int_0^L \phi^2 dx \\
&- 3EI_v q_1^2 q_2\int_0^L \phi_x^2\phi_{xx}^2 dx + EI_w\left[q_2\int_0^L \phi_{xx}^2 dx - 3q_2\left(q_1^2 + 2q_2^2\right)\int_0^L \phi_x^2\phi_{xx}^2 dx\right] \\
&- Pq_2\int_0^L \phi_x^2 dx + EAq_2\int_0^L \left(\int_0^x u_{\xi\xi}d\xi\right)\phi_x^2 dx = Q_2 \qquad (3.18)
\end{aligned}$$

In the above equations, the following substitution (found by integrating by parts) was used

$$m\int_0^L \left(\int_0^x \phi_\xi^2 d\xi\right)u_{tt}\,dx = EA\int_0^L \left(\int_0^x \phi_\xi^2 d\xi\right)u_{xx}\,dx = EA\int_0^L \left(\int_0^x u_{\xi\xi}d\xi\right)\phi_x^2\,dx$$

The Lagrangian equations of motion are identical to those obtained using the Galerkin approach. This is to be expected due to the presence of a functional which is to be minimized in order to obtain the governing equations. In such cases, the equations of motion derived via one of these methods may be obtained by performing integration by parts on the equations obtained using the alternate procedure.

Letting

$$\Phi_1 = \int_0^L \phi^2 dx \ , \quad \Phi_2 = \int_0^L \phi_x^2 dx \ , \quad \Phi_3 = \int_0^L \phi_{xx}^2 dx \ , \quad \Phi_4 = \int_0^L \phi_x^2 \phi_{xx}^2 dx$$

and dividing through by $m\Phi_1$ yields

$$M\ddot{q} + 2G\dot{q} + Kq + F(q,t) = Q \tag{3.19}$$

where q is the vector of generalized coordinates $(q_1, q_2)^T$, Q is the vector of generalized forces $(Q_1, Q_2)^T$, M is the 2×2 identity matrix, G represents terms arising from gyroscopic effects and K contains stiffness terms, i.e.

$$G = \begin{bmatrix} 0 & -\Omega \\ \Omega & 0 \end{bmatrix} \quad \text{and} \quad K = \begin{bmatrix} k_1 & 0 \\ 0 & k_2 \end{bmatrix}$$

The stiffness coefficients may be written as $k_i = \tilde{\omega}_i - \Omega^2$ where

$$\tilde{\omega}_1 = \frac{EI_v \Phi_3}{m\Phi_1} - \frac{\Phi_2}{m\Phi_1} P_0 = \bar{\omega}_1^2 - P^*$$

$$\tilde{\omega}_2 = \frac{EI_w \Phi_3}{m\Phi_1} - \frac{\Phi_2}{m\Phi_1} P_0 = \bar{\omega}_2^2 - P^*$$

The term $\bar{\omega}_i$ corresponds to the natural frequency in the ith direction in the absence of a static axial load, i.e. when $P_0 = 0$.

The function $F(q,t)$ consists of nonlinearities and forces which are derivable from a time-dependent potential $U(q,t)$, i.e.

$$F(q,t) = \frac{\partial U(q,t)}{\partial q}$$

The potential $U(q,t)$ is given by

$$U(q,t) = -\frac{3E\Phi_4}{2m\Phi_1} \left\{ I_v q_1^4 + (I_v + I_w) q_1^2 q_2^2 + I_w q_2^4 \right\}$$

$$- \frac{\Phi_2}{2m\Phi_1} \psi \mu H(t) \cos \nu t \left[q_1^2 + q_2^2 \right]$$

with

$$\psi = \int_0^L \frac{\cos \frac{\nu x}{\alpha}}{\cos \frac{\nu L}{\alpha}} \phi_x^2 dx$$

In the following section, the effects of internal and external damping on the equations of motion will be examined.

3.2.1 Dissipation

In addition to the conservative forces and time-dependent forces which are derivable from a potential, virtually all mechanical systems contain some mechanism by which energy is dissipated during vibration. These mechanisms are not fully understood and, as a result, the mathematical models describing the dissipation vary. Ultimately, the problem reduces to the addition of suitable terms to the governing equations such that the behavior observed analytically or through numerical simulation closely approximates that observed experimentally.

In the current analysis, the effects of dissipation are decomposed into external and internal damping. External damping may refer to the influence of friction, aerodynamic drag or other outside forces absorbing energy from the moving body, while internal damping describes the conversion of kinetic and strain energy in a vibratory mechanical system into heat. Both effects are included in Q_i on the right hand side of the Lagrangian equations of motion, Eq. (3.16). Note from Eq. (3.16) that Q_1 corresponds to generalized dissipation forces in the v direction and Q_2 to the w direction. Furthermore, let Q_{i-ext} describe external damping forces in the ith direction and Q_{i-int} describe internal damping forces in the ith direction.

First consider the effects of external damping. Recall Figure 3.4 and let F_Y and F_Z be the Y and Z components of the external damping. The generalized force Q_i associated with the generalized coordinate q_i is given by

$$Q_i = \sum_{j=1}^{n} F_j \frac{\partial \xi_j}{\partial q_i}$$

where n is the number of generalized coordinates and ξ_j represents the original coordinate system. Employ the transformation

$$\left\{ \begin{array}{c} Y \\ Z \end{array} \right\} = \left[\begin{array}{cc} \cos \Omega t & -\sin \Omega t \\ \sin \Omega t & \cos \Omega t \end{array} \right] \left\{ \begin{array}{c} v \\ w \end{array} \right\}$$

Assuming the external damping to be proportional to the velocity of the shaft center-line in the stationary frame, F_Y and F_Z can be expressed as

$$F_Y = -m d_e \dot{Y} \quad \text{and} \quad F_Z = -m d_e \dot{Z}, \quad d_e > 0$$

where d_e is the coefficient of external damping and $\dot{Y}$ and $\dot{Z}$ represent the components of the center-line velocity in the stationary frame. The negative sign indicates that the force is opposing the motion. Note that since m is mass per unit length, F_Y and F_Z are in units of force per unit length. Therefore, in order to determine the overall effect of external damping, the expressions for F_Y and F_Z must be integrated over the entire length of the shaft. The resulting generalized external damping forces are

$$
\begin{aligned}
Q_{1-ext} &= -m d_e \int_0^L (\dot{v} - \Omega w)\, dx \\
Q_{2-ext} &= -m d_e \int_0^L (\dot{w} + \Omega v)\, dx
\end{aligned}
$$

(3.20)

Assume a linear internal damping model in which the generalized forces associated with this dissipation are proportional to the velocities in the rotating frame, i.e.

$$Q_{1-int} = -m \zeta_1 \int_0^L \dot{v}\, dx \quad \text{and} \quad Q_{2-int} = -m \zeta_2 \int_0^L \dot{w}\, dx$$

In the above expressions, ζ_1 and ζ_2 are the coefficients of viscous damping in the two principal directions. Finally, the equations of motion including the effects of internal and external dissipation are given by Eqs. (3.17) and (3.18) with $Q_i = Q_{i-ext} + Q_{i-int}$, i.e.

$$Q_1 = -m\left[(d_e + \zeta_1)\dot{q}_1 - d_e\Omega q_2\right]\int_0^L \phi\,dx$$

$$Q_2 = -m\left[(d_e + \zeta_2)\dot{q}_2 + d_e\Omega q_1\right]\int_0^L \phi\,dx$$

In the following subsections, ordinary differential equations for simply supported and fixed-end shafts are derived using appropriate expressions for the shape function $\phi(x)$.

The choice of a linear internal damping model is justifiable in this situation since only small lateral displacements are considered. Thus, the contributions of the nonlinearities in a nonlinear model would be negligible. This choice is also convenient from the experimental system identification perspective since the identification techniques generally yield the coefficients of linear damping models.

3.2.2   Simply Supported And Fixed-End Shafts

The Rayleigh-Ritz or Galerkin approach yields the following general equation for the amplitudes $q_1(t)$ and $q_2(t)$:

$$M\ddot{q} + 2G\dot{q} + Kq + F(q,t) = Q \tag{3.21}$$

where Q is the vector of generalized forces $(Q_1, Q_2)^T$,

$$M = \begin{bmatrix} 1 & 0 \\ 0 & 1 \end{bmatrix}, \quad G = \begin{bmatrix} 0 & -\Omega \\ \Omega & 0 \end{bmatrix} \quad \text{and} \quad K = \begin{bmatrix} k_1 & 0 \\ 0 & k_2 \end{bmatrix}$$

The stiffness coefficients may be written as $k_i = \tilde{\omega}_i - \Omega^2$ where

$$\tilde{\omega}_1 = \frac{EI_v}{m}\left(\frac{\pi}{L}\right)^4 - \frac{\Phi_2}{m\Phi_1}P_0$$

$$\tilde{\omega}_2 = \frac{EI_w}{m}\left(\frac{\pi}{L}\right)^4 - \frac{\Phi_2}{m\Phi_1}P_0$$

The vector of nonlinear and periodic terms is

$$F(q,t) = -\frac{6E\Phi_4}{m\Phi_1}\begin{bmatrix} I_v & 0 \\ 0 & I_w \end{bmatrix}\begin{Bmatrix} q_1^3 \\ q_2^3 \end{Bmatrix} - \frac{3E\Phi_4}{m\Phi_1}(I_v + I_w)\begin{Bmatrix} q_1 q_2^2 \\ q_1^2 q_2 \end{Bmatrix}$$
$$- \frac{\Phi_2}{m\Phi_1}(\psi\mu\cos\nu t)\begin{Bmatrix} q_1 \\ q_2 \end{Bmatrix}$$

The dissipation terms are given by

$$Q_1 = -m\left[(d_e + \zeta_1)\dot{q}_1 - d_e\Omega q_2\right]\Phi_0$$
$$Q_2 = -m\left[(d_e + \zeta_2)\dot{q}_2 + d_e\Omega q_1\right]\Phi_0$$

where

$$\Phi_0 = \int_0^L \phi dx$$

The boundary conditions on the lateral motion determine the shape functions for each mode of vibration. The shape functions, in turn, provide the values for the coefficients in the equations governing $q_1(t)$ and $q_2(t)$. In the current analysis, the equations of motion for both simply supported (or pinned-pinned) and fixed-end (clamped-clamped) rotating shafts are presented. In subsequent chapters, the local and global stability of the shaft under both end conditions will be presented.

Pinned-Pinned Shaft

The simply supported shaft is one for which the ends are allowed to pivot in all directions. Hence, no moment is applied to the ends of the shaft by the support. A physical representation of such a system can be seen in shafts (or pipes) held in universal joints or bearing systems that are allowed to rotate with the shaft.

For this type of end condition, the shape function for the first mode must satisfy the following boundary conditions:

$$v(0,t) = v(L,t) = 0 \quad \text{and} \quad v_{xx}(0,t) = v_{xx}(L,t) = 0$$

$$w(0,t) = w(L,t) = 0 \quad \text{and} \quad w_{xx}(0,t) = w_{xx}(L,t) = 0$$

This leads to the mode shape approximation

$$\phi(x) = \sin \frac{\pi x}{L}$$

The equations of motion for this system are given by Eq. (3.21) with

$$\Phi_0 = \frac{2L}{\pi}, \quad \Phi_1 = \frac{L}{2}, \quad \Phi_2 = \frac{\pi^2}{2L}, \quad \Phi_3 = \left(\frac{\pi}{L}\right)^4 \Phi_1, \quad \Phi_4 = 4\pi \left(\frac{\pi}{2L}\right)^5$$

Clamped-clamped Shaft

The clamped-clamped, or fixed-end, support represents a shaft operating in a rigid bearing which prohibits any angular motion at the boundary. For the case in which the ends are clamped, the boundary conditions to be satisfied are

$$v(0,t) = v(L,t) = 0 \quad \text{and} \quad v_x(0,t) = v_x(L,t) = 0$$

$$w(0,t) = w(L,t) = 0 \quad \text{and} \quad w_x(0,t) = w_x(L,t) = 0$$

Thus, the shape function for the first mode can be expressed as [65]

$$\phi(x) = c_n \left(\cos \frac{\eta x}{L} - \cosh \frac{\eta x}{L} \right) (\sin \eta - \sinh \eta)$$
$$- \left(\sin \frac{\eta x}{L} - \sinh \frac{\eta x}{L} \right) (\cos \eta - \cosh \eta)$$

where η satisfies

$$\cos \eta \cosh \eta = 1$$

55

and c_n is a normalizing constant, i.e. $c_n \phi(L/2) = 1$. It can easily be shown that $\eta^2 = \omega \sqrt{\frac{L^4 m}{EI}}$. For the first mode of vibration of a clamped shaft, $\eta = 22.37$ corresponds to a first mode natural frequency of $\omega = 22.37 \sqrt{\frac{EI}{L^4 m}}$ where the appropriate moment of inertia must be used to obtain the natural frequency of vibration in the desired direction. The equations of motion for this system are given by Eq. (3.21) with

$$\Phi_0 = 0.5322\, L\,, \quad \Phi_1 = 0.3965\, L\,, \quad \Phi_2 = \frac{4.8777}{L}$$

$$\Phi_3 = \left(\frac{\eta}{L}\right)^4 \Phi_1\,, \quad \Phi_4 = 6.0497 \left(\frac{\eta}{2L}\right)^5 \quad \text{and} \quad c_n = 0.010923$$

3.3 Hamiltonian Equations of Motion

In deriving the Lagrangian equations of motion, it was not necessary to make any assumptions on the magnitude of the excitation or dissipation terms. However, if these quantities are assumed to be small, i.e. $O(\varepsilon), |\varepsilon| \ll 1$, then the system is nearly conservative and its dynamic response may be investigated via a Hamiltonian approach. The advantage of this approach lies in the fact that, under this formulation, the canonical structure of the undamped equations of motion is preserved. This structure is desirable since, in many cases, it significantly reduces the amount of algebraic manipulation required. Furthermore, the integrable structure of the Hamiltonian system of equations lends itself to the application of certain perturbation techniques used in predicting the global behavior of the system.

Throughout this work it is assumed that the dissipation, imperfections and amplitudes of parametric excitations are small. Thus, one can treat the proposed problems as weakly Hamiltonian systems. Most of the analysis is based on the recent work of perturbed Hamiltonian systems. Since, in the Hamiltonian treatment, the momenta p and the coordinates q constitute $2n$ independent variables, Hamilton's equations allow a much wider range of transformations than the point transformations. This enlargement of the class of possible transformations, which includes all $2n$ independent variables p and q, is one of the important advantages of the Hamiltonian treatment. Recent results on persistence of quasiperiodic motions will also enable us to develop global techniques to detect complicated dynamics.

Employing a Legendre transformation yields a set of $2n$ first order equations for the generalized coordinates q and conjugate momenta p. These equations are given by

$$\dot{q} = \frac{\partial H(q,p,t)}{\partial p} \quad \text{and} \quad \dot{p} = -\frac{\partial H(q,p,t)}{\partial q} + Q$$

where Q consists of all generalized forces which are not derivable from a potential. The Hamiltonian $H(q,p,t)$ represents the total energy of the system when all the forces are derivable from a conservative potential. The function $H(q,p,t)$ is determined by first calculating the Lagrangian. Let the kinetic and potential energies of the system be given by

$$T = \frac{1}{2}\dot{q}^T M \dot{q} + \dot{q}^T G q \quad \text{and} \quad V = \frac{1}{2} q^T K q + U(q,t)$$

where M, G, K and $U(q,t)$ are given above. In terms of these quantities, the Lagrangian of Eq. (3.15) becomes

$$L = T - V = \frac{1}{2}\dot{q}^T M \dot{q} + \dot{q}^T G q - \frac{1}{2} q^T K q - U(q,t)$$

56

The momenta may then be obtained from the Lagrangian as

$$p = \frac{\partial L(q, \dot{q}, t)}{\partial \dot{q}} = M\dot{q} + Gq$$

Rearranging yields

$$\dot{q} = M^{-1}(p - Gq)$$

Substituting this expression for the generalized coordinate back into the Lagrangian and noting the relationship

$$H(q, p, t) = p^T \dot{q} - L(q, \dot{q}(q, p), t)$$

the Hamiltonian, a scalar function of q and p, is

$$H(q, p, t) = \frac{1}{2} p^T M^{-1} p - p^T Gq + \frac{1}{2} q^T Cq + U(q, t) \tag{3.22}$$

where $C = G^T M^{-1} G + K$. The equation for the momenta can be obtained from the Hamiltonian as

$$\dot{p} = G^T (M^{-1})^T p - Cq - \frac{\partial U(q, t)}{\partial q} + Q$$

Let $z = (q_1, q_2, p_1, p_2)^T$. The time dependent Hamiltonian can be decomposed into a quadratic autonomous component and a component consisting of quadratic nonautonomous as well as higher order autonomous terms, i.e.

$$H(z, t) = H_0(z) + H_1(z, t)$$

where

$$H_0(z) = \frac{1}{2} z^T S z, \quad S = \begin{bmatrix} \tilde{\omega}_1 & 0 & 0 & -\Omega \\ 0 & \tilde{\omega}_2 & \Omega & 0 \\ 0 & \Omega & 1 & 0 \\ -\Omega & 0 & 0 & 1 \end{bmatrix}$$

and $H(z, t) = U(q(z), t)$. The equations of motion in the z coordinates are

$$\dot{z} = JSz + J\frac{\partial H_1(z, t)}{\partial z} - Bz \tag{3.23}$$

where J is the symplectic matrix

$$J = \begin{bmatrix} \mathbf{0} & I \\ -I & \mathbf{0} \end{bmatrix}$$

I is the 2×2 identity matrix and $\mathbf{0}$ is a 2×2 zero matrix. The matrix B represents the forces not derivable from a potential, i.e.

$$B = -\begin{bmatrix} \mathbf{0} & \mathbf{0} \\ \bar{D}_2 & \bar{D}_1 \end{bmatrix}$$

where

$$\bar{D}_1 = -\frac{\Phi_5}{\Phi_1} \begin{bmatrix} d_e + \zeta_1 & 0 \\ 0 & d_e + \zeta_2 \end{bmatrix} \quad \text{and} \quad \bar{D}_2 = -\frac{\Phi_5 \Omega}{\Phi_1} \begin{bmatrix} 0 & -\zeta_1 \\ \zeta_2 & 0 \end{bmatrix}$$

57

3.4 Conclusions

In this chapter, the equations governing the longitudinal and transverse vibrations of a rotating shaft subject to a time dependent axial load were derived. Although similar equations have been obtained previously by various authors, as indicated by the references cited in Section 3.1, this derivation is presented here for completeness. These equations were derived with the specific example of the rotating shaft in mind, yet the results are fairly general in the scope of gyroscopic systems. For example, these equations may also describe the transverse vibrations of a pipe conveying fluid with non-steady flow velocity. Hence, a wide variety of mechanical systems may be modeled by these equations with only slight modifications.

The primary motivation for deriving mathematical models of dynamical systems is the hope that these will provide valuable insight into the behavior, reliability and failure mechanisms of practical devices. Since the functionality of a component is the over-riding concern of designers, these models play an important role in predicting system behavior as well as outlining the limits of safe, or stable, operation. To this end, the derivation outlined in this chapter is only a starting point for the stability analysis to be presented in Chapters 4. In Chapter 4, the stability of the system in the neighborhood of a fixed point or limit cycle (local stability) will be examined. Parametric excitation terms are known to induce instabilities at certain *resonant* frequencies. Thus, in Chapter 4, the stability of the system developed in this chapter will be analyzed when the frequency of parametric excitation is near a system resonance. The results obtained are valid only in a small neighborhood of state space surrounding the fixed point, or in a small neighborhood of the parameter at which a fixed point or limit cycle undergoes a bifurcation.

Chapter 4

LOCAL NONLINEAR ANALYSIS OF GYROSCOPIC SYSTEMS

4.1   Introduction

In dynamical systems theory, it is often possible to bring a set of time-dependent equations to an *equivalent* set of autonomous equations via an asymptotic approximation. The theory of averaging, originally due to Krylov and Bogoliubov [52], provides such a method. The resulting set of averaged equations are *equivalent* to the original equations in the sense that the essential dynamics of the original system are preserved. Intuitively, this implies that the response of a given system to external excitation is determined more by the average influence than the fluctuations about the average. The aim of the averaging method is to establish the fact that the exact solution and the first approximation remain within $O(\varepsilon)$ of each other over time intervals of length $O(1/\varepsilon)$ where $\varepsilon \ll 1$. It is important to note that the results obtained from the method of averaging are valid only in a small region surrounding the fixed point. For detailed discussions of the method of averaging, see Hale [34], Sanders and Verhulst [75], Guckenheimer and Holmes [32] and Murdock [64].

The method of averaging, as described in Chapter 1, applies to T-periodic systems of the form

$$\dot{x} = \varepsilon f(x,t) \tag{4.1}$$

This is known as the standard form for this method. In such systems, the time evolution of solutions is "slow" in comparison to the T-periodic excitation due to the $O(\varepsilon)$ vector field. Averaging brings the above equations to the following set of autonomous differential equations:

$$\dot{y} = \varepsilon f_0(y) , \quad f_0(y) = {}_{t}^{M}\{f(y,t)\} \tag{4.2}$$

where ${}_{t}^{M}\{\cdot\}$ is the averaging operator defined as

$$
{}_{t}^{M}\{\cdot\} = \lim_{T \to \infty} \frac{1}{T} \int_{0}^{T} \{\cdot\}\, dt
$$

The study of the bifurcation behavior in a small region of state space surrounding the fixed point (or limit cycle) or in a small neighborhood of the bifurcation point is referred to as local analysis. In a local bifurcation, the stability of one fixed point or limit cycle is lost and a branching, or bifurcating, solution emerges. These local bifurcation scenarios are described by the dynamics in the variational equations.

59

In this chapter, the local stability and bifurcation behavior of a gyroscopic system subjected to periodic parametric excitation will be analyzed. Although the results obtained are valid for general parametrically excited gyroscopic systems, the motivating engineering problem is the lateral vibration of a rotating shaft. This example will be employed to interpret the general results. The method of averaging will be applied to obtain a set of autonomous ordinary differential equations. The stability of the trivial (non-vibratory) solution will be examined and the stability boundaries under various parametric resonance conditions will be determined. These boundaries are given in terms of the amplitude and frequency of the parametric excitation $P(t)$. The post-critical nontrivial solution branches will also be calculated.

4.2 Stability of the Linear System

The Hartman-Grobman Theorem (see, for example, Guckenheimer and Holmes [32]) states that if the Jacobian of the linear part of a set of nonlinear ordinary differential equations has no zero or purely imaginary eigenvalues, i.e. if the fixed points are hyperbolic, then the eigenvalues of this Jacobian are sufficient to determine the stability of the full nonlinear system. Hence in computing the stability boundaries, it is only necessary to consider the linear terms in the averaged equations of motion.

In the absence of a time dependent parameter, the stability of the linear system is determined simply by the location of the eigenvalues. Consider the linear system given by

$$x' = Ax , \quad x \in \mathbf{R}^d$$

The only steady state associated with this system is the trivial solution. If the eigenvalues of the matrix A are λ_i, $i = 1, \cdots, d$, the characteristic equation can be written as

$$\lambda^d + \sum_{i=1}^{d}(-1)^i c_i \lambda^{d-i} = 0$$

For the four-dimensional system under consideration, this reduces to

$$\lambda^4 - c_1 \lambda^3 + c_2 \lambda^2 - c_3 \lambda + c_4 = 0$$

where

$$
\begin{aligned}
c_1 &= \sum_i \lambda_i , \quad c_2 = \sum_{i,j} \lambda_i \lambda_j \\
c_3 &= \sum_{i,j,k} \lambda_i \lambda_j \lambda_k , \quad c_4 = \lambda_1 \lambda_2 \lambda_3 \lambda_4
\end{aligned}
$$

(see, for example, Abramowitz and Stegun [1]). The manner in which the system loses stability depends on how the eigenvalues cross into the right half plane. The various scenarios are summarized in Table 4.1. In Table 4.1, the spectrum of the critical eigenvalues is given along with necessary and sufficient conditions on the coefficients such that this eigenvalue configuration is attained. It is assumed that the rest of the eigenvalues have negative real parts where the notation $\Re(\lambda)$ denotes the real part of λ.

60

Critical Eigenvalue Spectrum	Condition (necessary & sufficient)
$\lambda_1 = 0$	$c_4 = 0$
$\lambda_1 = \lambda_2 = 0$	$c_3 = c_4 = 0$
$\Re(\lambda_i) = 0,\ i = 1, 2$	$c_1 \neq 0,\ c_3 \neq 0$ $c_1/c_3 > 0$ and $c_1 c_2 c_3 - c_1^2 c_4 - c_3^2 = 0$
$\Re(\lambda_i) = 0,\ i = 1, \cdots, 4$	$c_1 = c_3 = 0,$ $c_2 > 0$ and $c_2^2 - 4c_4 > 0$

Table 4.1: Critical Eigenvalue Conditions

In Hamiltonian systems, the stability conditions are somewhat different. The characteristic polynomial of a Hamiltonian system is an even polynomial. Thus, if λ is an eigenvalue of the system, then so is $-\lambda$, $\bar{\lambda}$ and $-\bar{\lambda}$, where $\bar{\lambda}$ denotes the complex conjugate of λ. The eigenvalue spectrum is symmetric with respect to both real and imaginary axes. Thus, the existence of a single zero eigenvalue is not possible. The necessary condition for stability is that the spectrum lies entirely on the imaginary axis. This type of stability is referred to as orbital stability. In this situation, it is impossible for all solutions to decay since all eigenvalues cannot be in the left half plane. Therefore, the origin cannot be an asymptotically stable fixed point of a Hamiltonian system.

The work of Krein [51] is the first to describe how the eigenvalues move in a generic nonsymmetric Hamiltonian system as the system parameters are varied. In such generic nonsymmetric situations, simple eigenvalues remain on the imaginary axis under Hamiltonian perturbations. However, the multiple (coincident) eigenvalues split and leave the imaginary axis. The generic families of symmetric Hamiltonian systems are affected by their symmetry type as shown by Dellnitz et al. [22]. The instability that takes place in a flexible rotating shaft is shown in Figure 4.1 where S denotes a stable region, D a divergence region (one eigenvalue has passed to the right half plane along the real axis) and F a region of flutter instability (a pair of eigenvalues has passed into the right half plane away from the real axis). Due to the symmetry of Hamiltonian systems, the divergence boundary represents two zero eigenvalues at every point.

In Figure 4.1(a), the system possesses S^1 (rotational) symmetry and the eigenvalues simply pass at the origin. As two pairs of eigenvalues meet on the imaginary axis, they may either pass or split according to Krein's analysis. The case of splitting is known as a Hamiltonian Hopf bifurcation. Figure 4.1(b) depicts the case in which the S^1 symmetry has been broken. The eigenvalues no longer pass at the origin inducing a saddle-center type fixed point configuration for that parameter value. The system loses then regains stability as the parameters are varied. The subsequent occurrence of coincident eigenvalues in the nonsymmetric case necessarily implies a Hamiltonian Hopf bifurcation. In the study of gyroscopic systems, the properties of symmetric systems will be used to examine these two bifurcation scenarios in more detail.

When the effect of damping is added, the system becomes *quasi-Hamiltonian*. The eigenvalue spectrum is then symmetric with respect to the real axis only. The stability boundaries for the dissipative system are depicted in Figure 4.2. Figures 4.2 (a-i) and (b-i) represent the divergence

61

(a) symmetric shaft: eigenvalues pass at origin

(b) unsymmetric shaft: eigenvalues split at origin
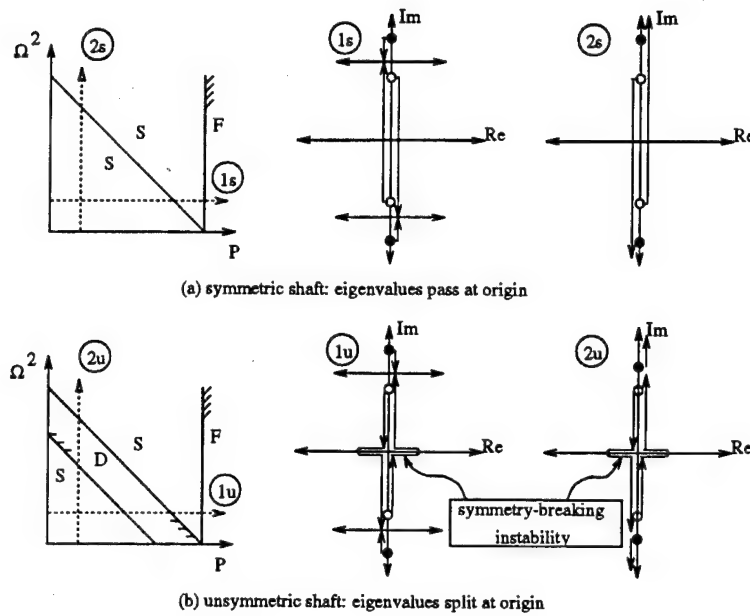
Figure 4.1: Stability boundaries of a rotating flexible shaft without dissipation.
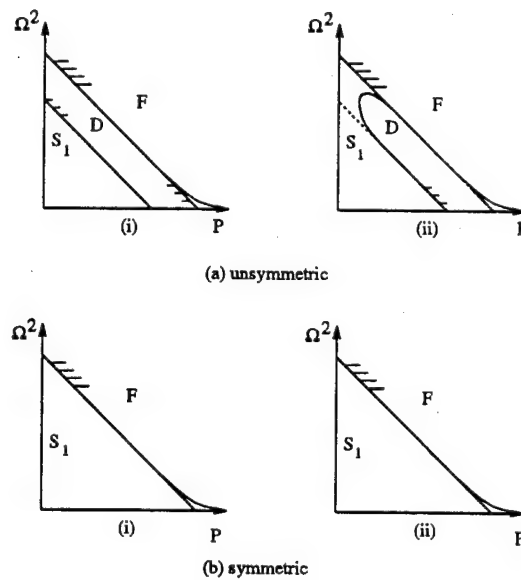

(a) unsymmetric

(b) symmetric

Figure 4.2: Stability boundaries of a rotating flexible shaft with dissipation.

62

and flutter boundaries in the presence of internal dissipation only. Compare these to the boundaries drawn in Figure 4.1 and note that the divergence boundary is unaffected by the addition of internal damping. The reason for this is simple. The internal dissipation as it is modeled here (linear proportional damping) enters the equations of motion multiplying a velocity term, not in the stiffness matrix. Hence, it cannot affect the static (divergent) bifurcations. Also note that since internal damping is *complete*, i.e. affects all modes, the restabilization region present in Figure 4.1 (above the divergent region) no longer exists. This is to be expected due to the results of Chetaev [15].

Figures 4.2 (a-ii) and (b-ii) show the effects of both internal and external dissipation. The addition of external damping affects both divergence and flutter boundaries since these terms enter into the stiffness matrix as well as the velocity terms. The divergent region of the damped system is bounded above and below by the boundaries of the system without damping. One important observation is that increasing the amount of external damping drives down the peak of the divergence region. The implication is that for the unsymmetric shaft, the initial loss of stability is not necessarily through divergence as it is in the conservative case. For the symmetric case, however, the initial loss of stability is always through flutter. Up to this point, the effects of the time dependent parametric excitation have not been considered. These effects will be examined in the following sections.

4.3 Stability of the Nonlinear System

In order to apply the method of averaging to the equations of motion of Chapter 3, it is first necessary to transform these equations to the standard form. To this end, three separate symplectic transformations will be performed. The first diagonalizes the conservative linear part. This will greatly simplify the algebra involved in the averaging operations. The second transformation scales the state variables and excitation amplitude such that all terms, except for the diagonalized linear part, are $O(\varepsilon)$. The final transformation employs a type-I (or F_1) generating function to eliminate the remaining $O(1)$ terms. The resulting equations are then in the standard form of Eq. (4.1).

Although the method of averaging may be applied to the equations of motion of a dynamical system beyond the systems critical divergence point, the canonical transformations outlined above are no longer valid in this region, i.e. when the eigenvalues of the Hamiltonian system are no longer purely imaginary. Therefore, in this study, the P_0-Ω parameter range is restricted such that the eigenvalues remain purely imaginary. For the parameters defined in Chapter 3, this condition reduces to

$$k_i = \bar{\omega}_i^2 - \Omega^2 - P^* > 0 , \quad i = 1, 2$$

This implies a positive stiffness. These regions of positive stiffness are indicated by S_1, the primary stable region, in Figure 4.2. When the time dependent axial load is added to P_0, the peak value of $P(t)$ must also remain in the S_1 parameter region.

Recall the Hamiltonian equations of motion given in Chapter 3,

$$\dot{z} = JSz + J\frac{\partial H_1(z,t)}{\partial z} - Bz \tag{4.3}$$

where the matrix B represents the forces not derivable from a potential, i.e.

$$B = - \begin{bmatrix} 0 & 0 \\ \bar{D}_2 & \bar{D}_1 \end{bmatrix}$$

63

and

$$\bar{D}_1 = -\frac{\Phi_5}{\Phi_1} \begin{bmatrix} d_e + \zeta_1 & 0 \\ 0 & d_e + \zeta_2 \end{bmatrix} \quad \text{and} \quad \bar{D}_2 = -\frac{\Phi_5 \Omega}{\Phi_1} \begin{bmatrix} 0 & -\zeta_1 \\ \zeta_2 & 0 \end{bmatrix}$$

A symplectic transformation which diagonalizes the linear conservative terms is given by

$$z = Ty \tag{4.4}$$

where

$$T^T S T = S = \text{diag}\{\omega_1, \omega_2, \omega_1, \omega_2\} \quad \text{and} \quad T^T J T = J$$

J is the symplectic matrix, ω_1 and ω_2 are the eigenvalues of the conservative system and are given ·by

$$\omega_i^2 = \frac{1}{2} \left\{ \tilde{\omega}_1 + \tilde{\omega}_2 + 2\Omega^2 \pm \sqrt{(\tilde{\omega}_1 - \tilde{\omega}_2)^2 + 8\Omega^2(\tilde{\omega}_1 + \tilde{\omega}_2)} \right\}$$

where "+" corresponds to ω_1 and "−" to ω_2. The transformation matrix T is given by

$$T = [t_{ij}] = \begin{bmatrix} \alpha_{11}\beta_1 & \alpha_{12}\beta_1 & \sigma_{11}\beta_1 & \sigma_{12}\beta_2 \\ \alpha_{21}\beta_1 & \alpha_{22}\beta_1 & \sigma_{21}\beta_1 & \sigma_{22}\beta_2 \\ \alpha_{31}\beta_1 & \alpha_{32}\beta_1 & \sigma_{31}\beta_1 & \sigma_{32}\beta_2 \\ \alpha_{41}\beta_1 & \alpha_{42}\beta_1 & \sigma_{41}\beta_1 & \sigma_{42}\beta_2 \end{bmatrix}$$

with

$$\alpha_{1i} = 1, \qquad \sigma_{1i} = -1$$

$$\alpha_{2i} = \sigma_{2i} = \frac{\omega_i^2 - k_1}{2\omega_i \Omega}$$

$$\alpha_{3i} = \sigma_{3i} = \omega_i - \frac{\omega_i^2 - k_1}{2\omega_i}$$

$$\alpha_{4i} = -\sigma_{4i} = \Omega - \frac{\omega_i^2 - k_1}{2\Omega}$$

$$\beta_i = \left\{ \frac{2k_1}{\omega_i} + \frac{(\omega_i^2 - k_1)^2}{2\omega_i \Omega^2} \right\}^{\frac{1}{2}}, \qquad\qquad i = 1, 2$$

The new Hamiltonian is simply

$$K(y, t) = H(z(y), t) = \frac{1}{2} y^T S y + K_1(y, t)$$

The Hamiltonian equations of motion are

$$\dot{y} = JSy + J\frac{\partial K_1}{\partial y} - \tilde{B}y \tag{4.5}$$

where $\tilde{B} = T^{-1} B T$.

The second transformation rescales the state variables and the excitation amplitude. To this end, introduce the nondimensional time $\tau = \nu t$ and the detuning parameter λ such that

$$\nu = \omega_0(1 - \varepsilon\lambda)$$

64

Next, note that the Hamiltonian $K(y, \tau)$ can be decomposed as follows: $K_0(y)$, generating the linear conservative terms in the equations of motion; $K_{1_n}(y)$, generating nonlinearities of order M in y; and K_{1_τ}, containing the parametric terms of order N in y. This yields

$$K(y, \tau) = K_0^{(2)} + K_{1_n}^{(M+1)} + K_{1_\tau}^{(N+1)} \mu \cos \tau$$

Note that K_0^2 is quadratic and $K_{1_\tau}^{(N+1)}$ is a homogeneous term of degree $N + 1$.

The state variables and excitation amplitude are scaled as follows:

$$y = \varepsilon^r x \quad \text{and} \quad \mu = \varepsilon^s h$$

Substituting the scaled quantities into Eq. (4.5) and solving for r and s such that the nonlinearities and parametric terms are $O(\varepsilon)$ yields $r = 1/2$, $s = 1$. The equations of motion in terms of x are

$$x' = J\hat{S}x + \varepsilon \left\{ \lambda J\hat{S}x + \frac{1}{\omega_0} \left[J\frac{\partial K_1(x, \tau)}{\partial x} - \delta^* \tilde{B}x \right] \right\} \tag{4.6}$$

where $\varepsilon \delta^* = 1$ and

$$\hat{S} = \frac{1}{\omega_0}S = \text{diag}\left\{\sigma_1, \sigma_2, \sigma_1, \sigma_2\right\} , \quad \sigma_i = \frac{\omega_i}{\omega_0} , \quad i = 1, 2$$

and $x = (\xi_1, \xi_2, \eta_1, \eta_2)^T$ or, more concisely, $x = (\xi, \eta)^T$. Differentiation with respect to the new time τ is denoted by ( )'.

In order to eliminate the $O(1)$ terms in the Hamiltonian $K(x, t)$, one additional transformation is needed. The new Hamiltonian (with $\varepsilon = 0$) can be written as

$$\hat{K}_0 = K_0 + \frac{\partial S}{\partial \tau}$$

where $S(a, \xi, \tau)$ is an F_1-type generating function and

$$K_0 = \frac{1}{2}x^T \hat{S}x = \frac{1}{2}\sum_{i=1}^{2} \sigma_i \left(\xi_i^2 + \eta_i^2\right)$$

The function $S(a, \xi, \tau)$ relates the old variables x to the new amplitude and phase variables $(a, \phi)^T$ through

$$\eta_i = \frac{\partial S}{\partial \xi_i} \quad \text{and} \quad \phi_i = -\frac{\partial S}{\partial a_i}$$

and $S(a, \xi, \tau)$ is chosen such that $\hat{K}_0 = 0$. Thus, $S(a, \xi, \tau)$ must solve the Hamilton-Jacobi equation

$$\frac{1}{2}\sum_{i=1}^{2} \sigma_i \left(\xi_i^2 + \left(\frac{\partial S}{\partial \xi_i}\right)^2\right) + \frac{\partial S}{\partial \tau} = 0 \tag{4.7}$$

Solving yields

$$\xi_i = \sqrt{2a_i}\cos(\sigma_i\tau - \phi_i) \quad \text{and} \quad \eta_i = -\sqrt{2a_i}\sin(\sigma_i\tau - \phi_i) , \quad i = 1, 2$$

65

The transformation is described by

$$\left\{ \begin{array}{c} \xi_i' \\ \eta_i' \end{array} \right\} = R \left[\left\{ \begin{array}{c} a_i' \\ \phi_i' \end{array} \right\} + \left\{ \begin{array}{c} 0 \\ -\sigma_i \end{array} \right\} \right] \qquad (4.8)$$

where, for $\Phi_i = \sigma_i \tau - \phi_i$ $(i = 1, 2)$,

$$
R = \left[\begin{array}{cc} \frac{\partial \xi_i}{\partial a_i} & \frac{\partial \xi_i}{\partial \phi_i} \\ \frac{\partial \eta_i}{\partial a_i} & \frac{\partial \eta_i}{\partial \phi_i} \end{array} \right]
$$

$$
= \left[\begin{array}{cccc} \frac{1}{\sqrt{2a_1}}\cos(\Phi_1) & 0 & \sqrt{2a_1}\sin(\Phi_1) & 0 \\ 0 & \frac{1}{\sqrt{2a_2}}\cos(\Phi_2) & 0 & \sqrt{2a_2}\sin(\Phi_2) \\ -\frac{1}{\sqrt{2a_1}}\sin(\Phi_1) & 0 & \sqrt{2a_1}\cos(\Phi_1) & 0 \\ 0 & -\frac{1}{\sqrt{2a_2}}\sin(\Phi_2) & 0 & \sqrt{2a_2}\cos(\Phi_2) \end{array} \right]
$$

Using Eq. 4.7, it can be easily verified that $\hat{K}_0 = 0$ and the symplectic condition $R^T J R = J$ holds. The new Hamiltonian is

$$\hat{K} = \hat{K}_0 + \hat{K}_1 = \frac{1}{\omega_0} K_1(\xi(a,\phi), \eta(a,\phi), \tau)$$

The equations of motion in standard form are

$$\left\{ \begin{array}{c} a_i' \\ \phi_i' \end{array} \right\} = \varepsilon \left\{ \begin{array}{c} \frac{\partial \hat{K}_1}{\partial \phi_i} \\ -\lambda\sigma_i - \frac{\partial \hat{K}_1}{\partial a_i} \end{array} \right\} - \frac{\varepsilon}{\omega_0} \left(\delta^* \bar{B} x(a,\phi) \right) \qquad (4.9)$$

where $\bar{B} = R^{-1}\tilde{B}$. It is also possible to obtain Eq. (4.9) directly from Eq. (4.6) via the transformation (4.8).

Since the equations of motion are obtained from the Hamiltonian through a linear operation, the system may be averaged in one of two ways: the equations of motion may be averaged directly or one can apply averaging to the Hamiltonian and obtain the averaged equations from the resulting autonomous Hamiltonian. The latter approach is generally simpler since it implies performing the averaging calculations only once.

Application of the method of averaging yields a set of equations of the form

$$\left\{ \begin{array}{c} \tilde{a}_i' \\ \tilde{\phi}_i' \end{array} \right\} = \varepsilon \left[\left\{ \begin{array}{c} 0 \\ -\lambda\sigma_i \end{array} \right\} + J \frac{\partial \tilde{K}_1}{\partial v_i} - \left\{ \begin{array}{c} f_i \\ -g_i \end{array} \right\} \right] \qquad (4.10)$$

where $v_i = (a_i, \phi_i)^T$. In the above equations, the notation $(\tilde{\ })$ indicates an averaged quantity and

$$\tilde{K}_1 = \underset{t}{M}\{\hat{K}_1\} \quad \text{and} \quad \left\{ \begin{array}{c} f_i \\ -g_i \end{array} \right\} = \frac{1}{\omega_0} \underset{t}{M}\{\delta^* \bar{B} x(a,\phi)\}$$

where $\underset{t}{M}$ is the averaging operator defined above.

The system described by Eq. (4.10) represents a first approximation of an asymptotic method. In some situations, the first approximation does not contain all the essential information that was present in the original set of equations. The influence of quadratic nonlinearities, for example, is

66

not retained in this first approximation. In such cases, in order for the resulting averaged equations to be *equivalent* to the original system, it is necessary to proceed to a second order approximation. Details of this procedure may be found in the book by Bogoliubov and Mitropolsky [13]. For the system under consideration, a first order approximation is sufficient to capture all the essential dynamics.

It can be shown (see, for example, Murdock [64]) that averaging to the first order is equivalent to removing terms from the Fourier series expansion of an equation. Complete averaging removes all but the constant term, i.e. the average, from the right hand side. In the presence of certain degeneracies, or *resonances*, however, additional terms will remain in the averaged system. A dynamical system is said to be in *internal resonance* if the parameter values are such that the following relation between the natural frequencies holds:

$$\sum_{i=1}^{n} m_i \omega_i = 0$$

for some set of integers $m = (m_1, m_2, \cdots, m_n)$. The system is said to be in *parametric resonance* if

$$\sum_{i=1}^{n} m_i \omega_i = \omega_0$$

for some set of integers $m = (m_1, m_2, \cdots, m_n)$ and some excitation frequency ω_0. In the local analysis presented here, the effects of the parametric excitation are to be examined. Thus, to simplify the analysis, only the case of parametric resonance in the original equations will be considered. It will be shown in Section 4.4.3 that the *averaged* system of equations may exhibit internal resonance under certain conditions on the parameter values.

In the subsequent local analysis of Eqs. (4.10), the stability of the fixed point and the emergence of limit cycles will be examined. As discussed in Section 4.1, one of the frequencies of the system has been removed. Hence, a fixed point in the averaged system corresponds to a periodic orbit in the original nonautonomous system. Similarly, a limit cycle in the averaged equations, corresponds to a 2-torus in the response of the original system.

4.4   Local Analysis of the Averaged Equations

In this section, the stability of the averaged equations will be examined under various parametric resonance conditions. As the frequency ν of the parametric excitation approaches some multiple of the natural frequency of one of the modes of vibration, the amplitude of vibration of that mode will dominate the dynamics of the response. If the excitation frequency approaches some algebraic combination of two or more modes, the response is more complicated and couples the modes involved. As stated above, the parametric resonance condition is

$$\sum_{i=1}^{n} m_i \omega_i = \omega_0 \quad \text{or} \quad \sum_{i=1}^{n} m_i \sigma_i = 1$$

where $\sigma_i = \omega_i/\omega_0$ and ω_0 is the resonance frequency.

Under first order averaging, it can be shown that the only possible parametric resonance conditions are those for which $\sum_{i=1}^{n} m_i = 2$, i.e. resonances of order 2. If the averaging procedure was

67

carried out to second order, one would see resonances of order 3 as well. The resonance conditions possible in the present analysis are: subharmonic resonance ($\omega_0 = 2\omega_i$ for $i = 1, 2$) and combination resonance ($\omega_0 = \omega_1 \pm \omega_2$). The stability of the equilibrium in the absence of parametric resonance will also be examined.

The following quantities are used in the analysis:

$$\gamma_{ii} = 2\left[I_v t_{1i}^2 (3t_{1i}^2 + t_{2i}^2) + I_w t_{2i}^2 (3t_{2i}^2 + t_{1i}^2) \right]$$

$$\gamma_{12} = 2\left[I_v \left(t_{11}^2 (3t_{12}^2 + t_{22}^2) + t_{12}^2 (3t_{11}^2 + t_{21}^2) \right) + I_w \left(t_{22}^2 (3t_{21}^2 + t_{11}^2) + t_{21}^2 (3t_{22}^2 + t_{12}^2) \right) \right]$$

$$\gamma_{i3} = \frac{1}{2}(t_{1i}^2 - t_{2i}^2)$$

$$\gamma_{i4} = \frac{1}{2}(t_{11}t_{12} + t_{21}t_{22})$$

$$\gamma_{i5} = \frac{1}{2}(t_{11}t_{12} - t_{21}t_{22})$$

$$\bar{\gamma}_{1i} = \frac{\Phi_5}{\Phi_1}\left\{ (t_{2i}t_{4i} - t_{1i}t_{3i})d_e + t_{1i}t_{2i}\Omega(\zeta_1 + \zeta_2) + t_{2i}t_{4i}\zeta_2 - t_{1i}t_{3i}\zeta_1 \right\}, \quad i = 1, 2$$

$$a_u = \frac{3E\Phi_4}{2m\Phi_1} \quad \text{and} \quad b_u = \frac{\Phi_2}{2m\Phi_1}$$

where t_{ij} are terms in the transformation matrix T defined for Eq. (4.4).

4.4.1 Nonresonant Case

First consider the case in which the resonance condition is not satisfied for any set of integers m_i. The averaged equations of motion in polar coordinates are given by

$$\tilde{a}_i' = \varepsilon\left\{ \left(\frac{2\bar{\gamma}_{1i}\delta^*}{\omega_0} \right) a_i \right\} \tag{4.11}$$

$$\tilde{\phi}_i' = \varepsilon\left\{ -\lambda\sigma_i + \frac{2a_u}{\omega_0}(\gamma_{11}a_1 + \gamma_{12}a_2) \right\} \tag{4.12}$$

for $i = 1, 2$. The fixed points of the system are found by setting $\tilde{a}_i' = 0$ and $\tilde{\phi}_i' = c_i$. The constant c_i can be included in the detuning parameter λ. Thus, the latter equilibrium equation may be replaced by $\tilde{\phi}_i' = 0$. Since the amplitude equations are linear, the only possible fixed point is the trivial solution, i.e. $(\tilde{a}_{01}, \tilde{a}_{02}) = (0, 0)$. It is important to note that in deriving Eq. (4.12), a factor of $\tilde{a}_i$ was divided out. Thus, in analyzing the resulting expressions, care must be taken not to omit the origin as a possible solution. In order to examine the stability of the trivial solution, it is necessary to transform Eqs. (4.11) and (4.12) to rectangular coordinates via

$$x_i = \sqrt{a_i}\cos\phi_i \quad \text{and} \quad y_i = \sqrt{a_i}\sin\phi_i, \quad i = 1, 2$$

In rectangular coordinates, Eqs. (4.11) and (4.12) become

$$x_i' = \varepsilon\left\{ \left(\frac{\bar{\gamma}_{1i}\delta^*}{\omega_0} \right) x_i + (\lambda\sigma_i)y_i - y_i\mathcal{F}_i(x, y) \right\}$$

$$y_i' = \varepsilon\left\{ \left(\frac{\bar{\gamma}_{1i}\delta^*}{\omega_0} \right) y_i - (\lambda\sigma_i)x_i + x_i\mathcal{F}_i(x, y) \right\}$$

68

The function $\mathcal{F}_i(x, y)$ contains the nonlinear terms and is given by

$$\mathcal{F}_i(x, y) = \frac{2a_u}{\omega_0} \left(\gamma_{1i} a_1 + \gamma_{i2} a_2 \right)$$

The stability of the trivial solution can be completely determined by the location of the eigenvalues of the system linearized about the origin. To this end, the linear system is given in matrix form by

$$\left\{ \begin{array}{c} x_1' \\ x_2' \\ y_1' \\ y_2' \end{array} \right\} = \frac{\varepsilon \delta^*}{\omega_0} \left[\begin{array}{cccc} \bar{\gamma}_{11} & 0 & \frac{\lambda \sigma_1 \omega_0}{\delta^*} & 0 \\ 0 & \bar{\gamma}_{12} & 0 & \frac{\lambda \sigma_2 \omega_0}{\delta^*} \\ -\frac{\lambda \sigma_1 \omega_0}{\delta^*} & 0 & \bar{\gamma}_{11} & 0 \\ 0 & -\frac{\lambda \sigma_2 \omega_0}{\delta^*} & 0 & \bar{\gamma}_{12} \end{array} \right] \left\{ \begin{array}{c} x_1 \\ x_2 \\ y_1 \\ y_2 \end{array} \right\}$$

The eigenvalues of this system are

$$\lambda_r = \frac{\varepsilon \delta^*}{\omega_0} \left(\bar{\gamma}_{1r} + i \frac{\lambda \sigma_r \omega_0}{\delta^*} \right) \quad \text{and} \quad \lambda_{r+2} = \frac{\varepsilon \delta^*}{\omega_0} \left(\bar{\gamma}_{1r} - i \frac{\lambda \sigma_r \omega_0}{\delta^*} \right), \quad r = 1, 2$$

Since $\delta^*/\omega_0 > 0$, the sign of $\bar{\gamma}_{1r}$ determines the stability of the linear, and therefore, the nonlinear system. It can be shown that $\bar{\gamma}_{1r} < 0$ for $r = 1, 2$. Thus, in the absence of parametric resonance, the trivial solution remains stable for all values of the excitation amplitude and frequency in the parameter range of interest.

4.4.2 Subharmonic Resonance: $\omega_0 = 2\omega_i$

The subharmonic resonance case corresponds to a parametric excitation with frequency near twice the frequency of one of the modes of the shaft. The averaged equations of motion for this situation are

$$\tilde{a}_i' = \varepsilon \left\{ \left(\frac{2hb_u \psi \gamma_{i3}}{\omega_0} \cos 2\phi_i \right) a_i + \left(2 \frac{\delta^* \bar{\gamma}_{1i}}{\omega_0} \right) a_i \right\} \tag{4.13}$$

$$\tilde{a}_j' = \varepsilon \left\{ \left(2 \frac{\delta^* \bar{\gamma}_{1j}}{\omega_0} \right) a_j \right\} \tag{4.14}$$

$$\tilde{\phi}_i' = \varepsilon \left\{ -\lambda \sigma_i + \frac{2a_u}{\omega_0} \left(\gamma_{1i} a_1 + \gamma_{i2} a_2 \right) - \left(\frac{hb_u \psi \gamma_{i3}}{\omega_0} \sin 2\phi_i \right) \right\} \tag{4.15}$$

$$\tilde{\phi}_j' = \varepsilon \left\{ -\lambda \sigma_j + \frac{2a_u}{\omega_0} \left(\gamma_{1j} a_1 + \gamma_{j2} a_2 \right) \right\} \tag{4.16}$$

From the amplitude equations, it is easy to see that one equilibrium solution is the trivial one, i.e. $(\tilde{a}_{0i}, \tilde{a}_{0j}) = (0, 0)$. As in the nonresonant case, it is necessary to transform Eqs. (4.13) through (4.16) to rectangular coordinates. This yields

$$x_i' = \varepsilon \left\{ \left(\frac{\delta^* \bar{\gamma}_{1i}}{\omega_0} + \frac{hb_u \psi \gamma_{i3}}{\omega_0} \right) x_i + (\lambda \sigma_i) y_i - y_i \mathcal{F}_i(x, y) \right\}$$

$$x_j' = \varepsilon \left\{ \left(\frac{\delta^* \bar{\gamma}_{1j}}{\omega_0} \right) x_j + (\lambda \sigma_j) y_j - y_j \mathcal{F}_i(x, y) \right\}$$

$$y_i' = \varepsilon \left\{ (-\lambda \sigma_i) x_i + \left(\frac{\delta^* \bar{\gamma}_{1i}}{\omega_0} - \frac{hb_u \psi \gamma_{i3}}{\omega_0} \right) y_i + x_i \mathcal{F}_i(x, y) \right\}$$

$$y_j' = \varepsilon \left\{ \left(\frac{\delta^* \bar{\gamma}_{1j}}{\omega_0} \right) y_j - (\lambda \sigma_j) x_j + x_j \mathcal{F}_i(x, y) \right\}$$

69

For $\omega_0 = 2\omega_r$, the eigenvalues of the system linearized about the origin are

$$\lambda_s = \frac{\varepsilon\delta^*}{\omega_0}\left(\bar{\gamma}_{1r} \pm i\frac{\lambda\sigma_r\omega_0}{\delta^*}\right), \quad r \neq s$$

$$\lambda_r = \frac{\varepsilon}{\omega_0}\left(\delta^*\bar{\gamma}_{1r} \pm i\sqrt{(\lambda\sigma_r\omega_0)^2 - (b_u\gamma_{r3}h\psi)^2}\right)$$

The first set of two eigenvalues, λ_s $(s \neq r)$, correspond to the mode that is *not* in resonance and possess negative real parts. This implies that $\tilde{a}_s \to 0$ as $\tau \to \infty$. Since the dynamics of the stable mode are only of interest in the manner in which they affect the mode in resonance, one can apply the Center Manifold Theorem outlined in Chapter 1. One can approximate the stable mode variables x_s and y_s as series expansions in x_r and y_r, each starting with a quadratic term. Since the resulting function $\mathcal{F}_i(x,y)$ is fourth order, to a first approximation, it is reasonable to take $x_s = y_s = 0$ in the analysis of the stability of the mode in resonance. This decouples the modes. In order to determine the steady state nontrivial solution, one only needs to examine the equations for x_r and y_r.

The second set of eigenvalues, λ_r, correspond to the mode that *is* in resonance. These eigenvalues can be complex, real or zero but not purely imaginary. Thus, the trivial solution loses stability through divergence. The condition for stability of the trivial solution, after dividing through by ε, can be expressed as

$$\mu < \frac{1}{b_u\gamma_{r3}|\psi|}\left\{\left(1 - \frac{\nu}{\omega_0}\right)^2\omega_r + \bar{\gamma}_{1r}^2\right\}^{1/2}$$

As stated above, if the stability condition is violated for some value of excitation amplitude μ or frequency ν, the system loses stability through divergence. Beyond the bifurcation point, the averaged set of equations exhibits a nonzero fixed point for each ν (or μ). Since fixed points of the averaged equations correspond to periodic orbits in the original system, this indicates that once the trivial solution loses stability, the shaft will begin to oscillate in the rth mode (with period ω_r). The amplitude of this oscillation may be determined by examining Eqs. (4.13) and (4.15) for the case in which $\tilde{a}_r \neq 0$. Setting $\tilde{a}_r' = 0$ yields two possible solutions for the steady state angle ϕ_{0r}

$$\sin 2\phi_{0r} = \pm\sqrt{1 - \left(\frac{\delta^*\bar{\gamma}_{1r}}{b_u\gamma_{r3}h\psi}\right)^2}$$

Substituting this into $\tilde{\phi}_r' = 0$ yields an expression for the nontrivial steady state amplitude $\tilde{a}_{0r}$,

$$\tilde{a}_{0r} = \frac{1}{2a_u\gamma_{rr}}\left\{\lambda\omega_r \pm \sqrt{(b_u\gamma_{r3}h\psi)^2 - (\delta^*\bar{\gamma}_{1r})^2}\right\}$$

It can be shown that the solution branch corresponding to the "+" in the expression for $\sin 2\phi_{0r}$ is stable for all values of h and λ and, therefore, for all values of μ and ν. The solution branch corresponding to the "−" is unstable for all values of μ and ν beyond the primary bifurcation point. Figures 4.3 and 4.4 depict the stability boundaries (in μ-ν parameter space) and subsequent nontrivial solutions for a rotating shaft which is pinned at each end. Figures 4.5 and 4.6 depict the stability boundaries and nontrivial solutions for a rotating shaft which is clamped at each end.

Figure 4.3: First subharmonic ($\omega_0 = 2\omega_1$) stability boundaries and nontrivial response of pinned-pinned rotating shaft ($a = a_{10}$).

Figure 4.4: Second subharmonic ($\omega_0 = 2\omega_2$) stability boundaries and nontrivial response of pinned-pinned rotating shaft ($a = a_{20}$).

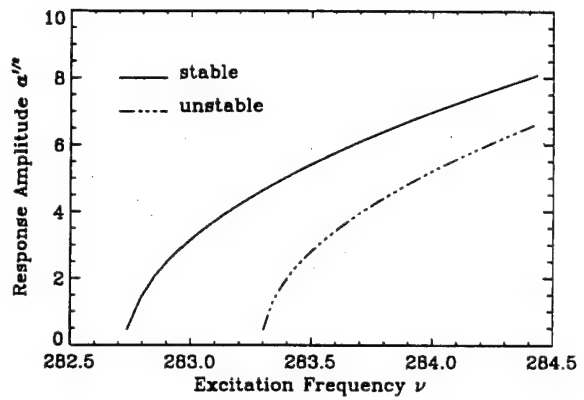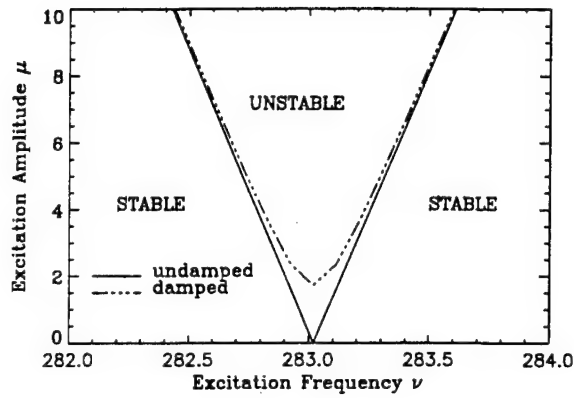Figure 4.5: First subharmonic ($\omega_0 = 2\omega_1$) stability boundaries and nontrivial response of clamped-clamped rotating shaft ($a = a_{10}$).
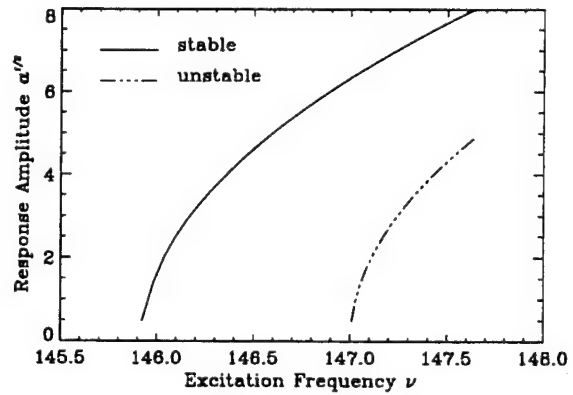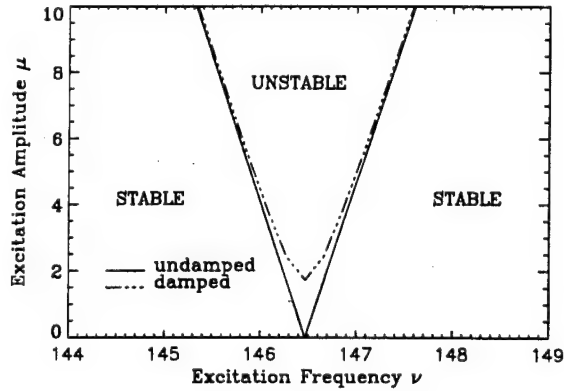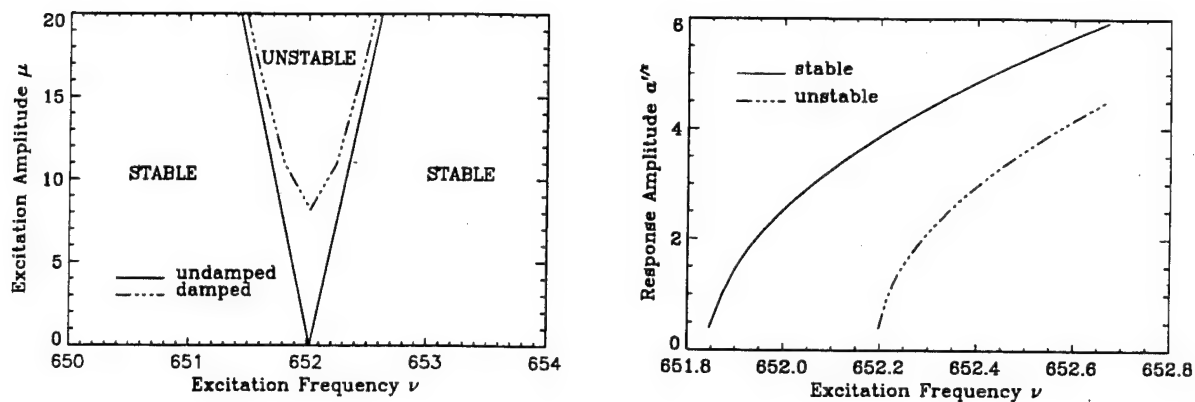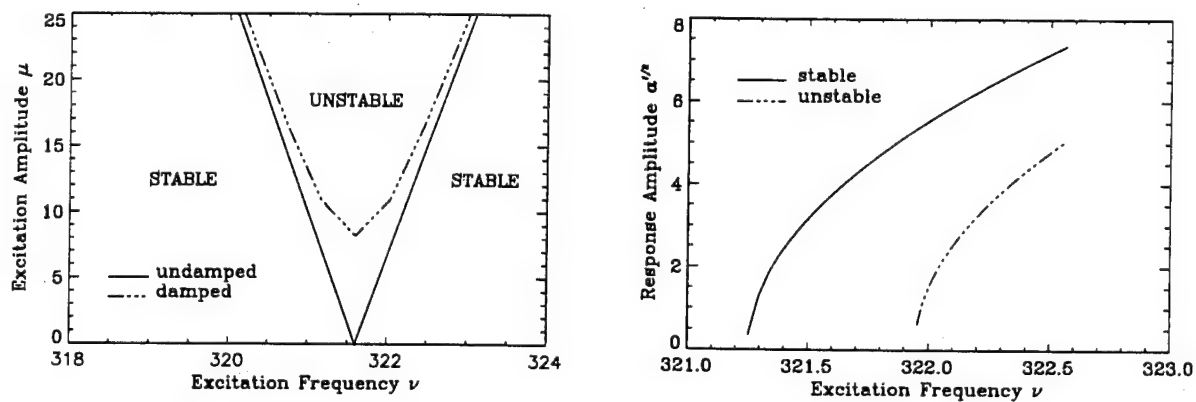

Figure 4.6: Second subharmonic ($\omega_0 = 2\omega_2$) stability boundaries and nontrivial response of clamped-clamped rotating shaft ($a = a_{20}$).

72

4.4.3 Additive Combination Resonance: $\omega_0 = \omega_i + \omega_j$

The next resonance case to be considered is that of additive combination resonance. In contrast to the subharmonic case discussed in the previous section, this resonance condition involves both modes instead of a single mode. As a result, the bifurcation behavior is more complicated than in the previous case. In this case, the averaged equations of motion in polar coordinates are

$$\tilde{a}_i' = \varepsilon \left\{ \left(\frac{2hb_u\psi\gamma_{i4}}{\omega_0} \cos(\phi_i + \phi_j) \right) \sqrt{a_i a_j} + \left(2\frac{\delta^* \bar{\gamma}_{1i}}{\omega_0} \right) a_i \right\} \tag{4.17}$$

$$\tilde{\phi}_i' = \varepsilon \left\{ -\lambda\sigma_i + \frac{2a_u}{\omega_0}(\gamma_{i1}a_1 + \gamma_{i2}a_2) - \left(\frac{hb_u\psi\gamma_{i4}}{\omega_0} \sin(\phi_i + \phi_j) \right) \sqrt{\frac{a_j}{a_i}} \right\} \tag{4.18}$$

$(i = 1, 2)$ for which the trivial solution $(\tilde{a}_{0i}, \tilde{a}_{0j}) = (0,0)$ is an equilibrium. Transformation to rectangular coordinates yields

$$x_i' = \varepsilon \left\{ \left(\frac{\delta^* \bar{\gamma}_{1i}}{\omega_0} \right) x_i + \left(\frac{hb_u\psi\gamma_{i4}}{\omega_0} \right) x_j + (\lambda\sigma_i) y_i - y_i \mathcal{F}_i(x, y) \right\}$$

$$y_i' = \varepsilon \left\{ (-\lambda\sigma_i) x_i + \left(\frac{\delta^* \bar{\gamma}_{1i}}{\omega_0} \right) y_i - \left(\frac{hb_u\psi\gamma_{i4}}{\omega_0} \right) y_j + x_i \mathcal{F}_i(x, y) \right\}$$

The eigenvalues of the system linearized about the origin are complicated. However, it is possible to simplify the expressions for these eigenvalues via an additional coordinate transformation. To this end, let

$$\chi_1 = x_1 + iy_1, \quad \bar{\chi}_1 = x_1 - iy_1$$
$$\chi_2 = x_2 + iy_2, \quad \bar{\chi}_2 = x_2 - iy_2$$

Note that this transformation is not symplectic. However, this is not detrimental to the analysis at this point since this new coordinate system is only used to calculate the eigenvalues, which are independent of the coordinates. The linear system in the new coordinates is

$$\left\{ \begin{array}{c} \chi_1' \\ \bar{\chi}_2' \\ \bar{\chi}_1' \\ \chi_2' \end{array} \right\} = \frac{\varepsilon}{\omega_0} \left[\begin{array}{cccc} \delta^* \bar{\gamma}_{11} - i\lambda\omega_1 & hb_u\psi\gamma_{14} & 0 & 0 \\ hb_u\psi\gamma_{24} & \delta^* \bar{\gamma}_{12} + i\lambda\omega_2 & 0 & 0 \\ 0 & 0 & \delta^* \bar{\gamma}_{11} + i\lambda\omega_1 & hb_u\psi\gamma_{14} \\ 0 & 0 & hb_u\psi\gamma_{24} & \delta^* \bar{\gamma}_{12} - i\lambda\omega_2 \end{array} \right] \left\{ \begin{array}{c} \chi_1 \\ \bar{\chi}_2 \\ \bar{\chi}_1 \\ \chi_2 \end{array} \right\}$$

This can be expressed as

$$\left\{ \begin{array}{c} \chi_1' \\ \bar{\chi}_2' \\ \bar{\chi}_1' \\ \chi_2' \end{array} \right\} = \mathcal{A} \left\{ \begin{array}{c} \chi_1 \\ \bar{\chi}_2 \\ \bar{\chi}_1 \\ \chi_2 \end{array} \right\}$$

The characteristic equation is obtained from

$$\det[\mathcal{A} - \rho I] = \det \left[\begin{array}{cc} \mathcal{R} & \mathbf{0} \\ \mathbf{0} & \bar{\mathcal{R}} \end{array} \right] = \det(\mathcal{R})\det(\bar{\mathcal{R}}) = 0$$

where the roots of $\det(\mathcal{R}) = 0$ are denoted by ρ and the roots of $\det(\bar{\mathcal{R}}) = 0$ are $\bar{\rho}$. Evaluating the determinant yields

$$
\begin{aligned}
\det(\mathcal{R}) &= \frac{\varepsilon^2}{\omega_0^2} \left[\left(\delta^* \bar{\gamma}_{11} - i\lambda\omega_1 - \rho \right) \left(\delta^* \bar{\gamma}_{12} + i\lambda\omega_2 - \rho \right) - (hb_u\psi)^2 \gamma_{14}\gamma_{24} \right] \\
&= (r_1 - is_1 - \rho)(r_2 + is_2 - \rho) - \frac{\varepsilon^2}{\omega_0^2}\hbar
\end{aligned}
$$

where, for convenience, $r_\ell = \varepsilon\delta^*\bar{\gamma}_{1\ell}/\omega_0$, $s_\ell = \varepsilon\lambda\omega_\ell/\omega_0$ $(\ell = 1, 2)$ and $\hbar = (hb_u\psi)^2\gamma_{14}\gamma_{24}$. The characteristic equation is given explicitly by

$$
\begin{aligned}
\rho^2 &- \rho \left[\frac{\varepsilon\delta^*}{\omega_0} (\bar{\gamma}_{11} + \bar{\gamma}_{12}) + i\frac{\varepsilon\lambda}{\omega_0}(\omega_2 - \omega_1) \right] \\
&+ \frac{\varepsilon^2}{\omega_0^2} \left[\left(\delta^{*2}\bar{\gamma}_{11}\bar{\gamma}_{12} + \lambda^2\omega_1\omega_2 - (hb_u\psi)^2\gamma_{14}\gamma_{24} \right) + i\delta^*\lambda(\bar{\gamma}_{11}\omega_2 - \bar{\gamma}_{12}\omega_1) \right] = 0 \quad (4.19)
\end{aligned}
$$

The characteristic equation (4.19) contains coefficients which are complex. In determining the sign of the real part of the eigenvalues, a complex version of the Routh-Hurwitz stability criterion will greatly simplify the analysis.

The condition for stability of the trivial solution is $\Re(\rho) < 0$. Let $\rho = i\kappa$. The stability condition becomes

$$
\Re(\rho) < 0 \quad \Rightarrow \quad \Im(\kappa) > 0
$$

where $\Im(\kappa)$ denotes the imaginary part of κ. In terms of κ, the characteristic equation is

$$
\begin{aligned}
-\kappa^2 &+ \kappa \left[\frac{\varepsilon\lambda}{\omega_0}(\omega_2 - \omega_1) - i\frac{\varepsilon\delta^*}{\omega_0}(\bar{\gamma}_{11} + \bar{\gamma}_{12}) \right] \\
&+ \frac{\varepsilon^2}{\omega_0^2} \left[\left(\delta^{*2}\bar{\gamma}_{11}\bar{\gamma}_{12} + \lambda^2\omega_1\omega_2 - (hb_u\psi)^2\gamma_{14}\gamma_{24} \right) + i\delta^*\lambda(\bar{\gamma}_{11}\omega_2 - \bar{\gamma}_{12}\omega_1) \right] = 0
\end{aligned}
$$

This is the characteristic equation of the following matrix:

$$
\mathcal{H} = \begin{bmatrix}
-1 & s_2 - s_1 & r_1 r_2 + s_1 s_2 - \hbar & 0 \\
0 & -(r_1 + r_2) & r_1 s_2 - s_1 r_2 & 0 \\
0 & -1 & s_2 - s_1 & r_1 r_2 + s_1 s_2 - \hbar \\
0 & 0 & -(r_1 + r_2) & r_1 s_2 - s_1 r_2
\end{bmatrix}
$$

The condition $\Im(\kappa) > 0$ is satisfied if and only if

$$
\begin{aligned}
\Delta_2 &= r_1 + r_2 < 0 \quad \text{and} \\
\Delta_4 &= (r_1 + r_2) \left[(s_2 - s_1)(r_1 s_2 - s_1 r_2) + (r_1 + r_2)(r_1 r_2 + s_1 s_2 - \hbar) \right] \\
&\qquad\qquad + (r_1 s_2 - s_1 r_2)^2 > 0
\end{aligned}
$$

Since $\bar{\gamma}_{11} < 0$ and $\bar{\gamma}_{12} < 0$, $\Delta_2 < 0$ is automatically satisfied. Thus, the stability condition for the trivial solution comes from satisfying $\Delta_4 < 0$. The final stability condition for the trivial solution is

$$
\left| 1 - \frac{\nu}{\omega_0} \right| > \sqrt{\frac{-(\bar{\gamma}_{11} + \bar{\gamma}_{12})^2(\bar{\gamma}_{11}\bar{\gamma}_{12} - \mu^2(b_u\psi\gamma_{14})^2)}{\bar{\gamma}_{11}\bar{\gamma}_{12}\omega_0^2}}
$$

Alternatively, this condition can be expressed as

$$\left|1 - \frac{\nu}{\omega_0}\right| > \frac{1}{\omega_0}\left[\left(\frac{\bar{\gamma}_{11}}{\bar{\gamma}_{12}}\right)^{\frac{1}{2}} + \left(\frac{\bar{\gamma}_{12}}{\bar{\gamma}_{11}}\right)^{\frac{1}{2}}\right]\sqrt{(\mu b_u \psi \gamma_{14})^2 - \bar{\gamma}_{11}\bar{\gamma}_{12}} \qquad (4.20)$$

In the absence of damping, this condition becomes

$$\left|1 - \frac{\nu}{\omega_0}\right| > \frac{2\mu(b_u \psi \gamma_{14})}{\omega_0}$$

In the presence of damping, the characteristic equation *along the stability boundary* is

$$\rho^2 \;-\; \frac{1}{\omega_0}\rho\left[(\bar{\gamma}_{11} + \bar{\gamma}_{12}) + i\varepsilon\lambda(\omega_2 - \omega_1)\right]$$

$$+ \; \frac{1}{\omega_0^2(\bar{\gamma}_{11} + \bar{\gamma}_{12})^2}\left[\varepsilon^2\lambda^2\left(\omega_1\omega_2(\bar{\gamma}_{11} + \bar{\gamma}_{12})^2 - \omega_0^2\bar{\gamma}_{11}\bar{\gamma}_{12}\right)\right.$$

$$\left. + i\varepsilon\lambda\left(\bar{\gamma}_{11}\omega_2 - \bar{\gamma}_{12}\omega_1\right)\left(\bar{\gamma}_{11} + \bar{\gamma}_{12}\right)^2\right] = 0 \qquad (4.21)$$

Thus

$$\rho_1 + \rho_2 = \frac{1}{\omega_0}\left[(\bar{\gamma}_{11} + \bar{\gamma}_{12}) + i\varepsilon\lambda(\omega_2 - \omega_1)\right]$$

and

$$\rho_1\rho_2 \;=\; \frac{1}{\omega_0^2(\bar{\gamma}_{11} + \bar{\gamma}_{12})^2}\left[\varepsilon^2\lambda^2\left(\omega_1\omega_2(\bar{\gamma}_{11} + \bar{\gamma}_{12})^2 - \omega_0^2\bar{\gamma}_{11}\bar{\gamma}_{12}\right)\right.$$

$$\left. + i\varepsilon\lambda\left(\bar{\gamma}_{11}\omega_2 - \bar{\gamma}_{12}\omega_1\right)\left(\bar{\gamma}_{11} + \bar{\gamma}_{12}\right)^2\right]$$

At $\lambda \equiv 0$, one (and only one) of these eigenvalues is identically 0. The other root is given by

$$\rho = \frac{1}{\omega_0}(\bar{\gamma}_{11} + \bar{\gamma}_{12}) < 0$$

This implies that two of the four system eigenvalues are zero. The other two have negative real parts.

For $\lambda \neq 0$, none of the eigenvalues may possess a zero real part. Along the stability boundary, the characteristic equation can be written in the form

$$\rho^4 - c_1\rho^3 + c_2\rho^2 - c_3\rho + c_4 = 0$$

where

$$c_1 \;=\; -\frac{2}{\omega_0}(\bar{\gamma}_{11} + \bar{\gamma}_{12})$$

$$c_2 \;=\; \left(\frac{2\varepsilon^2\lambda^2}{\omega_0^2(\bar{\gamma}_{11} + \bar{\gamma}_{12})^2}\right)\left[\omega_1\omega_2(\bar{\gamma}_{11} + \bar{\gamma}_{12})^2 - \omega_0^2\bar{\gamma}_{11}\bar{\gamma}_{12}\right] + \frac{1}{\omega_0^2}\left[(\bar{\gamma}_{11} + \bar{\gamma}_{12})^2 + \varepsilon^2\lambda^2(\omega_2 - \omega_1)^2\right]$$

$$c_3 \;=\; 2\left(\frac{\varepsilon^2\lambda^2}{\omega_0^3(\bar{\gamma}_{11} + \bar{\gamma}_{12})}\right)(\bar{\gamma}_{11}\omega_2 - \bar{\gamma}_{12}\omega_1)^2$$

$$c_4 \;=\; \frac{1}{\omega_0^4(\bar{\gamma}_{11} + \bar{\gamma}_{12})^4}\left[\varepsilon^4\lambda^4\left(\omega_1\omega_2(\bar{\gamma}_{11} + \bar{\gamma}_{12})^2 - \omega_0^2\bar{\gamma}_{11}\bar{\gamma}_{12}\right)^2\right.$$

$$\left. + \varepsilon^2\lambda^2\left(\bar{\gamma}_{11}\omega_2 - \bar{\gamma}_{12}\omega_1\right)^2\left(\bar{\gamma}_{11} + \bar{\gamma}_{12}\right)^4\right]$$

75

It can be shown that $c_1 \neq 0$, $c_3 \neq 0$, $c_1/c_3 > 0$ and

$$c_1 c_2 c_3 - c_1^2 c_4 - c_3^2 = 0$$

Thus, according to Table 4.1, this system possesses a single pair of purely imaginary eigenvalues. Therefore, the loss of stability in this case is through a Hopf bifurcation, i.e. a pair of eigenvalues passes into the right half plane after crossing the imaginary axis away from the origin. The nontrivial solution resulting from a Hopf bifurcation is periodic. Thus, the averaged equations possess periodic solutions beyond the bifurcation point. This motion in the averaged system corresponds to motion on a 2-torus in the original system. One of the frequencies involved in the oscillations of the original system is the response frequency $\omega_1 + \omega_2$. The second frequency relates the coupling between the ·modes.

In the undamped case, the system is purely Hamiltonian and the four eigenvalues are given by

$$\rho = \pm i \frac{\varepsilon}{2\omega_0} \left\{ \lambda(\omega_2 - \omega_1) \pm \sqrt{\lambda^2 \omega_0^2 - 4\hbar} \right\}$$

When the stability condition is satisfied, i.e. when $\lambda^2 \omega_0^2 \geq 4\hbar$, there are two conjugate pairs of purely imaginary eigenvalues. For $\lambda^2 \omega_0^2 = 4\hbar$, these pairs coalesce at

$$\rho = \pm i \frac{\varepsilon \lambda}{2\omega_0} (\omega_2 - \omega_1)$$

When $\lambda^2 \omega_0^2 > 4\hbar$, the eigenvalue spectrum is symmetric with respect to both real and imaginary axes and two of the eigenvalues possess positive real parts. This loss of stability is known as a Hamiltonian Hopf bifurcation.

For certain parameter values, either two or four eigenvalues of the nondissipative system will be located at the origin. Although the behavior of the system near all of these points will not be studied in detail here, certain characteristics of the system may be noted. Consider Figure 4.7. At the point $(\lambda, \mu) = (0,0)$ on the stability boundary, all four eigenvalues are located at the origin. As μ is increased while λ remains constant at 0 (along the dotted line), the quantity $4\hbar$ becomes positive, two equal eigenvalues move into the right half plane along the real axis (point F). Similarly, an equal pair moves into the left half plane at the same rate along the real axis.

For $\lambda \neq 0$, as μ is increased from zero, all four imaginary eigenvalues begin to move toward the origin (point A). Along the dashed line corresponding to $2\hbar = \lambda^2 \omega_1 \omega_2$, or, equivalently,

$$\mu_d = \left| \frac{\sqrt{2\omega_1 \omega_2}}{2b_u \psi \gamma_{14}} \left(1 - \frac{\nu}{\omega_0} \right) \right|$$

two eigenvalues are located at the origin (point B). The other two are purely imaginary. No splitting occurs in this region. As μ is increased further, the first pair of eigenvalues is moving away from the origin and the second pair is approaching the origin (point C). These two pairs meet at the stability boundary (point D). The unfolding and global dynamics of this internal resonance will be the focus of the next chapter.

The nontrivial solution may be determined by examining Eqs. (4.17) and (4.18) for the case in which $\tilde{a}_i \neq 0$ $(i = 1, 2)$. Setting $\tilde{a}_i' = 0$ yields two possible solutions for the steady state angle $\phi_0 = \phi_{01} + \phi_{02}$. Letting $M = |hb_u \psi \gamma_{14}| = |hb_u \psi \gamma_{24}|$ (since $\gamma_{14} = \gamma_{24}$) yields

$$\sin \phi_0 = \pm \frac{1}{M} \sqrt{M^2 - \delta^{*2} \bar{\gamma}_{11} \bar{\gamma}_{12}} = \pm \frac{\mathcal{P}}{M}$$
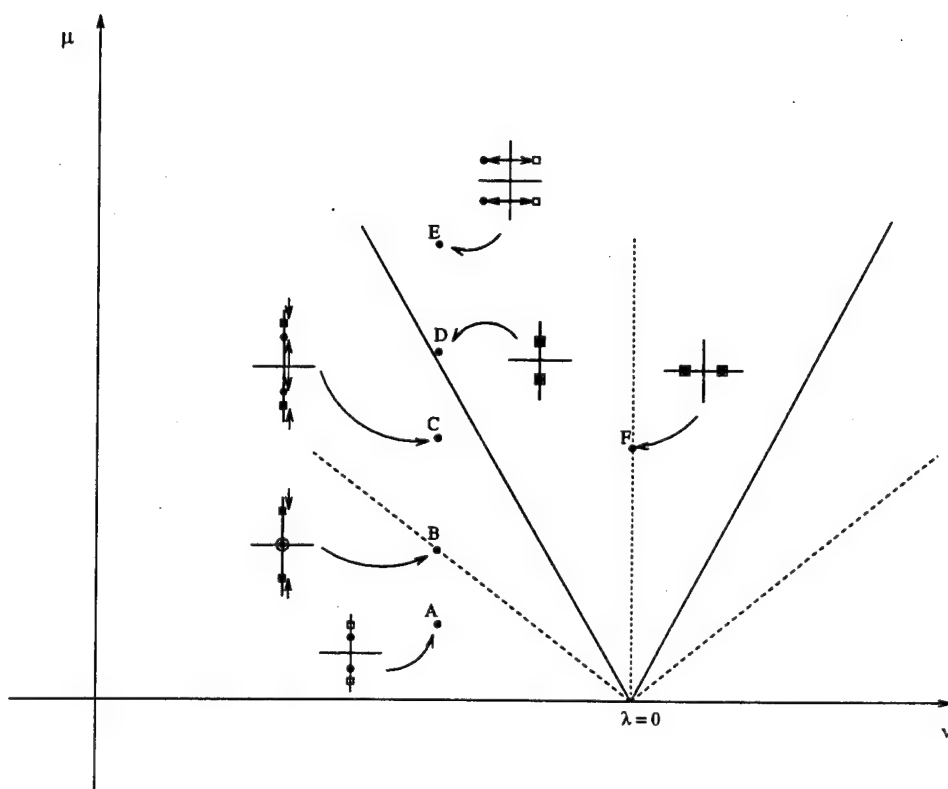
76

Figure 4.7: Eigenvalue location in ν-μ parameter space for the nondissipative case.
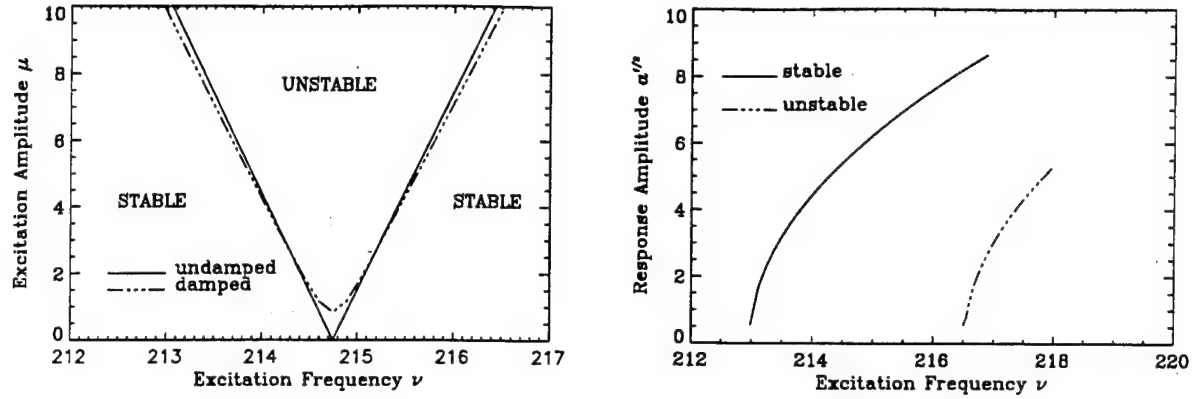
Figure 4.8: Combination resonance $(\omega_0 = \omega_1 + \omega_2)$ stability boundaries and nontrivial response of pinned-pinned rotating shaft $(a = a_{10})$.

Substituting this into $\tilde{\phi}_i' + \tilde{\phi}_j' = 0$ yields the following relation between the nontrivial steady state amplitudes and the excitation frequency (and amplitude):

$$1 - \frac{\nu}{\omega_0} = \frac{\varepsilon}{\omega_0} \left\{ 2a_u \left[(\gamma_{11} + \gamma_{12})a_{01} + (\gamma_{12} + \gamma_{22})a_{02} \right] \mp \frac{\bar{\gamma}_{11} + \bar{\gamma}_{12}}{\bar{\gamma}_{11}\bar{\gamma}_{12}} \mathcal{P} \right\}$$

The stability and bifurcation behavior of these nontrivial periodic solutions can also be determined. It can be shown that the periodic solution corresponding to "$+$" in the expression for $\sin \phi_0$ is unstable for all values of μ and ν beyond the primary bifurcation point. The periodic solution corresponding to "$-$" is shown to be a stable nontrivial solution. Furthermore, it can be shown that the steady state amplitudes are related through

$$\frac{a_{0i}}{a_{0j}} = \frac{\bar{\gamma}_{1j}}{\bar{\gamma}_{1i}}$$

The stability boundaries for the trivial solution, along with the nontrivial response amplitude $a_{10}^{1/2}$, are presented in Figures 4.8 and 4.9 for the rotating shaft. Figure 4.8 shows the boundaries and response amplitude for a shaft which is pinned at each end; Figure 4.9 depicts this information for a clamped shaft.

4.4.4 Difference Combination Resonance: $\omega_0 = \omega_i - \omega_j$

Now consider the final resonance case. Assuming the excitation frequency is near $\omega_i - \omega_j$, the averaged equations of motion are

$$\tilde{a}_i' = \varepsilon \left\{ \left(\frac{-2hb_u\psi\gamma_{i5}}{\omega_0} \sin(\phi_i - \phi_j) \right) \sqrt{a_i a_j} + \left(2\frac{\delta^*\bar{\gamma}_{1i}}{\omega_0} \right) a_i \right\} \tag{4.22}$$

$$\tilde{\phi}_i' = \varepsilon \left\{ -\lambda\sigma_i + \frac{2a_u}{\omega_0}(\gamma_{1i}a_1 + \gamma_{i2}a_2) - \left(\frac{hb_u\psi\gamma_{i5}}{\omega_0} \cos(\phi_i - \phi_j) \right) \sqrt{\frac{a_j}{a_i}} \right\} \tag{4.23}$$

78
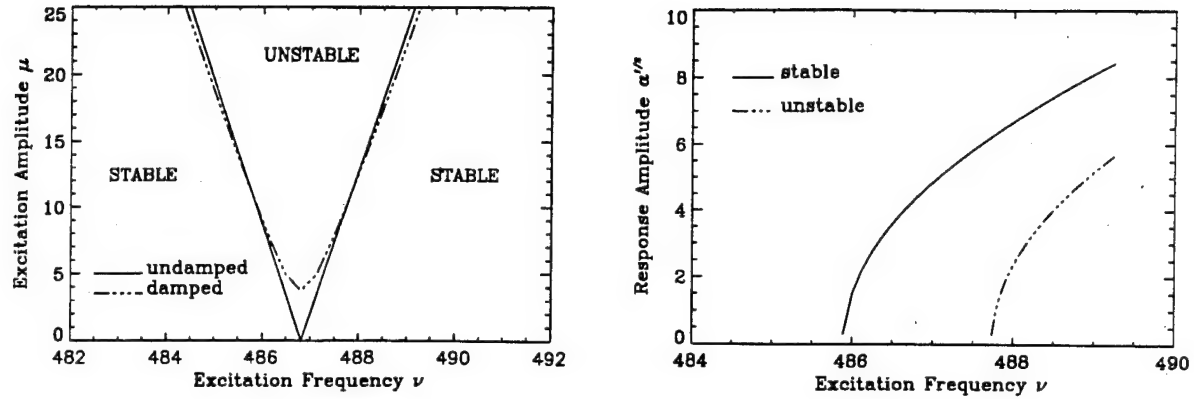
Figure 4.9: Combination resonance ($\omega_0 = \omega_1 + \omega_2$) stability boundaries and nontrivial response of clamped-clamped rotating shaft ($a = a_{10}$).

Again, one equilibrium solution is the trivial one, i.e. $(\tilde{a}_{0i}, \tilde{a}_{0j}) = (0,0)$. Transforming Eqs. (4.22) to (4.23) to rectangular coordinates yields

$$x_i' = \varepsilon \left\{ \left(\frac{\delta^* \bar{\gamma}_{1i}}{\omega_0} \right) x_i + (\lambda \sigma_i)\, y_i + \left(\frac{h b_u \psi \gamma_{i5}}{\omega_0} \right) y_j - y_i \mathcal{F}_i(x,y) \right\}$$

$$y_i' = \varepsilon \left\{ (-\lambda \sigma_i)\, x_i - \left(\frac{h b_u \psi \gamma_{i5}}{\omega_0} \right) x_j + \left(\frac{\delta^* \bar{\gamma}_{1i}}{\omega_0} \right) y_i + x_i \mathcal{F}_i(x,y) \right\}$$

As in the case of additive combination resonance, the expressions for the eigenvalues are complicated. Introducing the transformation

$$\chi_1 = x_1 + iy_1 , \quad \bar{\chi}_1 = x_1 - iy_1$$
$$\chi_2 = x_2 + iy_2 , \quad \bar{\chi}_2 = x_2 - iy_2$$

and proceeding as in the previous analysis, it can be shown that the conditions for stability of the trivial solution are always satisfied. Thus, in the difference combination resonance case, the trivial solution remains stable for all parameter values in the range of interest.

4.5 Conclusions

The method of averaging provides a powerful tool in the analysis of nonlinear systems with time-dependent parameters. In this chapter, the method of averaging was applied to the equations of motion derived in Chapter 3. The resulting set of autonomous ordinary differential equations were then examined to determine the limits of stability in the excitation amplitude/frequency parameter space. Depending on the excitation frequency, it was shown that the trivial (non-oscillatory) solution may lose stability through divergence or flutter. The subsequent nontrivial response for each case is also described.

79

In the case of combination resonance in the absence of dissipation, the system at criticality possesses two coincident pairs of purely imaginary eigenvalues. The linear system is in nonsemisimple 1:1 internal resonance and the trivial solution loses stability through a Hamiltonian Hopf bifurcation. The unfolding of this resonance and the global behavior near the stability boundary for this case is the subject of the next chapter.

Chapter 5

GLOBAL DYNAMICS OF SHALLOW ARCH STRUCTURES

5.1 Introduction

Shallow arch structures subjected to various load conditions have been investigated by many authors in the past. A large amount of literature exists on the stability behavior of shallow arch structures subjected to conservative static loads. It is well-known that such structures may go through *snap through* instability when the statically applied load exceeds a certain critical value. This instability behavior involves a sudden transition of the structural response from one stable equilibrium state to another non-adjoining stable equilibrium state. For a detailed review of snap through buckling and postbuckling behavior of thin-shell structures one is referred to Koiter [47] and Hutchinson and Koiter [39]. Under dynamic load conditions, the stability investigation requires the determination of the dynamic response as described by its nonlinear equations of motion. Mettler [56, 57, 58] investigated the dynamical behavior of a beam structure with small initial curvature under periodic loading, and demonstrated the occurrence of *dynamic snap through*, which is analogous to the jump phenomenon in the theory of nonlinear vibrations. Hsu [36], Humphreys [38], and Lock [53] examined the dynamic responses of shallow arches and spherical shells under step and impulsive loading. Huang [37] investigated the dynamic response of elastic shallow structures subjected to high frequency periodic loading. Plaut and Hsieh [72] numerically examined the nonlinear response associated with 1-DOF shallow arch system under two-frequency excitation. They studied the effects of arch rise and the excitation frequencies on the critical load, and observed various types of limit cycle behavior including the chaotic response.

Recently Sri Namachchivaya and Doyle [81] and Tien et al. [86, 87] studied the bifurcation behavior and the chaotic dynamics of a shallow arch subjected to small amplitude periodic excitation. Tien et al. [86, 87] examined the dynamic response of an initially deformed shallow arch, which is subjected to a spatially and temporally varying force, using analytical as well as numerical techniques. They considered a two-degree-of-freedom (2-DOF) nonlinear model governing the two fundamental modes of the transverse motion of the shallow arch. In the presence of initial deformations and nonlinear strain-displacement relationships, this model contains both quadratic and cubic nonlinearities. Assuming a very small forcing amplitude ($\mu = O(\epsilon^2)$), they obtained nonlinear variational equations corresponding to the forced system in the small neighborhood of *single mode equilibrium solutions* ($\eta_0, 0$). Next they investigated the global bifurcation behavior

associated with the averaged variational equations in the presence of 1:2 and 1:1 internal resonances near the harmonic frequency ($\nu = \omega_1$).

In this study we examine the dynamics associated with the 2-DOF shallow arch system near the principal subharmonic frequency ($\nu = 2\omega_1$), in addition to the presence of internal resonances. Here we take a more realistic approach owing to the observation that the forced system (3) allows single mode time dependent (periodic) solutions ($\eta(t), 0$) in the presence of external excitation. Assuming the forcing amplitude to be of $O(\epsilon)$, the single mode periodic solutions for the forced case are obtained using a power series expansion. We obtain the nonlinear variational equations governing the small perturbations in the neighborhood of the *single mode periodic solutions*. The external forcing appears as a parametric term in these perturbation equations. This approach allows one to .use higher values of excitation amplitude, and is more consistent for solving this class of problems as opposed to obtaining variational equations near the single mode equilibrium solutions.

By using the method of averaging [13], the first order approximation of the response of the perturbation equations is obtained in the presence of 1:2 internal resonance. We use the second order averaging to study the system response for the 1:1 internal resonance case. If one uses the approach used by Tien et al. [86, 87] to examine the response of the system near $\nu = 2\omega_1$, one finds that the forcing amplitude appears at a higher order than the lowest order nonlinear terms in the averaged equations. This suggests that the scaling used by [86, 87] is not appropriate to investigate the dynamics near $\nu = 2\omega_1$.

We use standard Melnikov type perturbation methods [89] to analytically show that the shallow arch structure, in the absence of any dissipation mechanism, may exhibit chaotic dynamics in the sense of Smale horseshoe for 1:2 internal resonance case. In this case it is shown that no attracting sets persists on the invariant manifold even in the presence of very small dissipation effects. However, the effect of dissipation can be examined in 1:1 internal resonance case where, using a perturbation technique due to [48], we show the existence of *Silnikov type homoclinic orbit* to a fixed point in the perturbed system, and consequently the chaotic behavior.

The organization of this chapter is as follows: A brief outline of the derivation of the 2-DOF model governing the two fundamental modes of the transverse motion of the shallow arch is given in section 2. The global bifurcation behavior associated with this model is investigated for 1:2 internal resonance case in section 3. In this section, first the perturbation equations are obtained in the neighborhood of single mode periodic solutions, and next we examine the averaged perturbation equations for the existence of complex behavior using analytical as well as numerical tools. In section 4, the 2-DOF shallow arch model is reconsidered for 1:1 internal resonance case and the perturbation equations are similarly obtained using a different scaling of variables and parameters. In this case, the effect of dissipation is examined on the global dynamics associated with the averaged perturbation equations, and the restrictions on the system parameters are obtained for the occurrence of Silnikov type homoclinic chaos. The physical interpretation of the results is given for the shallow arch dynamics in section 5. Finally the results are summarized in section 6.

5.2   Equations of Motion

The shallow arch is assumed to be subjected to a lateral loading $p(x,t)$, as shown in Figure 5.1. The equation of motion governing the lateral deflection $w(x,t)$ of a shallow arch, subjected to a lateral loading $p(x,t)$ as shown in Figure 5.1, can be derived by using the energy method, and is given as:
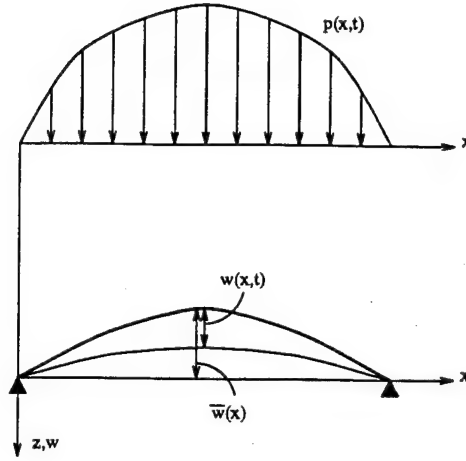
Figure 5.1: Geometry of the shallow arch structure subjected to lateral loading $p(x,t)$.

$$mw_{tt} + \beta w_t + EI w_{xxxx} - E\,A\,h(w,t)\,(\bar{w}_{xx} + w_{xx}) = p(x,t) \qquad (5.1)$$

where

$$
\begin{aligned}
h(w,t) &= \frac{1}{l}\left[u(l,t) + \int_0^l \left(\frac{1}{2}w_x^2 + \bar{w}_{xx}w_{xx}\right) dx\,\right] \\
\bar{w}(x) &= -q_0 \sin \frac{\pi x}{l} \\
p(x,t) &= (p_0 + f(t)) \sin \frac{\pi x}{l}
\end{aligned}
$$

Here $\bar{w}(x)$ represents the initial deflection of the unloaded arch, q_0 is the initial rise parameter, p_0 is the static loading, and $f(t)$ is time dependent part of the lateral loading. Here it is assumed that the external forcing is periodic, i.e., $f(t) = \mu \cos \nu t$, where μ and ν represent the amplitude and frequency of the harmonic excitation, respectively. The arch is subjected to the following boundary conditions:

$$w = 0, \quad w_{xx} = 0 \qquad\qquad at \quad x = 0, l$$

The Galerkin method is used to reduce the equation of motion to the ordinary differential equations by selecting appropriate shape functions. The transverse motion $w(x,t)$ of the arch is approximated by the following expression:

$$w(x,t) = q_1(t) \sin \frac{\pi x}{l} + q_2(t) \sin \frac{2\pi x}{l} \qquad (5.2)$$

The non-dimensional equations of motion describing the evolution of the amplitudes of two fundamental modes can be written in $(Q_1 = q_1 - q_0, Q_2 = q_2)$ coordinates as:

$$
\begin{aligned}
\ddot{Q}_1 &+ \beta_1 \dot{Q}_1 + Q_1 + Q_1(Q_1^2 - q_0^2 + 4Q_2^2) + (q_0 - \lambda_0) = \mu \cos \nu t \\
\ddot{Q}_2 &+ \beta_2 \dot{Q}_2 + 16Q_2 + 4Q_2(Q_1^2 - q_0^2 + 4Q_2^2) = 0
\end{aligned}
\qquad (5.3)
$$

83

where β_1 and β_2 are the viscous damping parameters for the first and second mode respectively, and λ_0 represents the non-dimensional loading parameter. The details of this derivation and the definitions of non-dimensional variables and parameters can be found in [85]. The linearized frequencies corresponding to the first and second modes are represented by ω_1 and ω_2, respectively (see next section).

5.3   One-to-Two Internal Resonance

This study deals with the dynamics, stability and bifurcation behavior of system described by Eqs. (5.3) in the presence of internal resonances. Resonances have long been known to cause complex or chaotic behavior in both dissipative and Hamiltonian dynamical systems. Since these resonances provide near-integrable structure in the governing equations, one can use certain analytical methods to study their global behavior. To this end, in this section, we consider Eqs. (5.3) in the presence of parametric subharmonic and 1:2 internal resonance.

5.3.1   Scaling and Averaged Equations

In order to investigate the dynamics of arch for 1:2 internal resonance, we assume the damping and the external forcing amplitude to be small as compared with the other terms. i.e.,

$$\mu = \epsilon\,\gamma, \qquad \beta_1 = \epsilon\,\delta_1, \qquad \beta_2 = \epsilon\,\delta_2 \tag{5.4}$$

where ϵ is a small parameter, i.e., $0 < \epsilon << 1$. As mentioned previously that the equations of motion (5.3) permit $(Q_1(t) = \eta(t), Q_2(t) = 0)$ as one of the solutions. The following form of $\eta(t)$ in the powers of ϵ is assumed,

$$\eta(t) = \eta_0 + \epsilon\,\eta_1(t) + \epsilon^2\,\eta_2(t) + O(\epsilon^3) \tag{5.5}$$

Next consider the small perturbations x_1 and x_2 in the neighborhood of single mode periodic solutions $(\eta(t), 0)$:

$$Q_1 = \eta(t) + \epsilon\,x_1, \qquad Q_2 = 0 + \epsilon\,x_2 \tag{5.6}$$

The nonlinear variational equations governing the perturbations can be written as:

$$
\begin{aligned}
\ddot{x}_1 + \omega_1^2 x_1 \quad &+ \quad \epsilon\left[\delta_1\dot{x}_1 + 6\eta_0\eta_1 x_1 + \eta_0(3x_1^2 + 4x_2^2)\right] \\
&+ \epsilon^2\left[3x_1(\eta_1^2 + 2\eta_0\eta_2) + \eta_1(3x_1^2 + 4x_2^2) + x_1^3 + 4x_1x_2^2\right] + O(\epsilon^3) = 0 \\
\ddot{x}_2 + \omega_2^2 x_2 \quad &+ \quad \epsilon\left[\delta_2\dot{x}_2 + 8\eta_0\eta_1 x_2 + 8\eta_0 x_1 x_2\right] \\
&+ \epsilon^2\left[4x_2(\eta_1^2 + 2\eta_0\eta_2) + 8\eta_1 x_1 x_2 + 4(x_1^2 x_2 + 4x_2^2)\right] + O(\epsilon^3) = 0
\end{aligned} \tag{5.7}
$$

where $\omega_1^2 = 3\eta_0^2 + (1 - q_0^2)$ and $\omega_2^2 = 4[\eta_0^2 + (4 - q_0^2)]$. Here η_0 is governed by a third order algebraic equation and the particular solutions for η_1, η_2 etc. are obtained in terms of known parameters and time as follows:

$$
\begin{aligned}
\eta_0^3 \quad &+ (1 - q_0^2)\eta_0 + (q_0 - \lambda_0) = 0 \\
\eta_1 \quad &= b_1\cos(\nu t) \\
\eta_2 \quad &= a_0 + a_1\cos(\nu t) + a_2\cos(2\nu t)
\end{aligned} \tag{5.8}
$$

84

where $b_1 = \frac{\gamma}{(w_1^2 - \nu^2)}$ and a_0, a_1, a_2 can be similarly expressed in terms of known quantities. We notice that the complementary solution (in η_1, η_2 etc.) is set to zero since we are only interested in periodic orbits with period $\frac{2\pi}{\nu}$. The Hamiltonian corresponding to (5.7) can be expressed as:

$$
\begin{aligned}
H(\mathbf{x_p}, \mathbf{x_q}) &= H_0 + \epsilon H_1 + O(\epsilon^2) \\
&= \frac{1}{2} \left[x_{p_1}^2 + x_{p_2}^2 + \omega_1^2 x_{q_1}^2 + \omega_2^2 x_{q_2}^2 \right] \\
&\quad + \epsilon \left[\eta_0 x_{q_1}^3 + 4\eta_0 x_{q_1}^2 x_{q_2} + \eta_0 \eta_1 (3x_{q_1}^2 + 4x_{q_2}^2) \right] + O(\epsilon^2)
\end{aligned}
\tag{5.9}
$$

where $x_{q_1} = x_1$, $x_{q_2} = x_2$, $x_{p_1} = \dot{x}_1$ and $x_{p_2} = \dot{x}_2$. The steady state behavior and bifurcation analysis of the system is best described when the following canonical change of variables is introduced:

$$
x_{q_i} = \sqrt{2a_i} \cos\left(\omega_i t + \frac{\phi_i}{\omega_i}\right), \qquad \dot{x}_{p_i} = -\omega_i \sqrt{2a_i} \sin\left(\omega_i t + \frac{\phi_i}{\omega_i}\right), \qquad \forall\, i = 1, 2
\tag{5.10}
$$

The following detuning parameters are introduced in order to examine the dynamics of the system in the presence of principal subharmonic resonance and 1:2 internal resonance.

$$
\omega_1^2 = \frac{1}{4}(\nu^2 - \epsilon\sigma_1), \qquad \omega_2^2 = \frac{1}{16}(\nu^2 - \epsilon\sigma_2)
\tag{5.11}
$$

where σ_1 is the measure of deviation of the forcing frequency from twice the natural frequency of the first mode, and $(\sigma_2 - \sigma_1)$ is proportional to the deviation from the 1:2 internal resonance. At this stage, the method of averaging [13] is applied to simplify the system. The averaged equations, giving the first order response of the system, can be expressed in terms of canonical variables $(a_1, \theta_1, a_2, \theta_2)$ as following:

$$
\begin{aligned}
\dot{a}_1 &= \epsilon \left[-\delta_1 a_1 + \frac{6}{\nu} a_1 b_1 \eta_0 \sin(2\theta_1) + \frac{4}{\nu}\sqrt{2a_1} a_2 \eta_0 \sin(\theta_1 - 2\theta_2) \right] + O(\epsilon^2) \\
a_1 \dot{\theta}_1 &= \epsilon \left[-\frac{1}{(4\nu)}\sigma_1 a_1 + \frac{3}{\nu} a_1 b_1 \eta_0 \cos(2\theta_1) + \frac{2}{\nu}\sqrt{2a_1} a_2 \eta_0 \cos(\theta_1 - 2\theta_2) \right] + O(\epsilon^2) \\
\dot{a}_2 &= \epsilon \left[-\delta_2 a_2 - \frac{16}{\nu}\sqrt{2a_1} a_2 \eta_0 \sin(\theta_1 - 2\theta_2) \right] + O(\epsilon^2) \\
a_2 \dot{\theta}_2 &= \epsilon \left[-\frac{1}{(2\nu)}\sigma_2 a_2 + \frac{8}{\nu}\sqrt{2a_1} a_2 \eta_0 \cos(\theta_1 - 2\theta_2) \right] + O(\epsilon^2)
\end{aligned}
\tag{5.12}
$$

where $\theta_i = \frac{\phi_i}{\omega_i}$. In order to analyze the trivial equilibrium solutions, the averaged equations can be transformed to the rectangular coordinates. One finds that the trivial solution $(a_1 = 0, a_2 = 0)$ may lose its stability only through a simple bifurcation and may give rise to one or two coupled mode nontrivial equilibrium branches or one single and one coupled solution branch.

5.3.2 Analytical Investigation of Chaotic Dynamics

In order to examine the possibility of the chaotic dynamics in the system, the higher dimensional Melnikov analysis is employed. The details of the framework of this method can be found in [89]. Originally this method is due to [55] who considered a two-dimensional non-autonomous system with a completely integrable unperturbed part and small ($O(\epsilon)$) time periodic terms. The non-resonant higher dimensional Melnikov method assumes the homoclinic structure of the unperturbed

85

system, along with arbitrary perturbations. Generically, certain invariant sets may persist under perturbations and thus, the knowledge of the global dynamics of the unperturbed integrable system can be used to develop a measure of the distance between the stable and unstable manifolds of that invariant set in the perturbed system. This measure is called the Melnikov Function, which provides crucial information on the possibility of the presence of chaotic behavior in certain class of nonlinear systems.

Reduction to the standard form

Consider the following canonical transformation in order to reduce the averaged system of equations to the form appropriate for applying the higher dimensional Melnikov theory as described in [89]:

$$q_1 = (\frac{\phi_1}{\omega_1} - 2\frac{\phi_2}{\omega_2}), \qquad q_2 = 2\frac{\phi_2}{\omega_2}, \qquad p_1 = a_1\omega_1, \qquad p_2 = \frac{1}{2}(a_2 + 4a_1)\omega_2 \qquad (5.13)$$

This transformation leads to the following set of equations in (p_1, q_1, p_2, q_2) coordinates:

$$
\begin{aligned}
\dot{p}_1 &= \epsilon\left[-\delta_1 p_1 + \frac{32\eta_0}{\nu^{\frac{3}{2}}}\sqrt{p_1}\,(p_2 - p_1)\sin q_1 + \frac{6b_1\eta_0}{\nu}p_1\sin 2(q_1 + q_2)\right] + O(\epsilon^2) \\
\dot{q}_1 &= \epsilon\left[-\frac{\sigma_1}{4\nu} + \frac{\sigma_2}{\nu} + \frac{16\eta_0}{\nu^{\frac{3}{2}}}\frac{(p_2 - 3p_1)}{\sqrt{p_1}}\cos(q_1) + \frac{3b_1\eta_0}{\nu}\cos 2(q_1 + q_2)\right] + O(\epsilon^2) \\
\dot{p}_2 &= \epsilon\left[-\delta_2 p_2 - (\delta_1 - \delta_2)p_1 + \frac{6b_1\eta_0}{\nu}p_1\sin 2(q_1 + q_2)\right] + O(\epsilon^2) \\
\dot{q}_2 &= \epsilon\left[-\frac{\sigma_2}{\nu} + \frac{32\eta_0}{\nu^{\frac{3}{2}}}\sqrt{p_1}\cos q_1\right] + O(\epsilon^2)
\end{aligned}
\qquad (5.14)
$$

In these equations the effect of excitation is present through the terms involving the coefficient b_1, as one recalls $b_1 = \frac{\gamma}{(w_1^2 - \nu^2)}$. This system (5.14) attains the desired form if the time is rescaled in addition to assuming the forcing terms to be smaller compared with the nonlinear terms. For this purpose, rescaling the variables and parameters in the following manner:

$$\gamma = \epsilon\gamma', \qquad \delta_{1,2} = \epsilon\delta'_{1,2}, \qquad t = \frac{t'}{\epsilon}, \qquad p_1 = \frac{p'_1}{A^2}, \qquad p_2 = \frac{p'_2}{A^2} \qquad (5.15)$$

where $A = (16\,\eta_0\,\nu^{-\frac{3}{2}})$ and t' denotes the slow time. For the sake of less cumbersome notation the prime ($'$) is dropped from the rescaled variables and parameters. The rescaled equations up-to $O(\epsilon)$ can now be written as:

$$
\begin{aligned}
\dot{p}_1 &= 2\,p_1^{1/2}\,(p_2 - p_1)\sin q_1 + \epsilon\left[-\delta_1 p_1 + 2\mu p_1\sin 2(q_1 + q_2)\right] \\
\dot{q}_1 &= \mu_1 + \mu_2 + p_1^{-1/2}\,(p_2 - 3p_1)\cos q_1 + \epsilon\left[\mu\,\cos 2(q_1 + q_2)\right] \\
\dot{p}_2 &= \epsilon\left[-\delta_2 p_2 - (\delta_1 - \delta_2)p_1 + 2\mu p_1\sin 2(q_1 + q_2)\right] \\
\dot{q}_2 &= -\mu_2 + 2p_1^{1/2}\cos q_1
\end{aligned}
\qquad (5.16)
$$

where

$$\mu_1 = -\frac{\sigma_1}{4\nu}, \qquad \mu_2 = \frac{\sigma_2}{\nu}, \qquad \mu = \frac{3}{\nu}\,b_1\eta_0$$

In these equations (5.16) the dot indicates differentiation with respect to t'. The objective is to study the global dynamics associated with this system (5.16). As a first step, the structure of the unperturbed system (obtained by setting $\epsilon = 0$) is examined, which can be expressed as:

$$
\begin{aligned}
\dot{p}_1 &= 2\, p_1^{1/2}\, (p_2 - p_1) \sin q_1 \\
\dot{q}_1 &= \mu_1 + \mu_2 + p_1^{-1/2}\, (p_2 - 3p_1) \cos q_1 \\
\dot{p}_2 &= 0 \\
\dot{q}_2 &= -\mu_2 + 2p_1^{1/2} \cos q_1
\end{aligned}
\tag{5.17}
$$

It is clear that the first two equations are completely independent of q_2, and $p_2 = p_{20} = $ constant, and thus it is sufficient to study the phase flow in (p_1, q_1) coordinates only. The canonical transformations (5.13) and the periodicity of q_1 suggests that the range of interest in (p_1, q_1) coordinates is: $0 < p_1 \le p_{20}$ and $0 \le q_1 \le 2\pi$. The Hamiltonian corresponding to the two-dimensional (p_1, q_1) vector field is given as:

$$
\hat{H}(p_1, q_1) = (\mu_1 + \mu_2)\, p_1 + 2\, p_1^{1/2}\, (p_2 - p_1) \cos q_1
\tag{5.18}
$$

It is obvious that the orbits in (p_1, q_1) phase space depend only on the three parameters (p_{20}, μ_1, μ_2). The fixed points of the reduced vector field in the range of interest are:

$$
(p_{20}, \hat{q}_1),\ (p_{20}, 2\pi - \hat{q}_1),\ (p_1^+, 0),\ (p_1^-, 2\pi),\ (p_1^+, \pi)
$$

where

$$
\begin{aligned}
\hat{q}_1 &= \cos^{-1} \frac{\sigma}{2\sqrt{p_{20}}} \\
p_1^\pm &= \frac{1}{18}[\sigma^2 + 6\, p_{20} \pm \sigma\sqrt{\sigma^2 + 12\, p_{20}}] \\
\sigma &= (\mu_1 + \mu_2)
\end{aligned}
$$

The linear stability analysis indicates that the phase flow has the qualitatively different behavior in region III as compared with regions I and II (Figure 5.2). These three regions are defined in the following manner:

$$
\begin{aligned}
I &: \quad \{(\sigma, p_{20}) \mid \sigma \ge 0,\ (\sigma^2 - 4p_{20}) < 0\} \\
II &: \quad \{(\sigma, p_{20}) \mid \sigma \le 0,\ (\sigma^2 - 4p_{20}) < 0\} \\
III &: \quad \{(\sigma, p_{20}) \mid (\sigma^2 - 4p_{20}) > 0\}
\end{aligned}
\tag{5.19}
$$

One can easily check that the equilibrium points $(p_{20}, \hat{q}_1)$ and $(p_{20}, 2\pi - \hat{q}_1)$ exist as *saddle* type fixed points in regions I and II, and the equilibrium points $(p_1^+, 0)$, $(p_1^+, 2\pi)$ and (p_1^-, π) exist as *center* type fixed points everywhere in (σ, p_{20}) parameter space. One also notices that there are no saddle points in region III, thus there do not exist any homoclinic/heteroclinic connections in region III. The phase portraits corresponding to these global bifurcation sets (I and II) are shown in Figure 5.3 These phase portraits indicate the existence of a heteroclinic cycle (A-A') connecting the two saddle points $(p_{20}, \hat{q}_1)$ and $(p_{20}, 2\pi - \hat{q}_1)$. The condition for the existence of this heteroclinic cycle is given as:
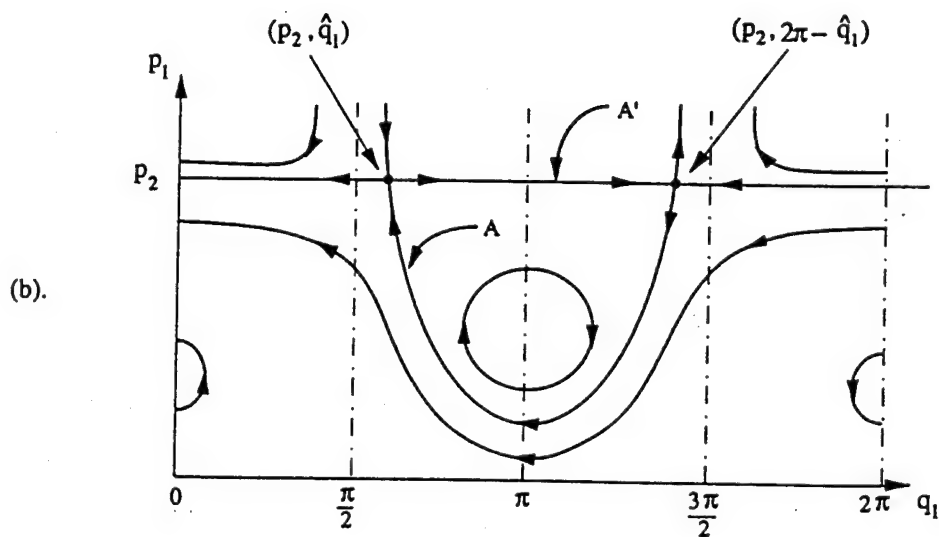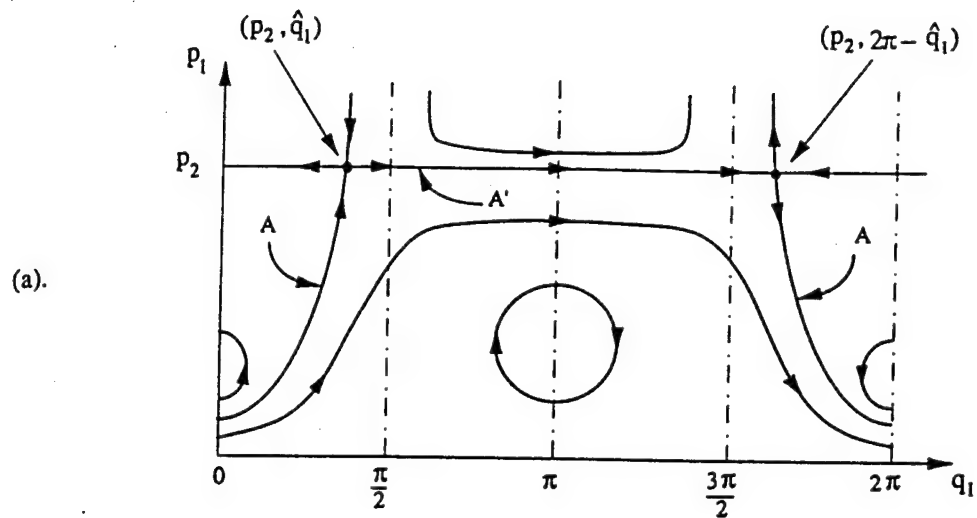
Figure 5.3: (a). Unperturbed phase-flow in (p_1, q_1) phase-space in region I (i.e., $\sigma > 0$), (b). Unperturbed phase-flow in (p_1, q_1) phase-space in region II (i.e., $\sigma < 0$).

$$p_{20} \geq \frac{\sigma^2}{4} \tag{5.20}$$

Hence it can be claimed that the Smale horseshoe type chaotic behavior is not possible for this system when the system parameters lie outside of region I and II. In the subsequent part of this section we assume that the above mentioned condition is satisfied for 1:2 internal resonance case.

The Invariant Manifolds and Associated Dynamics

As noted previously, the equilibrium points $(p_{20}, \hat{q}_1)$ and $(p_{20}, 2\pi - \hat{q}_1)$ exist as hyperbolic fixed points in (p_1, q_1) phase space. However, in the four dimensional phase space these fixed points represent a two-dimensional invariant manifold which is normally hyperbolic:

$$M_0 = \{(p_1, q_1, p_2, q_2) \mid p_1 = p_{20}, \ q_1 = \hat{q}_1 \text{ or } (2\pi - \hat{q}_1), \infty > p_2 = p_{20} \geq \frac{\sigma^2}{4}, \ q_2 \in T^1\}$$

It is obvious that the unperturbed manifold M_0 has a lower boundary at $p_2 = \frac{\sigma^2}{4}$ and no upper boundary. In general M_0 consists of periodic orbits for all values of $p_2 \geq \frac{\sigma^2}{4}$ as long as $\dot{q}_2 \neq 0$. We assume the non-resonant condition (i.e., $\dot{q}_2 \neq 0$) to be valid in this case.

Under small perturbations ($\epsilon \neq 0$), the manifold M_0 persists as M_ϵ due to its normal hyperbolicity property,

$$M_\epsilon = \{(p_1, q_1, p_2, q_2) \mid p_1^\epsilon = p_{20} + O(\epsilon), \ q_1^\epsilon = q_{10} + O(\epsilon), \ \infty > p_2^2 > p_2 > p_2^1 > \frac{\sigma^2}{4}, \ q_2 \in T^1\}$$

where $q_{10} = \hat{q}_1$ or $(2\pi - \hat{q}_1)$. The flow restricted to M_ϵ is described by the following equations (assuming $\delta_1 = \delta_2 = \delta$ for the sake of simplicity):

$$\dot{p}_2 = \epsilon \left[-\delta p_2 + 2\mu p_2 \sin 2(\hat{q}_1 + q_2) \right]$$
$$\dot{q}_2 = -\mu_2 + 2p_2^{1/2} \cos \hat{q}_1 + O(\epsilon) = \mu_1 + O(\epsilon)$$

M_ϵ is a locally invariant manifold with boundaries. Under small perturbations the periodic orbits on M_0 get destroyed, and in the absence of any attracting invariant sets on M_ϵ the trajectories may escape from the manifold by crossing the upper or lower boundary. It is easy to see that there are no invariant sets present on M_ϵ for $\mu_1 \neq 0$. On averaging the $\dot{p}_2$ equation with respect to q_2, we calculate the average rate of change of p_2 as $-\epsilon\delta$. Thus for positive dissipation $p_2 \to 0$ as $t \to \infty$, and hence all the trajectories with initial conditions on M_ϵ leave the manifold by crossing the lower boundary, and eventually get attracted to the trivial solution.

The Melnikov Function for Non-Dissipative Case

It is well known that in the absence of dissipation the nonlinear system (5.16) is non-integrable even for very small values of the forcing amplitude μ. It is also clear that in the presence of dissipation the Melnikov method can not be applied to obtain restrictions for the transversal intersection of the stable and unstable manifolds of M_ϵ. However, if we assume the dissipation to be zero (i.e., $\delta_{1,2} \to 0$), then all the periodic orbits on M_ϵ persist for the perturbed system and the *Melnikov Function* (for the non-integrable Hamiltonian system) gives the distance between the stable and unstable manifolds of M_ϵ for some p_2 corresponding to the attracting set in the domain. In this case the

89

Melnikov Function M provides a measure to ascertain whether the heteroclinic connections (A and A') break under small perturbations, and is given as follows [89]:

$$M = \int_{-\infty}^{\infty} [\frac{\partial \bar{H}}{\partial p_1} \cdot g^{p_1} + \frac{\partial \bar{H}}{\partial q_1} g^{q_1} + \frac{\partial \bar{H}}{\partial p_2} g^{p_2}] dt - \frac{\partial \bar{H}}{\partial p_2}\Big|_{(p_{20}, \hat{q}_1)} \int_{-\infty}^{\infty} g^{p_2} dt \qquad (5.21)$$

where, the integrand has been evaluated at any arbitrary point on the heteroclinic cycle. In the above expression, $g^{p_1}, g^{q_1}, g^{p_2}$, and g^{q_2} are the $O(\epsilon)$ terms in four-dimensional perturbed system of equations (5.16),

$$
\begin{aligned}
g^{p_1} &= 2\mu p_1 \sin 2(q_1 + q_2) \\
g^{q_1} &= \mu \cos 2(q_1 + q_2) \\
g^{p_2} &= 2\mu p_1 \sin 2(q_1 + q_2) \\
g^{q_2} &= 0
\end{aligned}
\qquad (5.22)
$$

and $\bar{H}$, the Hamiltonian corresponding to the four-dimensional unperturbed phase space, is given as:

$$\bar{H}(p_1, q_1, p_2, q_2) = \sigma \ p_1 + 2 \ p_1^{1/2} \ (p_2 - p_1) \cos q_1 - \mu_2 \ p_2 \qquad (5.23)$$

On substituting (5.22) and (5.23) in (5.21), the *Melnikov Function* for our system can be expressed as following,

$$
\begin{aligned}
M = \int_{-\infty}^{\infty} \ [\ & \{\sigma + p_1^{-1/2} \ (p_2 - 3p_1) \cos q_1\}\{2\mu p_1 \sin 2(q_1 + q_2)\} \\
- \ & \{2 \ p_1^{1/2} \ (p_2 - p_1) \sin q_1\}\{\mu \cos 2(q_1 + q_2)\} \\
+ \ & \{-\mu_2 + 2p_1^{1/2} \cos q_1\}\{2\mu p_1 \sin 2(q_1 + q_2)\} \ ] dt \\
- \ & \mu_1 \int_{-\infty}^{\infty} [2\mu p_1 \sin 2(q_1 + q_2)] \ dt
\end{aligned}
\qquad (5.24)
$$

Time parameterized expressions for heteroclinic orbits

In order to evaluate the Melnikov Function the explicit expressions for the heteroclinic orbits are required. The heteroclinic orbit A' is the horizontal line connecting the two saddle points as shown in Figure 5.3. This orbit is described by the following set of equations:

$$
\begin{aligned}
p_1(t) &= p_{20} \\
\dot{q}_1(t) &= \sigma - 2\sqrt{p_{20}} \cos q_1(t) \\
p_2(t) &= p_{20} \\
\dot{q}_2(t) &= -\mu_2 + 2\sqrt{p_{20}} \cos q_1(t)
\end{aligned}
\qquad (5.25)
$$

To evaluate the Melnikov Function for the heteroclinic orbit A' one does not require the explicit expressions for $q_1(t)$ and $q_2(t)$. On substituting $p_1(t) = p_{20}$ in (5.24), and further simplifying the integrand one gets

$$
\begin{aligned}
M_{A'}^{I,II} = \int_{-\infty}^{\infty} \ [\ & \{\sigma - 2\sqrt{p_{20}} \cos q_1\}\{2\mu p_{20} \sin 2(q_1 + q_2)\} \\
+ \ & \{-\mu_1 - \mu_2 + 2p_{20}^{1/2} \cos q_1\}\{2\mu p_{20} \sin 2(q_1 + q_2)\} \ ] \ dt
\end{aligned}
\qquad (5.26)
$$

90

using $\sigma = (\mu_1 + \mu_2)$ in (5.26), it is trivial to show $M_{A'}^{I,II} = 0$, which means the $O(\epsilon)$ distance between the stable and unstable manifolds of A' is always zero and hence, it can be concluded that the heteroclinic orbit A' does not break under order $O(\epsilon)$ perturbation.

The parameterized expression describing the heteroclinic orbit A can be obtained as:

$$\bar{H}(p_1, q_1) = \bar{H}(p_{20}, \hat{q}_1)$$

which implies,

$$p_1(t) = \frac{\sigma^2}{4 \cos^2 q_1(t)} \tag{5.27}$$

substituting this in the unperturbed equations of $\dot{q}_1$ and $\dot{q}_2$, one can get the explicit expressions for $q_1(t)$ and $q_2(t)$, hence the heteroclinic orbit A can be described by

$$p_1(t) = \frac{\sigma^2}{4} + \left(p_{20} - \frac{\sigma^2}{4}\right) \tanh^2 \sqrt{\left(p_{20} - \frac{\sigma^2}{4}\right)} \, t$$

$$q_1(t) = \tan^{-1}\left[\frac{2}{\sigma}\sqrt{\left(p_{20} - \frac{\sigma^2}{4}\right)} \, \tanh \sqrt{\left(p_{20} - \frac{\sigma^2}{4}\right)} \, t \,\right] + q_{10}$$

$$p_2(t) = p_{20} \tag{5.28}$$

$$q_2(t) = \mu_1 t + q_{20}$$

where q_{10} is the initial value of $q_1(t)$. For region I $(0 \leq \sigma < 2\sqrt{p_{20}})$, $q_{10} = 0$ and for region II $(-2\sqrt{p_{20}} < \sigma \leq 0)$, $q_{10} = \pi$. q_{20} is the initial value of $q_2(t)$ and is used as another parameter. Using these expressions in (5.24), and after some algebraic manipulation one can obtain the *Melnikov Function* for the heteroclinic orbit A as following,

$$M_A^{I,II} = 2\mu \sin 2q_{20} \int_{-\infty}^{\infty} \sqrt{p_1(t)} \, \{p_{20} - p_1(t)\} \, \cos\left(q_1(t) + 2\mu_1 t\right) \, dt$$

$$+ \; 2\mu \cos 2q_{20} \int_{-\infty}^{\infty} \sqrt{p_1(t)} \, \{p_{20} - p_1(t)\} \, \sin\left(q_1(t) + 2\mu_1 t\right) \, dt \tag{5.29}$$

One observes that the integrand associated with the second integral in this expression is an odd function of t, and thus the contribution due to this part is zero. The first integral can be computed easily using (5.27) and (5.28) to give

$$M_A^{I,II} = C(\mu_1, \mu_2, \mu, p_{20}) \; \sin 2q_{20} \tag{5.30}$$

where

$$C(\mu_1, \mu_2, \mu, p_{20}) = 2 \, \mu_1 \, (\mu_2 - \mu_1) \, \mu \, \pi \; \csc\left\{\frac{\mu_1 \pi}{\sqrt{\left(p_{20} - \frac{\sigma^2}{4}\right)}}\right\} \tag{5.31}$$

C depends upon the system parameters μ_1, μ_2, μ and p_{20}, and it is in general non-zero. Hence under the circumstances when C is non-zero, the *Melnikov Function* $(M_A^{I,II})$ will have a simple zero with respect to q_{20} at $q_{20} = \frac{n\pi}{2}$. In this case, the heteroclinic orbit A may break under small perturbation with transversal intersection and the system may exhibit chaotic dynamics in the sense of Smale Horseshoe.
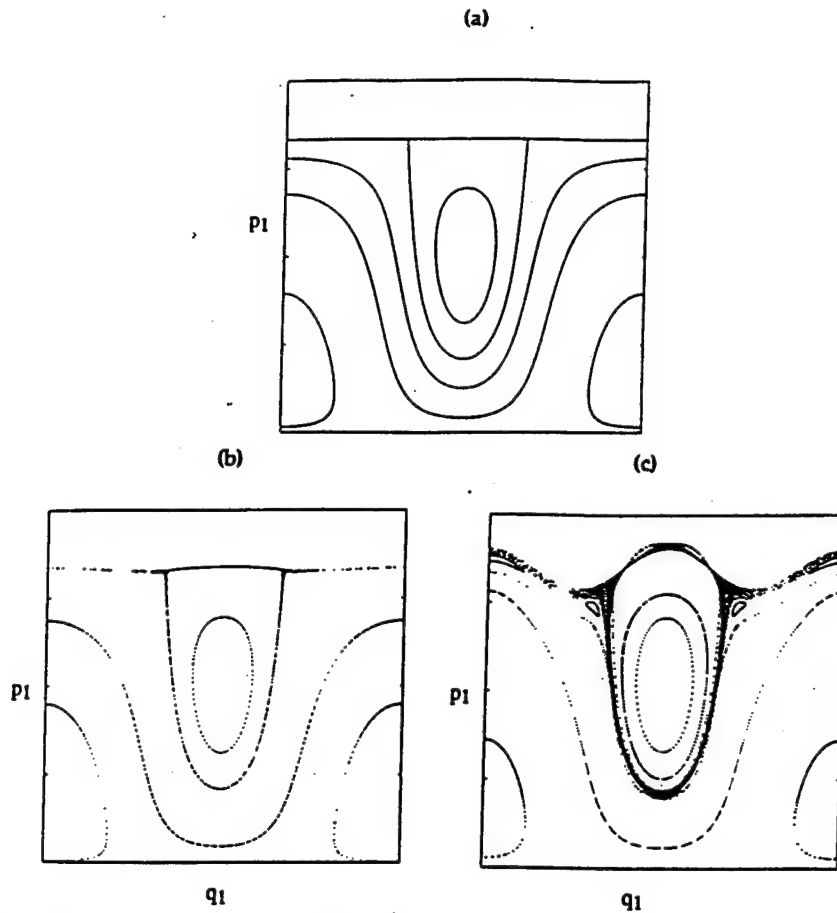
Figure 5.4: (a). The phase trajectories for the unperturbed system ($\epsilon = 0$) in (p_1, q_1) plane with $\sigma = -1.0, \mu_2 = 0.5$, and $p_2 = 1.0$, (b). The Poincare map for the perturbed system in (p_1, q_1) plane with $\sigma = -1.0, \mu_2 = 0.5$, and $\epsilon = 0.01$, (c). Same as part (b) except the parameter ϵ is increased to 0.1.

Numerical Results

In order to examine the effect of small perturbations on the dynamics of unperturbed system in more detail one often resorts to the numerical simulations. As noted previously, in the absence of any perturbations the system dynamics can be studied completely in (p_1, q_1) phase space (Figure 5.4). The introduction of small perturbation couples the dynamics of all the variables (p_1, q_1, I, θ) and in four-dimensional phase space this dynamics can be very complicated. Although the analysis considered earlier provides some insight on the global dynamics of the perturbed system but in general it does not yield the complete picture. However, the trajectories in the four-dimensional phase space can be numerically computed on a two-torus. Using the fact that $q_2 \in T^1$ is a phase variable with period π, three-dimensional Poincare maps can be constructed in (p_1, q_1, p_2) phase space, with $q_2 = q_{20} \bmod \pi$, where q_{20} can be set to zero without loss of generality. Futhermore, the variable p_2 varies very slowly for small perturbations, hence the Poincare map can be easily represented in (p_1, q_1) space.

Figure 5.4 (b) shows a Poincare map in (p_1, q_1) space for $\sigma = -1.0$, $\mu_2 = 0.5$, and $\epsilon \mu = 0.01$. In this diagram one finds that most of the periodic orbits of the unperturbed system survive as quasi-periodic orbits with non-commensurable frequencies on a 2-tori, while the initial conditions taken very close to the unperturbed heteroclinic orbit lead to chaotic dynamics in the perturbed system. As the perturbation strength ($\epsilon \mu$) is increased to 0.1, the extent of the chaotic attractor

increases and various small secondary regions appear in a symmetric fashion about $q_1 = 0$ axis (Figure 5.4 (c)). These secondary regions are small islands of quasi-periodic motion embedded in the layer of stochastic motion. The global dynamics of this system was studied for various values of the system parameters. It was observed that for a given perturbation strength the extent of chaotic layer is rather small for the non-zero values of the detuning parameter σ as compared with the case where $\sigma = 0$. The number, location and appearance of the secondary regions are also sensitive to the values of the detuning parameters. The influence of small perturbations arising from dissipation effects were also examined. It was found that even a very small damping causes the secondary regions to disappear, and the quasi-periodic orbits and the chaotic attractor shrink towards the trivial solution.

In this section the conditions on system parameters are examined for which the shallow arch system can exhibit chaotic dynamics under small harmonic excitations and in the absence of any dissipation mechanism. Under these circumstances it is shown that the equations governing shallow arch system can have heteroclinic connections for certain values of system parameters. Higher dimensional Melnikov's Method is used to show that one of the heteroclinic orbits may break under small time periodic excitations and thus leading to Smale Horseshoe type chaos. The drawback of this method is that one can not examine the effect of perturbations arising from the dissipation effects. In real life systems where the such effects are omnipresent, the application of Melnikov type perturbation methods may not provide strong enough restriction on the system parameters.

We next consider an alternative approach [48] that would allow us to consider the dissipation effects on the global dynamics of arch structures and thus provide more restrictive criterion for the existence of complicated dynamics in the class of system under consideration.

5.4 One-to-One Internal Resonance

In this case, it is possible to find orbits homoclinic to the fixed points that are created in resonance as a result of small perturbations arising from dissipation and excitation. We shall show that a resonance structure exists for some range of parameter values in the shallow arch system. The standard Melnikov type perturbation methods can not be used in these resonance problems without further refining the scaling of various dynamics that co-exist. An alternative technique which uses such scaling has been provided by Kovačič and Wiggins [48]. Their method gives conditions for the existence of a Silnikov type homoclinic orbit to a saddle-focus type fixed point that may be created near resonance structure under small perturbations. The existence of such a homoclinic orbit implies chaotic dynamics. A countably infinite number of unstable periodic orbits and aperiodic orbits exist in every neighborhood of this homoclinic orbit by a theorem of Silnikov [88].

5.4.1 Second order response of the shallow arch system

In order to examine the dynamics of shallow arch system in the presence of 1:1 internal and principal subharmonic resonance, we use a different scaling (as compared with 1:2 case) of parameters and obtain variational equations in the neighborhood of single mode time dependent solutions, and then these equations are averaged using the second order averaging. We proceed in a similar way as before, and introduce the following scaling in the system parameters.

$$\mu = \epsilon\, \gamma, \quad \beta_1 = \epsilon\, \delta_1, \quad \text{and} \quad \beta_2 = \epsilon\, \delta_2$$

Also, assuming the following expansion of $\eta(t)$ in the powers of ϵ,

$$\eta(t) = \eta_0 + \epsilon\,\eta_1 + O(\epsilon^2)$$

where η_0 and η_1 are same as given previously. Now consider the perturbations x_1 and x_2 in the neighborhood of the state $(Q_1(t) = \eta(t), Q_2(t) = 0)$ of (5.3) in the following fashion:

$$Q_1 = \eta(t) + \sqrt{\epsilon}\,x_1, \qquad Q_2 = 0 + \sqrt{\epsilon}\,x_2 \tag{5.32}$$

In this case, the nonlinear perturbation equations governing x_1 and x_2 are given as:

$$\ddot{x}_1 + \omega_1^2\,x_1 + \sqrt{\epsilon}\,[\,3\,\eta_0\,x_1^2 + 4\,\eta_0\,x_2^2\,]$$
$$+ \epsilon\,[\,\delta_1\,\dot{x}_1 + 6\,\eta_0\,\eta_1\,x_1 + x_1^3 + 4\,x_1\,x_2^2\,] + O(\epsilon^{3/2}) = 0 \tag{5.33}$$
$$\ddot{x}_2 + \omega_2^2 x_2 + \sqrt{\epsilon}\,[\,8\,\eta_0\,x_1\,x_2\,]$$
$$+ \epsilon\,[\,\delta_2\,\dot{x}_2 + 8\,\eta_0\,\eta_1\,x_2 + 4\,x_1^2\,x_2 + 16\,x_2^3\,] + O(\epsilon^{3/2}) = 0$$

where ω_1 and ω_2 are same as before. For the corresponding undamped system of (5.33), the Hamiltonian function can be expressed as:

$$
\begin{aligned}
H(\mathbf{x_p}, \mathbf{x_q}) &= H_0 + \sqrt{\epsilon}\,H_1 + \epsilon\,H_2 + O(\epsilon^{3/2}) \\
&= \frac{1}{2}\,[x_{p_1}^2 + x_{p_2}^2 + \omega_1^2\,x_{q_1}^2 + \omega_2^2\,x_{q_2}^2\,] \\
&\quad + \sqrt{\epsilon}\,[\eta_0\,x_{q_1}^3 + 4\eta_0\,x_{q_1}x_{q_2}^2\,] \\
&\quad + \epsilon\,[\frac{1}{4}x_{q_1}^4 + 4x_{q_2}^4 + 2x_{q_1}^2\,x_{q_2}^2 + \eta_0\,\eta_1(3x_{q_1}^2 + 4x_{q_2}^2)\,] + O(\epsilon^{3/2})
\end{aligned}
\tag{5.34}
$$

where $x_{q_1} = x_1$, $x_{q_2} = x_2$, $x_{p_1} = \dot{x}_1$ and $x_{p_2} = \dot{x}_2$. Introducing the following canonical change of variables given by (5.10), the following detuning parameters in order to examine the dynamics of the system in the vicinity of principal sub-harmonic resonance and 1:1 internal resonance.

$$\omega_1^2 = \frac{1}{4}(\nu^2 - \epsilon\sigma_1), \qquad \omega_2^2 = \frac{1}{4}(\nu^2 - \epsilon\sigma_2)$$

where σ_1 and σ_2 are the deviations of excitation frequency from twice the natural frequency of first and second mode, respectively. In other words, σ_1 represents the measure of deviation from principal subharmonic resonance with respect to the first natural frequency, while $(\sigma_2 - \sigma_1)$ represents the deviation from 1:1 internal resonance. At this stage, we apply the second order averaging to obtain the following system of equations in canonical variables (a_i, ϕ_i) using the transformation given by (5.10):

$$\dot{a}_1 = \epsilon[-\delta_1 a_1 - 2k_3 a_1 a_2 \sin 2(\theta_1 - \theta_2) + \frac{6}{\nu}a_1 b_1 \eta_0 \sin 2\theta_1\,] + O(\epsilon^2)$$

$$a_1\dot{\theta}_1 = \epsilon[-\frac{\sigma_1}{4\nu}a_1 - 2k_1 a_1^2 - (k_2 + k_4)a_1 a_2 - k_3 a_1 a_2 \cos 2(\theta_1 - \theta_2)$$
$$+ \frac{3}{\nu}a_1 b_1 \eta_0 \cos 2\theta_1\,] + O(\epsilon^2)$$

$$\dot{a}_2 = \epsilon[-\delta_2 a_2 + 2k_3 a_1 a_2 \sin 2(\theta_1 - \theta_2) + \frac{8}{\nu}a_2 b_1 \eta_0 \sin 2\theta_2\,] + O(\epsilon^2) \tag{5.35}$$

$$a_2\dot{\theta}_2 = \epsilon[-\frac{\sigma_2}{4\nu}a_2 - 2k_5 a_2^2 - (k_2 + k_4)a_1 a_2 - k_3 a_1 a_2 \cos 2(\theta_1 - \theta_2)$$
$$+ \frac{4}{\nu}a_2 b_1 \eta_0 \cos 2\theta_2\,] + O(\epsilon^2)$$

94

where

$$k_1 = \frac{15\,\eta_0^2}{4\,\omega_1^3} - \frac{3}{4\nu}, \qquad k_2 = \frac{13\,\eta_0^2}{3\,\omega_1^3} - \frac{1}{\nu}, \qquad k_3 = \frac{14\,\eta_0^2}{\omega_1^3} - \frac{2}{\nu},$$

$$k_4 = \frac{55\,\eta_0^2}{3\,\omega_1^3} - \frac{3}{\nu}, \qquad k_5 = \frac{20\,\eta_0^2}{3\,\omega_1^3} - \frac{12}{\nu}, \quad \text{and} \quad \theta_i = \frac{\phi_i}{\omega_i} \ \forall\, i = 1, 2.$$

5.4.2 Canonical change of variables

Consider the following canonical transformation to bring the averaged system to the appropriate form in order to apply the perturbation method given by Kovačič and Wiggins [48]:

$$q_1 = \left(\frac{\phi_1}{\omega_1} - \frac{\phi_2}{\omega_2}\right), \qquad q_2 = \frac{\phi_2}{\omega_2}, \qquad p_1 = a_1\omega_1, \qquad p_2 = (a_1 + a_2)\omega_2 \tag{5.36}$$

In addition to this transformation, we re-scale the variables and parameters in the following manner to further simplify the system,

$$\delta_{1,2} = \epsilon^2 \delta'_{1,2}, \qquad \sigma_{1,2} = \epsilon 4\nu \sigma'_{1,2}, \qquad b_1 = \epsilon^2 b'_1,$$

$$p_{1,2} = \epsilon \frac{2p'_{1,2}}{|k_3|}, \qquad q_{1,2} = (1 + sgn(k_3))\frac{\pi}{4} + q'_{1,2}, \qquad t = \frac{t'}{\epsilon^2}$$

As we recall, b_1 is like the amplitude of the forcing. On dropping the prime (') from the rescaled variables and parameters, the rescaled equations up-to $O(\epsilon)$ can be expressed as:

$$
\begin{aligned}
\dot{p}_1 &= 4\,p_1\,(p_2 - p_1)\sin 2q_1 + \epsilon\,[-\delta_1 p_1 + 6f_1 p_1 \sin 2(q_1 + q_2)\,] \\
\dot{q}_1 &= -2\beta + 2(2p_1 - p_2)(\alpha - \cos 2q_1) - 2\gamma_1 p_2 \\
&\quad + \epsilon\,[3f_1\,\cos 2(q_1 + q_2) - 4f_2 \cos 2q_2\,] \\
\dot{p}_2 &= \epsilon\,[-\delta_2 p_2 + (\delta_2 - \delta_1)p_1 + 6f_1 p_1 \sin 2(q_1 + q_2) + 8f_2(p_2 - p_1)\sin 2q_2\,] \\
\dot{q}_2 &= -\sigma_2 - 2(\gamma_1 + \alpha - \cos 2q_1)p_1 - 2\gamma_2 p_2 + \epsilon\,[4f_2 \cos 2q_2\,]
\end{aligned}
\tag{5.37}
$$

where

$$\alpha = \frac{k_2 + k_4 - k_1 - k_5}{|k_3|}, \qquad 2\beta = (\sigma_1 - \sigma_2), \qquad \gamma_1 = \frac{k_1 - k_5}{|k_3|}, \qquad \gamma_2 = \frac{2k_5}{|k_3|},$$

$$f_1 = \frac{b_1 \eta_0}{\nu}, \qquad f_2 = -\frac{b_1 \eta_0}{\nu} sgn(k_3)$$

This system depends upon various parameters. The parameters α, γ_1 and γ_2 are expressed in terms of nonlinear terms and other physical characteristics of the original system, and hence these can be fixed. The parameters σ_2 and β denote detuning terms, δ_1 and δ_2 are the dissipation coefficients and f_1 and f_2 are proportional to the amplitude of the external excitation. Systems similar to (5.37) have been studied by Feng and Sethna [26] and for the nonresonant case and Feng and Sethna [27] and Feng and Wiggins [28] for the resonant case. The presence of the parameter γ_1 makes the averaged equations of motion governing the shallow arch dynamics different than those considered by [28] in connection with investigation of global dynamics of parametrically excited almost square plates. The results obtained here are same as those obtained by [27] except a correction introduced

95

by parameter γ_1 in the results. In the absence of any damping, the equations of motion given by (5.37) represent a four-dimensional Hamiltonian system with the Hamiltonian function H expressed in (p_1, q_1, p_2, q_2) coordinates as following:

$$H(p_1, q_1, p_2, q_2) = H_0(p_1, q_1, p_2, q_2) + \epsilon H_1(p_1, q_1, p_2, q_2) \tag{5.38}$$

where

$$
\begin{aligned}
H_0(p_1, q_1, p_2, q_2) &= -[2\beta\ p_1 + \sigma_2 p_2 + 2\gamma_1 p_1 p_2 + \gamma_2 p_2^2 + 2p_1\ (p_2 - p_1)(\alpha - \cos 2q_1)] \\
H_1(p_1, q_1, p_2, q_2) &= 3\ f_1\ p_1\ \cos(q_1 + q_2) + 4\ f_2\ (p_2 - p_1)\ \cos 2q_2
\end{aligned}
$$

We observe that the coordinate system (p_1, q_1, p_2, q_2) is singular at $p_1 = 0$. Thus we introduce the following canonical transformation in order to avoid such singular behavior as we will soon see that the fixed points at $p_1 = 0$ play an important part in defining the dynamics of this system in our domain of interest.

$$x = \sqrt{2p_1}\sin q_1, \qquad y = \sqrt{2p_1}\cos q_1, \qquad I = p_2, \qquad \theta = q_2 \tag{5.39}$$

The integrable and non-integrable components of the Hamiltonian H assume the following form in the new coordinate system.

$$
\begin{aligned}
H_0(x, y, I, \theta) &= -[\ \beta(x^2 + y^2) + \sigma_2 I + \gamma_1 I(x^2 + y^2) + \gamma_2 I^2 \\
&\quad + \frac{1}{2}(2I - x^2 - y^2)\ [(\alpha + 1)x^2 + (\alpha - 1)y^2]\ ] \\
H_1(x, y, I, \theta) &= \frac{3}{2}\ f_1\ [(y^2 - x^2)\ \cos 2\theta - 2\ x\ y\ \sin 2\theta] \\
&\quad + 2\ f_2\ (2I - x^2 - y^2)\cos 2\theta
\end{aligned}
\tag{5.40}
$$

and thus the corresponding equations of motion are expressed as,

$$
\begin{aligned}
\dot{x} &= \frac{\partial H_0}{\partial y} + \epsilon\ g^x \\
\dot{y} &= -\frac{\partial H_0}{\partial x} + \epsilon\ g^y \\
\dot{I} &= -\frac{\partial H_0}{\partial \theta} + \epsilon\ g^I \\
\dot{\theta} &= \frac{\partial H_0}{\partial I} + \epsilon\ g^\theta
\end{aligned}
\tag{5.41}
$$

where

$$
\begin{aligned}
g^x &= -\frac{\delta_1}{2}x + \frac{\partial H_1}{\partial y} = -\frac{\delta_1}{2}x + 3f_1(y\cos 2\theta - x\sin 2\theta) - 4f_2 y\cos 2\theta \\
g^y &= -\frac{\delta_1}{2}y - \frac{\partial H_1}{\partial x} = -\frac{\delta_1}{2}y + 3f_1(x\cos 2\theta + y\sin 2\theta) + 4f_2 x\cos 2\theta \\
g^I &= -\delta_2 I + \frac{1}{2}(\delta_2 - \delta_1)(x^2 + y^2) - \frac{\partial H_1}{\partial \theta} \\
&= -\delta_2 I + \frac{1}{2}(\delta_2 - \delta_1)(x^2 + y^2) + 3f_1\ [(y^2 - x^2)\sin 2\theta + 2xy\cos 2\theta] \\
&\quad + 4f_2(2I - x^2 - y^2)\sin 2\theta \\
g^\theta &= \frac{\partial H_1}{\partial I} = 4f_2\cos 2\theta.
\end{aligned}
$$

In the subsequent analysis, we will use the system of equations in the above mentioned two coordinate systems alternately.

5.4.3   The unperturbed system

First, we examine the dynamics of the unperturbed system. Setting $\epsilon = 0$ in (5.41) yields the following set of completely integrable equations describing the unperturbed system:

$$
\begin{aligned}
\dot{x} &= -2[\beta + (\gamma_1 + \alpha - 1)I]y + 2\alpha x^2 y + 2(\alpha - 1)y^3 \\
\dot{y} &= 2[\beta + (\gamma_1 + \alpha + 1)I]x - 2(\alpha + 1)x^3 - 2\alpha x y^2 \\
\dot{I} &= 0 \\
\dot{\theta} &= -\sigma_2 - 2\gamma_2 I - [(\gamma_1 + \alpha + 1)x^2 + (\gamma_1 + \alpha - 1)y^2]
\end{aligned}
\tag{5.42}
$$

We observe that the first two equations are completely independent of θ, and $I = $ constant, and thus we need to study the phase flow in (x, y) phase space only. We recall that $p_1 < p_2$ and thus we are interested in the behavior of our system inside the paraboloid described by the following equation:

$$
x^2 + y^2 < 2I
\tag{5.43}
$$

Also, the periodicity in θ implies that we need to consider the system dynamics in the interval $0 \leq \theta \leq \pi$. All possible fixed points of the unperturbed vector field in (x,y) phase space, in the desired range of interest, can be classified as following:

$$
\begin{aligned}
&1. \quad (0,0) \\
&2. \quad (\pm\bar{x}, 0) = (\pm\sqrt{(I - I_1)(1 + a)}, 0) \\
&3. \quad (0, \pm\tilde{y}) = (0, \pm\sqrt{(I - I_2)(1 + b)})
\end{aligned}
\tag{5.44}
$$

where

$$
\begin{aligned}
I_1 &= \frac{-\beta}{(\alpha + 1)(1 + a)}, & a &= \frac{\gamma_1}{(\alpha + 1)} \\
I_2 &= \frac{-\beta}{(\alpha - 1)(1 + b)}, & b &= \frac{\gamma_1}{(\alpha - 1)}
\end{aligned}
$$

In the following analysis we restrict ourselves to the cases where $\alpha > 1, \beta < 0$ and $|\gamma_1| < (\alpha - 1)$, in order to ensure that $0 < I_1 < I_2$. It is obvious that all the fixed points given in (5.44) may not exist for every value of I. In fact, there are three distinct ranges of I where dynamics of the unperturbed system is qualitatively different. In the first case where $0 < I < I_1$, only trivial solution exists and it is of center type stability. At $I = I_1$, this trivial solution goes through a pitch fork bifurcation and gives rise to two branches of center type stability, while the trivial solution assumes the saddle type stability for $I_1 < I < I_2$. The two center type solution branches are described by type 2 fixed points (5.44). The saddle type zero solution goes through another pitchfork bifurcation at $I = I_2$ and this time it gives rise to two branches of saddle type stability. These nontrivial branches are given by type 3 fixed points (5.44). The zero solution itself adopts the center type stability behavior for $I > I_2$. The global bifurcation diagram for the unperturbed system in (x, y, I) space is shown in Figure 5.5. The phase portraits for three different ranges of I are shown in Figure 5.6 in (x, y)

97
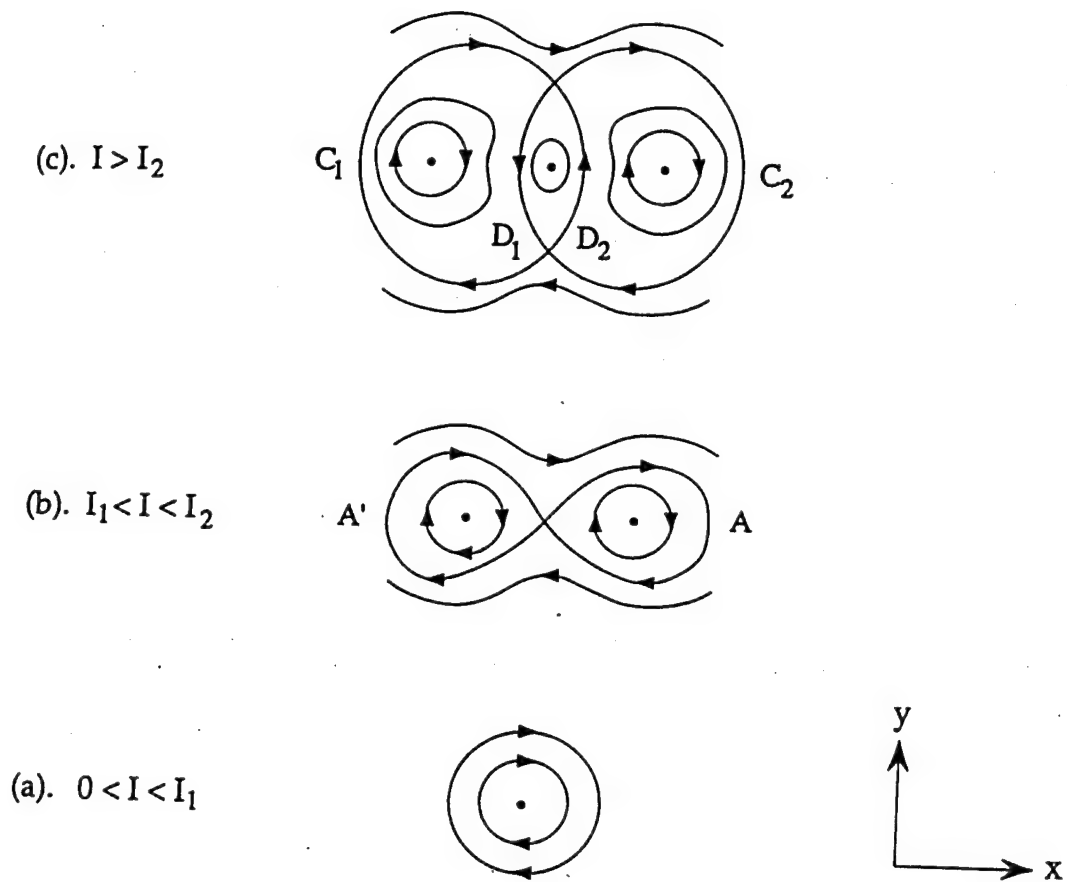
(c). $I > I_2$

(b). $I_1 < I < I_2$

(a). $0 < I < I_1$

Figure 5.6: Phase portraits in (x, y) space corresponding to the unperturbed bifurcation diagram

phase space. We notice that for $0 < I < I_1$, the flow consists of periodic orbits about the origin. For $I_1 < I < I_2$ we have two centers at $(\pm \bar{x}, 0)$ and a saddle at the origin. In this range, the origin is connected to itself by a pair of symmetric homoclinic orbits, each of which is described by:

$$(\beta + \gamma_1 I)(x^2 + y^2) + \frac{1}{2}(2I - x^2 - y^2)\left[(\alpha + 1)x^2 + (\alpha - 1)y^2\right] = 0 \tag{5.45}$$

For $I > I_2$, all five fixed points (5.44) exist. The two saddles at $(0, \pm \tilde{y})$ are connected to each other by heteroclinic connections in a complicated way as shown in Figure 5.6 (c). In this study we examine the conditions under which a Silnikov type homoclinic orbit may exist for $I \in (I_1, I_2)$.

5.4.4 Structure of the invariant manifolds

In the previous section we notice that for the unperturbed system the origin is a hyperbolic fixed point of saddle type stability for any $I \in (I_1, I_2)$. Thus in full four-dimensional phase space this fixed point is a two-dimensional invariant manifold M, and is given as follows:

$$M = \{(x, y, I, \theta) \mid x = 0, \ y = 0, \ I \in (I_1, I_2), \ \theta \in T^1\} \tag{5.46}$$

This invariant manifold M is normally hyperbolic i.e., the rate of expansion and contraction normal to M is dominant as compared to the rate tangent to M. M has a three-dimensional stable $W^s(M)$ and a three-dimensional unstable manifold $W^u(M)$. These manifolds intersect nontransversely along a three-dimensional homoclinic manifold Γ, which is given as:

$$\Gamma = \{(x, y, I, \theta) \mid \quad x = x^h(t, I), \ y = y^h(t, I), \ I \in (I_1, I_2),$$
$$\theta = \int_0^t D_I H_0(x^h(t, I), y^h(t, I), I) \ ds + \theta_0\} \tag{5.47}$$

where $(x^h(t, I), y^h(t, I))$ is the time parameterized expression for the homoclinic orbit. Any trajectory on Γ approaches M as $t \to \pm\infty$. $\theta_0 \in T^1$ is a constant, which is determined from the initial conditions. Due to normal hyperbolicity property, M persists under small perturbations along with its stable and unstable manifolds. The dynamics restricted to the invariant manifold M is described by:

$$\dot{I} = 0$$
$$\dot{\theta} = -\sigma_2 - 2\gamma_2 I \tag{5.48}$$

We can see that $\dot{\theta} = D_I H(0, 0, I) = 0$ for $I = I_r$ where

$$I_r = -\frac{\sigma_2}{2\gamma_2}$$

This represents the resonant value of I, and it corresponds to a circle of fixed points in $I - \theta$ plane. If $D_I H(0, 0, I) \neq 0$ then $I = $ constant represents a periodic orbit. Since we require a positive I value, thus if we assume $\gamma_2 > 0$ then we must have $\sigma_2 < 0$ for $I_r > 0$. In addition, we must ensure that I_r lies within the domain (I_1, I_2). This gives the following restriction on the system parameters as shown in Figure 5.7.

$$\frac{2\gamma_2}{\gamma_1 + \alpha + 1} < |\frac{\sigma_2}{\beta}| < \frac{2\gamma_2}{\gamma_1 + \alpha - 1} \tag{5.49}$$
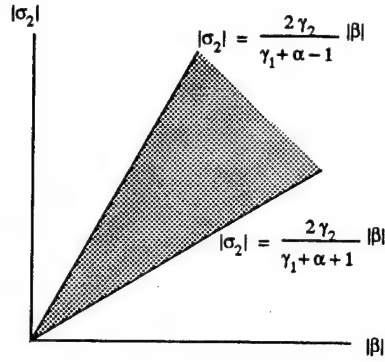
99

Figure 5.7: Region of existence of the resonant I value $I_r \in [I_1, I_2]$.

Following [48], we define a phase shift $\Delta\theta$ such that,

$$\Delta\theta = \theta(+\infty, I_r) - \theta(-\infty, I_r)$$

At the resonant value of I, by using the unperturbed equations in (p_1, q_1, p_2, q_2) coordinates we can show that,

$$\dot\theta = \dot q_2 = -\dot q_1 - 2\gamma_1 p_1$$

Hence the phase shift can be obtained by integrating this equation with respect to the time variable from $-\infty$ to $+\infty$.

$$\Delta\theta = \int_{-\infty}^{\infty} \dot\theta \ dt = -[\ q_1(+\infty, I_r) - q_1(-\infty, I_r)\ ] - 2\gamma_1 \int_{-\infty}^{\infty} p_1 \ dt \qquad (5.50)$$

In order to calculate $\Delta\theta$ we need to obtain the explicit expressions for the homoclinic orbit. The system of equations describing the unperturbed phase flow is integrable, and thus it is possible to obtain the time explicit expressions for the homoclinic manifold Γ. For this purpose, we write the unperturbed system in (p_1, q_1) phase space:

$$\begin{aligned}
\dot p_1 &= 4\ p_1\ (I - p_1)\sin 2q_1 \\
\dot q_1 &= -2\beta + 2(2p_1 - I)(\alpha - \cos 2q_1) - 2\gamma_1 I
\end{aligned} \qquad (5.51)$$

The phase portraits for for different I values (as shown in Figure 5.6) are reconstructed in (p_1, q_1) space and are shown in Figure 5.8. In this space we are interested in the dynamics associated with the heteroclinic connections B and B' for $I \in (I_1, I_2)$. The two saddle points in this space are located at $(0, \hat q_1)$ and $(0, \pi - \hat q_1)$ and the center is located at $(\hat p_1, \frac{\pi}{2})$. This implies $q_1(\infty) = (\pi - \hat q_1)$ and $q_1(-\infty) = \hat q_1$, where

$$\hat q_1 = \frac{1}{2}\cos^{-1}(\gamma_1 + \alpha + \frac{\beta}{I}). \qquad (5.52)$$

Figure 5.9 shows the variation of $\hat q_1$ as the detuning parameters σ_2 is varied. It is easy to see that the hyperbolic fixed point at the origin in (x, y) phase space is same as the heteroclinic connection B' in (p_1, q_1) space. While the homoclinic orbits A and A' in (x, y) phase space (as shown in

(c). $I > I_2$
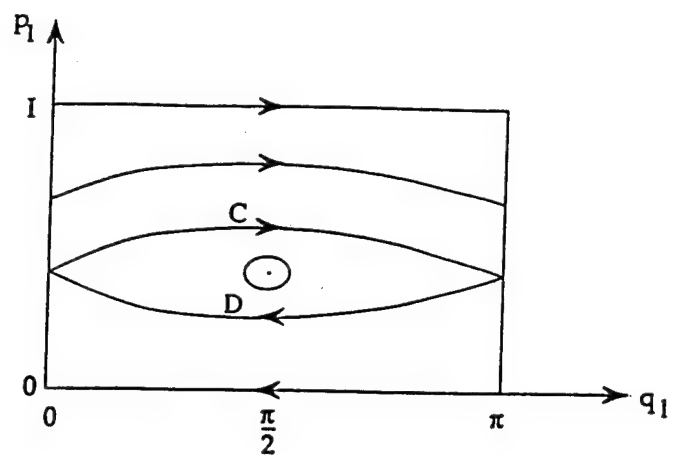
(b). $I_1 < I < I_2$
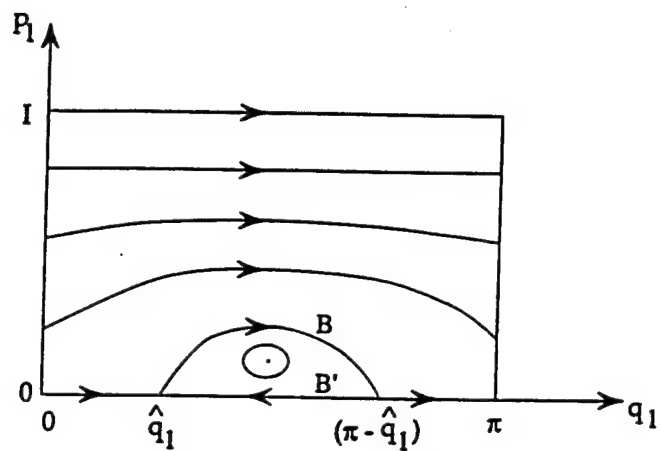
(a). $0 < I < I_1$
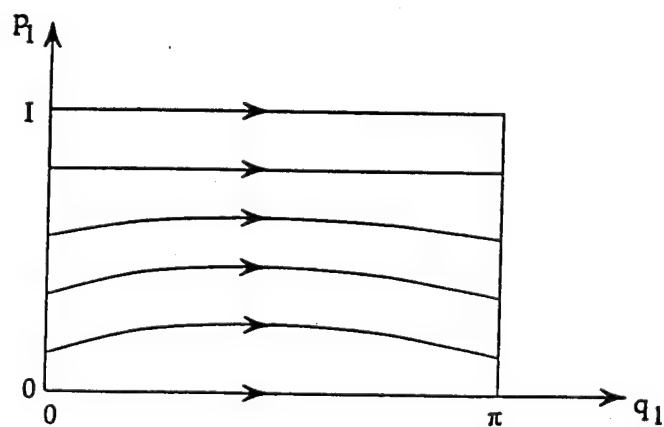
Figure 5.8: Phase portraits in (p_1, q_1) space corresponding to the global bifurcation diagram

101

Figure 5.9: Variation of $\hat{q}_1$ as the detuning parameter σ_2 is varied while $\alpha, \gamma_1, \gamma_2$, and β are fixed at 1.75, 0.25, 0.5, and -1.0, respectively.

Figure 5.6 (b)) coincide with the heteroclinic connection B in (p_1, q_1) phase space. The heteroclinic orbit B is characterized by $H_0(p_1, q_1) = H_0(0, \hat{q}_1)$, which gives:

$$p_1(t) = I + \frac{\beta + \gamma_1 I_r}{\alpha - \cos 2q_1} \tag{5.53}$$

This leads to the following differential equation in q_1,
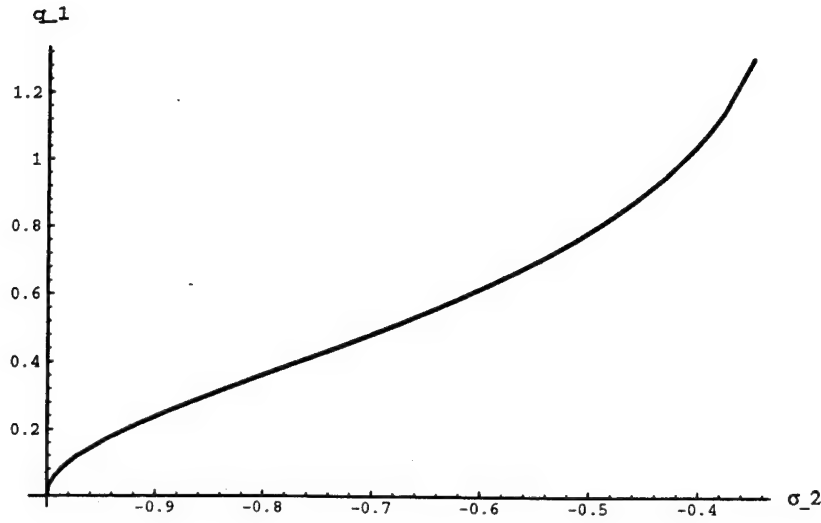
$$\dot{q}_1 = 2I(\cos 2\hat{q}_1 - \cos 2q_1) \tag{5.54}$$

which can be integrated to give,

$$\tan q_1(t) = - \tan \hat{q}_1 \coth(c\,t) \tag{5.55}$$

where $c = 2\,I\,\sin 2\hat{q}_1$, and we assume $q_1(0) = \frac{\pi}{2}$. On substituting (5.55) in (5.53) and after some algebraic manipulation we obtain the time explicit expression for $p_1(t)$.

$$p_1(t) = \frac{E}{\cos f + \cosh 2ct} \tag{5.56}$$

where

$$E = \frac{I\,\sin 2\hat{q}_1{}^2}{\alpha - \cos 2\hat{q}_1}, \qquad \cos f = \frac{1 - \alpha \cos 2\hat{q}_1}{\alpha - \cos 2\hat{q}_1}$$

Hence the phase shift (5.50) can be easily calculated using (5.56) as:

$$\Delta\theta = (2\hat{q}_1 - \pi) - \frac{2\gamma_1 E f}{c \sin f} \tag{5.57}$$

Figure 5.10 shows the phase shift ($\Delta\theta$) as a function of the system parameters σ_2. This quantity (phase shift) has a special significance. In fact the homoclinic orbit in (x, y) space is in general a heteroclinic connection in full four dimensional phase space (x, y, I, θ), and the phase shift gives the difference in θ value as a trajectory leaves and returns to the invariant manifold M.
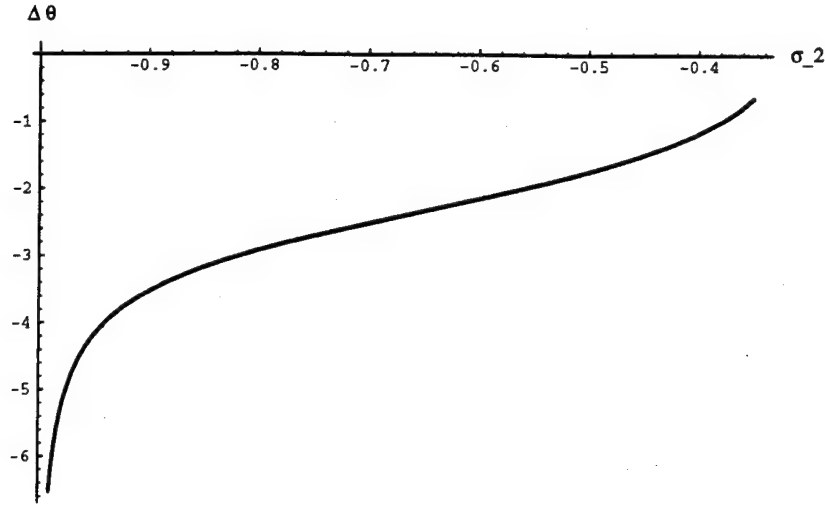
102

Figure 5.10: The phase shift ($\Delta\theta$) as a function of the detuning parameter σ_2.

5.4.5 Effect of Small Perturbations

Next we examine the effect of small perturbations on the normally hyperbolic manifold M and the associated dynamics. The normal hyperbolicity property of the manifold M implies that it persists along with its stable and unstable manifolds under sufficiently small perturbations. But in general, the dynamics within these manifolds changes dramatically. In this problem we notice that the hyperbolic fixed point at $(x = 0, y = 0)$ remains invariant for the perturbed system and thus the manifold M persists as M_ϵ for $\epsilon \neq 0$. The dynamics on M_ϵ is described by the following equations in $I - \theta$ plane.

$$
\begin{aligned}
\dot{I} &= \epsilon \left[8 f_2 \sin 2\theta - \delta_2\right] I \\
\dot{\theta} &= -\sigma_2 - 2\gamma_2 I + \epsilon \left[4 f_2 \cos 2\theta\right]
\end{aligned}
\tag{5.58}
$$

The fixed points of this system (5.58) are given as:

$$
1. \quad (I_c, \theta_c) = (-\frac{\sigma_2}{2\gamma_2} + \epsilon \left[\frac{2 f_2}{\gamma_2} \sqrt{1 - \delta^2}\right], \; \frac{1}{2} \sin^{-1}\delta)
$$

$$
2. \quad (I_s, \theta_s) = (-\frac{\sigma_2}{2\gamma_2} - \epsilon \left[\frac{2 f_2}{\gamma_2} \sqrt{1 - \delta^2}\right], \; \frac{1}{2} \left[\pi - \sin^{-1}\delta\right])
\tag{5.59}
$$

where $\delta = \frac{\delta_2}{8 f_2}$. The Jacobian matrix corresponding to (5.58) at the fixed points is given as follows:

$$
J_{c,s} = \begin{bmatrix} 0 & \pm\epsilon \left(16 f_2 \; I_{c,s} \sqrt{1 - \delta^2}\right) \\ -2\gamma_2 & -\epsilon \, \delta_2 \end{bmatrix}
\tag{5.60}
$$

The trace of the Jacobian matrix is given by $-\epsilon\delta_2$, and for $\gamma_2 > 0$ it is trivial to show that $Det(J_c) > 0$ and $Det(J_s) < 0$. Using this information, the eigenvalues of the Jacobian matrix J

103

corresponding to each of these fixed points is shown to be:

$$\lambda_{1,2}^c = \epsilon^{\frac{1}{2}} \left[\pm i \sqrt{Det(J_c)} + \epsilon^{\frac{1}{2}}(-\frac{1}{2}\delta_2) + O(\epsilon^{\frac{3}{2}}) \right]$$

$$\lambda_{1,2}^s = \epsilon^{\frac{1}{2}} \left[\pm \sqrt{|Det(J_s)|} + \epsilon^{\frac{1}{2}}(-\frac{1}{2}\delta_2) + O(\epsilon^{\frac{3}{2}}) \right].$$

Thus we conclude that (I_c, θ_c) is an asymptotically stable fixed point in $I - \theta$ subspace while (I_s, θ_s) is a hyperbolic saddle. A more refined study of the dynamics on M_ϵ in the vicinity of the resonant I value is performed in [48], which not only provides a more detailed description of the phase flow but also suggests a reasonable estimate for the domain of attraction of stable focus (I_c, θ_c). This is achieved by introducing the following localized coordinates in the neighborhood of I_r.

$$I = I_r + \sqrt{\epsilon}\, h, \qquad \theta = \theta, \qquad t = \frac{\tau}{\sqrt{\epsilon}} \tag{5.61}$$

where τ is the slow time. We can obtain the following equations describing the slow dynamics on M_ϵ near $I = I_r$,

$$h' = [8f_2 \sin 2\theta - \delta_2]\, I_r + \epsilon^{\frac{1}{2}}[8f_2 \sin 2\theta - \delta_2]\, h$$
$$\theta' = -2\gamma_2 h + \epsilon^{\frac{1}{2}}[4f_2 \cos 2\theta] \tag{5.62}$$

The prime $(\prime)$ in (5.62) indicates differentiation with respect to the slow time variable τ. We notice that the unperturbed system $(\epsilon \to 0)$ in $h - \theta$ phase space is integrable, and the corresponding Hamilton's function is expressed as:

$$K(h, \theta) = \gamma_2 h^2 - (4f_2 \cos 2\theta + \delta_2\, \theta)\, I_r \tag{5.63}$$

The integrable Hamiltonian structure at leading order near resonances is a very typical scenario. The unperturbed slow system restricted to $h - \theta$ space has two fixed points at $p_0 = (0, \theta_c)$ and $q_0 = (0, \theta_s)$ respectively. The equilibrium point at $(0, \theta_c)$ has elliptic type stability while $(0, \theta_s)$ has saddle type stability behavior. In addition, the fixed point at $(0, \theta_s)$ is connected to itself by a homoclinic orbit, which encloses infinitely many periodic orbits within. On introducing small perturbations, these periodic orbits are destroyed but the saddle type fixed point q_0 persists as a hyperbolic saddle q_ϵ. Using *Bendixon's Negative Criterion*, we find $D_h \dot{h} + D_\theta \dot{\theta} = -\sqrt{\epsilon}\, \delta_2 < 0$ everywhere inside the area enclosed by the homoclinic orbit in unperturbed (h, θ) space, and thus we can conclude that the elliptic fixed point at $(0, \theta_c)$ persists as a stable focus p_ϵ. It should be mentioned that the fixed points p_ϵ and q_ϵ of the perturbed system (5.62) are same as (I_c, θ_c) and (I_s, θ_s) respectively. A reasonable estimate of the domain of attraction of p_ϵ is provided by the area enclosed by the homoclinic orbit given by $K(h, \theta) = K(0, \theta_s)$. This domain of attraction is enclosed with $\theta \in [\theta_m, \theta_s]$, where θ_m is determined by solving $K(0, \theta_m) = K(0, \theta_s)$, which leads to the following transcendental equation.

$$\cos 2\theta_m + 2\, \delta\, \theta_m = \cos 2\theta_s + 2\, \delta\, \theta_s \tag{5.64}$$

Defining an annulus A_ϵ of width $O(\epsilon^{\frac{1}{2}})$ near $I = I_r$,

$$A_\epsilon = [(x, y, I, \theta) | \ x = 0, y = 0, (I_r - \sqrt{\epsilon}C) < I < (I_r + \sqrt{\epsilon}C), \theta \in T^1]$$

where $C > 0$ is a constant, which is chosen sufficiently large such that A_ϵ encloses the unperturbed homoclinic orbit. This annulus A_ϵ is a small segment of the perturbed invariant manifold M_ϵ and the stable and unstable manifolds of A_ϵ, denoted as $W^s(A_\epsilon)$ and $W^u(A_\epsilon)$, are the subsets of $W^s(M_\epsilon)$ and $W^u(M_\epsilon)$, respectively.

104

5.4.6 Existence of Silnikov type homoclinic orbit

We are interested in the existence of an orbit that leaves p_ϵ while coming out of the annulus A_ϵ in four-dimensional phase space, and under certain circumstances it may return to the annulus and eventually completing a Silnikov type homoclinic orbit. The existence of such an orbit connecting the saddle focus p_ϵ is examined in two steps. First using higher dimensional Melnikov theory, one obtains conditions for which $W^u(p_\epsilon) \cap W^s(A_\epsilon) \neq 0$, i.e. when a trajectory leaving p_ϵ comes back in the neighborhood of A_ϵ. Secondly, whether this orbit (in $W^u(p_\epsilon)$) comes back in the domain of attraction of p_ϵ. If it does not, then the trajectory may leave the annulus (A_ϵ) by crossing one of the boundaries of the annulus. But if it does, then the trajectory asymptotes to p_ϵ and a Silnikov type homoclinic loop, connecting p_ϵ to itself is completed. Here $W^u(p_\epsilon)$ and $W^s(A_\epsilon)$ are one and three dimensional manifolds respectively.

In order to ensure the first condition $(W^u(p_\epsilon) \cap W^s(A_\epsilon) \neq 0)$ we evaluate the Melnikov Function M^{I_r}, which gives a measure of $O(\epsilon)$ distance between $W^u(p_\epsilon)$ and $W^s(A_\epsilon)$, and is computed in the following manner:

$$M^{I_r} = \int_{-\infty}^{\infty} [\frac{\partial H_0}{\partial x} g^x + \frac{\partial H_0}{\partial y} g^y + \frac{\partial H_0}{\partial I} g^I]dt - \frac{\partial H_0}{\partial I}\Big|_{(0,0,I_r)} \int_{-\infty}^{\infty} g^I \, dt \qquad (5.65)$$

where, both the integrand have been evaluated at any arbitrary point on the homoclinic manifold Γ at $I = I_r$, and g^x, g^y and g^I the $O(\epsilon)$ terms in $\dot{x}, \dot{y}$ and $\dot{I}$ equations, respectively. For the sake of simplicity, let's assume $\delta_1 = \delta_2$. It is obvious that the second integral has no contribution to the Melnikov function. After some trivial calculations we can express the Melnikov Function as:

$$M^{I_r} = \int_{-\infty}^{\infty} [-\frac{\partial H_1}{\partial t} + \frac{\delta_2}{2}(x\dot{y} - \dot{x}y) - \delta_2 I_r \dot{\theta}]dt \qquad (5.66)$$

which can be further simplified to give,

$$M^{I_r} = -\Delta H_1 - \delta_2 \, I_r \, \Delta\theta + \frac{\delta_2}{2} \int_{-\infty}^{\infty} (x \, dy - y \, dx) \qquad (5.67)$$

We can show that,

$$\Delta H_1 = H_1(\infty) - H_1(-\infty) = 4f_2 I[\cos 2(\theta_c + \Delta\theta) - \cos 2\theta_c]$$

$$\int_{-\infty}^{\infty} (x \, dy - y \, dx) = -2 \int_{\hat{q}_1}^{\pi - \hat{q}_1} p_1 \, dq_1$$

$$\int_{\hat{q}_1}^{\pi - \hat{q}_1} p_1 \, dq_1 = I_r \, \Delta q_1 + (\beta + \gamma_1 I_r) \, S$$

where

$$\Delta q_1 = (\pi - 2\hat{q}_1),$$

$$S = \int_{\hat{q}_1}^{\pi - \hat{q}_1} \frac{1}{\alpha - \cos 2q_1} \, dq_1 = \frac{1}{\sqrt{\alpha^2 - 1}} [\pi - 2 \tan^{-1}(\sqrt{\frac{\alpha + 1}{\alpha - 1}} \tan \hat{q}_1)]$$

Using these expressions, the Melnikov Function can be obtained as:

$$M^{I_r} = -4f_2 I_r [\cos 2(\theta_c + \Delta\theta) - \cos 2\theta_c + 2\delta(\Delta\theta + \Delta q_1) + 2\delta(\gamma_1 + \frac{\beta}{I_r}) S] \qquad (5.68)$$
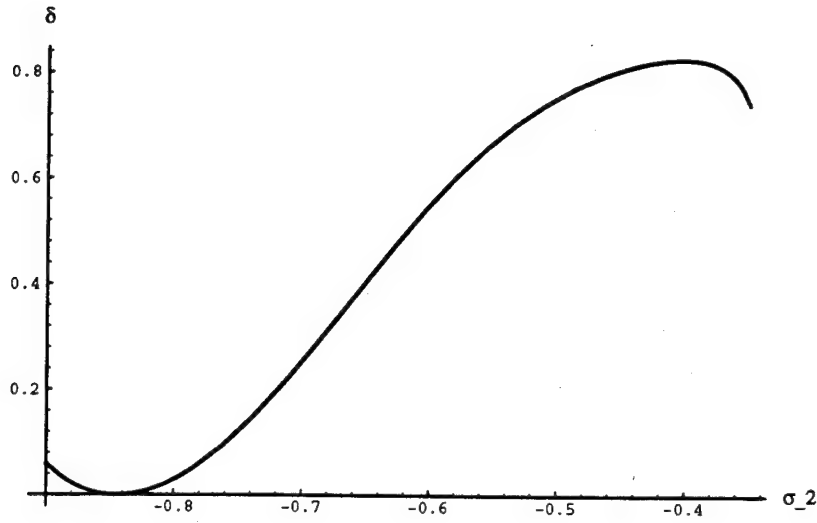
105

Figure 5.11: The curve representing the simple zeroes of the *Melnikov Function* in the $\delta - \sigma_2$ parameter space.

In order to show the existence of an orbit homoclinic to p_ϵ, we first need to examine the parameter values for which the Melnikov function has a simple zero. Substituting for θ_c in (5.68) we notice that M^{I_r} has a zero for:

$$\delta = \frac{1 - \cos 2\Delta\theta}{\sqrt{(1 - \cos 2\Delta\theta)^2 + [2(\Delta\theta + \Delta q_1) + 2S(\gamma_1 + \frac{\beta}{I_r}) - \sin 2\Delta\theta]^2}} \qquad (5.69)$$

It can be verified that the above condition gives a simple zero of M^{I_r}. The curve representing the simple zeroes of the Melnikov Function (M^{I_r}) is shown in Figure 5.11 in $\delta - \sigma_2$ parameters space. In addition, The following condition must be satisfied for the orbit in $W^u(p_\epsilon)$ to return to the basin of attraction of p_ϵ:

$$\theta_m < \theta_c + \Delta\theta + m\pi < \theta_s \qquad (5.70)$$

where m is any integer, and $\theta_c, \theta_s, \theta_m$ and $\Delta\theta$ are given by (5.59), (5.64) and (5.57), respectively. The two step calculation effectively determines the restrictions on the systems parameters for the existence of a homoclinic saddle focus.

If we fix $\alpha, \gamma_1, \gamma_2, \beta$ and σ_2 at 1.75, 0.25, 0.5, -1.0, and -0.61, respectively, then it is easily seen from Figure 5.12 that the phase condition (given by Eq. 70) is satisfied for $\delta < 0.585$. The corresponding critical value of δ which leads to a simple zero of the Melnikov function is 0.5224, and thus $\delta = 0.5224$ leads to the existence of a saddle focus or Silnikov type homoclinic orbit in the perturbed system. It is interesting to note that a slightly smaller value of σ_2 ($= -0.6$) does not lead to the Silnikov type phenomenon (Figure 5.13). In this case, the phase condition is satisfied for $\delta < 0.545$, but the critical value of delta ($= 0.5498$) leading to a simple zero of M^{I_r} is outside the domain.

This mechanism is fundamentally different from homoclinic tangency of a Poincare map (as observed in the previous section) as a source of chaotic dynamics. The mere existence of Silnikov
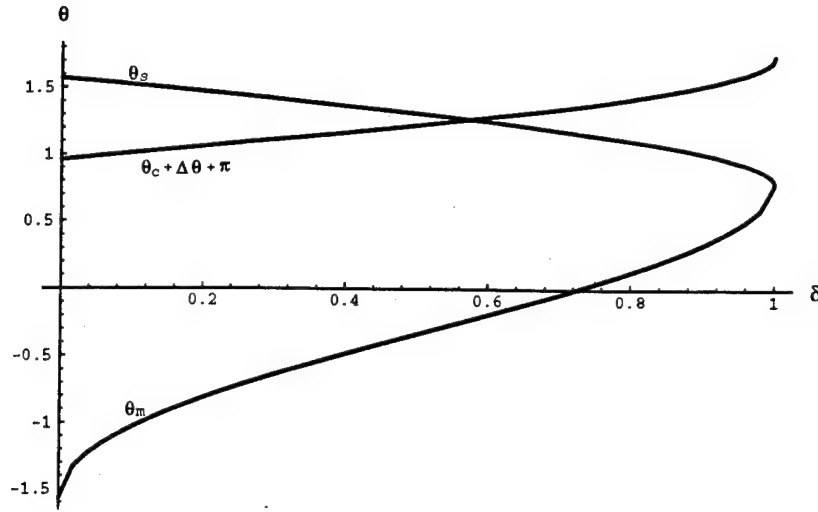
Figure 5.12: Graphical representation of the phase condition as given by Eq. 70. Various angle coordinates θ_s, θ_m and $(\theta_c + \Delta\theta + \pi)$ are plotted as the parameter δ is varied from 0.0 to 1.0. In this figure, $\alpha, \gamma_1, \gamma_2, \beta$ and σ_2 are fixed at 1.75, 0.25, 0.5, -1.0, and -0.61, respectively. The phase condition is satisfied for $\delta < 0.585$.
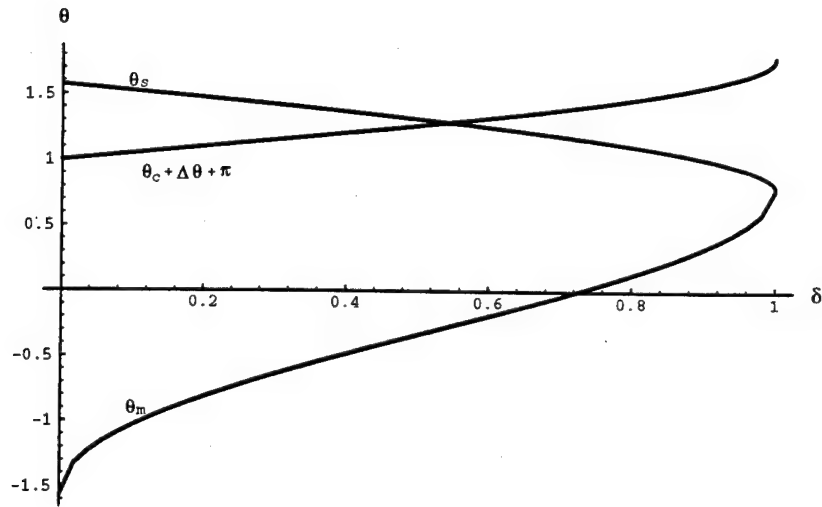
Figure 5.13: Same as figure before with the exception that the detuning parameter σ_2 is set at -0.6. In this case the phase condition is satisfied for $\delta < 0.545$.

type of homoclinic orbit provides a very robust mechanism for the existence of global chaos in the class of systems examined in this chapter. The chaotic behavior exists before, during, and after the creation of a Silnikov orbit.

5.5   Interpretation of Results

In this section we make an attempt to interpret the results corresponding to the perturbation variables x_1 and x_2 in terms of the response of the original system. We shall only discuss the one-to-two resonance case, as the interpretations for the one-to-one resonance case are similar. The amplitudes of the two fundamental modes ($Q_1(t)$ and $Q_2(t)$, respectively) of vibration of the shallow arch structure are expressed as:

$$
\begin{aligned}
Q_1(t) &= \eta(t) + \epsilon\sqrt{2a_1}\cos\left(\frac{\nu}{2}t+\theta_1\right) + O(\epsilon^2) \\
Q_2(t) &= \epsilon\sqrt{2a_2}\cos\left(\frac{\nu}{4}t+\theta_2\right) + O(\epsilon^2)
\end{aligned}
$$

where $\eta(t) = \eta_0 + \epsilon\,(b_1\cos\nu t) + O(\epsilon^2)$. It is well known that the solutions of the averaged equations (12) are related to the solutions of the original system (3), for sufficiently small values of ϵ. We make the following comments in regard to the dynamics in a_1 and a_2 variables with the response of the original system.

- The trivial solutions of (12) correspond to the single mode periodic motions (with base period of $\frac{2\pi}{\nu}$) of the original system.

- The non-trivial equilibrium solutions of (12) correspond to the periodic response of the original amplitudes. These additional non-trivial equilibrium solutions are the subharmonic periodic solutions with period $\frac{4\pi}{\nu}$ (which is twice the base period) for the first mode and periodic solutions with period $\frac{8\pi}{\nu}$ for the second mode.

- Similarly the periodic and quasi-periodic solutions of the averaged equations (12) correspond to the almost-periodic motions of the original system. One recalls that the periodic solutions of the averaged equations are over a slow time scale, thus the almost-periodic solutions of the original nonautonomous system shall be in the form of amplitude and phase modulated motions. The resulting motions of the shallow arch are slowly modulated periodic motions of frequency $\frac{\nu}{2}$ which are superimposed on the basic periodic response of frequency ν in the first mode of vibration.

- Whenever the system parameters are such that the averaged system has chaotic motions, it is expected that the original nonautonomous system will also undergo chaotic amplitude modulated motions.

- The present approach though more realistic can not be applied to study the response of the system near the harmonic excitation frequency because the coefficient b_1 becomes singular at $\nu = \omega_1$.

We have already described how the results corresponding to the averaged system relate to the original system (3). Now we comment on the nature of motions that may appear in the shallow

arch oscillations. In the remaining part of this section we consider the single mode periodic motions (with period of $\frac{2\pi}{\nu}$) to be the base state and solutions of the averaged system are superimposed over this state. For one–to–two internal resonance case the physical interpretation of the possible solutions is as follows:

- In the unperturbed phase space (see Figure 5.3), the elliptic type fixed points represent coupled mode constant amplitude motions over the base state, and the phase variable corresponding to both the modes varies slowly. The two types of elliptic fixed points, at (p_1^-, π) and $(p_1^+, 0 \text{ or } 2\pi)$ respectively, have different amplitude and phase structure. In this phase space the periodic orbits represent two types of coupled mode amplitude and phase modulated motions, which are separated by a different class of dynamics associated with the separatrix A (described next).

- If the initial conditions are chosen on the heteroclinic orbit A, the motion starts off as amplitude and phase modulated coupled mode vibration, and remains in such state for a long time (the initial conditions on heteroclinic connection A' start as constant single mode constant amplitude phase modulated periodic motions). But as the orbits (A or A$'$) approach the saddle point, the motion becomes single mode constant amplitude vibration (in the first mode).

- When we introduce small perturbations (due to excitation and dissipation effects) in the unperturbed system, first the amplitude and phase modulated motions appear and then amplitudes of both modes diminish slowly due to the presence of dissipation effects (no matter how small), and finally the motion settles down to the zero solution. This occurs for all the initial conditions in the phase space in the absence of any resonant structure on the invariant manifold M_ϵ.

- On introducing small forcing (with no dissipation) in the system, and if the initial point is chosen near the unperturbed heteroclinic connection A (i.e., the separatrix), the motion remains in the amplitude phase modulated coupled mode forever and never repeats itself. The amplitude and the phase of both the modes vary chaotically due to random exchange of energy between them. This occurs due to the presence of KAM tori in the perturbed system.

For one–to–one internal resonance case, a qualitatively different physical phenomena are observed for the damped and forced system:

- For the corresponding unperturbed system ($\epsilon = 0$), if the trajectory is on the invariant manifold M (given by Eq. 46) the motion occurs in the second mode only. In this motion the amplitude is constant (since $a_1 = 0$ and $a_2 = \frac{I}{\omega_2} = \text{const.}$) and the phase variable θ varies slowly.

- When the flow is outside the invariant manifold M and $x^2 + y^2 < 2I$ is satisfied, the trajectory is either on the elliptic fixed points, periodic manifolds or the homoclinic manifold Γ. In such a case the motions are similar to as described previously for the one–to–two resonance.

- In one–to–one case there exists a certain initial condition (I_r) on the hyperbolic manifold M for which the motion occurring in the second mode has constant amplitude and constant phase. The associated dynamics of the perturbed system has a very interesting structure on M_ϵ in the presence of small perturbations arising from dissipative effects and excitation.

- For the perturbed system ($\epsilon \neq 0$) we concentrate on the dynamics associated with trajectories coming out of hyperbolic sink p_ϵ. In this case ($x = 0, y = 0$) remains an invariant sub-space even for the perturbed system. The initial conditions on M_ϵ which lie outside the domain of attraction of p_ϵ lead the phase flow towards the stable trivial solution (which is an attracting invariant set in the presence of positive dissipation), and the motion settles down to the base state.

- But if the initial conditions lie within the domain of attraction of p_ϵ, the motion starts off as amplitude and phase modulated single mode vibration with slowly decreasing amplitude, and eventually the resulting motion becomes a constant amplitude constant phase vibration of the second mode.

- In the full four-dimensional phase space if the initial conditions are chosen near p_ϵ and close to $W^u(p_\epsilon)$, and if the *Melnikov Condition* and the *Phase Criterion* are simultaneously satisfied, the motion starts as a mixed mode amplitude and phase modulated vibrations, but soon the trajectory approaches the annulus disc A_ϵ and the motions appear to be in almost one mode (the second one) for a long time, and as it approaches p_ϵ the trajectory takes off again and repeats the similar motion in the four-dimensional phase space, and it goes on forever.

- On the other hand if the *Phase Criterion* is not satisfied, all the motions die out slowly as the trajectories move towards the trivial (zero) attracting set in M_ϵ.

It is easy to check that one-to-two internal resonance occurs for $q_0 = \lambda_0 = 5$, and one-to-one resonance takes place for $q_0 = \lambda_0 = \sqrt{7}$. In both the cases the constant part of the response (η_0) has two nontrivial solutions under resonant conditions (obtained by solving Eq. 8), which are $\eta_0 = \pm 2\sqrt{6}$ for 1:2 resonance, and $\eta_0 = \pm\sqrt{6}$ for 1:1 resonance. One can show that in both the cases the value of the loading parameter λ_0 is far from the critical values, and thus the arch oscillates in only one position (either top or bottom), and the motions described in this chapter are in the neighborhood of the non-trivial η_0 values. The snap through buckling does not take place as a result global bifurcations described in this chapter.

Chapter 6

DESIGN AND CONSTRUCTION OF LABORATORY FACILITIES

6.1 Introduction

Analytical techniques, such as the method of averaging and the theory of normal forms discussed in the previous chapters, provide a means of approximating the solutions of nonlinear and nonautonomous dynamical systems. These approximate solutions are then used to predict the local bifurcation behavior of the original system and estimate the nontrivial response in the post-critical regions. Furthermore, as in Chapter 5, the reduced equations form the basis for studying more complicated global bifurcations. While these techniques seem to provide engineers and scientists with the ability to predict the behavior of many practical dynamical systems without the expense and delay of complicated experiments, the accuracy of the approximations (as well as that of the mechanical models) is not fully known. Before relying on the results of such modeling and reduction techniques in the analysis of complex systems, it is imperative to verify the local and global predictions of simple (lower dimensional) dynamical systems through direct experimentation.

Experimental studies in nonlinear dynamics and chaotic motion of mechanical systems have been performed by several researchers [18, 61, 62]. Moon and co-workers considered various experimental methods to analyze elastic buckling dynamics [18], dry friction oscillators [61], superconducting levitation dynamics and fluid-elastic vibrations in an elastic tube [69]. Planar nonlinear motions of structural models with 2:1 internal resonance subjected to a harmonic base excitation were studied experimentally by Haddow et al. [33] and, recently, by Nayfeh and co-workers [66, 9].

In the case of stochastic systems, however, nonlinear experimental studies are scarce. Most of the investigations deal with linear stochastic models. Under this modeling restriction, the limits of stability (in some sense) of the trivial solution can be determined. However, in order to predict the post-critical (nontrivial) behavior, one needs to consider the full nonlinear problem. Some of the earliest nonlinear random vibration tests were conducted by Lyon et al. [54] and Bogdanoff and Citron [12]. Experimental results of Bogdanoff and Citron were used to substantiate the theoretical results that an inverted pendulum can be stabilized in mean square by applying a stationary random vertical base excitation with discrete power spectrum. Exploratory studies of liquid behavior in randomly excited tanks were reported by Dalzell [19, 20]. However, due to the complex nature of the model, no realistic comparisons with theory were possible. The work of Baxter and Evan-Iwanowski [10] is another early experimental investigation in which a series of experiments were

conducted to measure the stochastic response of an elastic column excited by a random parametric loading. In the early eighties, experimental studies on coupled nonlinear oscillators subjected to a random excitation were reported by Roberts [74].

Recently, some of these experiments on two-degree-of-freedom models with internal resonances have been repeated by Ibrahim and co-workers [41, 42]. A survey article by Ibrahim [40] presents an up-to-date literature review of experimental work in stochastic dynamics. Most of these experimental results were compared to those obtained analytically via the non-Gaussian closure technique. This technique, however, was found to predict erroneous behavior for the system near bifurcation points which are of primary interest in the determination of stability boundaries for dynamical systems [40].

The goal of the final portion of this research is the design and construction of an experimental rig. This rig will serve as a test bed for direct experimental verification of the validity of the results obtained from the various approximation techniques employed in the analysis of nonlinear differential equations. The theoretical results will serve as a guideline for locating stability boundaries and predicting post-critical behavior. The extent to which the theoretical and experimental results match will provide an insight into the accuracy of the mathematical models and theoretical approximations. The experiments will, in turn, guide the development and refinement of the analytical techniques to incorporate any new phenomena observed.

6.2 Design of Shaft Test Rig

In Chapter 3, the partial differential equations of motion governing the longitudinal and transverse vibrations (in the two principal directions) of a rotating shaft were derived. In the derivation, it is assumed that the shaft is rotating at a constant rate Ω and subjected to a time-dependent compressive load given by $P(t) = P_0 + \mu \cos \nu t$. In practical mechanical systems which rely on the transmission of power via a rotating shaft, transverse vibrations are unwanted and may even prove catastrophic. It is generally desired to operate in a parameter region in which the nonvibratory state is stable. The lowest order vibratory modes are the most frequently encountered and exhibit the largest amplitude oscillations. For this reason, it is imperative to be able to predict the onset of these vibrations in terms of the pertinent system parameters.

Using a Galerkin approximation and assuming only the first mode (in each lateral direction) of the rotating shaft to be excited, the partial differential equations of motion are reduced, in Chapter 3, to a set of ordinary differential equations. The stability of the trivial solution (the nonvibratory, or rest, state) and local bifurcation behavior of the averaged equations are examined in Chapter 4. The stability boundaries for the trivial solution are mapped out in the μ-ν parameter space. When the stability conditions for the trivial solution are violated, a stable nontrivial solution of the averaged equations emerges.

The focus of this chapter is to describe the experimental set-up designed to verify the local results obtained in Chapter 4. The test model is a brass shaft, rotating at a constant rate and parametrically excited by a time-dependent axial load. The model and the experimental subsystems are described in detail in this section. The goal of the investigations to be performed using this rig is the experimental determination of the local stability boundaries, in terms of the excitation amplitude μ and frequency ν, and a quantitative description of the post-critical nontrivial solutions.

The test shaft is machined from hard naval brass (#464). The published material properties of hard naval brass are shown in Table 6.1 along with the shaft characteristics of interest. A schematic

Shaft property	Characteristic value
Material	464 hard naval brass
Young's modulus, E	15.9 x 10^6 psi
mass/unit length, μ	7.92 x 10^{-4} lb_f-s^2/in^4
yield strength, S_y	60 ksi
length, L	25.1 in.
diameter, d	0.25 in.
1st mode natural frequency, f_n	50 Hz
buckling load, P_{cr}	191 lb_f
max. allowable strain, ε_{max}	2500 μin/in
max. allowable deflection, α_{max}	0.3 in
max. endpoint displacement, $(\Delta x)_{max}$	0.018 in

Table 6.1: Physical Characteristics of the Shaft

of the shaft assembly is shown in Figure 6.1. The shaft has a clamped length of $L = 25.1$ in. and a diameter of $d = 0.25$ in.

As shown in Table 6.1, the critical static buckling load of the shaft is $P_{cr} = 191$ lb_f and the angular natural frequency is $f_n = 50$ Hz. Assuming a safety factor of 1.5 ($\sigma_{max} = \sigma_{yield}/1.5$), the maximum allowable strain is $\varepsilon_{max} = 2500\mu$ in./in. corresponding to a centerline deflection of 0.3 in.

The bearing assemblies are designed to closely approximate clamped-clamped boundary conditions. With the use of super-precision bearings, the maximum angular deflection of the shaft at the bearings is calculated to be 0.013 degrees. In practice, perfectly clamped or pinned boundary conditions are difficult to achieve. To this end, the boundary conditions for a shaft rotating in a bearing may be described by

$$EI\frac{\partial^2 y}{\partial x^2} + c_L\frac{\partial y}{\partial x} = 0$$

where the factor c_L is included to describe a condition between a pinned boundary condition and a clamped boundary condition. The coefficient c_L ranges from zero to infinity. If the shaft is perfectly clamped, $c_L = \infty$. To satisfy the above condition, the slope $\partial y/\partial x$ must be identically zero. For a pinned end, $c_L = 0$. Thus, as one would expect, the above condition requires $\partial^2 y/\partial x^2 \equiv 0$. The value of c_L can be determined in such a way that an experimentally measured first mode natural frequency is equal to the theoretical value for such boundary conditions. This implies an altered mode shape which must be obtained theoretically using the above boundary condition with the appropriate value of c_L. However, the form of the temporal equations which describe the motion of the rotating shaft remain unchanged.

The detail of the motor-end bearing assembly is shown in Figure 6.2. The brass shaft is held in the motor-end bearing hub using a slit clamp, two bolts and four set screws. The large steel bearing blocks and large thrust bearing take the full load transmitted by the shaft. the bearing hub has eight port holes tapped through to allow for passage of strain gage leads from the shaft to the slip ring which is mounted on the bearing hub. The bearing hub is then passed through a radial bearing and coupled to the flywheel and motor.
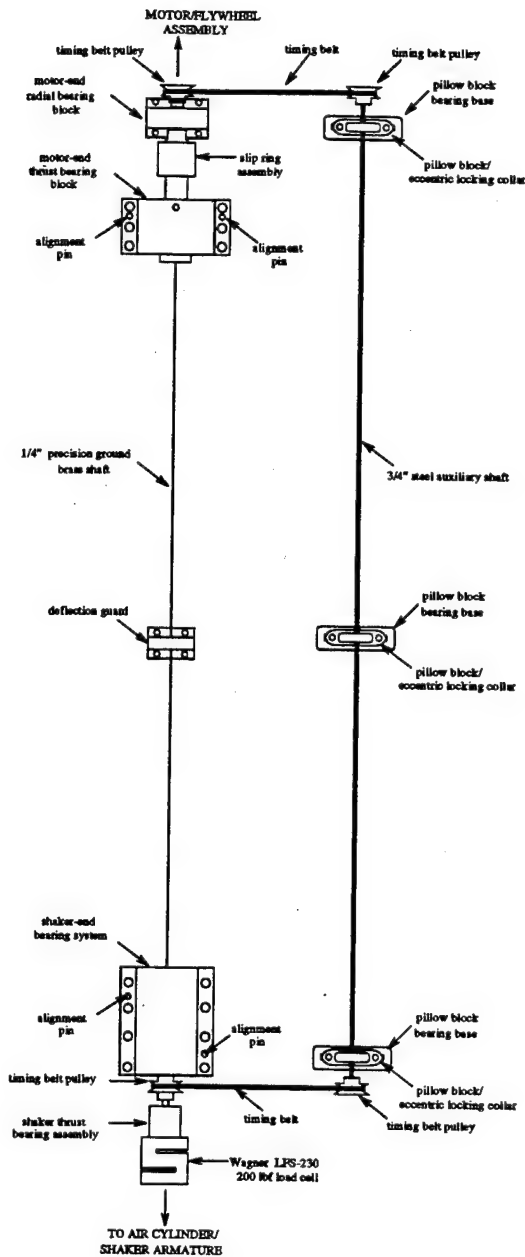
113

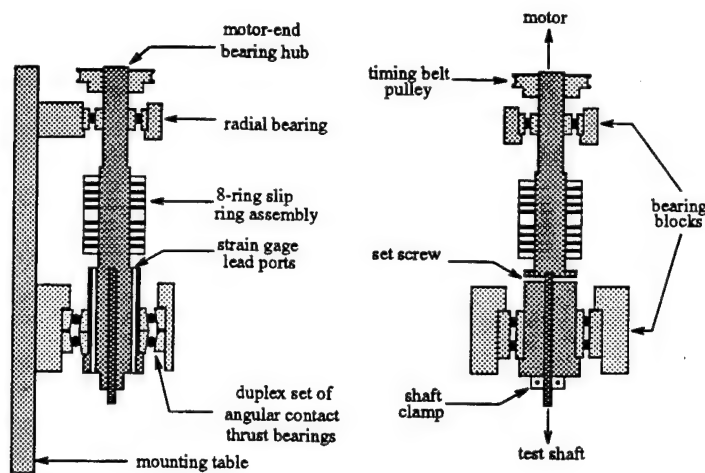Figure 6.1: Schematic of shaft assembly

Figure 6.2: Detail of the motor-end bearing assembly

The detail of the shaker-end bearing assembly is shown in Figure 6.3. The bearing hub is mounted in two bearings, one of which is a thrust bearing used to provide increased axial rigidity. Three 0.375 in. linear-rotary bearings are mounted inside the bearing hub to allow for axial movement of the shaft. The hardened stainless steel sleeves on which the linear-rotary bearings act are attached to the shaft using a shrink fit. The sleeves act as inner races for the ball bearings and also increase the stiffness of the shaft through the bearings. The major subsystems are described in detail below. Photographs of the existing setup and the excitation system are displayed in Figures 6.9 and 6.10 at the end of this chapter.

Loading/Excitation System

The axial load (static plus dynamic) is monitored by a Cooper Instruments LFS-230-200 shear beam load cell mounted to the lower end of the shaft as shown in Figure 6.3. This device has a 200 lb_f capacity (for tension or compression) and is connected to a Cooper Instruments model 460 Bridgesensor signal conditioning module with a cutoff frequency of 2000 Hz. The gain range for the 460 signal conditioner is 40-250. The bridge excitation is set to 9.5 Vdc and the amplifier gain to approximately 221. These values are chosen to obtain a high resolution signal from the analyzer. The raw output ("Load cell output") for a bridge excitation of 9.50 Vdc is 0.095 mV/lb_f. The load cell was mounted as close to the test shaft as possible to obtain the most accurate measurement of the actual static load. The calibration curve obtained for this load cell is shown in Figure 6.4. This data was obtained for both increasing and decreasing loads. No hysteresis effects were observed.

The static load is supplied by a double-acting Bimba air cylinder pressurized from a 125 psig capacity air tank. The cylinder has a power factor of 2.4, i.e. the maximum force exerted is 2.4 times the air line pressure. Thus, to achieve a 200 lb_f axial load, the line must be pressurized to 83.33 psig. The stroke length (7 in.) and bore diameter (1.75 in.) were selected using the ideal gas law to maintain pressure (i.e. applied static load) within acceptable limits as the end point of the shaft and, correspondingly, the piston head are displaced. The cylinder acts directly on the load
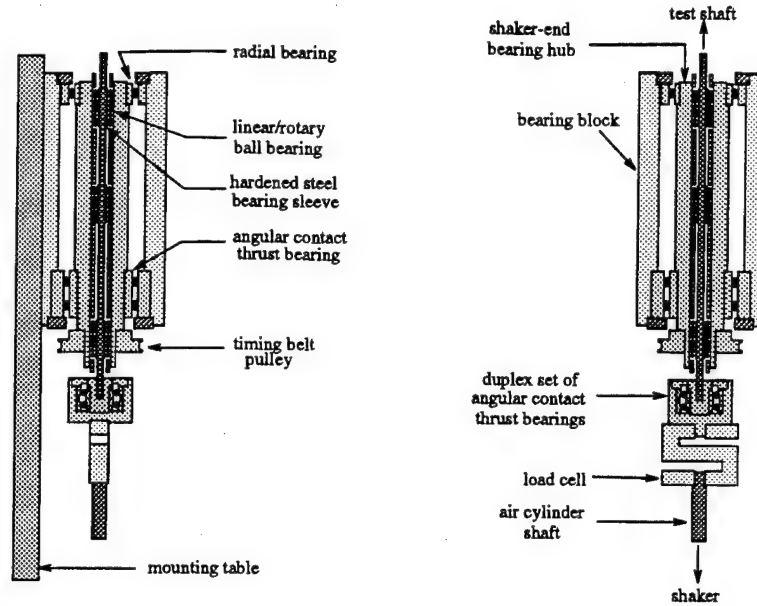
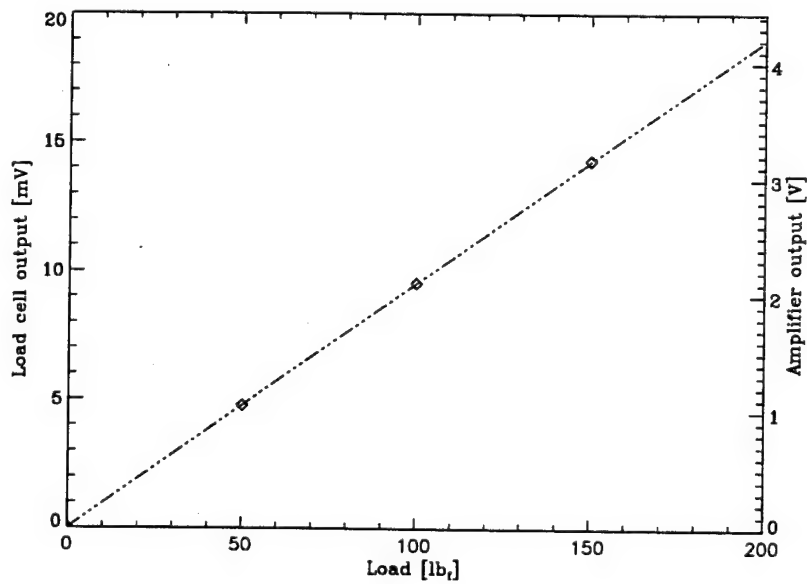Figure 6.3: Detail of the shaker-end bearing assembly

Figure 6.4: Load cell calibration curve for a bridge excitation of 9.5 Vdc

116

cell which transmits this load to the shaft through a small thrust bearing.

The time-dependent component of the axial load is provided by a Brüel & Kjær model # 4801T Exciter Body with a Brüel & Kjær model # 4812 Exciter Head. This shaker acts directly on the shaft of the air cylinder. Originally, it was desired to use the shaker to generate both static and dynamic forces simultaneously. The Brüel & Kjær 4801T/4812 is capable of generating a 30 lb$_f$ static load as well as a superimposed oscillating load. However, the DC current required to generate such an offset may, over a short period of time, cause the shaker to overheat. For this reason, the air cylinder described above was chosen to supply the static load.

The shaker is powered from a Brüel & Kjær # 2707 low distortion power amplifier. The frequency range of the amplifier is 40 Hz to 10 kHz at full capacity (220 VA) and DC to 100 kHz at reduced capacity. This shaker/amplifier system is capable of a 100 lb$_f$ peak sine excitation. The excitation amplitude required for the current tests, however, is well below this limit.

The 2707 amplifier may be set for *High* or *Low* output impedance, corresponding to constant drive current or constant drive voltage, respectively. The *High* impedance mode keeps the generated force unchanged when changes occur in the test object. This mode is particularly useful when monitoring force input rather than displacement. The *Low* impedance mode keeps the voltage applied to the exciter independent of changes in the test object, i.e. this regulates displacement of the exciter head. In the present investigation, the shaker operates in the *High* impedance mode since the force generated by this system is of primary importance.

Motor/Drive/Controller

The test shaft, auxiliary shaft, bearing system and flywheel are rotated by a Toshiba SMR-1-200 DC brushless servo motor/drive. The rated operating speed of this motor/drive system is 3000 rpm, the maximum is 4000 rpm. Quoted speed regulation of this system is "0.2% or better". The drive is controlled by a Motion Plus EDC 100 Encoder Digital Controller. The EDC 100 is a servo controller which allows full programming or direct operator control. The controller display screen also provides instantaneous position/velocity monitoring as well as error measurements. The rotation rate is also monitored by a tachometer consisting of a Pepperl+Fuchs inductive proximity probe sensing a 5-tooth gear mounted on the auxiliary shaft.

The motor shaft is connected to the motor-end bearing hub through a Gerwah #DK45/47 miniature metal bellows coupler. This coupler allows for both angular ($\pm$ 1.2 degrees) and axial (0.2 mm) misalignment. Directly below this coupler is a 6 in. diameter (1 in. thick) carbon steel flywheel used to regulate the rotation speed in the presence of any perturbations.

In order to eliminate torque in the test shaft, a timing belt/pulley system is employed. This system is depicted in Figure 6.1. The upper timing belt connects the motor-end hub to a 3/4 in. diameter steel shaft mounted parallel to the test shaft. The lower timing belt connects this auxiliary shaft to the shaker-end hub. The auxiliary shaft and timing belts are used to synchronize the rotation rate of the shaker end bearing hub with that of the motor-end hub in order to minimize torque in the experimental model. Therefore, the shaft will experience only axial movement with respect to the linear-rotary bearings, insuring that they do not bind. To include the effects of torque (due to bearing friction), the timing belts may be removed.

Figure 6.5: Axial view of the brass shaft showing strain gage configuration and the Wheatstone bridge corresponding to one pair of gages.

Lateral Displacement Measurements

The goal of the experiments is to measure the lateral displacement of the centerline of the brass test shaft. This quantity is measured indirectly through the strain. This is accomplished using four strain gages mounted directly on the test shaft. The gages are arranged in two half-bridge configurations as shown in Figure 6.5. Each pair (A or B) of gages constitutes two arms of the Wheatstone bridge. In this situation, there are two active gages with equal and opposite strains. Since the magnitudes of these signals are summed, this configuration provides a higher signal-to-noise ratio than the quarter bridge configuration.

The gages used are Measurements Group constantan foil gages with a gage factor of $F = 2.05$. The gage factor of a piezoelectric material is defined as

$$F = \frac{\Delta R/R_0}{\Delta L/L_0}$$

where $\Delta R/R_0$ is the change in resistance divided by the initial resistance of the gage ($R_0 = 350$ Ω, in this case), $\Delta L/L_0$ is the change in length divided by the initial length, i.e. strain, in the test object. In Figure 6.5, V represents the bridge excitation voltage, V_0, the output voltage and ϵ, the strain. These quantities are related through the gage factor by

$$\frac{V_0}{V} = \frac{F\epsilon}{2} \times 10^{-3}$$

where V_0 is measured in milliVolts, V in Volts and ϵ in microstrain (μin./in.).

Each pair of gages (A or B) is connected to a Measurements Group 2311 Signal Conditioning Amplifier. The signals are passed from the rotating to the stationary frame through a Fabricast 8-ring slip ring assembly. As stated, two gages make up two arms of the Wheatstone bridge. The remaining two arms are internal to the amplifier. The amplifier provides the bridge excitation V and filters and amplifies the incoming signal V_0.

Signal Analysis and Data Reduction

The signals obtained from the load cell, the tachometer proximity probe and the two strain gage amplifiers are fed into the four input channels of a Tektronix 2630 Fourier Analyzer run from a Gateway 486 PC. The analyzer implements the following standard data analysis functions:

- time domain waveform and orbit (x-y) plots

118

Channel	Signal
1	strain gage: bridge A
2	strain gage: bridge B
3	load cell
4	tachometer

Table 6.2: Data acquisition channel designation

- averaged and instantaneous power spectrum

- averaged and instantaneous auto- and cross-correlation

- impulse response function, transfer (frequency response) function and FFT

- real, imaginary, magnitude, phase and Nyquist displays

The analyzer also contains a signal generator which is used to give the Brüel & Kjær shaker/amplifier system the oscillatory signal which is translated into the time-dependent portion of the axial load. Both input and output channels process data at frequency ranges from DC to 5 Hz up to DC to 20 kHz.

The data assigned to each of the four input channels is given in Table 6.2. For reference, the strain gages are labeled (A or B) on the shaft according to the Wheatstone bridge, i.e. the 2311 amplifier, to which they are connected. Channels 1, 2 and 4 are AC coupled to filter out any DC offset since only dynamic signals are of interest in these measurements. Channel 3 monitors the axial load which contains both static and dynamic components. Hence, channel 3 is DC coupled to allow the DC component of the signal (the static load) to pass through the analog-to-digital converters.

Experimental Procedure

For the first set of experiments, the cross section of the test shaft used is symmetric (to within machining tolerances). An additional unsymmetric shaft has been machined for use in future tests. The first step in the experimental procedure is to determine an appropriate rotation rate Ω and static load P_0. Figure 6.6 shows the primary stable and restabilized regions described in Chapter 4 for a symmetric shaft in the absence of parametric excitation (and dissipation). The parameter region in which the experiments are to be conducted is the primary stable region since the mathematical model is no longer valid outside this region, i.e. beyond the buckling limit which separates the regions. Moreover, the static load and rotation rate are chosen such that the shaft is near the buckling limit. By choosing Ω and P_0 near this boundary, the stiffness of the shaft is effectively reduced.

Figure 6.7 shows a typical stability boundary for the case of additive combination resonance taken from Chapter 4. In this figure, $\Omega = 132.22$ rad/sec and $P_0 = 162.35$ lb$_f$. The predicted boundary provides a guide for locating the actual (experimental) stability boundary. For a given amplitude of parametric excitation μ, the frequency of excitation is gradually increased from some initial value ν_A until a change (a nonzero RMS value) is noticed in the steady state measurement
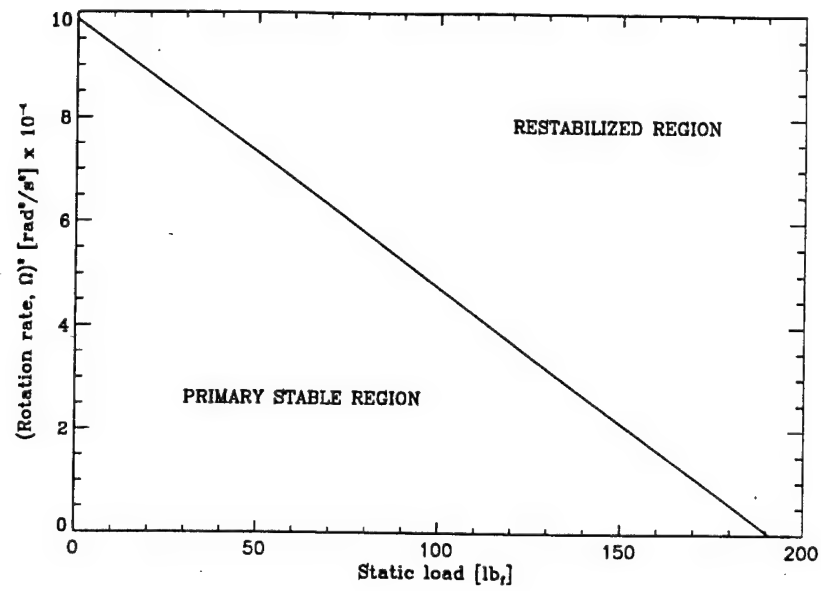
119

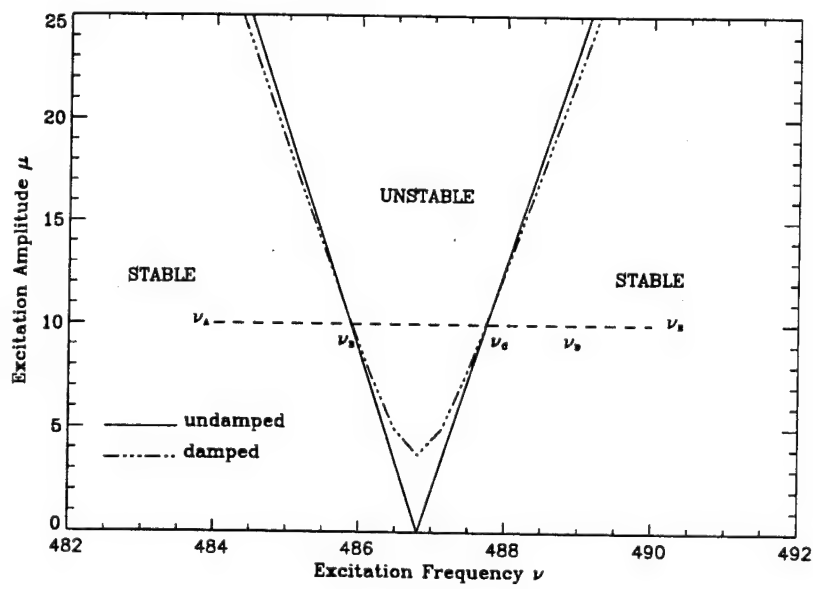Figure 6.6: Primary stable and restabilized regions

Figure 6.7: Typical stability boundary for the case of additive combination resonance.
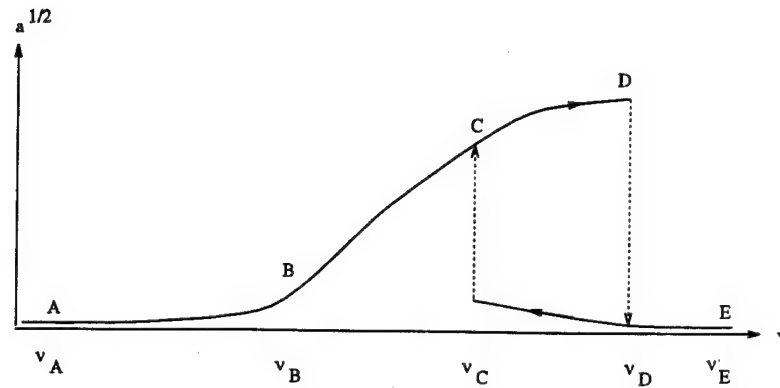
Figure 6.8: Hysteresis loop in the lateral vibration response.

of the strain. A qualitative description of the expected response amplitude a is given in Figure 6.8. The inferred shape of this curve is derived from experimental results on models described by similar equations of motion. As ν is increased, the frequency ν_B at which this nontrivial solution first exists marks the lower (frequency) bound of the stability boundary for that value of μ. As ν is increased beyond this point, the RMS amplitude will continue to grow. At some point, denoted by ν_D, the amplitude drops back down to zero. This occurs at a value of ν which is greater than that corresponding to the higher (frequency) bound of the stability boundary for that particular value of μ. If the frequency is increased beyond this point, the trivial solution remains stable until another such resonance band is encountered. The next resonance for the symmetric shaft corresponds to excitation of the second mode. The dynamics of this mode will not be considered in the current investigation. If this process is started from the point ν_E a nontrivial solution first begins to appear near the higher (frequency) bound of the stability boundary for the same μ. This point is denoted by ν_C. This increase, however, is not a smooth transition as is seen when the path is traversed in the original direction. In this case, a jump occurs at ν_C. The resulting RMS amplitude at point C is the same as when the path is traversed with increasing frequency. As the frequency is decreased further, the amplitude of oscillation dies down smoothly to zero.

The average and RMS value of any channel may be obtained at any time during the experiments. However, in the actual data analysis, frames of instantaneous temporal and spectral data are saved to a data file and reduced via post processing in Matlab. The RMS values of the time series obtained from channels 1 and 2 (the strain gage measurements) will be used to determine the stability of the trivial solution, approximate the location of the stability boundaries and record the growth of the nontrivial solutions. Any effects of hysteresis will also be noted.

6.3 Nonstandard Analysis of Experimental Data

Fourier and spectral analysis is indeed the most frequently applied technique for understanding experimental data. Such analysis is useful for obtaining the frequency components and power distribution as a function of frequency. For a given periodic or nonperiodic signal $f(t)$, one can define a frequency spectrum $F(\omega)$ as the Fourier transform of $f(t)$. Most modern spectral analysis

utilizes the discrete version of the above equation with an efficient algorithm called the Fast Fourier Transform (FFT). The book by Bendat and Piersol [11] on random data analysis and measurement procedures gives a detailed discussion on these and various other data processing techniques.

While such standard techniques provide useful information regarding frequency content and power distribution, some information is generally lost or averaged out. As the system response becomes more complicated, more information is lost. Thus, in order to gain a more detailed description of the nonlinear dynamics, it is imperative to utilize nonstandard time series analysis. Wavelet transforms, Lyapunov exponents, fractal dimensions and probability density functions are important examples of such techniques.

Wavelet Transforms

The ability to extract useful information from a time series often depends on the representation used to examine this data. Wavelet transformation provides an easily interpretable visual representation. The most often used methods of power spectral densities and Fourier transforms are essential tools for data analysis in many fields. However, these are poor choices when knowledge of spectral change over time is desired. The coefficients produced via the Fourier transform reflect the aggregate frequency content over the entire signal but say nothing about how the spectrum evolves with time. One way around this difficulty is to split the signal into segments to be analyzed separately. This is the basis for the procedure known as the windowed Fourier transform (WFT) which computes, for a given function $f(x)$,

$$G(\omega, u) = \int_{-\infty}^{\infty} e^{-i\omega x} f(x) g(x - u) dx$$

where $G(\omega, u)$ measures the frequency ω around the time point u and $g(x - u)$ is a fixed window function. A common choice for g is a Gaussian window but many other window functions may be used. In this method, one simply takes a Fourier transform of small pieces of the signal obtaining a set of spectra corresponding to different regions of time. However, as these windows of data grow smaller and smaller (yielding better resolution in time), the uncertainty principle dictates a loss of information about the frequency content in each region. Therefore, based on the type of information desired, a choice must be made to either transform short segments in order to understand time behavior at the expense of spectral resolution or deal with long segments of data to resolve the spectrum well, but lose the ability to pinpoint events in time. Thus, in the WFT method, the trade-off between time and frequency resolution is unavoidable.

For many applications, information is needed on a variety of scales. There may not be a single transform length which suitably illustrates small scale characteristics while yielding meaningful large scale data. In such cases, computationally expensive multiple transforms using different lengths may be performed. However, an inexpensive transformation which changes its resolution on different intervals, perhaps using large sections of data to clearly understand certain frequency ranges and small segments to nail down the time behavior where spectral accuracy is not that important, is needed. This is the basic idea behind wavelet transforms.

A wavelet is a function h which decays rapidly outside an interval in both time and frequency domains. This can be considered as the admissibility condition and is given explicitly by Morlet et al. [63] as

$$c_h = \int_0^{\infty} \frac{|\hat{h}(\omega)|}{\omega} d\omega < \infty$$

122

where $\hat{h}$ is the Fourier transform of h. This condition forces the frequency response to decay to zero at both zero and infinity, restricting the wavelet function to a class of band-pass filters. A detailed discussion on the type of functions satisfying this and other conditions is given by Daubechies [21]. The wavelet transform is thus a projection of a signal onto a set of functions which are translations and dilations of a given wavelet h. This transform was proposed by Morlet as a transformation of a function $f(x)$ at scale a and location b as

$$w(a, b) = \frac{1}{\sqrt{a}} \int_{-\infty}^{\infty} h\left(\frac{x - b}{a}\right) f(x) dx$$

It is clear from these definitions that both the WFT and wavelet transforms are scalar products of $f(x)$ with

$$g_{\omega, u}(x) = e^{-i\omega x} g(x - u) \quad \text{and} \quad h_{a, b}(x) - |a|^{-1/2} h\left(\frac{x - b}{a}\right)$$

respectively. These scalar products analyze the function f in a neighborhood of a time-frequency point. However, the frequency analysis performed by the wavelet transform is quite different from the WFT. The wavelet transform has a selected analyzing waveform modified by a given envelope and defined to have a fixed number of oscillations inside this envelope. The width of the envelope and the frequency scale work together as the frequency is increased to hold the number of oscillations constant. This property gives good resolution in the frequency domain and good localization in the time domain. Furthermore, the nonstationarity of the signal becomes less significant in the wavelet analysis since it does not depend on the long time behavior of the signal. This method also proves to be an important tool for analyzing the transient behavior of any dynamical system.

Lyapunov Exponent and Fractal Dimension

The Lyapunov exponent for a stochastic system is the analog of the real part of the eigenvalue in the deterministic case. It is a measure of the exponential divergence of nearby orbits in phase space and is, therefore, a characterization of the stability of the system. Lyapunov exponents thus provide a qualitative, as well as quantitative,description of the behavior of dynamical systems. In the context of deterministic systems, the Lyapunov exponent provides a measure of the system's sensitivity to variations in the initial conditions. Thus, any system possessing at least one positive Lyapunov exponent is defined to be chaotic. The computation of the spectrum of Lyapunov exponents when only a time series is available is difficult. Wolf et al. [90] present general algorithms which yield approximate values of the non-negative Lyapunov exponents for a time series.

There are several measures of the dimension of a set of points. The four most useful definitions for time series analysis will be discussed in this section. For detailed discussions on these measures, refer to Farmer [24] and the recent books by Moon [60] and Rasband [73].

Let A be the set of points of interest and assume that A is a bounded subset of $\mathbf{R}^n$. Let $N(\varepsilon)$ denote the minimum number of n-dimensional cubes of side ε needed to cover A. Then one can define the Hausdorff or capacity dimension of the set A as

$$d_{cap} = \lim_{\varepsilon \to 0} \frac{\ln[N(\varepsilon)]}{\ln[1/\varepsilon]}$$

which depends on the metric properties of space only.

123

The information dimension depends on the frequency at which each cell is visited by the map or, for the continuous flows, the fraction of time spent in each cell. In order to calculate the information dimension one counts the number of points N_i in each of the N cells and the probability P_i of finding a point in the ith cell where $P_i = N_i/N_0$ with $\sum P_i = 1$ where N_0 is the total number of points in set A. The information dimension is defined by the expression

$$d_I = \lim_{\varepsilon \to 0} \frac{I(\varepsilon)}{\ln[1/\varepsilon]} \quad \text{where} \quad I(\varepsilon) = \sum_{k=1}^{N(\varepsilon)} P_i \ln(1/P_i)$$

The correlation dimension is defined as

$$d_{corr} = \lim_{\varepsilon \to 0} \frac{\ln[c(\varepsilon)]}{\ln[\varepsilon]} \quad \text{where} \quad c(\varepsilon) = \lim_{N \to \infty} \frac{1}{N^2} \sum_{j,k=1(j \neq k)}^{N} H\left(\varepsilon - \| x_j - x_k \|\right)$$

and represents the number of pairwise correlations in an ε neighborhood about points on an attracting set A. In the above definition, $H(\cdot)$ is the Heaviside function, $H(\alpha) = 1$ if $\alpha > 0$, $H(\alpha) = 0$ if $\alpha \leq 0$ and $\| x_j - x_k \|$ denotes some convenient norm for the distance between x_j and x_k.

For an n-dimensional phase space, the Lyapunov exponents can be ordered as $\lambda_1, \cdots, \lambda_n$. Note that the sum of Lyapunov exponents is the average convergence which, for a dissipative system, must always be negative. The Lyapunov dimension is then

$$d_L = k + \frac{\sum_{j=1}^{k} \lambda_j}{|\lambda_{k+1}|}$$

where k labels the last λ_i for which $\lambda_1 + \cdots + \lambda_k \geq 0$. If $\lambda_1 < 0$, then define $d_L = 0$ and if $k = m$, define $d_L = m$. This definition is suggested by Kaplan and Yorke [44].

For dissipative dynamical systems exhibiting strange attractors, the fractal dimension defined through the various definitions above provides a good measure of the strangeness of the attractor. It is important to note that the fractal dimension D is always smaller than the dimension of the dynamical system F. One can choose the type of measure used to characterize the chaotic time series depending on the nature of the dynamical system. For example, it has been shown by Grassberger and Procaccia [31] that the calculation of the capacity dimension is exceedingly hard and, in fact, impractical for systems of dimension greater than 2. The correlation dimension appears to be the easiest and most useful measure of the fractal dimension. In addition, the correlation dimension allows one to distinguish between deterministic chaos and random noise.

Probability Distribution

Calculation of the probability distribution and density functions are important in both stochastic and chaotic dynamic experiments. In these experiments, the distribution of a signal is obtained by determining the length of the time intervals (Δt_i) the signal record $x(t)$ spent above a specified level, say a. The cumulative probability distribution is estimated by using the relation

$$P\{x(t) > a\} = \frac{1}{T} \sum \Delta t_i$$

where T is the whole sample interval. In a two dimensional phase-space, one can determine the same by partitioning the phase-space into cells and counting the number of time-sampled points
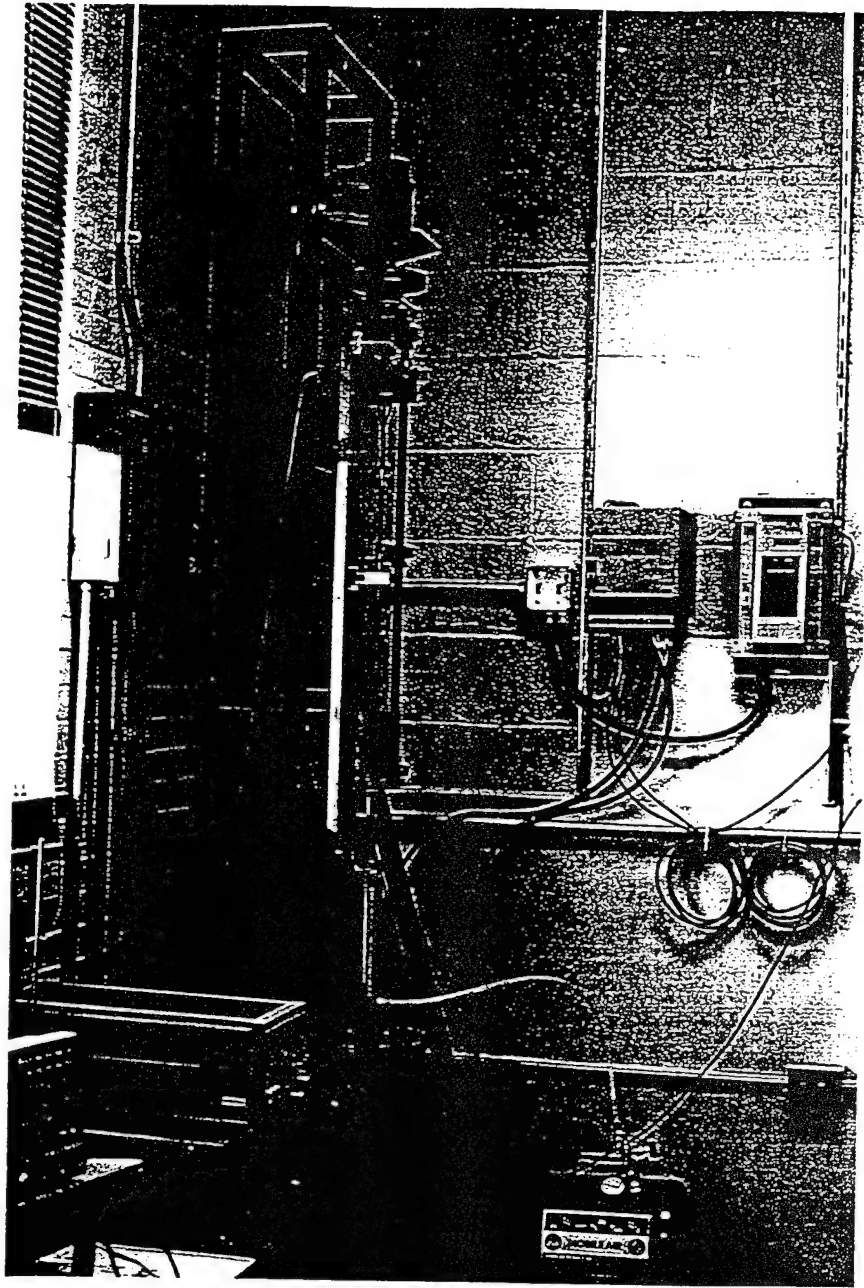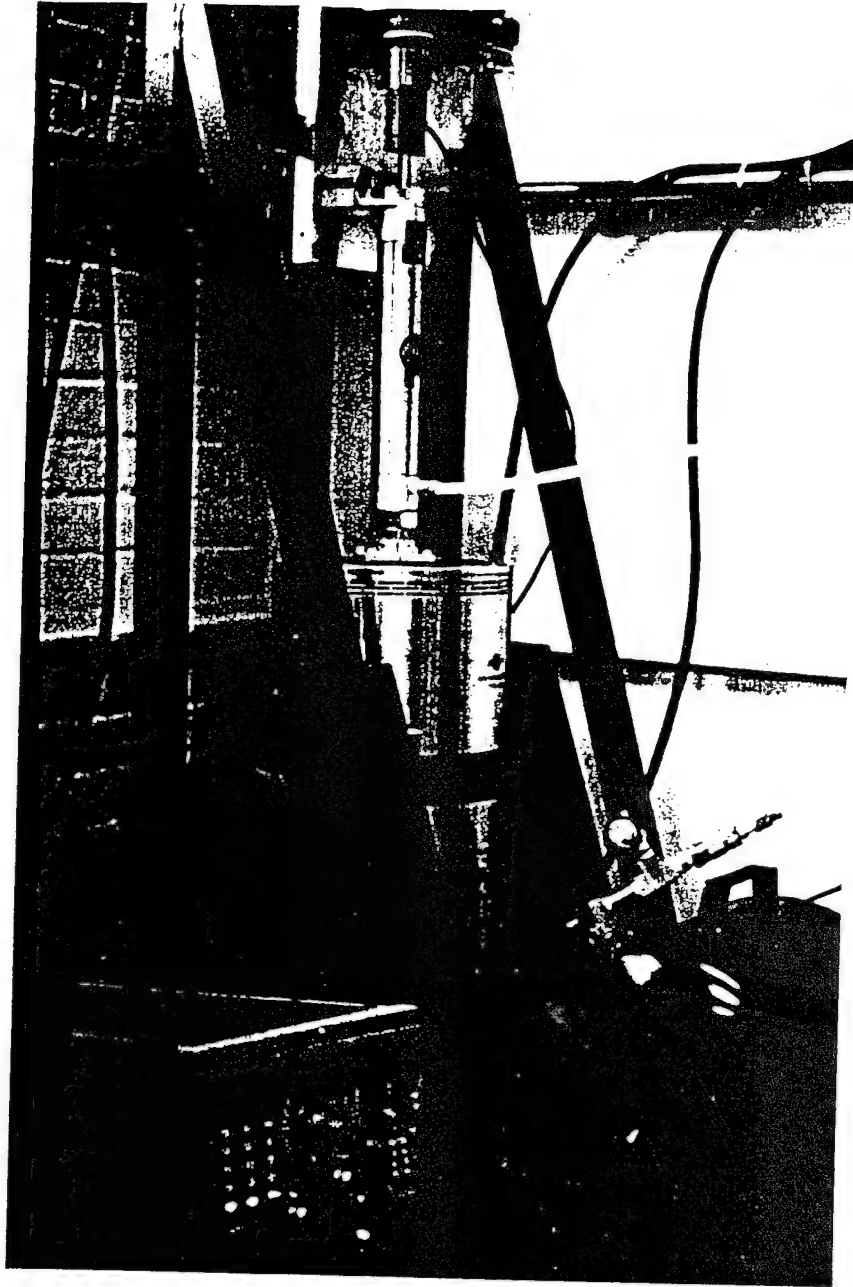
Figure 6.9: Rotating shaft test rig.

Figure 6.10: Close-up of excitation system.

Chapter 7

CONCLUSIONS

The motivation for this research was the determination and prediction of steady-state motions of practical dynamical systems and their corresponding stability. Of primary interest was the stability and bifurcation behavior of gyroscopic mechanical systems. The specific objectives for this research were as follows:

- develop analytical techniques to yield the almost-sure and moment stability of two- and four-dimensional linear systems parametrically excited by noise;

- investigate the local and global bifurcation behavior of deterministic nonlinear gyroscopic systems subject to periodic parametric excitation with application to rotordynamics;

- develop laboratory facilities in order to verify the local stability results through direct experimentation.

The results obtained from this research provide valuable insight into the mechanisms which cause instability and give rise to more complicated behavior. Moreover, it is hoped that the analytical techniques developed will have an important impact on the design of advanced mechanical/structural components and system reliability.

The first portion of this research dealt with the determination of the effect of adding parametric noise to linear mechanical systems for which the corresponding deterministic system is stable. In Chapter 2, an asymptotic expansion for the maximal Lyapunov exponent, the exponential growth rate of solutions to a linear stochastic system, and the rotation numbers for a general four-dimensional dynamical system driven by a small intensity real noise process were constructed. The almost-sure asymptotic stability boundaries, defined as the point at which the maximal Lyapunov exponent becomes zero can be obtained provided the infinitesimal generator associated with the noise process has an isolated simple zero eigenvalue. This assumption was made to make the solution tractable. In the absence of noise and dissipation, the system under consideration in Chapter 2 is critical and possesses two pairs of purely imaginary eigenvalues with non-commensurable frequencies. By imposing certain restrictive conditions on the manner in which the stochastic terms enter the system, the method of stochastic averaging may be applied to determine the top Lyapunov exponent. However, in certain important physical examples (such as the problem of flow-induced oscillations discussed in Chapter 2), these conditions are unrealistic. The advantage of the current method over the method of stochastic averaging is the applicability of the perturbation approach to problems without imposing any conditions on the form of the stochastic terms. The results obtained have a wide range of applications. Specifically, the perturbative technique developed in this

chapter was applied to study the lateral vibration instability in rotating shafts subject to stochastic axial loads and stationary shafts in cross flow with randomly varying flow velocity.

Sample or almost-sure stability of a stationary solution of a random dynamical system is of importance in the context of dynamical systems theory since it guarantees all samples except for a set of measure zero tend to the stationary solution as time goes to infinity. However, from the applications viewpoint, one may not be satisfied with such guarantees since a sample stable process may still exceed some threshold values or may possess a slow rate of decay. Although sample solutions may be stable with probability one, the mean square response of the system for the same parameter values may grow exponentially. For this reason, it is wise to also consider the behavior of the moments of the response over time. To this end, an asymptotic expansion for the moment Lyapunov exponent is being derived by the *Nonlinear Systems Group* at the University of Illinois. In the process of calculating the moment Lyapunov exponent, the maximal Lyapunov exponent, and thus the almost-sure stability, will also be computed. The moment Lyapunov exponent, based solely on the linear operator, provides insight into the response of the full nonlinear equations of motion. It provides the parameter value necessary to attain a normalizable density function for the nonlinear response and parameter values at which this density function undergoes qualitative changes.

The second portion of this research studies the bifurcation behavior of nonlinear gyroscopic systems. Throughout this work, it is assumed that the dissipation, imperfections and amplitudes of parametric excitations are small. In this way, it is possible to treat these problems as weakly Hamiltonian systems. Most of the analysis presented here was based on the recent work of perturbed Hamiltonian systems.

Although the local and global results presented in Chapters 4 and 5 have a wide range of applications, the motivating problems throughout this phase of the research have been the investigation of the dynamics and stability of the rotating shaft and structural arch subject to a periodic parametric excitation. Shaft is a fundamental component in many mechanical and power generating systems. The parametric excitations in this system arise due to the action of adjacent components on the rotating shaft. These inputs are included as time-dependent parameters in the equations of motion of the component under investigation and may lead to large amplitude vibrations or chaotic motion. In the second problem we examine the dynamics associated with the 2-DOF shallow arch system near the principal subharmonic frequency ($\nu = 2\omega_1$), in addition to the presence of internal resonances. Here we take a more realistic approach owing to the observation that the forced system (3) allows single mode time dependent (periodic) solutions ($\eta(t), 0$) in the presence of external excitation. In Chapter 3, the partial differential equations of motion of a rotating shaft were derived. These equations describe the longitudinal as well as lateral motions (in the two principal directions) of the shaft. The equation governing the longitudinal motion decouples from the rest. Assuming only the first mode of vibration to be excited in each of the lateral directions, the partial differential equations were reduced to ordinary differential equations via a Galerkin approximation. The parameter range under consideration must be restricted such that the shaft is not allowed to buckle. Once the shaft buckles, the governing equations are no longer valid.

In Chapter 4, the method of averaging was applied to yield a set of autonomous differential equations of motion governing the transverse vibrations of the shaft. These equations were then employed to examine the local bifurcation behavior of the shaft in the presence of all possible parametric resonance conditions that can exist in the first order averaged equations. The limits of stability for the trivial (non-oscillatory) solution of the averaged equations were determined in terms

of the excitation amplitude μ and frequency ν. The natural frequency of vibration in each direction is denoted by ω_r, $r = 1, 2$. In the nonresonant case, as well as the difference combination resonance case (i.e. for ν near $|\omega_1 - \omega_2|$), the nontrivial solution remains stable for all values of μ and ν in the parameter range of interest. It was shown that in the case of subharmonic parametric resonance (ν near $2\omega_r$), the trivial solution loses stability through divergence. Beyond the bifurcation point, the averaged set of equations exhibits a nonzero fixed point for each ν (or μ). Since fixed points of the averaged equations correspond to periodic orbits in the original system, this indicates that once the trivial solution loses stability, the shaft will begin to oscillate in the rth mode (with period ω_r). In the presence of additive combination resonance (ν near $\omega_1 + \omega_2$), depending on the excitation frequency, it was shown that the trivial solution may lose stability through divergence or flutter. The subsequent nontrivial response for each case was also described. In the case of combination resonance in the absence of dissipation, the system at criticality possesses two coincident pairs of purely imaginary eigenvalues. The linear system is in nonsemisimple 1:1 internal resonance and the trivial solution loses stability through a Hamiltonian Hopf bifurcation.

The specific goal of Chapter 5 was to determine the effects of non-Hamiltonian perturbations on the global behavior of otherwise Hamiltonian dynamical systems. The non-Hamiltonian terms in this analysis appear at the linear level only. In Chapter 5, the conditions on system parameters are explored for which the shallow arch system can exhibit chaotic dynamics under small perturbations arising due to dissipation and external excitation effects. In the first case it is shown that the averaged system corresponding to the nonlinear variational equations can have heteroclinic connections for certain values of system parameters in the absence of any perturbations. For one-to-two resonant case higher dimensional Melnikov's Method is used to show that one of the heteroclinic orbits may break under small time periodic excitations. Under these conditions the averaged system may have Smale Horseshoe type chaos whenever the system parameters σ and p_{20} lie inside the domain I and II. Using a standard theorem these results can be extended for the original system. It must be noted that the existence of a simple zero of the *Melnikov Function* only provides the necessary condition for the chaotic conditions to occur. The applicability of this method is restricted in this class of problems in the sense that one can not examine the effect of perturbations arising from the dissipation effects. In this case, the presence of even very small dissipation leads to destroy any attracting invariant sets on the perturbed manifold M_ϵ and the phase flow escapes by crossing the lower boundary, and the shallow arch system finally settles down to the periodic behavior as $t \to \infty$. The numerical simulations were also performed to confirm the predictions made in the analysis and to further explore the effect of small perturbations on the periodic and heteroclinic orbits. These simulations reveal very exciting details of the underlying structure of the quasi-periodic orbits and chaotic regions in the perturbed system.

In the second part of this Chapter 5, we have used a perturbation technique due to [48] to study the shallow arch dynamics near one-to-one internal resonance. Using this technique the effect of small perturbations arising from periodic excitations and dissipative forces are examined on the averaged system, and the explicit restrictions on system parameters are obtained which may lead to the existence of a *Silnikov type homoclinic orbit* to a saddle-focus type fixed point in the perturbed system, and consequently the complex dynamics is resulted. This mechanism provides a more restrictive criterion for the existence of chaotic dynamics in the presence of small dissipation and small periodic excitation effects. The results of this analysis are also interpreted in terms of the oscillations of the shallow arch system.

The final phase of this research was the design and construction of a test rig dedicated to the verification of the analytical techniques developed in this research through direct experimentation. Chapter 6 describes the laboratory facilities that have been developed. The theoretical results will serve as a guideline for locating stability boundaries and predicting post-critical behavior. The extent to which the theoretical and experimental results match will provide an insight into the accuracy of the mathematical models and theoretical approximations. The experiments will, in turn, guide the development and refinement of the theories developed to incorporate any new phenomena observed.

Bibliography

[1] ABRAMOWITZ, M., AND STEGUN, I. A. *Handbook of Mathematical Functions.* Dover, New York, 1972.

[2] ARIARATNAM, S. T., AND SRI NAMACHCHIVAYA, N. Periodically perturbed linear gyroscopic systems. *Journal of Structural Mechanics 14*, 2 (1986), 127–151.

[3] ARIARATNAM, S. T., AND SRI NAMACHCHIVAYA, N. Periodically perturbed nonlinear gyroscopic systems. *Journal of Structural Mechanics 14*, 2 (1986), 153–175.

[4] ARIARATNAM, S. T., AND XIE, W. C. Lyapunov exponents and stochastic stability of coupled linear systems under real noise excitation. *ASME Journal of Applied Mechanics 59*, 3 (1992), 664–673.

[5] ARNOLD, L. A formula connecting sample and moment stability of linear stochastic systems. *SIAM Journal of Applied Mathematics 44*, 4 (1984), 793–802.

[6] ARNOLD, L., AND KLIEMANN, W. *Probabilistic Analysis and Related Topics*, vol. 3 of *Qualitative Theory of Stochastic Systems.* Academic Press, New York, 1983. A.T. Bharucha-Reid ed.

[7] ARNOLD, L., PAPANICOLAOU, G., AND WIHSTUTZ, V. Asymptotic analysis of Lyapunov exponent and rotation number of the random oscillator and applications. *SIAM Journal of Applied Mathematics 46*, 3 (1986), 427–450.

[8] ARNOLD, L., AND SAN MARTIN, L. A multiplicative ergodic theorem for rotation numbers. *Journal of Dynamics and Differential Equations 1*, 1 (1989), 95–119.

[9] BALACHANDRA, B., AND NAYFEH, A. H. Nonlinear motions of beam-mass structure. *Nonlinear Dynamics 1*, 1 (1990), 39–61.

[10] BAXTER, G. K., AND EVAN-IWANOWSKI, R. M. Response of a column in random vibration tests. *Journal of Structural Mechanics 101* (1975), 1749–1761.

[11] BENDAT, J. S., AND PIERSOL, A. G. *Random Data: Analysis and Measurement Procedures*, 2nd edition ed. Wiley-Interscience, New York, 1986.

[12] BOGDANOFF, J. L., AND CITRON, S. J. Experiments with an inverted pendulum subjected to random parametric excitation. *Journal of the Acoustal Society of America 38* (1965), 447–452.

[13] BOGOLIUBOV, N., AND MITROPOLSKY, Y. A. *Asymptotical Methods in the Theory of Nonlinear Oscillations.* Gordon and Breach, New York, 1961.

[14] BOLOTIN, V. V. *The Dynamic Stability of Elastic Systems.* Holden-Day, San Francisco, 1964.

[15] CHETAEV, N. G. *The Stability of Motion.* Pergamon Press, New York, 1961.

[16] CHOI, S. H., PIERRE, C., AND ULSOY, A. G. Consistent modeling of rotating Timoshenko shafts subject to axial loads. *Journal of Vibration and Acoustics 114* (April 1992), 249–259.

[17] CRANDALL, S. H. Rotordynamics. In *Nonlinear Dynamics and Stochastic Mechanics*, W. H. Kliemann and N. Sri Namachchivaya, Eds. CRC Press, Boca Raton, FL, 1995.

[18] CUSUMANO, J. P., AND MOON, F. C. Low-dimensional behavior in chaotic nonplanar motions of a forced linearly elastic rod: Experiment and theory. In *IUTAM Symposium on Nonlinear Dynamics in Engineering Systems* (New York, 1990), Springer-Verlag.

[19] DALZELL, J. F. Exploratory studies of liquid behavior in randomly excited tanks: Lateral excitation. Tech. Rep. 2, Southwest Research Institute, San Antonio, TX, 1967.

[20] DALZELL, J. F. Exploratory studies of liquid behavior in randomly excited tanks: Longitudinal excitation. Tech. Rep. 1, Southwest Research Institute, San Antonio, TX, 1967.

[21] DAUBECHIES, I. The wavelet transform, time-frequency localization and signal analysis. *IEEE Transactions on Information Theory 36*, 5 (1990), 961–1005.

[22] DELLNITZ, M., MELBOURNE, I., AND MARSDEN, J. E. Generic bifurcation of Hamiltonian vector fields with symmetry. *Nonlinearity 5* (1992), 979–996.

[23] DOYLE, M. M., AND SRI NAMACHCHIVAYA, N. Almost-sure asymptotic stability of a general four dimensional dynamical system driven by real noise. *Journal of Statistical Physics 75*, 3/4 (1994), 525–552.

[24] FARMER, J. D. Chaotic attractors of an infinite-dimensional dynamical system. *Physica D 4* (1982), 366–393.

[25] FELLER, W. Diffusion process in one dimension. *Transactions of American Mathametical Society 77* (1954), 1–31.

[26] FENG, Z., AND SETHNA, P. R. Global bifurcations and chaos in parametrically forced systems with one-one resonance. *Dynamics and Stability of Systems 5* (1990), 201–225.

[27] FENG, Z., AND SETHNA, P. R. Global bifurcations in the motion of parametrically excited thin plates. *Nonlinear Dynamics 4* (1993), 398–408.

[28] FENG, Z., AND WIGGINS, S. On the existence of chaos in a class of two-degree-of-freedom , damped, strongly parametrically forced mechanical systems woth broken o(2) symmetry. *Journal of Applied Mathematics and Physics (ZAMP) 44* (1993), 1–48.

[29] FORRAY, M. J. *Variational Calculus in Science and Engineering.* McGraw - Hill, 1968.

[30] GOLDSTEIN, H. *Classical Mechanics.* Addison-Wesley, 1980.

[31] GRASSBERGER, P., AND PROCACCIA, I. Measuring the strangeness of strange attractors. *Physica D 9* (1983), 189–208.

133

[32] GUCKENHEIMER, J., AND HOLMES, P. *Nonlinear Oscillations, Dynamical Systems, and Bifurcations of Vector Fields.* Springer-Verlag, New York, 1983.

[33] HADDOW, A. G., BARR, A. D. S., AND MOOK, D. T. Theoretical and experimental study of modal interaction in two degree-of-freedom structure. *Journal of Sound and Vibration 97* (1984), 451–473.

[34] HALE, J. K. *Ordinary Differential Equations.* Wiley, New York, 1969.

[35] HARTLEN, R. T., AND CURRIE, I. G. Lift oscillator model of vortex-induced vibration. *Journal of Engineering Mechanics, Proceedings of the ASCE 96* (1970), 577–591.

[36] HSU, C. S. Stability of shallow arches against snap-through under time-wise step loads. *AIAA Journal 35*, 1 (1969), 31–39.

[37] HUANG, N. C. Dynamic buckling of some elastic shallow structures subjected to periodic loading with high frequency. *International Journal of Solids of Structures 8* (1972), 315–326.

[38] HUMPHREY, J. S. On dynamic snap buckling of shallow arches. *AIAA Journal 4*, 5 (1966), 878–886.

[39] HUTCHINSON, J. W., AND KOITER, W. T. Postbuckling theory. *Appl. Mech. Rev. 23* (1970), 1353–1366.

[40] IBRAHIM, R. A. Nonlinear random vibration: Experimental results. *Applied Mechanics Review 44*, 10 (1991), 423–446.

[41] IBRAHIM, R. A., EVANS, M., AND YOON, Y. J. Experimental investigation of random excitation of nonlinear systems with autoparametric coupling. *Structural Safety 6* (1989), 161–176.

[42] IBRAHIM, R. A., AND SULLIVAN, D. G. Experimental investigation of structural linear and nonlinear autoparametric interactions under random excitation. *AIAA Journal 28* (1990), 338–344.

[43] KAPITANIAK, T. Combined bifurcations and transition in a non-linear oscillator with two external periodic forces. *Journal of Sound and Vibration 121*, 2 (1988), 259–268.

[44] KAPLAN, J., AND YORKE, J. Chaotic behavior of multidimensional difference equations. In *Functional Differential Equations and the Approximation of Fixed Points*, vol. 730 of *Lecture Notes in Mathematics*. Springer-Verlag, New York, 1979, pp. 228–232.

[45] KARLIN, S., AND TAYLOR, H. M. *A Second Course in Stochastic Processes.* Academic Press, New York, 1972.

[46] KHAS'MINSKII, R. Z. Necessary and sufficient conditions for the asymptotic stability of linear stochastic systems. *Theory of Probability and Applications 12*, 1 (1967), 144–147.

[47] KOITER, W. T. On the nonlinear theory of thin shell structures. *Proc. Koninkl. Ned. Acad. Wetenschap. B70* (1966), 1–54.

[48] KOVAČIČ, G., AND WIGGINS, S. Orbits homoclinic to resonances, with an application to chaos in a model of the forced and damped sine-gordon equation. *Physica D 57* (1992), 185–225.

[49] KOZIN, F., AND PRODROMOU, S. Necessary and sufficient conditions for almost-sure sample stability of linear itô equations. *SIAM Journal of Applied Mathematics 21*, 3 (1971), 413–424.

[50] KOZIN, F., AND SUGIMOTO, S. Relations between sample and moment stability for linear stochastic differential equations. In *Proceedings of Conference on Stochastic Differential Equations and Applications* (1977), J. D. Mason, Ed., Academic Press, pp. 145–162.

[51] KREIN, M. G. A generalization of several investigations of A. M. Lyapunov on linear differential equations with periodic coefficients. *Dokl. Akad. Nauk. SSSR 73* (1950), 445–448.

[52] KRYLOV, N. M., AND BOGOLIUBOV, N. N. *New Methods of Nonlinear Mechanics in Their Application to the Investigation of the Operation of Electronic Generators, I.* United Scientific and Technical Press, Moscow, 1934.

[53] LOCK, M. H. The snapping of a shallow sinusoidal arch under a step pressure load. Tech. Rep. TRD-469 (5240-10-16), Air Force Systems Command, Los Angeles, 1965.

[54] LYON, R. H., HECKL, M., AND HAZELGROVE, C. B. Response of hard-spring oscillator to narrow-band excitation. *Journal of the Acoustal Society of America 33* (1961), 1404–1411.

[55] MELNIKOV, M. H. On the stability of the center for time periodic perturbations. *Trans. Mosc. Math. Soc. 12*, 1 (1963), 1–57.

[56] METTLER, E. Dynamic buckling. In *Handbook of Engineering Mechanics*. McGraw-Hill, New York, 1962.

[57] METTLER, E. Stability and vibration problems of mechanical systems under harmonic excitation. In *Proceedings of the International Conference on Nonlinear Dynamic Stability of Structures* (London, 1967), G. Herrman, Ed., Pergamon, pp. 169–188.

[58] METTLER, E. Combination resonances in mechanical systems under harmonic excitation. In *Proceedings of the Fourth Conference on Nonlinear Oscillations* (Prague, 1968), Academia, pp. 51–70.

[59] MITCHELL, R. R., AND KOZIN, F. Sample stability of second order linear differential equations with wide-band noise coefficients. *SIAM Journal of Applied Mathematics 27*, 4 (1974), 571–604.

[60] MOON, F. C. *Chaotic Vibrations*. Wiley, New York, 1987.

[61] MOON, F. C., CUSUMANO, J., AND HOLMES, P. F. Evidence of homoclinic orbits as a precursor to chaos in magnetic pendulum. *Physica D 24* (1987), 383–390.

[62] MOON, F. C., AND HOLMES, P. J. A magneto elastic strange attractor. *Journal of Sound and Vibration 65* (1979), 275–296.

[63] MORLET, J., ARENS, G., FOURGEAU, I., AND GIARD, D. Wave propagation and sampling theory. *Geophysics 47* (1982), 203–236.

[64] MURDOCK, J. Qualitative theory of nonlinear resonance by averaging and dynamical systems methods. *Dynamics Reported 1* (1988), 91–172.

[65] NAYFEH, A. H., AND MOOK, D. T. *Nonlinear Oscillations*. Wiley, New York, 1979.

[66] NAYFEH, A. H., AND ZAVODNEY, L. D. Experimental observation of amplitude and phase modulated responses of two internally coupled oscillators to a harmonic excitation. *Journal of Applied Mechanics 55* (1988), 706–711.

[67] NISHIOKA, K. On the stability of two-dimensional linear stochastic systems. *Kodai Mathematics Seminar 27* (1976), 211–230.

[68] OSELEDEC, V. I. A multiplicative ergodic theorem. Lyapunov characteristic numbers for dynamical systems. *Transaction of Moscow Mathematical Society 19* (1968), 197–231.

[69] PAIDOUSSIS, M. P., AND MOON, F. C. Nonlinear and chaotic fluidelastic vibrations of a flexible pipe conveying fluid. In *Nonlinear Interaction Effects and Chaotic Motion* (1988), M. Reischman, M. Paidoussis, and R. Hansen, Eds., ASME, pp. 107–133.

[70] PARDOUX, E., AND WIHSTUTZ, V. Lyapunov exponent and rotation number of two-dimensional linear stochastic systems with small diffusion. *SIAM Journal of Applied Mathematics 48*, 2 (1988), 442–457.

[71] PINSKY, M. A., AND WIHSTUTZ, V. Lyapunov exponents for white and real noise driven two-dimensional systems. *Lectures in Applied Mathematics 27* (1991), 201–213.

[72] PLAUT, R. H., AND HSIEH, J. C. Oscillations and instability of a shallow arch under two-frequency excitation. *Journal of Sound and Vibration 102*, 2 (1985), 189–201.

[73] RASBAND, S. N. *Chaotic Dynamics of Nonlinear Systems*. Wiley, New York, 1909.

[74] ROBERTS, J. W. Random excitation of a vibratory system with autoparametric interaction. *Journal of Sound and Vibration 69* (1980), 101–116.

[75] SANDERS, J. A., AND VERHULST, F. *Averaging Methods in Nonlinear Dynamical Systems*. Springer-Verlag, New York, 1985.

[76] SETHNA, P. R., AND BAJAJ, A. K. Bifurcations in dynamical systems with internal resonance. *ASME Journal of Applied Mechanics 45* (1978), 895–902.

[77] SETHNA, P. R., AND SCHAPIRO, S. M. Nonlinear behavior of flutter unstable dynamical systems with gyroscopic and circulatory forces. *ASME Journal of Applied Mechanics 44*, 4 (1977), 755–762.

[78] SRI NAMACHCHIVAYA, N. Mean square stability of a rotating shaft under combined harmonic and stochastic excitations. *Journal of Sound and Vibration 133*, 2 (1989), 323–336.

[79] SRI NAMACHCHIVAYA, N. Almost-sure stability of dynamical systems under combined harmonic and stochastic excitations. *Journal of Sound and Vibration 151*, 1 (1991), 77–90.

[80] SRI NAMACHCHIVAYA, N., AND ARIARATNAM, S. T. Almost-sure asymptotic stability of stochastically coupled two degree of freedom mechanical systems. Tech. Rep. UILU ENG 90-0502, University of Illinois at Urbana-Champaign, 1990.

[81] SRI NAMACHCHIVAYA, N., AND DOYLE, M. M. Chaotic motion of a shallow arch. In *Proceeding of 29th Structures, Structural Dynamics and Materials Conference* (1988), AIAA, pp. 198–209.

[82] SRI NAMACHCHIVAYA, N., AND TALWAR, S. Maximal Lyapunov exponents for stochastically perturbed co-dimension two bifurcations. *Journal of Sound and Vibration 69*, 3 (1993), 349–372.

[83] SRI NAMACHCHIVAYA, N., AND VAN ROESSEL, H. J. Maximal Lyapunov exponent and rotation numbers for two coupled oscillators driven by real noise. *Journal of Statistical Physics 71*, 3/4 (1993), 549–567.

[84] STAKGOLD, I. *Green's Functions and Boundary Value Problems*. Wiley-Interscience, New York, 1979.

[85] TIEN, W. M. *Chaotic and Stochastic Dynamics of Structural Systems*. PhD thesis, University of Illinois at Urbana-Champaign, 1992.

[86] TIEN, W. M., SRI NAMACHCHIVAYA, N., AND BAJAJ, A. K. Nonlinear dynamics of a shallow arch under periodic excitation, part I: 1:2 internal resonance. *International Journal of Nonlinear Mechanics 29*, 3 (1994), 349–366.

[87] TIEN, W. M., SRI NAMACHCHIVAYA, N., AND MALHOTRA, N. Nonlinear dynamics of a shallow arch under periodic excitation, part II: 1:1 internal resonance. *International Journal of Nonlinear Mechanics 29*, 3 (1994), 367–386.

[88] ŠIL'NIKOV, L. P. A case of the existence of a countable number of periodic motions. *Sov. Math. Dokl. 6* (1965), 163–166.

[89] WIGGINS, S. *Global Bifurcations and Chaos*. Springer-Verlag, New York, 1988.

[90] WOLF, A., SWIFT, J. B., SWINNEY, H. L., AND VASTANO, J. A. Determining Lyapunov exponents from a time series. *Physica D 16* (1985), 285–317.

[91] YAZICI, M. On the stability of dissipative gyroscopic systems. Master's thesis, University of Waterloo, Waterloo, Ontario, 1976.

[92] ZAUDERER, E. *Partial Differential Equations of Applied Mathematics*. Wiley-Interscience, New York, 1989.